CATALYTIC PARTIAL OXIDATION OF METHANE TO VALUE ADDED PRODUCTS BY N_2O OVER FE-BASED CATALYSTS AT MODERATE TEMPERATURES

A Thesis Submitted for the Degree of

DOCTOR OF PHILOSOPHY

Guangyu Zhao

B.Eng. (Environmental)

THE UNIVERSITY OF NEWCASTLE AUSTRALIA

Discipline of Chemical Engineering

Faculty of Engineering and Built Environment

The University of Newcastle, Australia

August, 2019

STATEMENT OF ORIGINALITY

I hereby certify that the work embodied in the thesis is my own work, conducted under normal supervision. The thesis contains no material which has been accepted, or is being examined, for the award of any other degree or diploma in any university or other tertiary institution and, to the best of my knowledge and belief, contains no material previously published or written by another person, except where due reference has been made. I give consent to the final version of my thesis being made available worldwide when deposited in the University's Digital Repository, subject to the provisions of the Copyright Act 1968 and any approved embargo.

Guangyu Zhao

ACKNOWLEDGMENT OF AUTHORSHIP

I hereby certify that the work embodied in this thesis contains published paper/s/scholarly work of which I am a joint author. I have included a written declaration below endorsed in writing by my supervisor, attesting to my contribution to the joint publication/s/scholarly work.

By signing below I confirm that Guangyu Zhao contributed conduction of experiments, data analysis and manuscripts writing to the paper/ publication entitled "Comparison of Direct, Selective Oxidation of Methane by N_2O over Fe-ZSM-5, Fe-Beta and Fe-FER Catalysts", "Catalysed Conversion of Methane to Value Added Products", "Formation of Surface Oxygen Species and the Conversion of Methane to Value Added Products with N_2O as Oxidant over Fe-FER Catalysts" and "Direct Methane Conversion to Value added Products at Moderate Temperature by N_2O over Fe-FER Catalysts Prepared by Different Methods".

Eric Kennedy, Michael Stockenhuber

STATEMENT OF CONTRIBUTION OF OTHERS

I, the undersigned, attest that Research Higher Degree candidate, Guangyu Zhao, has carried out the experimental programs, conducted experiments, result analysis and has written all papers included in this thesis.

Guangyu Zhao

ACKNOWLEDGMENT

I would like to express my sincerest gratitude to my supervisors, Professor Eric Kennedy and Professor Michael Stockenhuber for their guidance, support, encouragement and advice throughout the fulfilment of my thesis. Their wise ideas and inimitable knowledge inspired me and enhanced my research ability. The accomplishment of the thesis was basing on our fruitful meetings and their patient editing.

I am grateful to The University of Newcastle for awarding me the International Postgraduate Research Scholarship (UNIPRS) and Postgraduate Research Scholarship (UNPRS).

I would like to acknowledge Mr Penghui Yan, Dr Naseer Ahmed Khan and Mr Jarrod Friggieri who assisted me in the design of the experimental setup, thank you for your suggestions. I really appreciate the input of Dr Emad Benhelal for providing valuable support in the ICP and TGA analysis, Dr Matthew Drewery and Dr Meng Jung Li for their great help in proof reading my thesis. My sincere appreciation is extended to Dr Glenn Bryant, Mr Scott Molly, Mr Luke Harvey, Dr Vahid Shadravan, Dr Hadi Hosseiniamoli, and Dr Omid Mowla who provided me with insightful suggestions for FTIR spectroscopy, H_2-TPR, TPD, and CO chemisorption analysis. I also thank Dr Tiesheng Wang and Mr Eleanor Kearns for helping me with UV-vis spectroscopy measurement.

My sincere thanks to the staff of the Chemical Engineering Department, especially Mrs Jane Hamson, Ms Jane Power, Mr Matt Laver and Mr Con Safouris for their technical and administrative assistance.

I would like to thank the Electron Microscope and X-ray Unit of the University of Newcastle and their fantastic staff. I am grateful to Dr Yun Lin for her help with SEM analysis and Mrs Jennifer Zobec for her help with XRD analysis.

I am truly grateful to my partner, Mingzhe, who is my love, my companion, my motivation and my strength. She always supported, encouraged and brighten me in those dark moments. I would like to express my gratitude to my family for their constant support, I am thousands miles away but my heart always be with you.

I would also like to thank my friends in Newcastle, Jiajie, Yingxin, Yi, Duanduan, Meng, Ming, Zheqian, Jianhua, Wenlong, they became my family here in Australia.

Finally, thank all my colleagues and friends in ATC and EB, Dr Faeze Farhang, Pedram Ghaseminejad, Dr Sara Mosallanejad, Hamed Mootabadi, Dr Timothy Oliver, Dr Gizelle Sanchez, Cameron Keast, Jim Mensah, Umar Isha, Nirmala Dharmarathne, Taslima Akhter. It was such great experience to study with all of you.

ABSTRACT

A laboratory scale process for catalytic partial methane oxidation to methanol and derivatives by N_2O over Fe-based catalysts in a continuous operation mode at moderate temperatures was constructed.

Examination of the partial methane oxidation to methanol over Fe-ZSM-5 catalysts at moderate temperatures showed that methanol and formaldehyde were produced at a temperature range from 275 ℃ to 400 ℃ with selectivity decreasing with increasing temperature. Incorporation of 0.1 wt% iron to H-ZSM-5 promoted methane and N_2O conversion, as well as the selectivity to C_1-oxygenates. Further loading of iron enhanced methane conversion via complete oxidation. With an increase in the CH_4/N_2O ratio, selectivity of both carbon oxides and C_1-oxygenates decreased, while the selectivity of ethylene showed an opposite trend. In addition, a relatively high GHSV elevated selectivity to desired products.

In order to explore the correlation of structure properties of zeolites to active sites for methanol formation, activity and selectivity over Fe-ZSM-5, Fe-Beta and Fe-FER catalysts were studied at 350 °C for the catalytic partial oxidation of methane. Ammonia adsorption data suggested that among the studied zeolites, H-FER zeolite contained the highest concentration of framework Al atoms which are essential for the formation of active extra-framework Fe species. Fe-FER catalyst contained more active sites for N_2O conversion in comparison to Fe-Beta and Fe-ZSM-5 catalysts, as demonstrated by H_2-TPR profiles and IR spectra of NO adsorbed on the Fe zeolites. The catalytic activity studies showed that Fe-FER was the most active catalyst based on

methane and N_2O conversion, and displayed the highest selectivity to C_1-oxygenates and dimethyl ether (DME), while Fe-ZSM-5 obtained the highest selectivity to ethylene among the three catalysts. Fe-ZSM-5 was found to deactivate significantly due to coke formation.

Fe-FER catalysts prepared by incipient wetness impregnation (IMP), liquid ion exchange (IE) and solid state ion exchange (SSIE) methods were studied at 350 °C. UV-vis spectra indicated that the main component present in Fe-FER-IMP, Fe-FER-IE and Fe-FER-SSIE was isolated Fe species, dimeric Fe species and oligomeric iron oxides clusters, respectively. The active oxygen sites for the selective conversion of methane were identified by a TPR feature at 220 ℃ . This sites were s also characterised by an infrared band observed at 1872 cm^{-1} and 1892 cm^{-1} upon adsorption of NO. The correlation of the area of the unique reduction peak in the H_2-TPR profiles and the area of a band at 1892 cm^{-1} in the IR spectra of NO adsorption on the catalysts suggested that the active sites for N_2O decomposition were binuclear Fe species, and Fe-FER-SSIE contained the largest number of active Fe species among the three catalysts. The activity test showed that Fe-FER-SSIE obtained the highest N_2O decomposition at 250 ℃ but Fe-FER-IE achieved the highest N_2O conversion at elevated temperatures due to the greater likelihood of transformation from active oxygen species to oxygen molecules over Fe-FER-IE. Selectivity to desired products (methanol, formaldehyde, DME and ethylene) over Fe-FER-IMP, Fe-FER-IE and Fe-FER-SSIE was 12.5%, 16.5% and 19.8% (coke took into account), respectively.

Formation of active oxygen species from N_2O over Fe-FER catalyst prepared by SSIE method at moderate temperatures was studied using spectroscopic

and solid characterisation techniques including H_2-TPR, N_2O-TPD and *in situ* FTIR. These bands observed at 1872 cm^{-1} and 1892 cm^{-1} in IR spectra of NO adsorption on catalyst were NO stretching vibrations of NO adsorbed on iron oxygen clusters, present in the zeolite cages and responsible for selective oxidation. It was shown that these oxidised clusters reacted with methane to form oxygenates but at higher temperatures formed molecular oxygen. IR Bands of surface methoxy groups were observed in significant concentration in the FTIR spectra and were suggested to be intermediate species of the selective oxidation of methane. Studies using continuous reactor demonstrated that co-feeding of methane and N_2O promoted generation of desired products from methane conversion by N_2O over Fe-FER catalyst can be enhanced by optimizing the feed ratio of CH_4/N_2O.

LIST OF PUBLICATIONS

Peer-reviewed Journal Articles

Guangyu Zhao, Emad Benhelal, Adesoji Adesina, Eric Kennedy, Michael Stockenhuber. Comparison of Direct, Selective Oxidation of Methane by N_2O over Fe-ZSM-5, Fe-Beta and Fe-FER Catalysts. J. Phys. Chem. C 2019, 123, 45, 27436-27447.

Guangyu Zhao, Matthew Drewery, Eric Kennedy, Michael Stockenhuber. Catalysed Conversion of Methane to Value Added Products. Energy Technology (doi: 10.1002/ente.201900665).

Guangyu Zhao, Adesoji Adesina, Eric Kennedy, Michael Stockenhuber. Formation of Surface Oxygen Species and the Conversion of Methane to Value Added Products with N_2O as Oxidant over Fe-FER Catalysts. ACS Catal. 2020, 10, 1406−1416.

Guangyu Zhao, Eleanor Kearns, Eric Kennedy, Deanna D'Alessandro, Michael Stockenhuber. Direct Methane Conversion to Value added Products at Moderate Temperature by N_2O over Fe-FER Catalysts Prepared by Different Methods. (In preparation).

Conference papers

Guangyu Zhao, Eric Kennedy, Michael Stockenhuber. Direct Conversion of Methane to Oxygenates over Fe-ZSM-5 Catalyst at Relatively Low

Temperature. 9th International Conference on Environmental Catalysis, 10th-13th July 2016, Newcastle, Australia.

Guangyu Zhao, Eric Kennedy, Michael Stockenhuber. Methane Oxidation to Value-Added Products over Fe-Beta Catalysts. 13th European Congress on Catalysis, 27th-31th August 2017, Florence, Italy.

Guangyu Zhao, Eric Kennedy, Michael Stockenhuber. Direct Conversion of Methane to Value-Added Products over Fe-based Catalysts at Medium Temperature. 18th International Symposium on Relations between Homogeneous and Heterogeneous Catalysis, 22th-25th July 2018, Sydney, Australia.

Guangyu Zhao, Eric Kennedy, Michael Stockenhuber, Adesoji A. Adesina, Meng Jung Li, Direct Methane Conversion to Value-Added Products over Fe-FER Catalysts. 12th Natural Gas Conversion Symposium, 2th-6th June 2019, Texas, USA.

Guangyu Zhao, Eric Kennedy, Michael Stockenhuber. Mechanism of Methane Conversion over Fe-FER Catalyst Using N_2O at 350°C. 19th International Zeolite Conference, 7th-12 July 2019, Perth, Australia.

TABLE OF CONTENTS

LIST OF FIGURES

LIST OF TABLES

CHAPTER 1

1 INTRODUCTION

1.1 Research background

Natural gas, of which methane makes up typically 95% is one of the most important fossil fuels [1, 2]. Natural gas has been increasingly widely used for power generation and heating for domestic and industry use in the past decades, because natural gas with abundant reserves (which are still rapidly increasing) is considered a “cleaner” fuel than coal and oil [1, 3-6].

Over 60% of worldwide natural gas consumption was used for electricity and heat generation [1], and it is known that the combustion of methane more than 35% of the exergy is lost due to engineering restrictions [7]. In addition, natural gas is currently transported using gas pipelines which adds significant costs to its use because natural gas is normally located in remote areas [8]. Therefore, it would be beneficial to convert natural gas to more easily transportable liquid products from the viewpoint that the abundant natural gas resource will play an important role in easing a petroleum shortage in the future [9].

On the other hand, methane indeed is an excellent feedstock and has been used to produce fuels and chemicals via various routes as shown in Figure 1.1. Current commercial applications of methane for this purpose is still quite limited, mainly focusing on synthesis gas generation via steam reforming [3, 10, 11].

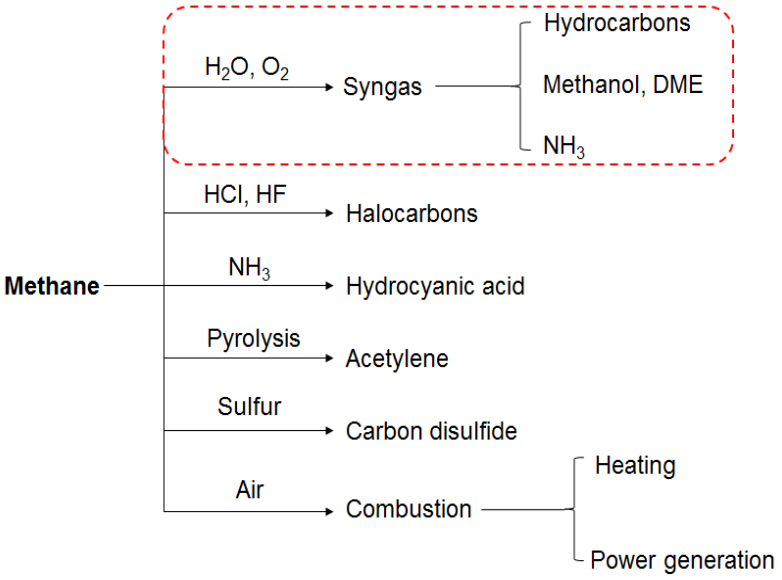

Figure 1.1. Methane conversion in developing process technologies

Currently, many important products can be generated from synthesis gas including methanol, ammonia and synthetic fuels [3]. These processes have been implemented on a large industrial scale, and are environmentally valued because they avoid generating various pollutants associated when coal is used as input carbonaceous feed [12]. However, these technologies are generally regarded as expedient strategies because the products are not generated directly from methane, but via synthesis gas which is produced by an energy-intensive reforming process [7]. It has been reported that the generation of synthesis gas by methane reforming consumed 60% or even more of the capital of Gas to Liquid (GTL) plants [3].

To reduce energy consumption during methane conversion, there has been an extensive research effort made to develop methods for direct conversion of methane when used to produce valuable products. Among the desired products of direct methane conversion, methanol and formaldehyde are among the most valuable raw materials in the chemical industry [13]. The

production methods of methanol and formaldehyde from methane currently involve multi-step processes which include the relatively high energy consumption steam reforming steps [13-15]:

$$CH_4 + H_2O \rightarrow CO + H_2 \quad (1)$$

$$CO + H_2 \rightarrow CH_3OH \quad (2)$$

$$2CH_3OH + O_2 \rightarrow 2CH_2O + 2H_2O \quad (3)$$

Therefore, direct conversion of methane to methanol and formaldehyde provides an attractive methanol and formaldehyde producing technology. In addition, direct methane conversion, in the scope of changing the raw material base, would invoke an attractive, efficient and sustainable utilization approach for natural gas resources, and reducing net greenhouse gas emissions since natural gas is known as a “cleaner” resource. To date, there are many examples of catalytic methane conversion which have been tested, but these processes suffer from drawbacks of unsatisfactory selectivity, hash reaction conditions and complicated operating procedures.

Initially, processes developed for the generation of methanol via direct the partial oxidation of methane were conducted at relatively high temperatures (normally in excess of 500 °C), which usually lead to complete oxidation of methane and poor selectivity to desired products [16]. The approach to develop the partial oxidation of methane at low temperature (lower than 200 °C) was developed based on the formation of a reactive “α”-oxygen species which were formed over the combination of Fe-ZSM-5 and N_2O, and exhibited good selectivity favouring methanol production [17], although an additional extraction

procedure is needed for obtaining methanol at such conditions, and this is not a common catalytic reaction.

Recently, there have been intriguing studies of the partial oxidation of methane at moderate temperature (from 200 ℃ to 400 ℃), in an effort to minimise the complete combustion of methane and eliminate the extraction procedure, and based on the conversion of methane by α-oxygen species at moderate temperature over Fe-ZSM-5 catalysts [18-20]. Notwithstanding relatively low yield of methanol observed, these studies have broken new ground and provide an inspiring and exciting results involving the selective, partial oxidation of methane by unique oxidation species at moderate temperatures.

1.2 Objectives of the research

The current project aims to develop a laboratory scale process for catalytic partial methane oxidation to methanol and derivatives by N_2O as oxidant over Fe-based catalysts in a continuous mode of operation at moderate temperatures. The strategies for optimizing catalytic performance in terms of methane conversion and desired products selectivity were explored by investigating the effect of reaction temperature, iron loading, feed gas composition and zeolite structure. Mechanisms involved in the catalytic partial oxidation of methane were studied using spectroscopic and solid characterisation tools including temperature programed reduction (TPR), Fourier transform infrared spectroscopy (*in situ* FTIR), N_2 gas adsorption, CO chemisorption and Thermal gravimetric analyses (TGA) to analyze the nature of active sites which remains to be a controversial issue. Formation and

dissociation of surface oxygen species generated from N_2O over solid catalysts at moderate temperatures were studied for obtaining deep insight of utilization of the surface oxygen species for partial oxidation of methane to value added products at elevated temperatures. To reach the above objects, following activities should be completed:

1. Investigating the effect of reaction conditions (reaction temperature, metal loading amount and feed gas composition) on catalytic performance of catalysts.
2. Examining Fe incorporated on various zeolites for catalytic partial oxidation of methane to methoxy groups and methanol.
3. Comparing the catalytic performance of catalysts prepared by different methods which are associated with various Fe species compositions.
4. Monitoring the N_2O decomposition products and formation of surface oxygen species over solid catalyst at moderate temperatures.
5. Employing characterization techniques such as *in situ* FTIR, H_2-TPR, N_2O-TPD, N_2-adsorption, TGA, Powder X-ray diffraction (XRD), Scanning electron microscope (SEM) to obtain deep understanding of the role of Fe species in catalytic partial oxidation of methane.

1.3 Thesis structure

The thesis comprises eight chapters in total, a brief outline of the chapters are:

Chapter 1: Introduction.

The chapter described the current approaches of methane consumption, and provided an overview of the potential routes of methane utilization under the

background of severe energy and chemical demands. The processes for direct methane conversion to value-added products were briefly discussed in terms of significance, current progress and remaining issues.

Chapter 2: Literature review.

The chapter presented a literature review of previous publications regarding direct methane oxidation technological options for various value-added products. In particular, the progress of study on direct methane conversion to methanol at low temperature was provided with the details of catalytic performance and proposed mechanisms. Followed by the introduction of latest attempts of direct methane conversion at moderate temperatures.

Chapter 3: Materials and experimental methodologies.

Preparation methods of catalysts employed in this work were described. Details on activity tests and characterization techniques were provided with all the reactants, experimental equipment and operating conditions.

Chapter 4: Direct methane conversion using N_2O over Fe-ZSM-5 to value added products.

Effect of temperature, iron loading on the catalysts, feed gas composition and GHSV on methane conversion, N_2O decomposition and products selectivity was investigated, to examine the feasibility of methane partial oxidation at moderate temperatures, and to estimate the appropriate reaction conditions for the process.

Chapter 5: Comparison of direct, selective oxidation of methane by N_2O over Fe-ZSM-5, Fe-Beta and Fe-FER catalysts.

In this chapter, the activity of Fe-ZSM-5, Fe-Beta and Fe-FER was studied through combination of catalyst characterization and catalytic activity to explore the reasons that led to different selectivities to products. N_2-adsorption, CO-chemisorption, ICP, H_2-TPR, *in situ* FTIR and TGA-MS were employed to reveal the active sites and the formation of intermediates.

Chapter 6: Direct methane conversion to value-added products by N_2O over Fe-FER catalysts prepared by different Methods.

Incipient wetness impregnation (IMP), aqueous ion exchange (IE) and solid state ion exchange (SSIE) methods were used to load 0.5wt% iron on FER zeolite to make Fe-FER catalysts. This chapter contributed to determining the number and the nature of the active sites for N_2O conversion and methanol formation over Fe-FER catalysts, to reveal the relation between catalytic activity and nature of the Fe species over Fe-FER catalysts.

Chapter 7: Formation of surface oxygen species and the conversion of methane to value-added products with N_2O as oxidant over Fe-FER Catalysts.

Formation and stability of surface oxygen species over Fe-FER catalyst prepared by solid state ion exchange method over a temperature range of 250 °C to 350 °C were studied through application of characterization techniques including N_2O-TPD and H_2-TPR, and catalyst activity trials were conducted in batch mode using an *in situ* FTIR and continuous mode in a fix-bed stainless steel tube reactor. Optimization aimed at maximising products yield was undertaken by controlling the ratio of CH_4/N_2O in the feed gas.

Chapter 8: Conclusion and recommendations.

The key findings of this study were listed and suggestions for future work were provided.

1.4 Reference

1. Neumann, C.; von Hirschhausen, C. Natural Gas: An Overview of a Lower-Carbon Transformation Fuel. *Rev. Environ. Econ. Policy* **2015,** *9*, 64-84.
2. Maggio, G.; Cacciola, G. When will oil, natural gas, and coal peak? *Fuel* **2012,** *98*, 111-123.
3. Holmen, A. Direct conversion of methane to fuels and chemicals. *Catal. Today* **2009,** *142*, 2-8.
4. Holz, F.; Richter, P.M.; Eggingy, R. A Global Perspective on the Future of Natural Gas: Resources, Trade, and Climate Constraints. *Rev. Environ. Econ. Policy* **2015,** *9*, 85-106.
5. Gradass, M.J.; Green, N.W. Economics of natural gas conversion processes. *Fuel Process. Technol.* **1995,** *42*, 65-83.
6. Lunsford, J.H. Catalytic conversion of methane to more useful chemicals and fuels. *Catal. Today* **2000,** *63*, 165–174.
7. Heyden, A.; Peters, B.; Bell, A.T.; Keil, F.J. Comprehensive DFT Study of Nitrous Oxide Decomposition over Fe-ZSM-5. *J. Phys. Chem. B* **2005,** *109*, 1857-1873.
8. Knops-Gerrits, P.P.; Goddard, W.A. Oxidation hydroxylation using dinitrogen monoxide a possible route for organic synthesis. *J. Mol. Catal. A Chem.* **2001**, *166*, 135-145
9. Jia, J. One-step oxidation of benzene to phenol with nitrous oxide over Fe/MFI catalysts. *J. Catal.* **2004,** *221*, 119-126.

10. Taylor, S.H.; Hargreaves, J.S.J.; Hutchings, G.J.; Joyner, R.W.; Lembacher, C.W. The partial oxidation of methane to methanol: An approach to catalyst design. *Catal. Today*, **1998**, *42*, 217-224.
11. Xu, J.; Zheng, A.; Wang, X.; Qi, G.; Su, J.; Du, J.; Gan, Z.; Wu, J.; Wang, W.; Deng, F. Room temperature activation of methane over Zn modified H-ZSM-5 zeolites: Insight from solid-state NMR and theoretical calculations. *Chem. Sci.* **2012,** *3*, 2932.
12. Bjørn, C.E.; Lødeng, R.; Holmen, A. A review of catalytic partial oxidation of methane to synthesis gas with emphasis on reaction mechanisms over transition metal catalysts. *Appl. Catal. A: Gen.* **2008,** *346*, 1-27.
13. Ravi, M.; Ranocchiari, M.; van Bokhoven, J.A. The direct catalytic oxidation of methane to methanol—A critical assessment. *Angew. Chem., Int. Ed.* **2017**, *56*, 16464-16483.
14. Zhang, Q.; He, D.; Zhu, Q. Recent Progress in Direct Partial Oxidation of Methane to Methanol. *J. Nat. Gas Chem.* **2003,** *12*, 81-89.
15. Groothaert, M.H.; Smeets, P.J.; Sels, B.F.; Jacobs, P.A.; Schoonheydt, R.A. Selective Oxidation of Methane by the Bis(í-oxo)dicopper Core Stabilized on. *J. Am. Chem. Soc.*, **2005**, *127*,1394–1395
16. Wang, B.; Albarracín-Suazo, S.; Pagán-Torres, Y.; Nikolla, E. Advances in methane conversion processes. *Catal. Today*, **2017**, *285*, 147-158.
17. Zakaria, Z.; Kamarudin, S.K. Direct conversion technologies of methane to methanol: an overview. *Renew. Sustain. Energy Rev.* **2016**, *65*, 250-261.
18. Kameoka, S.; Nobukawa, T.; Tanaka, S. I.; Ito, S. I.; Tomishige, K.; Kunimori, K. Reaction between N_2O and CH_4 over Fe ion-exchanged BEA

zeolite catalyst: A possible role of nascent oxygen transients from N_2O. *Phys. Chem. Chem. Phys.* **2003,** *5*, 3328-3333.

19. Parfenov, M. V.; Starokon, E. V.; Pirutko, L. V.; Panov, G. I. Quasicatalytic and Catalytic Oxidation of Methane to Methanol by Nitrous Oxide over FeZSM-5 Zeolite. *J. Catal.* **2014**, *318*, 14-21.
20. Chow, Y. K.; Dummer, N. F.; Carter, J. H.; Meyer, R. J.; Armstrong, R. D.; Williams, C.; Shaw, G.; Yacob, S.; Bhasin, M. M.; Willock, D. J. *et al.* A Kinetic study of methane partial oxidation over Fe-ZSM-5 using N_2O as an oxidant. *ChemPhysChem* **2018**, *19*, 402-411.

CHAPTER 2

2 LITERATURE REVIEW

2.1 Introduction

Research into methane valorisation has garnered significant interest due to the abundance of natural gas and the unique properties of methane, which is recognised as a potential substitute for crude oil and a raw material for the synthesis of a variety of chemical compounds [1-2]. Methane conversion can proceed via both direct and indirect routes, with the latter associated with production of syngas (CO and H_2) via methane steam reforming (Equation 1) and dry reforming (Equation 2), and the formation of value-added product from syngas (Equation 3) [3-5]:

$$CH_4 + H_2O \rightarrow CO + 3H_2 \quad (1)$$

$$CH_4 + CO_2 \rightarrow 2CO + 2H_2 \quad (2)$$

$$CO + 2H_2 \leftrightarrow CH_3OH \quad (3)$$

These reactions are usually catalysed by transition metals, such as nickel, which is the most commonly utilised industrial catalyst owing to its high activity and low capital cost [6]. Conversely, indirect methods of methane conversion are considered complicated and costly as these are energy-intensive processes [7], making direct conversion, which avoids synthesis gas production, an attractive alternative.

There are a significant number of studies which focus on practical catalysts, which are optimised for conditions and reactions favouring direct methane conversion, including oxidative coupling of methane for C_{2+} carbon species, non-oxidative conversion of methane to aromatics and partial oxidation of methane to methanol [7-12]. This study focuses on direct methane conversion to methanol as methanol is an important solvent and precursor for the formation of a large number of chemicals [6].

The process of direct methane conversion to methanol has been extensively studied for both homogenous and heterogeneous catalytic processes with temperatures ranging from 25 ℃ to 600 ℃ and pressures from 1 bar to 50 bar [8, 11, 13-18]. Heterogeneous processes are of particular interest due to the ease of catalyst separation and typically consist of noble or transition metals on different supports such as Al_2O_3, SiO_2 and zeolitic materials [16, 19-22].

In spite of the clear economic and environmental benefit for a direct process for the conversion of methane to methanol, there have been no breakthroughs in either heterogeneous or homogenous catalysis and more recent studies are unable to be applied to industrial processes to compete with indirect methanol production due to low oxygenate yields [7, 23-24]. This has been attributed to the high stability of C-H bonds in methane which makes conversion thermodynamically unfavourable [25]. In addition, methane is generally less active than its conversion products as shown in Table 2.1, with reaction products likely to undergo further oxidation to generate carbon monoxide, carbon dioxide and water, resulting in poor selectivity [26-28]. Therefore, in recent years the attention being paid to direct methane conversion to methanol is mainly focusing on exploration of the use of novel oxidants in various techniques and prevention of deep oxidation of methanol using optimized reaction conditions [29-32].

Table 2.1 Molecule bond dissociation energies

Chemicals	C-H Bond Energy [kcal.mol^{-1}]
CH_3-H	104.99 ± 0.03
H-CH_2OH	96.1 ± 0.2
CH_3O-H	104.6 ± 0.7
H-CHO	88.144 ± 0.008

The processes for direct methane conversion to methanol have been previously reviewed by categorizing as homogenous reaction and heterogeneous reaction and the performance of various processes in terms of methane conversion and methanol selectivity was discussed [33]. In this work, we review progress in this area as an evolution of techniques pursuing greater active oxidative species. Studies on direct methane conversion to methanol were initially established with high-temperature processes where lattice oxygen species are used to active methane [34], followed by emergence of processes conducting under mild conditions as consequence of the successful development of more active oxidative species via different approaches [30-32]. The latter processes are becoming increasingly more attractive as these active oxidative species allow operation of methane conversion at low temperature which is beneficial for methanol selectivity [35]. The progress in catalytic partial oxidation of methane to methanol is accordingly described, and the active sites that are responsible for forming powerful oxidative species to convert methane over solid catalysts at mild conditions are extensively discussed, to provide a comprehensive sight for better understanding.

2.2 Catalysis

Catalysis, as a phenomenon, was firstly utilized in the production of mining lamp in early 19th century [36]. The followed establish and significant progress in kinetics and advent of characterization techniques opened the opportunity of study of catalysis, which consequently became a scientific discipline to study the relation between catalytic performance and the properties of catalysts experimentally and theoretically in 21st century. To date, the

catalysts are responsible to over 80% of the products in modern chemical industry and hence are believed to be the workhorse in the fields of fine chemicals, fuels and pharmaceuticals [36].

A catalyst is a material that accelerates the rate of a chemical reaction, in which the catalyst participates but recovers in its initial form at the end of a reaction cycle. The catalyst does so by providing an alternative approach that associates with much lower activation energy than that required to be overcome in a non-catalytic way [37].

Fig. 2.1 showed a simplified representation of the potential energy diagram of non-catalytic and catalytic reactions. In the non-catalytic route, energy is required for the reactants A and B to overcome the barrier to reach the intermediate state, and then to form products C. Conversely, in the catalytic route, the reactants A and B bind to the catalyst, where the reaction between A and B occurs and forms product C. Finally, the product separates from the catalyst in an endothermic step. In the latter route, the activity energy is associated as well but much lower than that in the non-catalytic route as shown in Fig. 2.1 [38].

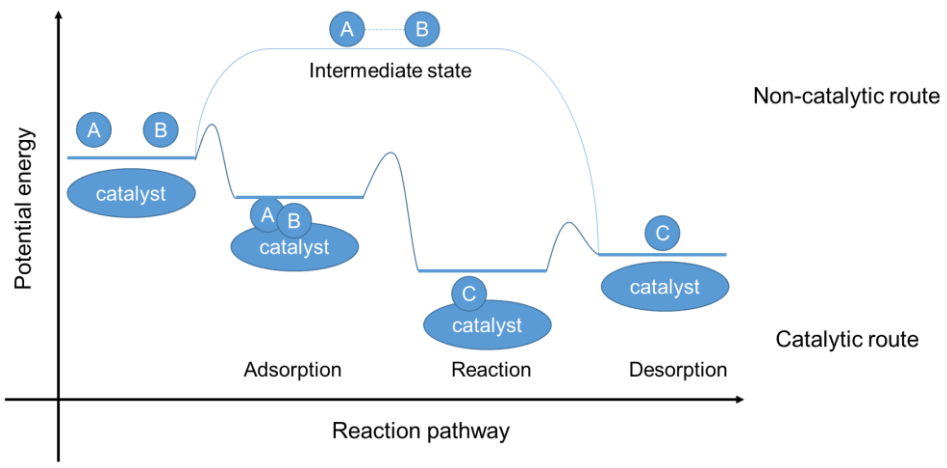

Figure 2.1 Potential energy diagram for non-catalytic and catalytic reactions [38]

Therefore, the application of catalysts provides a more complex but energetically favorable path, and enhances the rate of the chemical reaction. In the case of methane conversion, a variety of catalysts have been utilized to convert methane to ethylene, aromatics, methanol and formaldehyde as presented in previous studies [7, 12, 17, 39].

The catalysis consists of three subdisciplines which are homogeneous catalysis, heterogeneous catalysis and bio catalysis. Homogeneous and heterogeneous catalysis are the primary processes for the purpose of methane conversion to value products [8, 11, 13-14, 17-18]. Relative studies especially the heterogeneous catalytic oxidation of methane will be reviewed.

2.3 Direct, catalytic methane conversion routes

Currently, indirect process for transform methane to desired products via syngas has been applied in large scale industry for multitude products [40-41]. However, the production of syngas is an energy-intensive process [24]. There have been several direct methane conversion approaches developed aiming to utilize methane in an economic and sustainable way, such as methane non-oxidative aromatization to aromatics, oxidative coupling of methane to ethylene and ethane, and partial oxidation of methane to methanol.

2.3.1 Methane non-oxidative aromatization

The non-oxidative conversion of methane to aromatics was first reported in 90's in the 20th century, Mo-ZSM-5 catalyst was firstly used to convert methane to benzene which was shown to be the only hydrocarbon product at

high temperature (over 700 °C) [9]. The result inspired studies in this field, and thereafter researchers reported that non-cyclic hydrocarbons were observed as well from methane non-oxidative conversion [12, 42].

Literature reported that the loading of Mo particles would modified the acid sites on ZSM-5 zeolites by changing the OH groups [5]. The Mo oxides stay or diffuse into the channels of and form distinct active sites such as Mo_{6c}^{6+} and Mo_{5c}^{5+} and MoO_xC_y [43], with the concentration of Mo exhibiting strong impact on catalytic activity. It was noted that the loading above 16% would lead to marked decline in both methane conversion and aromatics selectivity [44].

Porosity would affect the catalytic performance of non-oxidative methane conversion as well. The Mo-ZSM-5 was modified by using mesoporous H-ZSM-5, and was demonstrated to be more active than the conventional Mo-ZSM-5 catalysts [45]. It was determined that the catalyst could be modified to enhance the activity and stability via the introduction of a second metal, such as Cu, Co, Ni, Fe or Pt [44, 46-48].

Loading the active metals on different zeolitic supports has also been investigated, with MCM-22 shown as another potential catalyst, exhibiting higher methane conversion and aromatic selectivity compared to Mo/ZSM-5 with the same metal loading [6].

Although research into non-oxidative aromatization has progressed significantly, there are still a number of issues which need to be addressed. There are a number of active sites which could be responsible for the activation of methane and current research has been unable to clearly identify which is more catalytically effective [12].

2.3.2 Oxidative coupling of methane

The oxidative coupling of methane (OCM) is the process that makes methane react with oxygen in the presence of catalysts to generate longer chain carbonaceous species, such as ethane or ethylene [6, 49]. Ethylene is considered as an important platform chemical for petrochemical products, thus its production via OCM is considered a potential process for the utilisation of methane [50]. Early research reports that ethylene was formed via methane oxidation over metal oxides on α-alumina at temperatures above 500 ℃ [51], with the active sires believed to be the reactive surface oxygen species. It is hypothesised that the reaction begins with the removal of hydrogen from the methane via these reactive oxygen species, leading to the generation of methyl free radicals, followed by the formation of ethane by the coupling of the radicals before dehydrogenation producing ethylene [39].

$$4CH_4 + O_2 \rightarrow 2CH_3CH_3 + 2H_2O \quad (4)$$

$$2CH_3CH_3 + O_2 \rightarrow 2CH_2CH_2 + 2H_2O \quad (5)$$

A number of catalysts have been developed for OCM, with metal oxides such as Li/MgO, SrO/La_2O_3 and $Mn/Na_2WO_4/SiO_2$ producing some of the best results, with C_2 yields from 16-19% [52-53]. It was noted that in addition to producing ethylene, undesired side reactions forming carbon monoxide and carbon dioxide significantly limit selectivity to ethylene, particularly for high methane conversions [54]. Theoretical studies have suggested that a compromise between the activation energy of C-H bonds and CH_3* adsorption must be made to enhance catalyst performing, predicting a maximum ethylene yield of 30% [55].

$$2CH_4 + 3O_2 \rightarrow 2CO + 4H_2O \quad (6)$$

$$CH_4 + 2O_2 \rightarrow CO + 2H_2O \quad (7)$$

In an attempt to overcome the limitations identified in the OCM process with molecular oxygen oxidant, a membrane reactor was developed. In this experiment, oxygen ions produced on one side of the membrane diffuse to the other where methane was fed for the OCM reaction [56]. It was reported that controlling the partial pressure of oxygen in the reactor can be used to enhance both methane conversion and ethylene selectivity [57]. The processes examined for OCM are not currently commercially viable due to the generation of carbon monoxide and dioxide being thermodynamically favoured at the conditions required [56].

2.3.3 Direct oxidation of methane to methanol

Methanol is an important feedstock for chemical and petrochemical industries, playing a major role in the energy economy [7, 58], and making direct routes from methane an appealing process. Research towards this has been extensively conducted; developing catalysts, optimising reaction conditions and clarifying mechanisms, however the process needs further development for industrial applications [24]. The challenge is that methane is a very stable molecule, which makes the conversion of methane to value added products thermodynamically unfavourable [25], as methane is generally more inactive than its conversion productions, and hence the products would undergo further oxidation to generate CO, CO_2 and H_2O, resulting in poor selectivity [26]. Processes for catalytic partial oxidation of methane conducted under mild conditions exhibit remarkable selectivity to methanol, however the processes are suffered with low conversion amount of methane or high cost brought by addition of reactant

(H_2O_2) [30-32]. Therefore more effort is expected for achieving high yield of desired products with reasonable economic cost.

2.4 Direct methane conversion to methanol at high temperatures

Economic optimisation is a key challenge for a direct methane conversion process to compete with current commercial processes. Oxygen, typically in the form of air, is the most popular oxidant as it is the most economically viable co-reactant for potential partial oxidation of methane in large scale applications [59]. The processes with oxygen as oxidant are normally conducted at high temperature (above 450 ℃) as strong energy is required to break the O=O bonds and form surface oxygen species [60-61].

2.4.1 Catalytic partial oxidation of methane by oxygen at atmospheric pressure

A variety of solid catalysts have been implemented in an attempt to produce methanol at atmospheric pressure, both with and without metal loading, among the most widely used catalysts. The performance of these catalysts are present in Table 2.2.

Methane conversion lower than 4.8% with formaldehyde selectivity less than 50% was obtained over SiO_2 [13, 34, 62], but no methanol was observed. SiO_2 incorporated with MoO_3, V_2O_5, W and Fe was investigated at a temperature range of 450 ℃ to 650 ℃ , formaldehyde yield less than 5% was reported [13, 63-66]. Catalytic partial oxidation of methane over MoSnP/SiO_2 catalyst was conducted, obtaining a maximum formaldehyde selectivity of 64.8% with methane conversion of 7.2% [67]. VO_x/MCM-41 catalyst was examined over 595 ℃ , with conversion less than 11% and formaldehyde selectivity less than

30% [68-69]. Catalytic partial oxidation of methane over VO_x/SBA-15 in a temperature range of 540 ℃ to 650 ℃ exhibited methane conversion less than 1.1 % with formaldehyde selectivity lower than 60% [70]. It is noteworthy that the formaldehyde was the sole C_1-oxygenate produced from the above studies and the methanol selectivity was ignorable.

Methanol was successfully produced using MoO_3/SiO_2 prepared by sol/gel method with the addition of an excess of water vapour in the feed at a temperature range of 500 ℃ to 650 ℃ , with conversion up to 12% and methanol selectivity less than 13%. It was hypothesised that the formation of silico-molybdic acid over the silica surface was the critical compound to improve methanol selectivity [71]. V_2O_5-SiO_2 xerogels was reported to convert up to 4.9% of methane with methanol selectivity less than 20% and formaldehyde selectivity up to 56% at a temperature range of 550 ℃ to 650 ℃ [72]. Partial oxidation of methane by oxygen over Fe-ZSM-5 with different Si/Fe ratios at 630 ℃ exhibited methane conversion up to 31.5% with methanol selectivity less than 17% [73]. In addition, a special prepared SiO_2@$V2O_5$@Al_2O_3 catalyst by atomic layer deposition exhibited methane conversion of 22.2% with formaldehyde selectivity of 57.8% [74].

Table 2.2 Methane conversion and C_1-oxygenates selectivity over various solid catalysts

Material	T (℃)	CH_4 conversion (%)	HCHO selectivity (%)	CH_3OH selectivity (%)	Ref.
SiO_2	580-620	1.4-4.8	24-48	0	62
	650	5.2	18.7	0	13
	610	ca. 3.7	ca. 13	0	34
	625	0.3	45.0	7.8	72
W/ SiO_2	650	3.3	14.5	0	13

	610	ca. 5.2	ca. 24.0	0	[34]
[a]MoO_3/SiO_2	500-650	0.58-6.6	1.0-32.0	0-2.0	[63]
	575-625	ca. 0.1-5.3	ca. 30.0-83.0	0	[64]
$Mo/P/SiO_2$	675	7.2	64.8	0	[67]
V_2O_5/SiO_2	550-600	1.0-5.1	6.0-45.0	0	[65]
	590	0.9	41.0	0	[66]
	610	ca. 13.0	ca. 10.0	0	[34]
	500-550	ca. 0.1-6.0	ca. 8.0-84.0	0	[64]
VO_x/MCM-41	595-656	3.0-11.0	8.4-29.1	0	[68]
	575-625	ca. 4.6-5.8	ca. 24.0-20.0	0	[69]
VO_x/SBA-15	540-650	ca. 0.2-1.1	ca. 35.0-60.0	0	[70]
[b]MoO_3/SiO_2	500-650	1.0-12.0	11.0-73.0	4.0-13.0	[71]
V_2O_5/SiO_2	550-650	0.3-4.9	7.1-56.0	4.3-19.7	[72]
Fe-HZSM-5	630	31.5	17.1	10.8	[73]
SiO_2@V2O_5 @Al_2O_3	600	22.2	57.8	0	[74]

a. prepared by impregnation method

b. prepared by sol/gel method

It was reported that elevated temperatures (generally in excess of 500 ℃) are required for methane activation by surface oxygen species derived from the dissociative adsorption of gaseous oxygen or diffusion from the bulk lattice of $Fe_2(MoO_3)_4$, generating methyl or methoxide species [1]. The surface oxygen species were further suggested to be doubly bonded lattice oxygen (M=O) [75], or bridging lattice oxygen (M-O-M) [76]. At such temperature, the formed methyl or methoxide species would be further oxidized to formaldehyde or carbon monoxide and dioxide [61, 77], which is the reason of low selectivity to methanol observed in the previous studies. It has been reported that minimising reactant contact time with the catalyst increases formaldehyde and C_2 products, but inevitably leads to lower methane conversion [78].

2.4.2 Strategies to enhance catalytic performance

Catalytic partial oxidation of methane over solid catalysts at temperature above 450 ℃ exhibited methane conversion less than 35% with C_1-oxygenates (formaldehyde is the main product) yield less than 15% as shown in Table 2.2. Researchers proposed multiple strategies to enhance methane conversion and C_1-oxygenates selectivity, as summarized in Table 2.3.

Table 2.3 Strategies to enhance catalytic performance

Strategy	Effect	Reason of enhancement	Ref.
Conducting reaction at high pressure	Enhances methanol formation (methanol becomes the main product instead of formaldehyde)	Increasing partial oxygen pressure is beneficial for methanol formation	79-82
NO_x addition	Enhances methane conversion	Energy for methane activation is reduced with presence of NO_x	14, 83-88
Using inert reactor (quartz reactors)	Enhances methanol selectivity	Inert reactor increases the rate of free radical chain termination reactions	89
Addition of higher molecular weight carbon	Enhances methane conversion	These carbons act as a trigger to provide free radicals	79
Using recycle reactor	Enhances C_1-oxygenates production	Recycle the flow rate	40
Vapor addition	Enhances methanol production	Vapor is beneficial for formation of silicomolybdic acid on MoO_3/SiO_2	63

2.4.2.1 Catalytic partial oxidation of methane by oxygen at high pressure

Significant research has focussed on high pressure reactions for improving methanol selectivity [79-82]. It was reported that under elevated pressures (20 bar to 125 bar) and temperatures (400 ℃ to 480 ℃), methanol was formed in a homogeneous reaction with selectivity exceeded 80% however methane conversion was less than 8% [79]. Partial oxidation of methane over active iron oxo centres was investigated at pressures of 50 bar and 430 ℃ , achieving 5.8% methane conversion with methanol selectivity of 25% [80]. The study on catalytic partial oxidation of methane over MoO_x/la-C-O at 420 ℃ reported maximum methanol selectivity of 60.0% with methane conversion of 11.2% under 42 bar [82].

It has been stated that the presence of solid do not improve methane conversion under high pressure [26], thus the possibility of producing a high yield is controlled by gas phase, radial reactions, as verified by both experimental and theoretical results [90]. It was theorised that the homogenous reaction of gaseous methane with oxygen is a degenerate, chain branching reaction [91]. In this, methane is first attacked by molecular oxygen at high temperature (450 ℃ to 650 ℃) to generate radicals (CH_3*), which then reacts further with oxygen producing CH_3COO* radicals, which is dependent on temperature, pressure and oxygen pressure. Methanol can then be formed with this radical reacting with either another CH_3COO* or CH_4 [7, 91]. The formation of the methyl radicals from the cleavage of C-H bonds is believed to be the rate-limiting step according to thermodynamic and kinetic analysis [92]. The optimum conditions for maximising yield were determined with

pressures between 30 bar to 60 bar and temperatures from 450 ℃ to 500 ℃ yielding 40% methanol with 10% conversion [81]. The yield of C_1-oxygenates from partial oxidation of methane without solid catalysts was still low for industrial applications. In addition to this, the high pressures employed would result in high costs, limiting industrial implementation [24].

2.4.2.2 Enhancement effect of nitrogen oxides on direct methane conversion

The enhancement effect of NO_2 on partial oxidation of methane by O_2 was first demonstrated in 1934 [83], and was later confirmed by followed research [84]. Further research reported methane conversion was 1.0% at 693 ℃ in CH_4-O_2 reaction, but methane conversion reached 10.0% at 535 ℃ with addition of 0.25% of NO [85]. In addition, it was reported that the addition of small amounts of NO could dramatically improve the production of C_1-oxygenates, and selectivity to methanol reached to a maximum with 0.5% of NO and decreased as further increase of NO concentration [85]. NO_2 was also found to effect both methane conversion and selectivity to C_1-oxygenates, methane conversion was less than 2% with 0.125% of NO_2 at 520 ℃ , but increased to ca. 35% with 0.75% of NO_2, and selectivity to methanol increased from ca. 11% to ca. 27% with NO_2 concentration increased from 0.1% to 0.5% [86]. NO_x was reported to have a promoting effect on methane conversion and methanol generation as the transition barrier of hydrogen cleavage is lower than compared with O_2 [87]. It is hypothesised that the utilisation of NO_x can promote radical formation by the following reactions [85]:

$$NO + O_2 \rightarrow NO_2 \quad (8)$$

$$NO_2 + CH_4 \rightarrow CH_3^* + HNO_2 \quad (9)$$

$$CH_3^* + O_2 \rightarrow CH_3O_2^* \quad (10)$$

$$CH_3^* + NO_2 \rightarrow CH_3O^* + NO \quad (11)$$

$$CH_3O_2^* + NO \rightarrow CH_3O^* + NO_2 \quad (12)$$

In comparison to NO, it was calculated that NO_2 has a higher activity for removal of hydrogen from methane, with activation energy for NO calculated to be 65.6 kcal.mol^{-1}, but only 37.6 kcal.mol^{-1} for that of NO_2 [87], which was verified experimentally by followed study [86]. Additionally, the difference between the effect of NO and NO_2 on methane conversion reactions was examined, and it was believed that NO_2 was the critical component for the promotion of methane conversion. If NO_2 was not initially present in the reaction, it could be generated from NO and O_2 to promote alkane conversion [14, 88].

Partial oxidation of methane with addition of NO_x has also been examined over solid catalysts, with V_2O_5/SiO_2 obtaining oxygenate yields of 7% at atmospheric pressure [19]. Furthermore, it was demonstrated that $Cu/ZnO/Al_2O_3$ could enhance methanol selectivity in the direct oxidation of methane with O_2 and NO [93]. High pressure could lead to similar promotion of methane conversion, with the highest yield of methanol was 2.3% was obtained when the ratio of CH_4:N_2O was 8 at 0.4 MPa [94]. The promotion of methane conversion as well as selectivity to formaldehyde was observed in the presence of MoO_3 when methane was directly oxidised by O_2 and NO_2, however methanol selectivity decreased, indicating the generation of formaldehyde is attributed to the solid catalyst but the generation of methanol was a found to be a gas-phase reaction [93, 95]. Negative effects of solid catalysts in the presence of NO were observed, and it was reported that NO

could enhance formaldehyde production, but Mo/SiO_2 and V/SiO_2 decomposed the products, predicting a maximum yield of 4% [96].

2.4.2.3 Other strategies

In addition to elevated pressure and NO_x addition, other strategies for enhancing methane conversion or C_1-oxygenates selectivity have also been examined. It has been stated that reactor inertness is beneficial for methanol formation [89]. Higher molecular weight carbon chains were found to contribute to lowering the reaction temperature for activating methane, as they act to a trigger to provide free radicals. The addition of 2, 3-dimethylbutane was reported to increased methanol selectivity to 76.6% at 320 ℃ [79]. Recycle reactor was also proposed, obtaining a formaldehyde yield of 12% over SiO_2 [40]. Vapor was proved to enhance methanol production by promote formation of silicomolybdic acid on MoO_3/SiO_2 [63].

2.4.3 Discussion

As discussed above, yield of C_1-oxygenates is less than 15% over the various catalysts. In addition, the identification of active oxygen formed in above catalysts is still a matter of discussion, terminal or bridging lattice oxygen are the candidatures that are responsible for methane conversion, and both types of lattice oxygen species require high temperature to active methane [97]. At such condition the desired oxygenate products react more readily than methane, further generating CO, CO_2 and H_2O [26]. The increased temperature promotes methane conversion however decreases selectivity of desired products [63]. Studies are thus conducted to achieve low temperature catalytic

partial oxidation of methane and avoid further oxidation of intermediates and improve selectivity.

2.5 Direct methane conversion at low temperatures

2.5.1 Low temperature catalytic partial oxidation of methane in strong acids

It is theorised that catalytic partial oxidation of methane can be completed homogeneously in aqueous conditions, with initial studies examining strong acids [98]. Catalysts such as $HgSO_4$, V_2O_5, I_2 and $PtCl_2$ were investigated [29, 99-103]. $HgSO_4$ was dissolved in sulphuric acid to produce methyl bisulphate, and the selectivity reached 85% with 50% methane conversion at low temperatures before transformation [99]. A methanol yield of 45.5% with methane conversion of 54.5% was reported over V_2O_5 in oleum [100]. It was reported that $PtCl_2$ obtained methane conversions up to 90% with methyl bisulphate selectivity of 81%, identifying the better catalytic performance of Pt as a result of stability against protolytic ligand loss and irreversible reduction, preventing further oxidation of desired products [103]. Further studies on catalytic partial oxidation of methane over Pt-based catalysts in sulfuric acid/oleum reported turnover frequencies of more than 25000 h^{-1} with selectivities above 98% by using K_2PtCl_4 as catalyst, and it was conjectured that excess of Cl^- is detrimental for the catalytic activity, and variation of the surrounding ligand sphere corresponds to different catalytic properties [29, 101]. In addition, high selectivity to methyl sulphate (over 90%) was achieved with the application of I_2 in weak oleum [102].

The study of catalytic partial oxidation of methane to methanol in sulphuric acid has been expanded to include the application of metals and salts and

other acids such as trifluoroacetic acid, with the optimization of operation parameters producing higher selectivity and methanol yields [104]. However, the difficulty of separating desired liquid products from the acid, the strong corrosion and severe pollution caused by the utilization of strong acid in the system inhibit commercialisation due to increased capital costs required [92].

2.5.2 Low temperature catalytic partial oxidation of methane in hydrogen peroxide

In contrast, a known mild and controlled catalytic partial oxidation of methane was performed in an enzymatic system in methanotrophic bacteria which uses methane monooxygenase (MMO) enzymes to convert methane to methanol under ambient conditions [22]. The MMO can be particulate MMO (pMMO) which contains copper-based active sites with low concentration or soluble MMO (sMMO) with higher concentration of copper species or, more commonly, with bi-nuclear iron species [22]. These MMO enzymes capture molecular oxygen from the atmosphere to form active oxygen on active centres, where methane can be oxidised with a low activation energy [105]. The results published have led to additional research examining biomimetic strategies for methane conversion to valuable products catalytically at mild conditions. Direct methane conversion using H_2O_2 as the aqueous media was extensively explored recently [11, 30, 106-108]; a parent benefit is that H_2O_2 has significantly less environmental impact in comparison to strong acids [107].

It was reported that the combination of Fe/ZSM-5 and hydrogen peroxide could provide a low-energy pathway for catalytic partial oxidation of methane, in which methyl hydrogen peroxide was formed on the active sites as a result of the reaction between hydrogen peroxide molecules and specific Fe species

[30, 108]. Two types of Fe species were considered the active sites for methane dissociation: Fe(III)-oxo and Fe(IV)-oxo complexes, and three reaction mechanisms might be involved in the activation of methane and formation of methanol: heterolytic methane dissociation, homolytic methane dissociation, and Fenton-type reaction [106]. In addition, it was found that the addition of copper on Fe-ZSM-5 could promote methanol selectivity from less than 40% to over 80%, because copper could avoid the generation of hydroxyl radicals which are produced with the hydrolysis of a surface-bound methoxy species and facilitate the further oxidation of methanol to formic acid and CO_2 [30]. Promotion was also observed upon the incorporation of Al^{3+} and Ga^{3+} cations into the zeolite, as these species are beneficial for the formation and maintaining of extra-framework active iron sites [107].

Additionally, catalysts with other metals loading were also examined. Au-Pd/TiO_2 was demonstrated to be effective for catalytic partial oxidation of methane to methanol with hydrogen peroxide as oxidant [11]. The combination of Au and Pd exhibited better performance than Cu and Fe, with a selectivity to methanol up to 93.4% obtained when 5% Au-Pd/TiO_2 was employed at 2 ℃ . It was predicted that the formation of Au-Pd alloys contributes to the enhancement of catalytic performance, which was shown by the determination of active sites using x-ray energy dispersive spectroscopy (XEDS) analysis [11]. Despite the selectivity of methanol is enhanced with hydrogen peroxide as oxidant, the cost of hydrogen peroxide is comparably high [109]. Additionally, there are other issues including separation and recyclability of aqueous media and catalysts and disposal of waste need to be addressed prior to large scale implementation [98].

2.5.3 Low temperature, gas phase oxidation

2.5.3.1 Catalytic partial oxidation of methane over iron-based zeolites

In addition to catalytic partial oxidation of methane at low temperature in liquid phase, effort has been made toward the reaction in gas phase, however early studies were unable to generate equally active oxygen species with various oxygen donors investigated [22], until Fe/ZSM-5 was used together with N_2O as suggested by Panov [110-111]. The iron species in a ZSM-5 matrix lose their ability to activate the oxygen molecule but are able to dissociate nitrous oxides in a particular way and lead to the generation of a reactive surface oxygen, α-oxygen, which performs as a uniquely active oxidant responsible for methane conversion and C_1-oxygenates generation. The so-called α-oxygen could be readily oxidized at 200 ℃ to 250 ℃ [22, 31].

$$(Fe^{II})_\alpha + N_2O \rightarrow (Fe^{III}–O^-)_\alpha + N_2 \quad (13)$$

The generated α-oxygen then leads to the formation of methoxy and hydroxyl groups [20, 112].

$$CH_4 + (O)_\alpha \rightarrow (CH_3O)_\alpha + (OH)_\alpha \quad (14)$$

Water is required for the subsequent formation of methanol.

$$(CH_3O)_\alpha + H_2O \rightarrow CH_3OH + (OH)_\alpha \quad (15)$$

Instead of utilising oxygen, N_2O has been examined as the oxidant in this process. Although for industrial implementation this would result in higher capital cost, N_2O is an important greenhouse gas, with a greenhouse potential 300 times that of CO_2 [113]. Therefore, the reaction of methane with N_2O as the co-reactant for producing methanol is of great significance from the perspective of greenhouse gas emission control. In addition it is

recommended that the reaction is conducted at lower temperatures, reducing the costs associated with commercialisation of the process.

Catalytic partial methane oxidation by N_2O over Fe-ZSM-5 at room temperature obtained methanol concentration of ca. 20 μmol/g, with yield of over 90% [111]. Observed catalytic performance of Fe-ZSM-5 in followed studies is shown in Table 2.4.

Enhancement effect of high temperature pre-treatment on α-oxygen generation, and the activity of N_2O decomposition over Fe-ZSM-5 was investigated ,and it was reported that after high-temperature treatment activity of Fe-ZSM-5 was three times higher than after calcination [114]. Fe-ZSM-5 can be modified via the introduction of extra-framework aluminium because the concentration of α-oxygen increased linearly with the amount of introduced aluminium [115]. Introduction of H_2O was predicted to enhance the formation of methanol, based on density functional theory (DFT) calculation [116], which was experimentally proved and interpreted by the suppression of coke formation with addition of water [117]. On the other hand, inhibition of N_2O decomposition by water was observed, due to the transformation of active Fe^{2+} species to inactive hydroxylated Fe^{3+} sites in the presence of N_2O and H_2O [118-119]. Additionally, it was assumed that even in trace amounts, H_2O would affect the surface composition and increase the apparent activation barriers for N_2O decomposition on Fe sites based on DFT calculations [120-121].

Nature of the active sites that are responsible for N_2O decomposition over Fe/ZSM-5 is not yet clear due to these species are challenging to probe [122]. Panov proposed that in Fe/ZSM-5, the tetrahedral positions of the crystalline lattice were occupied by Fe^{3+} atoms, which would migrate into the micropores

of the ZSM-5 by high temperature activation, forming α-sites [123]. The Mössbauer spectra indicated that the active sites were binuclear Fe^{2+} species, which were indicated by isomer shifts of around 1.2 and 1.0 $mm.s^{-1}$ [123], which was supported by followed DFT calculation and EXAFS spectra [124-126]. However another study predicted that N_2O was decomposed over mononuclear FeO^+ sites [127], which was proved in followed studies by the combination of DFT calculations, EXAFS spectra and site-selective spectroscopic method [122, 128]. Other researchers suggested that oligo-nuclear represented the most active sites for N_2O decomposition basing on results from UV-vis and IR spectroscopy [114, 129]. A combination of spectroscopic and magnetic techniques led to a proposition of small-sized Fe_xO_y nanoparticles were the most active species for N_2O decomposition [130]. Similar propose was reported that the spinel structure of the oxide favoured the formation of Fe_3O_4 clusters, which were believed to be the active site [131]. These results provided compelling evidence that more complicated reaction mechanisms should be involved in alkane oxidation by N_2O, and the specific active sites for catalytic partial oxidation of methane have yet to be identified.

The formation process of methanol is another controversial issue. It has been proposed that methanol is formed from hydrolysis of methoxy groups via the addition of water vapour [22, 112], while other research proposed that methanol was already present as a surface-adsorbed compound to metal or zeolite lattice oxygens [132]. For both proposed pathways of methanol formation, an additional extraction procedure is required to obtain methanol at low temperature, because methanol or its precursor would generally bind on the surface of catalysts under this condition. The additional extraction procedure

complicates the catalytic partial oxidation of methane process, inhibiting industrial applications. This problem was suggested to be overcame by using a mixture of helium and water vapour to desorb methanol from catalysts after the reaction, so the catalysts do not need to be removed from the reactor, eliminating the need for solvent extraction. However, in this instance, an additional desorption process is still required to close the reaction cycle [16].

2.5.3.2 Catalytic partial oxidation of methane over Cu-based zeolites

Copper, which was found to be present in MMO, has received much attention as the copper incorporated catalysts for catalytic partial oxidation of methane using O_2 as the oxidant [32, 133-137]. Similar to Fe-based catalysts, direct methane conversion over Cu-based catalysts is performed in a multi-step process. First, specific oxygen species are produced from reaction between Cu-based catalysts and the oxidant (usually O_2) at high temperature (typically higher than 400 ℃), followed by the oxidation of methane by these oxygen species at relatively low temperature (120℃ to 200 ℃) [32, 133-139]. The catalytic test results of Cu-based catalysts are summarized in Table 2.4.

Activity of dicopper cores in Cu-MOR for methane conversion was investigated using X-ray absorption spectroscopy and DFT calculations, and bis(μ-oxo)dicopper cores were proposed as the active sites [32]. Copper-containing small-pore zeolites and zeotypes was examined to convert methane to methanol, it was reported that a mono-μ-oxo dicopper complex was the possible active site that could be generated by oxidation of catalysts at high temperature [139], which was confirmed by DFT calculations, XANES and EXFS spectra [140]. Cu/MOR with only type of active sites was developed and the active sites were demonstrated to be the trinuclear Cu-oxo clusters

which was supported by followed study [35, 135]. The successfully prepared catalysts showed an extremely higher activity, which was reported to be at least 10 times higher than those reported in previous publications as shown in Table 2.4 [35].

The results presented highlight the potential application of copper loaded zeolites in successful direct, catalytic partial methane oxidation to methanol and other value products. It should be noted, however, that all the methods discussed need an additional extraction step for obtaining methanol and future modifications are required in prior to industrial scale application.

2.5.3.3 Other metals

In addition to iron and copper, further efforts have been made toward methane conversion via the utilisation of other metals [15, 141-142]. Ni/ZSM-5 consisting of bent mono (μ-oxo) dinickel species was synthesized on the internal way of ZSM-5, and the results showed that bent mono (μ-oxo) dinickel species were active for methane conversion to methanol under mild conditions [141]. Co/ZSM-5 was reported to convert methane to methanol and formaldehyde, where it was identified that the preparation method effected formation of Co species which exhibited different selectivity to a variety of oxygenates [15, 142].

2.5.4 Discussion

Methanol is successfully formed from catalytic partial oxidation of methane over the catalysts as compared in Table 2.4, indicating a promising way for catalytic partial oxidation of methane to value added products. The difference in concentration may be due to different reaction temperatures, catalyst preparation methods and used oxidants. However, the nature of active sites

is still a matter of discussion, various active sites over these catalysts were proposed basing on evidences from various characterization techniques as summarized in Table 2.5. In addition, above discussed processes for catalytic partial oxidation of methane at low temperature are stepwise and include an additional extraction or desorption procedure for obtaining the methanol. Further effort is expected to identify the state of active sites over catalysts for promoting formation of surface oxygen species and close the catalytic cycle.

Table 2.4 Comparison of methanol formation over various metal-based catalysts

Catalyst	T (℃)	CH_3OH concentration (μmol/g cat.)	CH_3OH concentration (μmol/mol metal)	CH_3OH selectivity (%)	Ref.
Fe-ZSM-5	R.T.	5.0	-	ca. 80	110
	R.T.	20.3	214	-	111
	R.T	23.0	64.4	45	22
	160	213.2	597.0	87	117
	160	160.0	448.0	76	31
	175	238.7	668.4	77	117
	200	265.2	742.3	68	117
Cu-ZSM-5	150	16	30	-	139
	150	1.6	4.7	-	136
Cu-SSZ	150	39	50	-	139
	150	31	60	-	139
	200	28.1	50		138
Cu-MOR	200	ca. 12.0	ca. 18.0	-	137
	150	31.0	40.0	-	139
	200	ca. 170	ca. 340	-	35
	200	59.4	ca. 160	-	134
	150	97.0	ca. 310		135
Cu-SiO_2	200	11.5	37.5	-	133
Co-ZSM-5	150	ca. 0.39	ca. 2.1	ca. 38.0	142
	150	ca. 1.0	ca. 1.4	ca. 75	15

Ni-ZSM-5	175	2.0	5.9	-	141

Table 2.5 Proposed active sites for producing surface oxygen species

Material	Proposed nature of active sites	Evidence source	Ref.
Fe-ZSM-5	mononuclear iron cations	XAFS spectroscopy	127
Fe-Beta	mononuclear, high-spin, square planar Fe^{2+} sites	Magnetic circular dichroism spectroscopy	122
Fe-ZSM-5	dinuclear iron-containing complexes	Mössbauer spectroscopy, DFT calculations, XAFS spectroscopy	123-126
	oligonuclear iron oxide species	IR spectroscopy, UV–vis spectroscopy, Raman spectroscopy,	114, 129
	small-sized Fe_xO_y nanoparticles	DR spectroscopy	130
Cu-MOR	bis(μ-oxo)dicopper cores	X-ray absorption spectroscopy, DFT calculations	32
	mono-μ-oxo dicopper complex	UV-vis spectroscopy, DFT calculations, XANES and EXFS spectroscopy	139-140
	trinuclear Cu-oxo clusters	UV-vis-NIR spectroscopy, EXAFS, *in situ* X-ray absorption spectroscopy	35, 135
Ni-ZSM-5	mono(μ-oxo)dinickel species	XANES and EXAFS spectroscopy	141

2.6 Catalytic partial oxidation of methane by N_2O at moderate temperatures

To avoid the need for additional extraction, continuous partial oxidation reactions were examined, with a focus on Fe-based catalysts, particularly Fe/MFI catalysts due to their high stability of structure and well-arranged pores [20, 112, 117, 143]. The selectivity to methanol from catalytic partial oxidation of methane over Fe-Al/MFI was less than 2% at temperatures above 250°C due to combustion of methane [112]. Beta is another potential zeolite material, and the conversion of CH_4 and N_2O over Fe ion exchanged Beta zeolite with a temperature range from 200 ℃ to 400 ℃ was reported to be very low even at 350 ℃ and no product selectivity information was provided [20]. Panov and co-workers proved that water could enhance the selectivity to methanol from catalytic partial oxidation of methane over Fe/ZSM-5 up to approximately 30% at 300 ℃ with methane conversion of 0.8% [117]. Similar observation was reported with carbon balance data showed that over 60% of methane was converted to coke [143]. Of great interest is that the α-oxygen was reported to be stable up to 300 ℃ , where it would transfer into molecular oxygen, which is inactive for catalytic partial oxidation of methane [22, 61]. The results that suggest methane can be transformed to methanol over Fe-based catalysts using N_2O at temperatures over 300 °C indicated that methane might be oxidized by short-lived oxygen species which are formed from N_2O dissociation [144].

As discussed above, the study on continuous methane conversion to value-added products over Fe-based catalysts is relatively limited and selectivity to desired products is unsatisfactory. On the other hand, in enzymatic studies,

the active sites of catalytic partial oxidation of methane were proposed to be the binuclear iron species [145], which are also believed to be the active centre for N_2O decomposition. Therefore, catalysts which show better performance for N_2O decomposition might also convert more methane to value added products. There were plenty of zeolites studied aiming to achieve high conversion of N_2O, such as ZSM-5, Beta, Al_2O_3, AlPO-5, MOR and Ferrierite (FER) [20, 143, 146-151]. Among those zeolites, FER has been proved to be an attractive alternative of ZSM-5, since the N_2O decomposition over FER was observed to be significantly higher than ZSM-5 [152]. It was believed that there were local structures with two β adjacent sites in the eight-member ring over FER where the anchored Fe-Fe distance was calculated to be comparable to the length of N_2O molecular, with the unique arrangement of the two Fe ions providing potential for cooperation of Fe cations on N_2O splitting [152]. However, this research was not concerned with the stability of the active oxygen species and the feasibility of utilization of the active oxygen species for methane activation at moderate temperature.

2.7 Conclusions

Overall, the direct oxidation of methane to valuable products has been widely studied in terms of oxidant comparisons, catalyst modifications and operating conditions optimization; the results obtained in these processes are currently unable to compete with traditional adopted technologies. The oxidation of methane by oxygen with or without solid catalysts was not reported to produce C_1-oxygenates with a satisfactory yield. Methane conversion under mild conditions proposed a promising way, in which the selectivity to methanol and formaldehyde are likely to be enhanced, but the process has not yet been

performed either as an economically catalytic reaction with sufficient methanol selectivity or in a closed catalytic cycle. The conduction of reaction at moderate temperature produces methanol continuously in gas phase, however the selectivity to desired products is reduced at such condition. The yield of desired products is likely to be enhanced with the development of superior catalysts by attempting incorporation of iron or copper on more suitable zeolites basing on deeper understanding of the nature of the active sites and surface oxygen species.

2.8 Reference

1. Otsuk, K; Wang, Y. Direct conversion of methane into oxygenate. *Appl. Catal. A: Gen*. **2001**, *222*, 145-161.
2. Wang, Q.; Chen, X.; Jha, A.N.; Rogers, H. Natural gas from shale formation – The evolution, evidences and challenges of shale gas revolution in United States. *Renew. Sustain. Energy Rev.* **2014**, *30*, 1-28.
3. Jin, D.; Zhu, B.; Hou, Z.; Fei, J.; Lou, H.; Zheng, X. Dimethyl ether synthesis via methanol and syngas over rare earth metals modified zeolite Y and dual Cu–Mn–Zn catalysts. *Fuel* **2007**, *86*, 2707-2713.
4. Horn, R.; Schlögl, R. Methane Activation by Heterogeneous Catalysis. *Catal. Lett.* **2014**, *145*, 23-39.
5. Hu, J.; Wu, S.; Li, Z.; Peng, L.; Fu, X.; Wang, X.; Guan, J.; Kan, Q. Nano-MoO_3-modified MCM-22 for methane dehydroaromatization. *Appl. Organomet. Chem.* **2015**, *29*, 638-645.

6. Wang, B.; Albarracín-Suazo, S.; Pagán-Torres, Y.; Nikolla, E. Advances in methane conversion processes. *Catal. Today* **2017**, *285*, 147-158.

7. Han, B.; Yang, Y.; Xu, Y.; Etim, U. J.; Qiao, K.; Xu, B.; Yan, Z. A review of the direct oxidation of methane to methanol. *Chin. J. Catal.* **2016**, *37*, 1206-1215.

8. Xu, Y. Direct conversion of methane under nonoxidative conditions. J. Catal. **2003**, *216*, 386-395.

9. Xu, C.; Liu, H.; Jia, M.; Guan, J.; Wu, S.; Wu, T.; Kan, Q. Methane non-oxidative aromatization on Mo/ZSM-5: Effect of adding triethoxyphenylsilanes into the synthesis system of ZSM-5. *Appl. Surf. Sci.* **2011**, *257*, 2448-2454.

10. Gambo, Y.; Jalil, A. A.; Triwahyono, S.; Abdulrasheed, A. A. Recent advances and future prospect in catalysts for oxidative coupling of methane to ethylene: A review. *J. Ind. Eng. Chem.* **2018**, *59*, 218-229.

11. Ab Rahim, M. H.; Forde, M. M.; Jenkins, R. L.; Hammond, C.; He, Q.; Dimitratos, N.; Lopez-Sanchez, J. A.; Carley, A. F.; Taylor, S. H.; Willock, D. J.; Murphy, D. M.; Kiely, C. J.; Hutchings, G. J., Oxidation of methane to methanol with hydrogen peroxide using supported gold-palladium alloy nanoparticles. *Angew. Chem. Int. Ed. Engl.* **2013**, *52*, 1280-1284.

12. Galadima, A. Muraza, O. Advances in Catalyst Design for the Conversion of Methane to Aromatics: A Critical Review. *Catal. Surv. Asia* **2019**, 1-22

13. De Lucas, A.; Valverde, J. L.; Canizares, P.; Rodriguez, L. Partial oxidation of methane to formaldehyde over W/SiO_2 catalysts. *Appl. Catal. A: Gen.* **1999**, *184*, 143–152.

14. Bendtsen, A. B.; Glarborg, P.; Dam-Johansen, K. I. M. Low temperature oxidation of methane: the influence of nitrogen oxides. *Combust. Sci. Technol.* **2000**, *151*, 31-71.

15. Beznis, N. V.; van Laak, A. N. C.; Weckhuysen, B. M.; Bitter, J. H., Oxidation of methane to methanol and formaldehyde over Co–ZSM-5 molecular sieves: Tuning the reactivity and selectivity by alkaline and acid treatments of the zeolite ZSM-5 agglomerates. *Micropor. Mesopor. Mat.* **2011**, *138*, 176-183.

16. Alayon, E. M.; Nachtegaal, M.; Ranocchiari, M.; van Bokhoven, J. A. Catalytic conversion of methane to methanol over Cu-mordenite. *Chem. Commun.* **2012**, *48*, 404-406.

17. Parmaliana, A.; Frusteri, F.; Mezzapica, A.; Scurrell, M. S.; Giordano, N. Novel high activity catalyst for partial oxidation of methane to formaldehyde. *Chem. Comm.* **1993**, *9*, 751-753.

18. Arutyunov, V. S.; Strekova, L. N. The interplay of catalytic and gas-phase stages at oxidative conversion of methane: A review. *J. Mol. Catal. A: Chem.* **2017**, *426*, 326-342.

19. Bañares, M. A.; Cardoso, J. H.; Hutchings, G. J.; Bueno, J. M. C.; Fierro, J. L. Selective oxidation of methane to methanol and formaldehyde over V_2O_5/SiO_2 catalysts. Role of NO in the gas phase. *Catal. Lett.* **1998**, *56*, 149–153.

20. Kameoka, S.; Nobukawa, T.; Tanaka, S. I.; Ito, S. I.; Tomishige, K.; Kunimori, K. Reaction between N_2O and CH_4 over Fe ion-exchanged BEA zeolite catalyst: A possible role of nascent oxygen transients from N_2O. *Phys. Chem. Chem. Phys.* **2003**, *5*, 3328.

21. Wang, Z. C.; Dietl, N.; Kretschmer, R.; Ma, J. B.; Weiske, T.; Schlangen, M.; Schwarz, H. Direct conversion of methane into formaldehyde mediated by $[Al_2O_3]$ + at room temperature. *Angew. Chem. Int. Ed.* **2012**, *51*, 3703-3707.

22. Starokon, E.V.; Parfenov, M. V.; Pirutko, L. V.; Abornev, S. I.; Panov, G. I. Room-Temperature Oxidation of Methane by α-Oxygen and Extraction of Products from the FeZSM-5 Surface. *J. Phys. Chem. C* **2011**, *115,* 2155-2161.

23. Ravi, M.; Ranocchiari, M.; van Bokhoven, J. A. The Direct Catalytic Oxidation of Methane to Methanol-A Critical Assessment. *Angew. Chem. Int. Ed.* **2017**, *56*, 16464-16483.

24. Zakaria, Z.; Kamarudin, S. K. Direct conversion technologies of methane to methanol: An overview. *Renew. Sustain. Energy Rev.* **2016**, *65*, 250-261.

25. Majhi, S.; Mohanty, P.; Wang, H.; Pant, K. K. Direct conversion of natural gas to higher hydrocarbons: A review. *J. Energy Chem.* **2013**, *22*, 543-554.

26. Holmen, A. Direct conversion of methane to fuels and chemicals. *Catal. Today* **2009**, *142*, 2-8.

27. Blanksby, S. J.; Ellison, G. B. Bond Dissociation Energies of organic molecule. *Acc. Chem. Res.* **2003**, *36*, 255-263.

28. Silva, M. J. d. Synthesis of methanol from methane: Challenges and advances on the multi-step (syngas) and one-step routes (DMTM). *Fuel Process. Technol.* **2016**, *145*, 42-61.

29. Zimmermann, T.; Bilke, M.; Soorholtz, M.; Sch th, F. Influence of Catalyst Concentration on Activity and Selectivity in Selective Methane Oxidation with Platinum Compounds in Sulfuric Acid and Oleum. *ACS Catal.* **2018**, *8*, 9262-9268.

30. Hammond, C.; Forde, M. M.; Ab Rahim, M. H.; Thetford, A.; He, Q.; Jenkins, R. L.; Dimitratos, N.; Lopez-Sanchez, J. A.; Dummer, N. F.; Murphy, D. M.; Carley, A. F.; Taylor, S. H.; Willock, D. J.; Stangland, E. E.; Kang, J.; Hagen, H.; Kiely, C. J.; Hutchings, G. J. Direct catalytic conversion of methane to methanol in an aqueous medium by using copper-promoted Fe-ZSM-5. *Angew. Chem. Int. Ed. Engl.* **2012**, *51*, 5129-33.

31. Starokon, E. V.; Parfenov, M. V.; Arzumanov, S. S.; Pirutko, L. V.; Stepanov, A. G.; Panov, G. I. Oxidation of methane to methanol on the surface of FeZSM-5 zeolite. *J. Catal.* **2013**, *300*, 47-54.

32. Alayon, E. M. C.; Nachtegaal, M.; Bodi, A.; Ranocchiari, M.; van Bokhoven, J. A. Bis (μ-oxo) versus mono (μ-oxo) dicopper cores in a zeolite for converting methane to methanol: an in situ XAS and DFT investigation. *Phys. Chem. Chem. Phys.* **2015**, *17*, 7681-7693.

33. Ravi, M.; Ranocchiari, M.; van Bokhoven, J. A. The direct catalytic oxidation of methane to methanol—A critical assessment. *Angew. Chem. Int. Ed.* **2017**, *56*, 16464-16483.

34. Banares, M.; Alemany, L.; Granados, M. L.; Faraldos, M.; Fierro, J. Partial oxidation of methane to formaldehyde on silica-supported transition metal oxide catalysts. *Catal. Today* **1997**, *33*, 73-83.

35. Grundner, S.; Markovits, M. A. C.; Li, G.; Tromp, M.; Pidko, E. A.; Hensen, E. J. M.; Jentys, A.; Sanchez-Sanchez, M.; Lercher, J. A. Single-site trinuclear copper oxygen clusters in mordenite for selective conversion of methane to methanol. *Nat. Commun.* **2015**, *6*, 7546.

36. Chorkendorff, I.; Niemantsverdriet, J. W. Concepts of modern catalysis and kinetics. *John Wiley & Sons*. **2017**.

37. Fino, D.; Specchia, V. Compositional and structural optimal design of a nanostructured diesel-soot combustion catalyst for a fast-regenerating trap. *Chem. Eng. Sci.* **2004**, *59*, 4825-4831.

38. Bowker, M.; The basis and applications of heterogeneous catalysis. *Oxford chemistry primers, New York: Oxford University Press.* **1998**.

39. Galadima, A.; Muraza, O. Revisiting the oxidative coupling of methane to ethylene in the golden period of shale gas: A review. *J. Ind. Eng. Chem.* **2016**, *37*, 1-13.

40. Parmaliana, A.; Frusteri, F.; Arena, F.; Mezzapica, A.; Sokolovskii, V. Synthesis of methyl formate via two-step methane partial oxidation. *Catal. Today* **1998**, *46*, 117–125.

41. Enger, B. C.; Lødeng, R.; Holmen, A. A review of catalytic partial oxidation of methane to synthesis gas with emphasis on reaction mechanisms over transition metal catalysts. *Appl. Catal. A: Gen.* **2008**, *346*, 1-27.

42. Guo, X.; Fang, G.; Li, G.; Ma, H.; Fan, H.; Yu, L.; Ma, C.; Wu, X.; Deng, D. H.; Wei, M. M. *et. al.* Direct, nonoxidative conversion of methane to ethylene, aromatics, and hydrogen. *Sci*. **2014**, *344*, 616-619.

43. Liu, H.; Shen, W.; Bao, X.; Xu, Y. Identification of Mo active species for methane dehydro-aromatization over Mo/HZSM-5 catalysts in the absence of oxygen: 1 H MAS NMR and EPR investigations. *J. Mol. Catal. A* **2006**, *244*, 229-236.

44. Tshabalala, T. E.; Coville, N. J.; Scurrell, M. S. Dehydroaromatization of methane over doped Pt/Mo/H-ZSM-5 zeolite catalysts: The promotional effect of tin. *Appl. Catal. A: Gen.* **2014**, *485*, 238-244.

45. Liu, H.; Yang, S.; Hu, J.; Shang, F.; Li, Z.; Xu, C.; Guan, J. Kan, Q. A comparison study of mesoporous Mo/H-ZSM-5 and conventional Mo/H-ZSM-5 catalysts in methane non-oxidative aromatization. *Fuel Process. Technol.* **2012**, *96*, 195-202.

46. Abdelsayed, V.; Shekhawat, D.; Smith, M. W. Effect of Fe and Zn promoters on Mo/HZSM-5 catalyst for methane dehydroaromatization. *Fuel* **2015**, *139*, 401-410.

47. Lónyi, F.; Solt, H. E.; Valyon, J.; Boix, A.; Gutierrez, L. B. The SCR of NO with methane over In,H- and Co,In,H-ZSM-5 catalysts: The promotional effect of cobalt. *Appl. Catal. B: Environ.* **2012**, *117-118*, 212-223.

48. Aboul-Gheit, A. K.; El-Masry, M. S.; Awadallah, A. E. Oxygen free conversion of natural gas to useful hydrocarbons and hydrogen over monometallic Mo and bimetallic Mo–Fe, Mo–Co or Mo–Ni/HZSM-5

catalysts prepared by mechanical mixing. *Fuel Process. Technol.* **2012**, *102*, 24-29.

49. Keller, G. E.; Bhasin, M. M. Synthesis of ethylene via oxidative coupling of methane: I. Determination of active catalysts. *J. Catal.* **1982**, *73*, 9-19.

50. Penteado, A.; Esche, E.; Salerno, D.; Godini, H. R.; Wozny, G. Design and assessment of a membrane and absorption based carbon dioxide removal process for oxidative coupling of methane. *Ind. Eng. Chem. Res.* **2016**, *55*, 7473-7483.

51. Kondratenko, E. V.; Peppel, T.; Seeburg, D.; Kondratenko, V. A.; Kalevaru, N.; Martin, A.; Wohlrab, S. Methane conversion into different hydrocarbons or oxygenates: current status and future perspectives in catalyst development and reactor operation. *Catal. Sci. Technol.* **2017**, *7*, 366-381.

52. Liu, H.; Wu, S.; Guo, Y.; Shang, F.; Yu, X.; Ma, Y.; Xu, C.; Guan, J.; Kan, Q. Synthesis of Mo/IM-5 catalyst and its catalytic behavior in methane non-oxidative aromatization. *Fuel* **2011**, *90*, 1515-1521.

53. Liu, H.; Hu, J.; Li, Z.; Wu, S.; Liu, L.; Guan, J.; Kan, Q. Synthesis of zeolite IM-5 under rotating and static conditions and the catalytic performance of Mo/H-IM-5 catalyst in methane non-oxidative aromatization. *Kinet. Catal.* **2013**, *54*, 443-450.

54. Kim, I.; Lee, G.; Na, H. B.; Ha, J. M.; Jung, J. C. Selective oxygen species for the oxidative coupling of methane. *Mol. Catal*. **2017**, *435* 13-23.

55. Labinger, J. A. Oxidative coupling of methane: an inherent limit toselectivity? *Catal. Lett.* **1988**, *1*, 371-375.

56. Farrell, B. L.; Igenegbai, V. O.; Linic, S. A viewpoint on direct methaneconversion to ethane and ethylene using oxidative coupling on solidcatalysts. *ACS Catal.* **2016**, *6*, 4340-4346.

57. Eng, D.; Stoukides, M. Catalytic and electrocatalytic methane oxidation withsolid oxide membranes. *Catal. Rev.* **1991**, *33*, 375-412.

58. Olah, G. A. Beyond oil and gas: the methanol economy. *Angew. Chem. Int. Ed.* **2005**, *18*, 2636-2639.

59. Gunsalus, N. J.; Koppaka, A.; Park, S. H.; Bischof, S. M.; Hashiguchi, B. G.; Periana, R. A. Homogeneous functionalization of methane. *Chem. Rev.* **2017**, *117*, 8521-8573.

60. Nobukawa, T.; Yoshida, M.; Okumura, K.; Tomishige, K.; Kunimori, K. Effect of reductants in N_2O reduction over Fe-MFI catalysts. *J. Catal.* **2005**, *229*, 374-388.

61. Nobukawa, T.; Sugawara, K.; Okumura, K.; Tomishige, K.; Kunimori, K. Role of active oxygen transients in selective catalytic reduction of N_2O with CH_4 over Fe-zeolite catalysts. *Appl. Catal. B: Environ.* **2007**, *70*, 342-352.

62. Kastanas, G. N.; Tsigdinos, G. A.; Schwank, J. Selective oxidation of methane over vycor glass, quartz glass and various silica, magnesia and alumina surfaces. *Appl. Catal. A: Gen.* **1988**, *44*, 33-51.

63. Aoki, K.; Ohmae, M.; Nanba, T.; Takeishi, K.; Azuma, N.; Ueno, A.; Ohfune, H.; Hayashi, H.; Udagawa, Y. Direct conversion of methane

into methanol over MoO_3/SiO_2 catalyst in an excess amount of water vapor. *Catal. Today* **1998**, *45*, 29-33.

64. Amiridis, M. D.; Rekoske, J. E.; Dumesic, J. A.; Rudd, D. F.; Spencer, N. D.; Pereira, C. J. Simulation of methane partial oxidation over silica-supported MoO_3 and V_2O_5. *AIChE J.* **1991**, *37*, 87-97.

65. Koranne, M. M.; Goodwin Jr, J. G.; Marcelin, G. Carbon pathways for the partial oxidation of methane. *J. Phys. Chem.* **1993**, *97*, 673-678.

66. Shimura, K.; Fujitani, T. Effects of promoters on the performance of a VO_x/SiO_2 catalyst for the oxidation of methane to formaldehyde. *Appl. Catal. A: Gen.* **2019**, *577*, 44-51.

67. Weng, T.; Wolf, E. E. Partial oxidation of methane on mo/sn/p silica supported catalysts. *Appl. Catal. A: Gen.* **1993**, *96*, 383-396.

68. Berndt, H.; Martin, A.; Brückner, A.; Schreier, E.; Müller, D.; Kosslick, H.; Lücke, B. Structure and catalytic properties of VO_x/MCM materials for the partial oxidation of methane to formaldehyde. *J. Catal.* **2000**, *191*, 384–400.

69. Dang, T. T. H.; Seeburg, D.; Radnik, J.; Kreyenschulte, C.; Atia, H.; Vu, T. T. H.; Wohlrab, S. Influence of V-sources on the catalytic performance of VMCM-41 in the selective oxidation of methane to formaldehyde. *Catal. Commun.* **2018**, *103*, 56-59.

70. Wallis, P.; Wohlrab, S.; Kalevaru, V. N.; Frank, M.; Martin, A. Impact of support pore structure and morphology on catalyst performance of VO_x/SBA-15 for selective methane oxidation. *Catal. Today* **2016**, *278*, 120-126.

71. Sugino, T.; Kido, A.; Azuma, N.; Ueno, A.; Udagawa, Y. Partial Oxidation of Methane on Silica-Supported Silicomolybdic Acid Catalysts in an Excess Amount of Water Vapor. *J. Catal.* **2000**, *190*, 118-127.

72. Wang, C. B.; Herman, R. G.; Shi, C.; Sun, Q.; Roberts, J. E. V_2O_5-SiO_2 xerogels for methane oxidation to oxygenates: preparation, characterization, and catalytic properties. *Appl. Catal. A: Gen.* **2003**, *247*, 321-333.

73. Michalkiewicz, B. Partial oxidation of methane to formaldehyde and methanol using molecular oxygen over Fe-ZSM-5. *Appl. Catal. A: Gen.* **2004**, *277*, 147-153.

74. Yang, E.; Lee, J. G.; Kim, D. H.; Jung, Y. S.; Kwak, J. H.; Park, E. D.; An, K. SiO_2@ V_2O_5@ Al_2O_3 core–shell catalysts with high activity and stability for methane oxidation to formaldehyde. *J. Catal.* **2018**, *368*, 134-144.

75. Smith, M.; Ozkan, U. The partial oxidation of methane to formaldehyde: role of different crystal planes of MoO_3. *J. Catal.* **1993**, *141*, 124-139.

76. Wachs, I. E. Recent conceptual advances in the catalysis science of mixed metal oxide catalytic materials. *Catal. Today* **2005**, *100*, 79-94.

77. Otsuka, K.; Wang, Y.; Yamanaka, I.; Morikawa, A. Kinetic study of the partial oxidation of methane over $Fe_2(MoO_4)_3$ catalyst. *Faraday Trans.* **1998**, *89*, 4225-4230.

78. Sun, Q.; Herman, R. G.; Klier, K. Selective oxidation of methane with air over silica catalysts. *Catal. Lett.* **1992**, *16*, 251-261.

79. Hunter, N. R.; Gesser, H. D.; Morton, L. A.; Yarlagadda, P. S.; Fung, D. P. C. Methanol Formation at High Pressure by the Catalyzed Oxidation of Natural Gas and by the Sensitized Oxidation of Methane. *Appl. Catal.* **1990**, *1*, 45-54.

80. Lyons, J. E.; Ellis Jr, P. E.; Durante, V. A. Active Iron Oxo Centers for the Selective Catalytic Oxidation of Alkanes. *Stud. Surf. Sci. Catal.* **1991**, *67*, 99–116.

81. Zhang, Q.; He, D.; Li, J.; Xu, B.; Liang, Y.; Zhu, Q. Comparatively high yield methanol production from gas phase partial oxidation of methane. *Appl. Catal. A: Gen.* **2002**, *224*, 201-207.

82. Zhang, X.; He, D.; Zhang, Q.; Xu, B.; Zhu, Q. Comparative studies on direct conversion of methane to methanol/formaldehyde over La–Co–O and ZrO_2 supported molybdenum oxide catalysts. *Top. Catal.* **2005**, *32*, 215-223.

83. Norrish, R. G. W.; Wallace, J. The reaction of methane and oxygen sensitized by nitrogen peroxide. Part I—Thermal ignition. Proceedings of the Royal Society of London. Series A, Containing Papers of a Mathematical and Physical Character **1934**, *145*, 307-321.

84. Ashmore, P.; Preston, K. Sensitized ignitions of methane and oxygen. *Combust. Flame* **1967**, *11*, 125-134.

85. Teng, Y.; Sakurai, H.; Tabata, K.; Suzuki, E. Methanol formation from methane partial oxidation in CH_4–O_2–NO gaseous phase at atmospheric pressure. *Appl. Catal. A: Gen.* **2000**, *190*, 283–289.

86. Tabata, K.; Teng, Y.; Yamaguchi, Y.; Sakurai, H.; Suzuki, E. Experimental Verification of Theoretically Calculated Transition

Barriers of the Reactions in a Gaseous Selective Oxidation of CH_4−O_2−NO_2. *J. Phys. Chem. A* **2000**, *104*, 2648-2654.

87. Takemoto, T.; Tabata, K.; Teng, Y.; Nakayama, A.; Suzuki, E. The effects of reaction pressures on the production of methanol through the selective oxidation of methane in CH_4–O_2–NO_x (x= 1 or 2). *Appl. Catal. A: Gen.* **2001**, *205*, 51-59.

88. Otsuka, K.; Takahashi, R.; Amakawa, K.; Yamanaka, I. Partial oxidation of light alkanes by NO_x in the gas phase. *Catal. Today* **1998**, *45*, 23-28.

89. Onsager, O.; Lødeng, R.; Søraker, P.; Anundskaas, A.; Helleborg, B. The homogeneous gas phase oxidation of methane and the retarding effect of basic/inert surfaces. *Catal. Today* **1989**, *4*, 355-363.

90. Lodeng, R.; Lindvaag, O. A.; Soraker, P.; Roterud, P. T.; Onsager, O. T. Experimental and Modeling Study of the Selective Homogeneous Gas Phase Oxidation of Methane to Methanol. *Ind. Eng. Chem. Res.* **1995**, *34*, 1044–1059.

91. Brown, M.; Parkyns, N. Progress in the partial oxidation of methane to methanol and formaldehyde. *Catal. Today* **1991**, *8*, 305-335.

92. Alvarez-Galvan, M. C.; Mota, N.; Ojeda, M.; Rojas, S.; Navarro, R. M.; Fierro, J. L. G. Direct methane conversion routes to chemicals and fuels. *Catal. Today* **2011**, *171*, 15-23.

93. Takemoto, T.; He, D.; Teng, Y.; Tabata, K.; Suzuki, E. The optimization of methanol yield in direct selective oxidation of methane with O_2 and NO in the presence of Cu-ZnO/Al_2O_3. *J. Mol. Catal. A: Chem.* **2002**, *179*, 279-286.

94. Blanksby, S. J.; Ellison, G. B. Bond Dissociation Energies of organic molecule. *Acc. Chem. Res.* **2003**, *36*, 255-263.

95. Sklenak, S.; Andrikopoulos, P. C.; Boekfa, B.; Jansang, B.; Nováková, J.; Benco, L.; Bucko, T.; Hafner, J.; Dědeček, J.; Sobalík, Z. N_2O decomposition over Fe-zeolites: Structure of the active sites and the origin of the distinct reactivity of Fe-ferrierite, Fe-ZSM-5, and Fe-beta. A combined periodic DFT and multispectral study. *J. Catal.* **2010**, *272*, 262-274.

96. Irusta, S.; Lombardo, E. A.; Miro, E. E. Effects of NO and solids on the oxidation of methane to formaldehyde. *Catal. Lett.* **1994**, *29*, 339-348.

97. Panov, G. I.; Dubkov, K. A.; Starokon, E. V. Active oxygen in selective oxidation catalysis. *Catal. Today* **2006**, *117*, 148-155.

98. Forde, M. M.; Grazia, B. C.; Armstrong, R.; Jenkins, R. L.; Ab Rahim, M. H.; Carley, A. F.; Hutchings, G. J. Methane oxidation using silica-supported N-bridged di-iron phthalocyanine catalyst. *J. Catal.* **2012**, *290*, 177-185.

99. Hickman, D.; Schmidt, L. Production of syngas by direct catalytic oxidation of methane. *Sci.* **1993**, *259*, 343-346.

100. Chen, L.; Yang, B.; Zhang, X.; Dong, W.; Cao, K.; Zhang, X. Methane oxidation over a V_2O_5 catalyst in the liquid phase. *Energ. Fuels* **2006**, *20*, 915-918.

101. Zimmermann, T.; Soorholtz, M.; Bilke, M.; Sch th, F. Selective methane oxidation catalyzed by platinum salts in oleum at turnover frequencies of large-scale industrial processes. *J. Am. Chem. Soc.* **2016**, *138*, 12395-12400.

102. Gang, X.; Zhu, Y.; Birch, H.; Hjuler, H. A.; Bjerrum, N. J., Iodine as catalyst for the direct oxidation of methane to methyl sulfates in oleum. *Appl. Catal. A: Gen.* **2004**, *261*, 91-98.

103. Periana, R. A.; Taube, D. J.; Gamble, S.; Taube, H.; Satoh, T.; Fujii, H. Platinum catalysts for the high-yield oxidation of methane to a methanol derivative. *Sci.* **1998**, *280*, 560-564.

104. Li, T.; Wang, S. J.; Yu, C. S.; Ma, Y. C.; Li, K. L.; Lin, L. W. Direct conversion of methane to methanol over nano-[Au/SiO_2] in [Bmim]Cl ionic liquid. *Appl. Catal. A: Gen.* **2011**, *398*, 150-154.

105. Xu, J., Zheng, A., Wang, X., Qi, G., Su, J., Du, J.; Gan, Z.; Wu, J.; Wang, W.; Deng, F. Room temperature activation of methane over Zn modified H-ZSM-5 zeolites: Insight from solid-state NMR and theoretical calculations. *Chem. Sci.* **2012**, *3*, 2932-2940.

106. Szecsenyi, A.; Li, G.; Gascon, J.; Pidko, E. A. Mechanistic Complexity of Methane Oxidation with H_2O_2 by Single-Site Fe/ZSM-5 Catalyst. *ACS Catal.* **2018**, *8*, 7961-7972.

107. Hammond, C.; Dimitratos, N.; Lopez-Sanchez, J. A.; Jenkins, R. L.; Whiting, G.; Kondrat, S. A.; ab Rahim, M. H.; Forde, M. M.; Thetford, A.; Hagen, H. Aqueous-phase methane oxidation over Fe-MFI zeolites; promotion through isomorphous framework substitution. *ACS Catal.* **2013**, *3*, 1835-1844.

108. Hammond, C.; Jenkins, R. L.; Dimitratos, N.; Lopez-Sanchez, J. A.; ab Rahim, M. H.; Forde, M. M.; Thetford, A.; Murphy, D. M.; Hagen, H.; Stangland, E. E. Catalytic and mechanistic insights of the low-

temperature selective oxidation of methane over Cu-promoted Fe-ZSM-5. *Chem. Eur. J.* **2012**, *18*, 15735-15745.

109. Tomkins, P.; Ranocchiari, M.; van Bokhoven, J. A. Direct conversion of methane to methanol under mild conditions over Cu-zeolites and beyond. *Acc. Chem. Res.* **2017**, *50*, 418-425.

110. Sobolev, V.; Dubkov, K.; Panna, O.; Panov, G. Selective oxidation of methane to methanol on a FeZSM-5 surface. *Catal. Today* **1995**, *24*, 251-252.

111. Panov, G. I.; Uriarte, A. K.; Rodkin, M. A.; Sobolev, V. I. Generation of active oxygen species on solid surfaces. Opportunity for novel oxidation technologies over zeolites. *Catal. Today* **1998**, *41*, 365-385.

112. Wood, B. R.; Reimer, J. A.; Bell, A. T.; Janicke, M. T.; Ott, K. C. Methanol formation on Fe/Al-MFI via the oxidation of methane by nitrous oxide. *J. Catal.* **2004**, *225*, 300-306.

113. KA, S. Nitrous oxide and climate change. *Earthscan* **2010**, 167-176.

114. Sun, K.; Xia, H.; Feng, Z.; van Santen, R.; Hensen, E.; Li, C. Active sites in Fe/ZSM-5 for nitrous oxide decomposition and benzene hydroxylation with nitrous oxide. *J. Catal.* **2008**, *254*, 383-396.

115. Sun, K.; Zhang, H.; Xia, H.; Lian, Y.; Li, Y.; Feng, Z.; Ying, P.; Li, C. Enhancement of alpha-oxygen formation and N_2O decomposition on Fe/ZSM-5 catalysts by extraframework Al. *Chem. Commun.* **2004**, *21*, 2480-2481.

116. Fellah, M. F.; Onal, I. Direct methane oxidation to methanol by N_2O on Fe-and Co-ZSM-5 clusters with and without water: A density functional theory study. *J. Phys. Chem. C* **2010**, *114*, 3042-3051.

117. Parfenov, M. V.; Starokon, E. V.; Pirutko, L. V.; Panov, G. I. Quasicatalytic and Catalytic Oxidation of Methane to Methanol by Nitrous Oxide over FeZSM-5 Zeolite. *J. Catal.* **2014**, *318*, 14-21.

118. El-Malki, E. M.; Van Santen, R. A.; Sachtler, W. M. H. Active Sites in Fe/MFI Catalysts for NO_x Reduction and Oscillating N_2O Decomposition. *J. Catal.* **2000**, *196*, 212-223.

119. Bulushev, D. A.; Prechtl, P. M.; Renken, A.; Kiwi-Minsker, L Water Vapor Effects in N_2O Decomposition over Fe-ZSM-5 Catalysts with Low Iron Content. *Ind. Eng. Chem. Res.* **2007**, *46*, 4178-4185.

120. Heyden, A.; Peters, B.; Bell, A. T.; Keil, F. J. Comprehensive DFT Study of Nitrous Oxide Decomposition over Fe-ZSM-5. *J. Phys. Chem. B* **2005**, *109*, 1857-1873.

121. Hansen, N.; Heyden, A.; Bell, A. T.; Keil, F. J. A Reaction Mechanism for the Nitrous Oxide Decomposition on Binuclear Oxygen Bridged Iron Sites in Fe-ZSM-5. *J. Phys. Chem. C* **2007**, *111*, 2092-2101.

122. Snyder, B. E.; Vanelderen, P.; Bols, M. L.; Hallaert, S. D.; Böttger, L. H.; Ungur, L.; Pierloot, K.; Schoonheydt, R. A.; Sels, B. F.; Solomon, E. I. The active site of low-temperature methane hydroxylation in iron-containing zeolites. *Nat.* **2016**, *536*, 317.

123. Dubkov, K. A.; Ovanesyan, N. S.; Shteinman, A. A.; Starokon, E. V.; Panov, G. I. Evolution of Iron States and Formation of α-Sites upon Activation of FeZSM-5 Zeolites. *J. Catal.* **2002**, *207*, 341-352.

124. Li, G.; Pidko, E. A.; Filot, I. A.; van Santen, R. A.; Li, C.; Hensen, E. J. Catalytic properties of extraframework iron-containing species in ZSM-5 for N_2O decomposition. *J. Catal.* **2013**, *308*, 386-397.

125. Yakovlev, A. L.; Zhidomirov, G. M.; van Santen, R. A. DFT Calculations on N_2O Decomposition by Binuclear Fe Complexes in Fe-ZSM-5. *J. Phys. Chem. B* **2001**, *105*, 12297-12302.

126. Park, J. H.; Choung, J. H.; Nam, I. S.; Ham, S. W. N_2O decomposition over wet-and solid-exchanged Fe-ZSM-5 catalysts. *Appl. Catal. B: Environ.* **2008**, *78*, 342-354.

127. Choi, S. H.; Wood, B. R.; Ryder, J. A.; Bell, A. T. X-ray Absorption Fine Structure Characterization of the Local Structure of Fe in Fe− ZSM-5. *J. Phys. Chem. B* **2003**, *107*, 11843-11851.

128. Snyder, B. E.; Böttger, L. H.; Bols, M. L.; Yan, J. J.; Rhoda, H. M.; Jacobs, A. B.; Hu, M. Y.; Zhao, J.; Alp, E. E.; Hedman, B. Structural characterization of a non-heme iron active site in zeolites that hydroxylates methane. *Proc. Natl. Acad. Sci.* **2018**, *115*, 4565-4570.

129. Sun, K.; Xia, H.; Hensen, E.; Vansanten, R.; Li, C. Chemistry of N_2O decomposition on active sites with different nature: Effect of high-temperature treatment of Fe/ZSM-5. *J. Catal.* **2006**, *238*, 186-195.

130. Moretti, G.; Fierro, G.; Ferraris, G.; Andreozzi, G.; Naticchioni, V., N_2O decomposition over [Fe]-MFI catalysts: Influence of the Fe_xO_y nuclearity and the presence of framework aluminum on the catalytic activity. *J. Catal.* **2014**, *318*, 1-13.

131. Fejes, P.; Lázár, K.; Marsi, I.; Rockenbauer, A.; Korecz, L.; Nagy, J. B.; Perathonerf, S.; Centi, G. Isomorphously substituted Fe-ZSM-5 zeolites as catalysts Causes of catalyst ageing as revealed by X-band EPR, Mössbauer and ^{29}Si MAS NMR spectra. *Appl. Catal. A: Gen.* **2003**, *252*, 75-90.

132. Baber, A. E.; Lawton, T. J.; Sykes, E. C. H. Hydrogen-Bonded Networks in Surface-Bound Methanol. *J. Phys. Chem. C* **2011**, *115*, 9157-9163.

133. Bozbag, S. E.; Sot, P.; Nachtegaal, M.; Ranocchiari, M.; van Bokhoven, J. A.; Mesters, C. Direct Stepwise Oxidation of Methane to Methanol over Cu–SiO_2. *ACS Catal.* **2018**, *8*, 5721-5731.

134. Le, H. V.; Parishan, S.; Sagaltchik, A.; G bel, C.; Schlesiger, C.; Malzer, W.; Trunschke, A.; Schom cker, R.; Thomas, A. Solid-state ion-exchanged Cu/mordenite catalysts for the direct conversion of methane to methanol. *ACS Catal.* **2017**, *7*, 1403-1412.

135. Kim, Y.; Kim, T. Y.; Lee, H.; Yi, J. Distinct activation of Cu-MOR for direct oxidation of methane to methanol. *Chem. Commun.* **2017**, *53*, 4116-4119.

136. Beznis, N. V.; Weckhuysen, B. M.; Bitter, J. H. Cu-ZSM-5 Zeolites for the Formation of Methanol from Methane and Oxygen: Probing the Active Sites and Spectator Species. *Catal. Lett.* **2010**, *138*, 14-22.

137. Bozbag, S. E.; Alayon, E. M. C.; Pecháček, J.; Nachtegaal, M.; Ranocchiari, M.; van Bokhoven, J. A. Methane to methanol over copper mordenite: yield improvement through multiple cycles and different synthesis techniques. *Catal. Sci. Technol.* **2016**, *6*, 5011-5022.

138. Ipek, B.; Wulfers, M. J.; Kim, H.; G ltl, F.; Hermans, I.; Smith, J. P.; Booksh, K. S.; Brown, C. M.; Lobo, R. F., Formation of $[Cu_2O_2]^{2+}$ and $[Cu_2O]^{2+}$ toward C–H Bond Activation in Cu-SSZ-13 and Cu-SSZ-39. *ACS Catal.* **2017**, *7*, 4291-4303.

139. Wulfers, M. J.; Teketel, S.; Ipek, B.; Lobo, R. F. Conversion of methane to methanol on copper-containing small-pore zeolites and zeotypes. *Chem. Commun.* **2015**, *51*, 4447-50.

140. Alayon, E. M. C.; Nachtegaal, M.; Bodi, A.; van Bokhoven, J. A. Reaction Conditions of Methane-to-Methanol Conversion Affect the Structure of Active Copper Sites. *ACS Catal.* **2014**, *4*, 16-22.

141. Shan, J.; Huang, W.; Nguyen, L.; Yu, Y.; Zhang, S.; Li, Y.; Frenkel, A.I.; Tao, F. Conversion of methane to methanol with a bent mono(mu-oxo)dinickel anchored on the internal surfaces of micropores. *Langmuir* **2014**, *30*, 8558-8569.

142. Beznis, N. V.; Weckhuysen, B. M.; Bitter, J. H. Partial Oxidation of Methane Over Co-ZSM-5: Tuning the Oxygenate Selectivity by Altering the Preparation Route. *Catal. Lett.* **2009**, *136*, 52-56.

143. Chow, Y. K.; Dummer, N. F.; Carter, J. H.; Meyer, R. J.; Armstrong, R. D.; Williams, C.; Shaw, G.; Yacob, S.; Bhasin, M. M.; Willock, D. J. *et al.* A Kinetic study of methane partial oxidation over Fe-ZSM-5 using N_2O as an oxidant. *ChemPhysChem* **2018**, *19*, 402-411.

144. Kondratenko, E. V.; Pérez-Ramírez, J. Importance of the lifetime of oxygen species generated by N_2O decomposition for hydrocarbon activation over Fe-silicalite. *Appl. Catal. B: Environ.* **2006**, *64*, 35-41.

145. Gherman, B. F.; Baik, M. H.; Lippard, S. J.; Friesner, R. A. Dioxygen activation in methane monooxygenase: a theoretical study. *J. Am. Chem. Soc.* **2004**, *126*, 2978-2990.

146. Guesmi, H.; Berthomieu, D.; Kiwi-Minsker, L. Reactivity of oxygen species formed upon N_2O dissociation over Fe–ZSM-5 zeolite: CO oxidation as a model. *Catal. Commun.* **2010**, *11*, 1026-1031.

147. Sobolev, V. I.; Koltunov, K. Y. Location, stability, and reactivity of oxygen species generated by N_2O decomposition over Fe-ZSM-5 and Fe-Beta zeolites. J*. Mol. Catal. A: Chem.* **2011**, *347*, 22-27.

148. Alvarez, P.; Araya, P.; Rojas, R.; Guerrero, S.; Aguila, G. Activity of alumina supported Fe catalysts for N_2O decomposition: effects of the iron content and thermal treatment. *J. Chil. Chem. Soc.* **2017**, *62*, 3752-3759.

149. Chen, F.; Do, M. H.; Zheng, W.; Cheng, D. G.; Zhan, X. Catalytic reduction of N_2O with CH_4 over FeAlPO-5 catalyst. *Catal. Commun.* **2008**, *9*, 2481-2484.

150. Pietrogiacomi, D.; Campa, M. C.; Carbone, L. R.; Occhiuzzi, M. N_2O decomposition and reduction on Co-MOR, Fe-MOR and Ni-MOR catalysts: in situ UV–vis DRS and operando FTIR investigation. An insight on the reaction pathways. *Appl. Catal. B: Environ.* **2019**, *240*, 19-29.

151. Sobalik, Z.; Novakova, J.; Dedecek, J.; Sathu, N. K.; Tabor, E.; Sazama, P.; Wichterlova, B. Tailoring of Fe-ferrierite for N_2O decomposition: On the decisive role of framework Al distribution for catalytic activity of Fe species in Fe-ferrierite. *Micropor. Mesopor. Mat.* **2011**, *146*, 172-183.

152. Jíša, K.; Nováková, J.; Schwarze, M.; Vondrová, A.; Sklenák, S.; Sobalik, Z. Role of the Fe-zeolite structure and iron state in the N_2O

decomposition: Comparison of Fe-FER, Fe-BEA, and Fe-MFI catalysts. *J. Catal.* **2009**, *262*, 27-34.

CHAPTER 3

3 MATERIALS AND EXPERIMENTAL METHODOLOGIES

3.1 Catalysts preparation

A variety of chemicals were used for catalyst preparation in this study. Fe $(NO_3)_3 \cdot 9H_2O$ (98%) and $FeCl_3 \cdot 6H_2O$ (99%) were purchased from Sigma Aldrich. ZSM-5 with Al/Si ratio of 15, Beta with Al/Si ratio of 12.5 and FER with Al/Si ratio of 10 were purchased from Zeolyst.

The catalysts employed in this project were synthesised by various methods including incipient wetness impregnation, aqueous ion exchange and solid state ion exchange methods, and details outlining the preparation procedures are provided in this section.

Incipient wetness impregnation method is the most widely used catalyst preparation method as the method contains simple procedures and costs less than other methods [1]. When incipient wetness impregnation method was used, the volume of metal salt solution was pre-determined based on the capacity of saturated water adsorption of zeolite. The mass of metal salts were varied, according to the desired metal loading (0.1 wt%, 0.5 wt%, 1.0 wt% and 2.0 wt%). The precursor salt was dissolved in a given volume of deionized water to prepare the metal salt solutions which was added dropwise to the zeolite (in powder form), which was then mixed with the support by the mortar and pestle under ambient conditions. The well mixed paste then was transferred to a crucible and dried at 110 °C overnight, which was then followed by calcination in air at 550 °C for 5 hours with a heating rate of 3 °C/min from room temperature. The powder was then pressed and sieved, and the particles within the size range of 250 μm to 425 μm were chosen to be used for catalyst activity examination.

Aqueous ion exchange is another popular preparation method, which involves replacement of ionic species on surface of zeolites using metallic species in the precursor under aqueous conditions. Ion exchange process can be expressed as [2]:

$$A^{n+}_{Solution} + nB^{+}_{Solid} \leftrightarrow A^{n+}_{Solid} + nB^{+}_{Solutions} \quad (1)$$

Where A^{n+} and B^{+} are the ions present in precursor and support, espectively. During the aqueous ion exchange process, the precursor and zeolite are allowed to contact sufficiently in solution and generally improved (higher) dispersion in comparison to incipient wetness impregnation method can be achieved.

A pre-determined mass of iron salt ($FeCl_3 \cdot 6H_2O$ from Sigma Aldrich) was dissolved in 200 ml deionized water to prepare the iron solution. The (calcined) FER was added into the solution, which was then heated and maintained at 80 °C and stirred for 24 h in a fume cupboard. The solution was washed extensively and centrifuged 5 times, and the paste then dried overnight at 80 °C. The powder thus prepared was calcined at 550 °C for 5 h with a heating rate of 3 °C/min, followed by press and sieve, and the particles within the size range of 250 μm to 425 μm were used in this study.

Solid state ion exchange technique performs the ion exchange process via physically milling in solid phase instead of in a solution, and has some advantages over aqueous ion exchange method. Firstly, the solid state ion exchange method allows one to control the amount of metal which is loaded on the zeolites. Secondly, it avoids the generation of hydrates metal complex, which may form in a solution with large sizes and hinder the process of ion exchange [3]. In addition, it has been reported that the active sites formed by

solid state ion exchange method are different from that by aqueous ion exchange method [4], because molecular diffusion determines the formation of active sites in the solid state ion exchange, while ionic interaction is the key in the conventional aqueous ion exchange [5].

When the solid state ion exchange method was employed, the Fe salt ($FeCl_3 \cdot 6H_2O$ from Sigma Aldrich) was weighed according to the desired concentration of metal prior to mixing. The precursor was mechanically mixed with the pre-determined FER to reach a desired Fe-exchange level. The mixture was then charged into a crucible and rapidly heated to 500 °C (in a half hour) and maintained at 500 °C for 3 h, and then cooled to room temperature, followed by calcination at 550 °C for 5 hours at a heating rate of 3 °C/min. The catalyst was then pressed and sieved, and the particles within the size range of 250 μm to 425 μm were chosen to be used in the reaction.

3.2 Catalytic experimental setup

3.2.1 Experimental rig

In this study, a laboratory scale experimental rig which consisted of gas supply systems, reactor, Varian micro-GC and FTIR was employed.

Gas cylinders in the apparatus of the experiments were used to supply high purity grade methane, nitrous oxide and helium, and the flow rate of reactant gas mixture was controlled with Aalborg and Brooks mass flow controllers (MFC). Methane, N_2O and helium were well mixed prior to entering the reactor via a four-way valve, which controlled the steam to pass through the stainless steel tube or a bypass line. The effluent gas from the reactor and the bypass line was connected with a Varian micro-GC or a vent via another four-way valve. In addition, gasbags were used to collect the effluent gas for the

measurement of methanol, DME and formaldehyde by a FTIR measurement. The schematic of the experimental rig is shown in Fig. 3.1 and the setup of reactor is shown in Fig. 3.2.

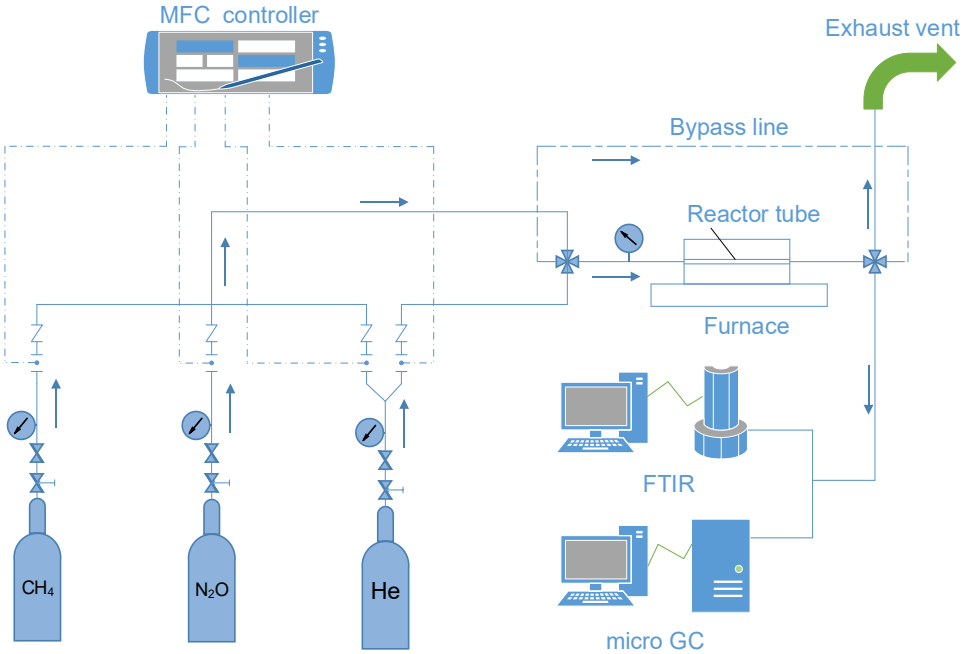

Figure 3.1 Schematic diagram of the experimental rig

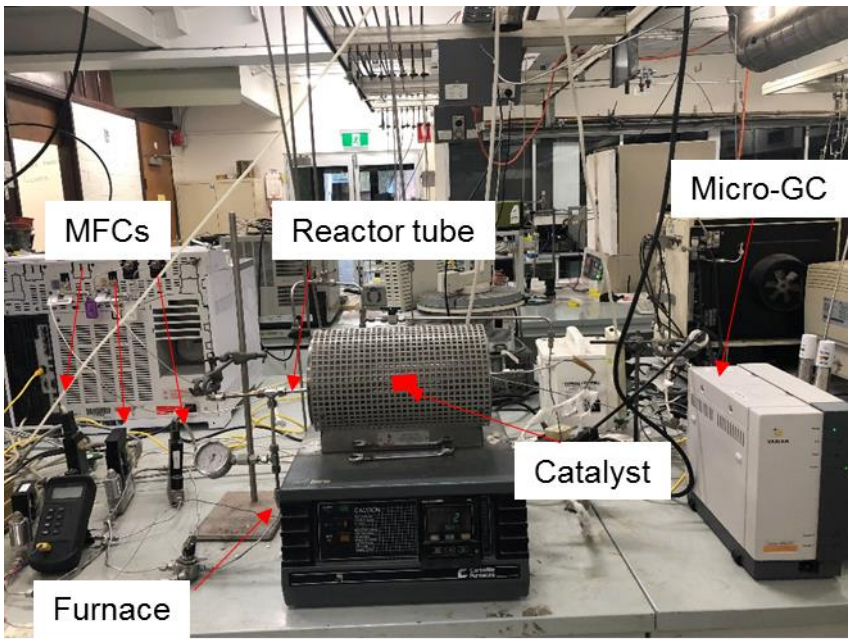

Figure 3.2 Laboratory setup of catalytic methane oxidation

3.2.2 Tubular reactor

A single-pass, stainless steel tubular reactor with an external diameter of ¼ inch was use for activity test of catalysts, as shown in Fig. 3.3. For each experiment, 200 mg of catalyst was located in the middle of the stainless steel tube and was held by two packs of quartz wool plugs at both sides to prevent the movement of catalyst with feed gas flow, and the temperature in the catalyst bed was monitored by a thermocouple (k-type) located coaxially as shown in Fig. 3.4. A pressure gauge was employed to monitor the feed gas pressure at the entry point of stainless steel tube, and hence the mixture of various gases with constant inlet pressure was fed into the reactor in all experiments. The temperature was controlled by a carbolite tubular furnace and a Eurotherm temperature controller.

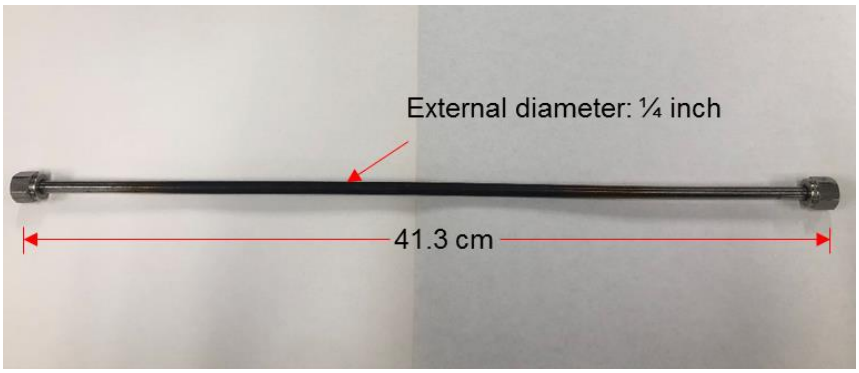

Figure 3.3 Single-pass stainless steel tubular reactor

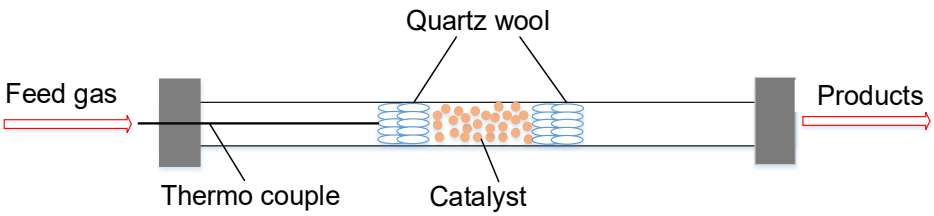

Figure 3.4 Schematic of catalyst loading in the tubular reactor

3.2.3 Mass flow controllers

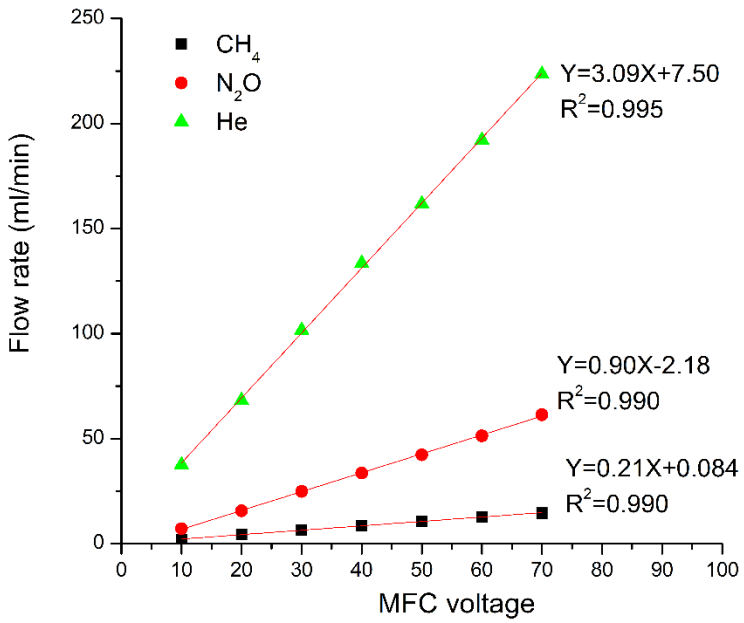

Figure 3.5 Calibration curves of MFCs

Mass flow controllers (Aalborg and Brooks) were used to control the molar flow rate of feed gas including helium, methane and nitrous oxide. Mass flow controllers were used to adjust the flow rate by setting the control voltage between 0 and 100 % for each mass flow controller, where the value of the voltage corresponds to a flow rate which was measured using a bubble meter attached to the exhaust line. The flow rates obtained from measurement using the bubble meter were compared against the set voltages and were plotted as the calibration curves, which are shown in Fig. 3.5.

3.2.4 Gas cylinders

Compress methane (99.9995%) and compress nitrous oxide (99%) were used as the reactant gas, and compress helium (99.999%) was used as the balance gas. In addition, compress helium (99.999%) and argon (99.999%) were used as the carrier gas of the micro-GC.

3.3 Catalytic activity test

3.3.1 Reaction

Catalytic reaction experiments were conducted within a temperature range from 250 °C to 400 °C at atmospheric pressure. For catalytic methane oxidation and N_2O decomposition experiments, 200 mg of catalyst was used for each reaction. Two quartz wool plugs were employed to hold the catalyst in the stainless steel tube reactor. The catalyst was initially activated in presence of helium at a heating rate of 3 °C/min to 550 °C and was held at the temperature for 3 h. After activation, the catalyst was cooled to the desired reaction temperature. Pressure regulators for the methane and nitrous oxide cylinders were kept at 4 bar and the mass flow controllers were adjusted to prepare a mixture of gases with desired flow rates and CH_4/N_2O ratios. Products in the exhaust line were sampled in an interval of 30 min, and were determined directly by the micro-GC or collected to a gas bag and measured by the FTIR. In addition, a bypass line was built to allow the measurement of concentrations of methane and N_2O in the feed.

3.3.2 Gas products analysis

The sample in the gas bag was used for measurement of methanol, formaldehyde and dimethyl ether by the FTIR, and other products (CO, CO_2, ethylene, methane and N_2O) were measured by the online micro-GC.

3.3.2.1 Online micro-GC

A micro-GC (Varian) was used to measure the feed gas and generated products in gas phase from the reactor, and was calibrated before use. The micro-GC contained a Molsieve 5A column and a PoraPLOT Q (PPQ) column,

directing separately to two thermal conductivity detectors for separation and determination of gaseous mixtures. CH_4 and CO were measured in the Molsieve 5A column, while N_2O, CO_2 and ethylene were quantified in the PPQ column. Helium was used as the carrier gas of the PPQ column, while argon for the Molsieve 5A column. A specific method was built for the determination of gas samples as shown in Table. 3.1.

Table 3.1 micro-GC operation methods

Specifications	Column	
	Moseive 5A	PoraPLOT Q
Carrier gas	Ar	He
Injector temperature (℃)	50	90
Column temperature (℃)	50	90
Initial pressure (psi)	20	8
Sampling Frequency (Hz)	12.5	12.5

A standard mixture gas consists of methane, carbon monoxide, carbon dioxide, ethylene, ethane, propane, propene, iso-butane and n-butane, and another standard mixture gas consists of nitrous oxide and nitrogen were used to calibrate the micro-GC for identity and quantity of various gaseous compounds. The chromatographs of various standard gases are shown in Fig. 3.6, and the response factors of each gas are shown in Table 3.2. The standard gases were determined 5 times and the average response areas were used to calculate the response factors. In this study the obtained response factors varied from that reported in previous publication [6], which may be due to the different polarities of the columns. In addition,

chromatographs of sample from reaction between methane and N_2O over Fe-FER catalyst at 350 °C are shown in Fig. 3.7.

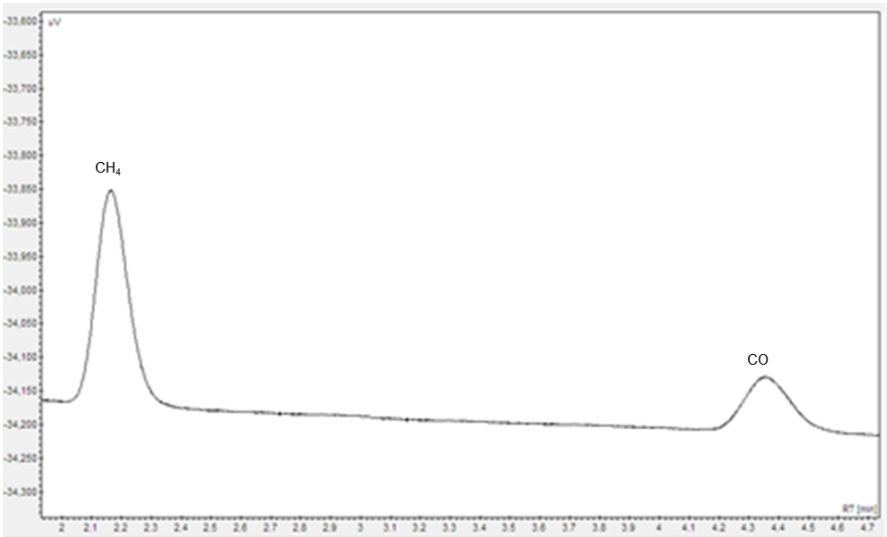

a. CH_4 and CO in Molsieve 5A column

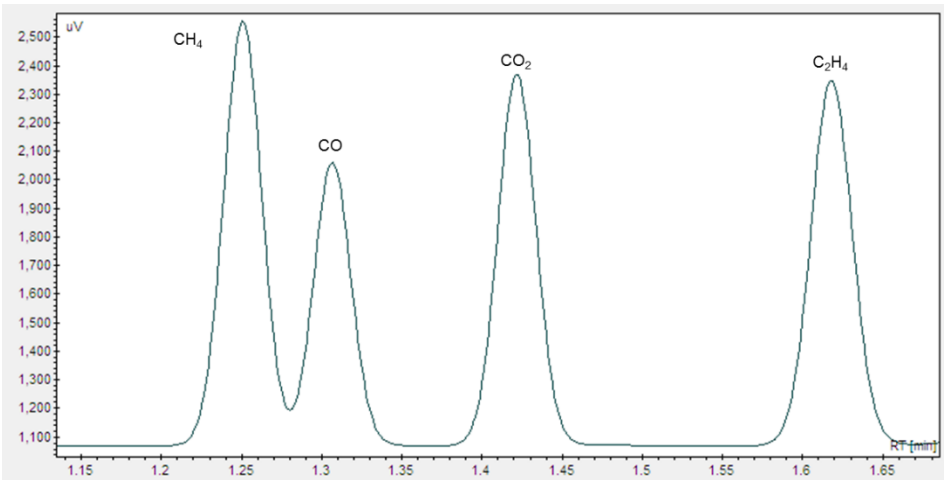

b. CO_2 and C_2H_4 in PPQ column

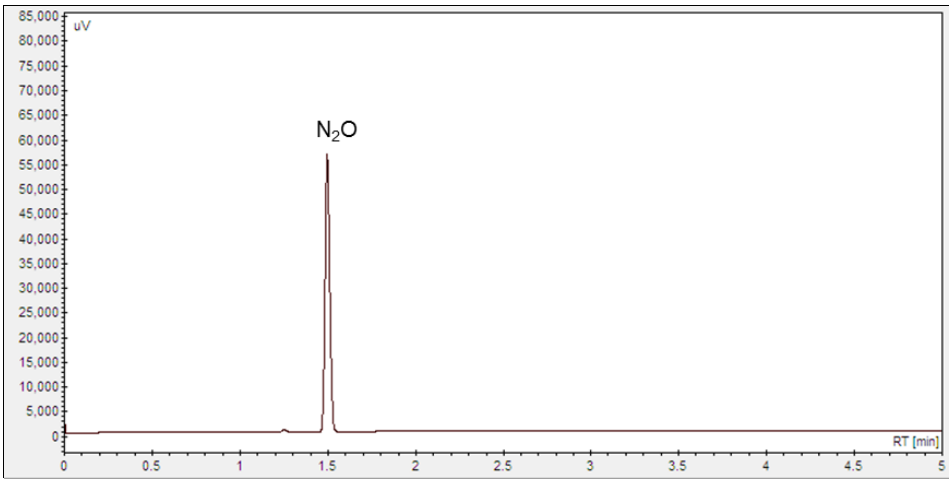

c. N_2O in PPQ column

Figure 3.6 Chromatographs of calibration gases (CH_4, CO, CO_2, C_2H_4 and N_2O)

Table 3.2 Response factors of micro-GC measurement

Gas	Concentration (ppm)	Average Peak area	STDEV	Response factor
CH_4	2010	39.7	0.23	50.6
N_2O	49700	1147.5	13.8	43.3
CO	2003	14.2	0.15	140.7
CO_2	2008	38.1	0.31	52.7
C_2H_4	2049	40.3	0.38	50.9

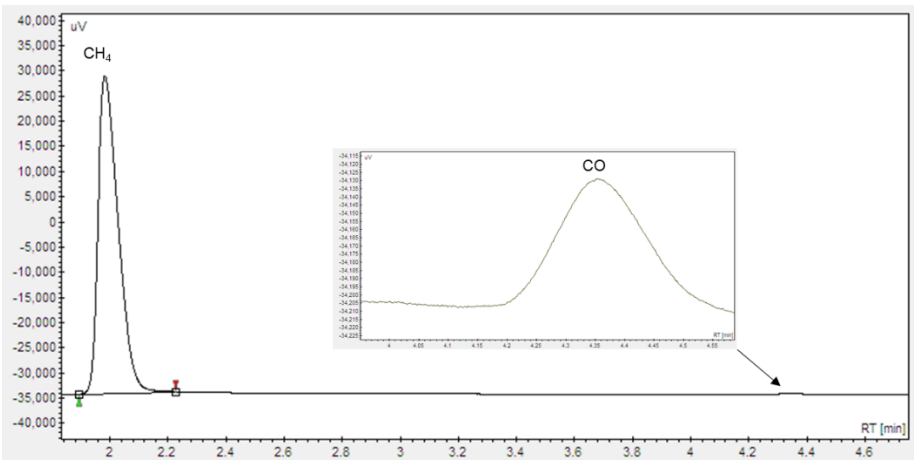

a. CH_4 and CO in Molsieve 5A column

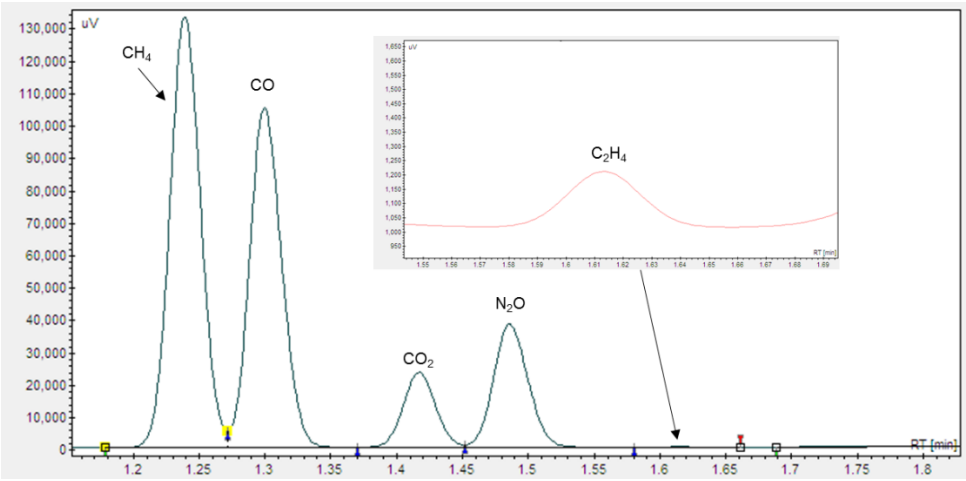

b. CO_2, C_2H_4 and N_2O in PPQ column

Figure 3.7 Chromatographs of sample from reaction between methane and N_2O over Fe-FER catalyst at 350 °C

3.3.2.2 Fourier transform infrared spectroscopy (FTIR)

FTIR is a widely used technique which can be used to analyse liquid, solid and gas samples by detecting the change of dipole moment of molecules in samples [7]. The gaseous species absorb infrared radiation with characteristic frequency that is emitted from a fixed stationary source, and then the molecules of these species release energy with a specific wavelength which is recorded and compared with library traces to obtain quantitative information of the species [8].

In this study, A IR Prestige21 Shimadzu FTIR QP 5000 was used to quantify methanol, DME and formaldehyde in the products as shown in Fig. 3.8. The FTIR consisted of a Michelson interferometer, KCl windows, and a 2.3 L gas cell with path length of 10 meters. A powerful rotary pump was connected with

the cell for maintaining vacuum inside. Plastic gas bags were used to collect the gas products and were connected with the cell via ¼ inch plastic tubing to introduce the gas samples into the cell to reach the desired pressure in the FTIR cell. A nitrogen cylinder was connected with the cell for clearance before and after sampling and analysis. Before the sampling, spectra of background were collected with the cell under vacuum, and the spectra were then subtracted from the spectra of samples to minimize the influence of background. Each sample was scanned 32 times with a resolution of 0.5 cm^{-1} from 4000 cm^{-1} to 400 cm^{-1}. An IR spectrum of sample from the reaction between methane and N_2O over Fe-FER catalyst at 350°C is shown Fig. 3.9.

QAsoft (Infrared Analysis, Inc) and Grams AI (Thermo Scientific) were applied for identification and quantitation of gas samples by comparing sample spectra with reference spectra library. Methanol, formaldehyde and DME among the products formed from methane oxidation, were quantified with FTIR scans. For instance, for identification and quantification of methanol shown in Fig. 3.9, a total of 91.8 torr of sample was injected into the cell. The pressure inside the cell before sampling was 2.9 torr, thus the total pressure of sample present inside the cell was 88.9 (91.8-2.9) torr. Similarly the atmospheric pressure was measured to be 766.5 torr, and subtracted the minimum pressure which is 2.9 torr, thus having the value of 763.6 torr, and then a factor of 8.6 (763.6/88.9) was obtained. The concentration of methanol obtained by comparing with the library trace (60.3 ppm as shown in Fig. 3.10) was multiplied by the factor to obtain the real concentration of methanol in the sample (517.9 ppm).

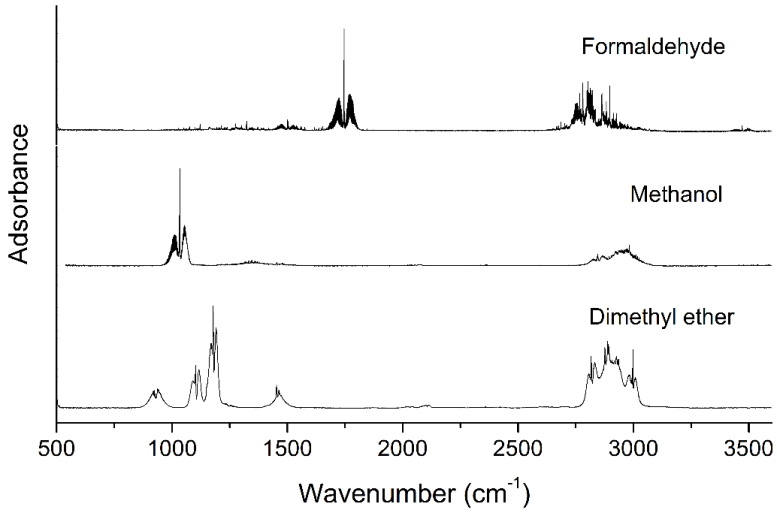

Figure 3.8 FTIR spectra of gases (NIST library trace)

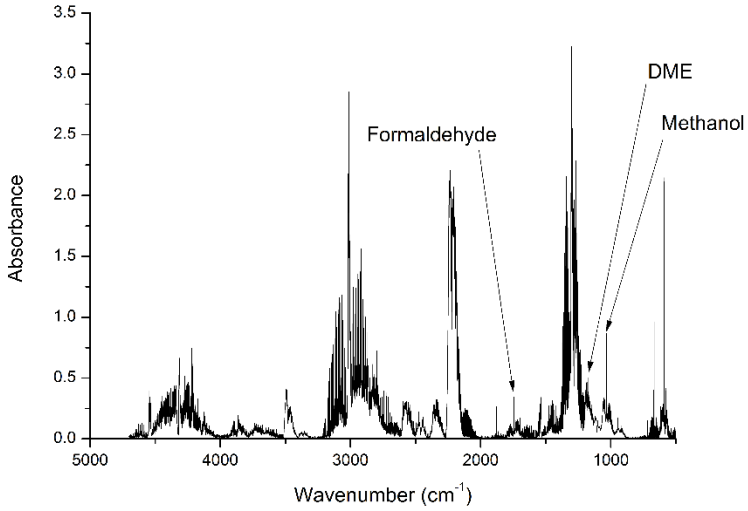

Figure 3.9 IR spectrum of sample from reaction between methane and N_2O over Fe-FER at 350 °C

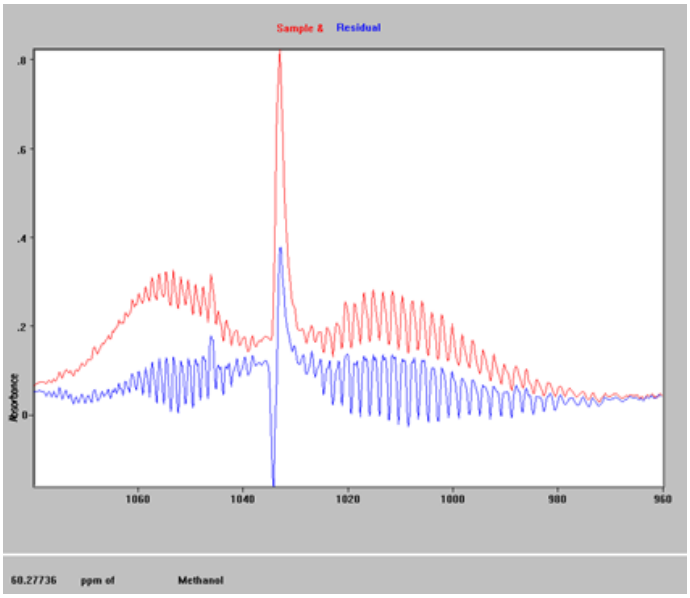

Figure 3.10 Analysis of methanol in the IR spectrum using Grams.

3.3.2.3 Data analysis

In this work, the conversion of methane and decomposition of nitrous oxide were calculated as:

$$X = \left(1 - \frac{C_p}{C_f}\right) \times 100 \quad (2)$$

Where X represents the total conversion or decomposition, C_p is concentration of methane or nitrous oxide in product stream (ppm), while C_f is concentration in the feed (ppm).

The selectivity to a gaseous product i was calculated by the equation:

$$S_i = \frac{C_i}{\sum C_i} \times 100 \quad (3)$$

Where S_i is the selectivity to the product i, and C_i is the concentration of the product (ppm).

The balance of the total carbon going in a reactant feed with the total carbon present in product was calculated as the equation unless states otherwise:

$$B = \frac{\sum n_i + n_{p,CH_4}}{n_{f,CH_4}} \times 100 \quad (4)$$

Where B is the total carbon balance, $\sum n_i$ is the sum of average concentration of the carbon in the product steam during the reaction (mole of carbon·L^{-1}), $n_{f, CH4}$ and $n_{p, CH4}$ is the average concentration of methane in the feed and outlet during the reaction (mole of carbon·L^{-1}), respectively.

The activity of catalysts can be assessed by turn over frequency (TOF), which refers to the total number of moles of methane or N_2O converted per number of active site over the catalyst per time unit. The TOF (h^{-1}) can be calculated as shown in eq. 3.5:

$$\mathrm{TOF} = \frac{60 \times \frac{V}{1000 \times 22.4} X}{\frac{m \times \Delta W \times d}{M}} \tag{5}$$

Where V is the amount of methane or N_2O in the feed gas (ml/min), X is the conversion of methane or N_2O (%), ΔW is the concentration of iron in the catalysts (%), d is the dispersion of iron active site (%) which will be explained in 3.4.5, M is the mole mass of iron (g/mol), m is the amount of catalyst used in each reaction (g).

3.4 Characterization technologies

Characterization technologies have been extensively employed in the study of catalysis to gain insights into structure, composition, porosity and surface properties of solid catalysts. The characterization results are crucial for heterogeneous catalysis study, as they provide enormous information that are essential to analyze the involved mechanisms and suggest the strategies for achieving better catalytic performance. In this project, a variety of characterization technologies were used, including powder X-Ray diffraction patterns (XRD), scanning electron microscopy (SEM), inductively coupled

plasma optical emission spectrometry (ICP-OES), nitrogen absorption (BET), CO-chemisorption, fourier transform infrared spectroscopy (FTIR), temperature programed reduction (TPR), temperature-programmed desorption (TPD), thermal gravimetric analyses (TGA), and ultraviolet and visible spectroscopy (UV-vis spectroscopy).

3.4.1 Powder X-ray diffraction (XRD)

XRD is an efficient and convenient technique to identify and quantification of crystalline content in materials, as well as to determine and refine the lattice parameters of a crystal structure [9]. The diffraction patterns are identifiable as most of the materials contain unique atomic arrangement which leads to specific diffractions peaks, and the positions of the diffraction peaks are determined by the distance between atom layers, which is described by Bragg's law [9] as expressed in eq. 3.6 and shown in Fig. 3.11:

$$n\lambda = 2d' \sin\theta \tag{6}$$

Where λ is the wavelength of the X-rays, n is an integer, d' is the spacing between atoms layers, θ is the angle of the incidence of the X-ray.

To perform the acquisition and analyse of X-ray diffraction patterns of materials, the X-ray diffractometers consist of an X-ray source, a sample holder and an X-ray detector. In this study, XRD was performed on a Phillips X'pert Pro diffractometer utilizing Cu Kα radiation. Samples were placed on a zero diffraction Si holder and were scanned from 5° to 90°. Analysis was carried out with Highscore Plus Analysis software equipped with a standard ICDD diffraction database supplied by Panalytical. A XRD pattern of H-Beta zeolites is shown in Fig. 3.12.

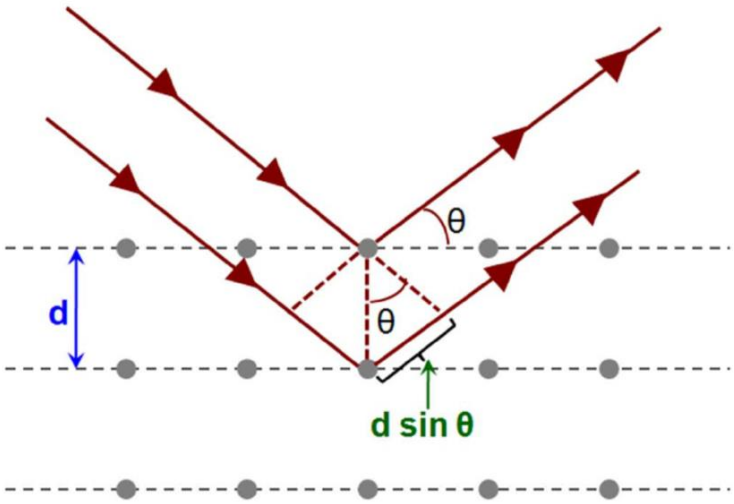

Figure 3.11 Bragg's law [10].

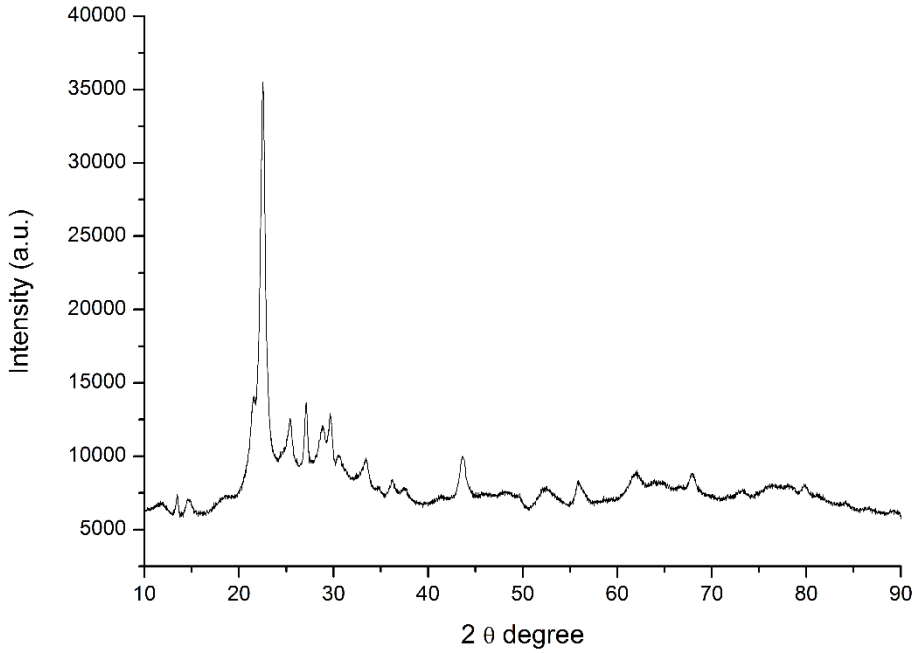

Figure 3.12 XRD pattern of H-Beta

3.4.2 Scanning electron microscope (SEM)

SEM has been wildly used to characterize the morphology of materials by providing high resolution images of samples surface [11, 12]. SEM apparatus consists of an electron source, electromagnetic lenses, electron detectors and sample champers. In SEM, a focused high-energy electron beam scans across the powder sample, and the interaction of electrons in the beam with

the sample leads to the emission of low-energy secondary electron, which can be detected and employed to the construction of surface image. Additionally, SEM can be combined with an energy dispersive X-ray spectroscopy (EDS) to quantify the amount of elements in the sample. A SEM image of Fe-FER catalyst is shown in Fig. 3.13.

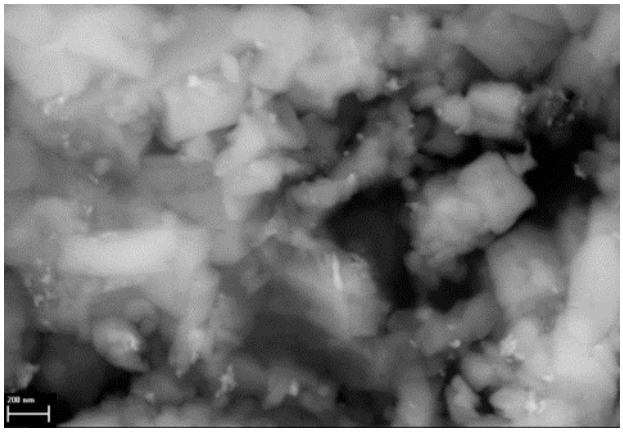

Figure 3.13 SEM image of Fe-FER (0.5 wt%)

In this study, the SEM images were provided by a Zeiss Sigma VP Field Emission SEM, three detectors including a secondary detector (SE), a backscattered detector (BSD) and a Bruker light element SSD Energy-dispersive X-ray spectroscopy (EDS) detector were available depending on the research purpose. The samples were coated by carbon tape prior to placing in the chamber, where the pressure was maintained at $2 \cdot 10^{-5}$ mbar.

3.4.3 Surface area and micropore analysis

Nitrogen adsorption is widely used for acquisition of information about surface area and pore size distribution of various solids [13]. This knowledge is beneficial for understanding the relation between catalytic activity and morphological properties of catalysts. The nitrogen adsorption is conducted by exposing nitrogen gas to the surface of sample at 77K, and the adsorption

amount of nitrogen molecules versus the corresponding pressure of nitrogen gas is plotted in the form of isotherm. According to the International Union of Pure and Applied Chemistry (IUPAC), the types of adsorption isotherms can be categorised into 6 types, and these types of isotherms are characteristic of materials that are microporous materials, nonporous or macroporous materials, typical of weak solids gas interactions, mesoporous materials, again typical of weak solids gas interactions, and uniform ultra-microporous materials [14] as shown in Fig. 3.14.

It is known that as the increase of N_2 pressure, the adsorption occurred in a monolayer first, and then in multiple layers. The further increase of system pressure would cause capillary condensation in mesorpores, and finally the saturation pressure makes the pores filled with N_2, where the pore volume can be estimated. There are a few methods developed to estimate the surface properties of a material basing on the given adsorption-desorption data collected from nitrogen adsorption experiments. Among the methods, Brunauer, Emmet and Teller (BET) theory and Langmuir model are commonly used.

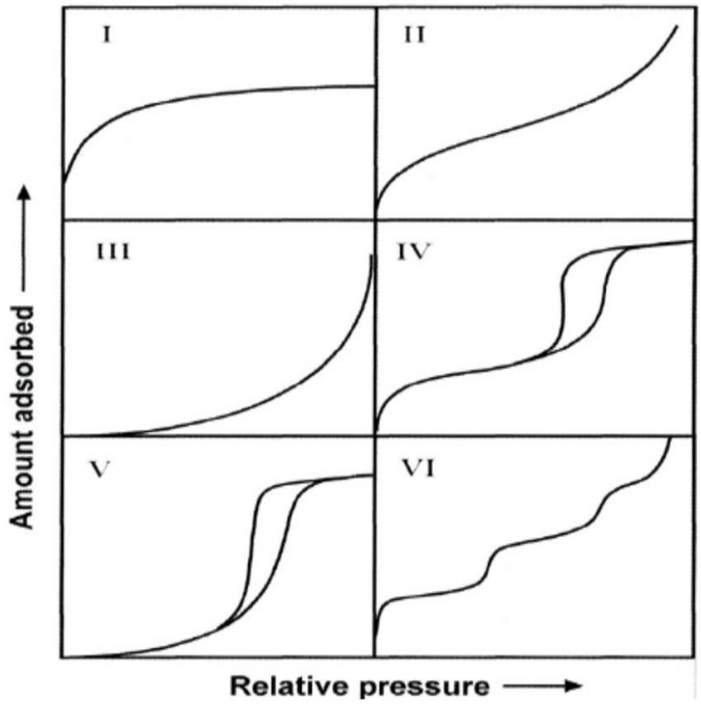

Figure 3.14 Types of adsorption-desorption isotherms [14]

For Langmuir model, when the adsorption and desorption reach to an equilibrium, the Langmuir equation can be represented as:

$$\theta = \frac{bp}{(1+bp)} \tag{7}$$

Where, θ is the fraction of occupied sites, p is the system pressure and b is the adsorption coefficient, which can be represented as:

$$b = Ke^{\frac{E}{RT}} \tag{8}$$

Where K is the pre-exponential factor. It should be noticed that the Langmuir model is a model of monolayer adsorption, and hence is inappropriate for the estimation of surface area of zeolites.

While BET equation can be written as:

$$\frac{p}{n(p_0-p)} = \frac{1}{n_m C} + \frac{C-1}{n_m C}\frac{p}{p_0} \tag{9}$$

Where p_0 is the saturation pressure of the adsorbate, n_m is the amount of adsorbate for formation of a monolayer, and C is the constant of BET, which can be represented as:

$$C = e^{\frac{E_1 - E_L}{RT}} \quad (10)$$

Where E_1 and E_L are the enthalpies of adsorption of the first layer and liquefaction, respectively.

In addition to BET and Langmuir models, t-plot method was developed to determine the external surface area and micropore volume of microporous materials, and Barrett-Joyner-Halenda (BJH) method applies mainly to calculate the pore size distribution in mesporous materials.

In this study, surface properties of fresh catalysts were analyzed by physical adsorption of N_2. The isotherm of N_2 adsorption and desorption over Fe-FER is shown in Fig. 3.15.

Catalyst samples (100 mg) were loaded in the quartz tubes and vacuum-degassed using a Micromeritics Vac Prep 061 sample preparation device at 200 °C for overnight to remove surface moisture and pre-adsorbed gases before exposing the samples to the adsorption gas. The adsorption-desorption data collected by the experiments was analysed by a Micromeritics software Tristar 3000, and the micropore volumes and micropore areas were analyzed using the *t*-plot and Barrett-Joyner-Halenda (BJH) models, respectively.

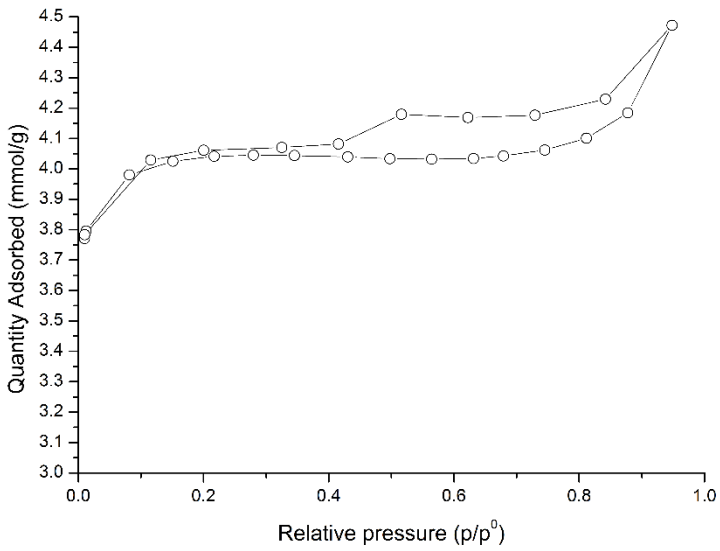

Figure 3.15 Isotherm of nitrogen adsorption and desorption on H-FER

3.4.4 Chemisorption measurement

Chemisorption measurement is a useful technique to quantify the surface active sites that are potentially responsible for specific reactions by measuring the amount of chemical gas adsorbed on materials. For a catalyst with known metal loading amount, its metal dispersion, which reveals the accessibility of adsorption and reaction sites to gas reactants in a catalyst, can be then estimated by combining the quantity of probe gas chemisorbed per gram of catalyst by chemisorption measurement with the knowledge of stoichiometry of the adsorption.

A chemisorption apparatus was built to measure the dispersion of iron on the employed catalysts in this study as shown in Fig. 3.16, the schematic of the apparatus is shown in Fig. 3.17. The chemisorption measurement set up consists of a U-shape quartz tube for loading samples, a furnace and a temperature controller with a thermocouple to heat up and maintain required temperatures, glass bulbs for containing gaseous adsorbates, a glass manifold, isolated valves, a rotary vacuum pump and a turbo pump with

gauges for monitoring the pressure in the system, and a flow rate controller to control the flow rate of air, H_2 or He depending the purpose.

Figure 3.16 Chemisorption apparatus

For chemisorption analysis, 250 mg of sample was loaded in the U-shape quartz tube, which was located in the furnace. Air was used to activate the sample with a flow rate of 100 ml/min at 450 °C for 1 h, and then He was fed in for half hour to clean the residential air, followed by H_2 reduction for at 450 °C for 1 h. Subsequently, the remained gas was evacuated by the vacuum pumps to 10^{-3} mbar. The system was maintained at vacuum for overnight and cooled to room temperature. CO was fed in the system with a pressure of around 90 mbar, and then the bulb V_1 was isolated from the system, where the CO was evacuated. The chemisorption of CO over catalysts was performed as gradually opening the isolate valve of bulb to release the stored CO.

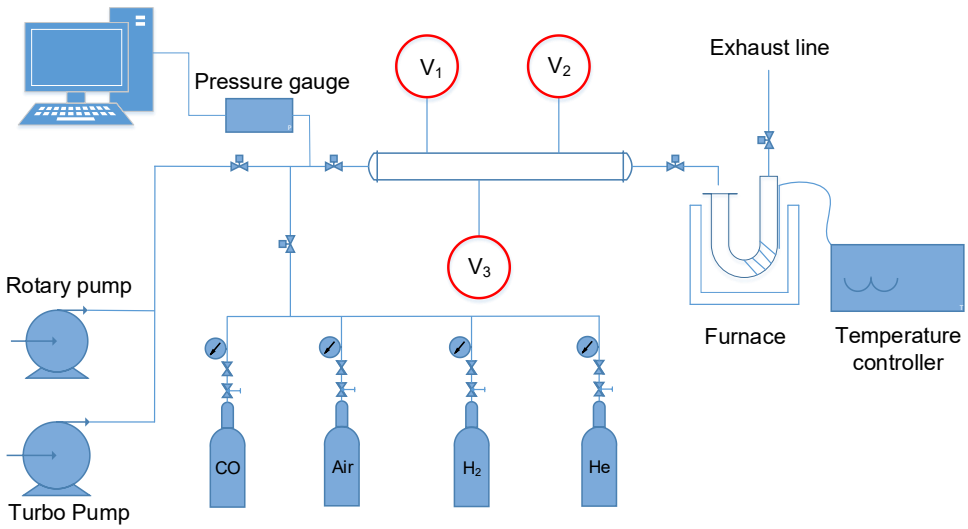

Figure 3.17 Schematic of chemisorption apparatus

The measurement pressure was determined by Pfeiffer CMR 362-TPG 261, and data logging was facilitated by LabVIEW version 7.1.1. The temperature of chemisorption was controlled at 35 °C, and the total amount of CO adsorbed on the catalyst was calculated applying the ideal gas law (eq. 3.11).

$$n_{CO} = (P_1V_1 - P_2V_2)/RT \quad (10)$$

Where the n_{CO} is the amount of adsorbed CO (mol), P_1 is the initial CO pressure in the system, P_2 represents the CO pressure after adsorption, V_1 is the volume of CO glass bulb, V_2 is the volume of the combination of glass manifold, the glass bulbs and the U-shape quartz tube, which was measured before the adsorption.

The dispersion of iron can be calculated using eq. 3.12:

$$D\ (\%) = \frac{M_{iron} \times n_{CO} \times 10^4}{SF \times x \times W} \quad (12)$$

Where the M_{iron} is the atonic mass of iron, SF is the stoichiometric factor of metal, which is 0.5 for iron [15]. *x* is the concentration of iron in the sample, and *W* is the weight of sample.

3.4.5 Inductively Coupled Plasma optical Emission Spectroscopy (ICP-OES)

ICP-OES, or sometimes refers to ICP atomic emission spectrometry (AES), is a powerful technique based on atomic emission spectrometry to measure concentrations of elements in a wide range of concentrations in a material [16]. The technique involves destroying the molecular bonds and ionizing the elements of materials within an argon-based plasma at temperature up to 10000 K [17].

In this project, the ICP-OES consists of a Varian Radial 715-ES inductively coupled plasma optical emission spectrometer, a quartz torch, a SPS 3 autosampler and a Sturman-Maters spray chamber.

The concentrations of iron, Aluminium, Silicon were determined using the ICP-OES. Approximately 10 mg powder of each catalyst was dissolved in a mixture solution of 4 ml HNO_3 (65% w/w), 4 ml HCl (37% w/w) and 2.5 ml HBF_4 (50% w/w), followed by digestion conducted in a microwave digestion unit. After the digestion, 10 ml of the solution was then transferred into the ICP-OES to be analysed. A thulium solution, as the internal standard, was digested and analysed together with unknown samples in each sequence.

3.4.6 Hydrogen temperature programmed reduction (H_2-TPR)

H_2-TPR is wildly used for characterization of metal oxides by providing quantitative information of the reducibility within this metal-based catalysts employed in catalytic study, where metal species are present in different valence states [18]. In this study, H_2-TPR is a useful technology to reveal the reducibility of the Fe-based catalysts, and hence suggests the distribution of

various valence states of iron species, which are relevant to preparation methods, iron loading amounts and catalytic activity of the catalysts.

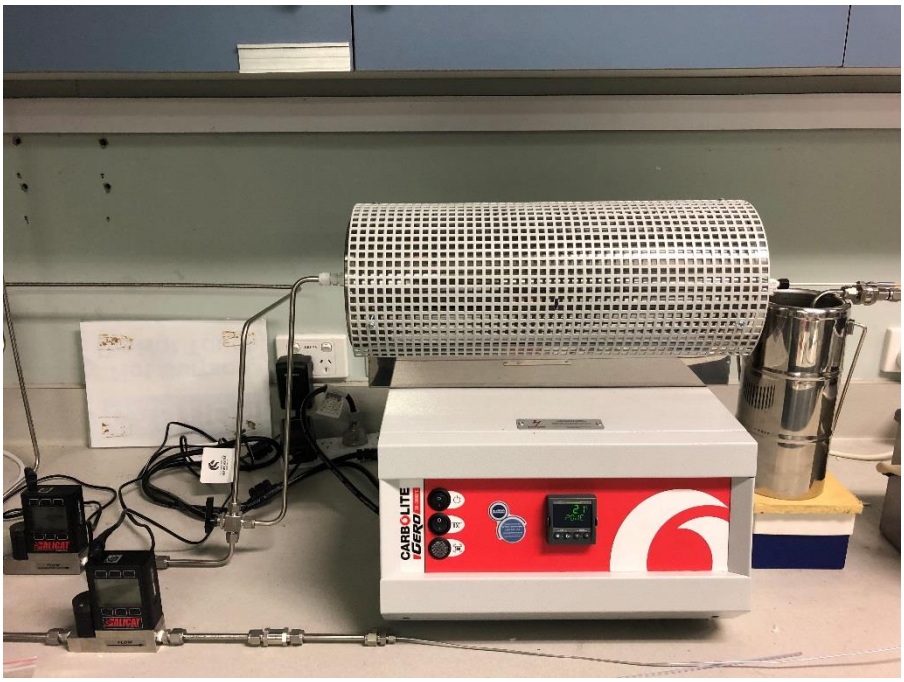

Figure 3.18 Temperature programmed reduction apparatus

In order to measure the reducibility of Fe-based catalysts, a custom-built H_2-TPR was used as shown in Fig. 3.18. Fig. 3.19 shows the schematic of the H_2-TPR set-up used in this project. The set-up consists of a furnace to heat up the sample to required temperatures, a sample quartz tube to load the sample, three flow controllers to control the flow rate of air/He, H_2/Ar and Ar in reaction tube and reference tube, a outgas condenser to remove water from the effluent, a thermal conductivity detector to measure the hydrogen concentration and a signal amplifier. A H_2-TPR profile of Fe-ZSM-5 (2.0 wt%) is shown in Fig. 3.20.

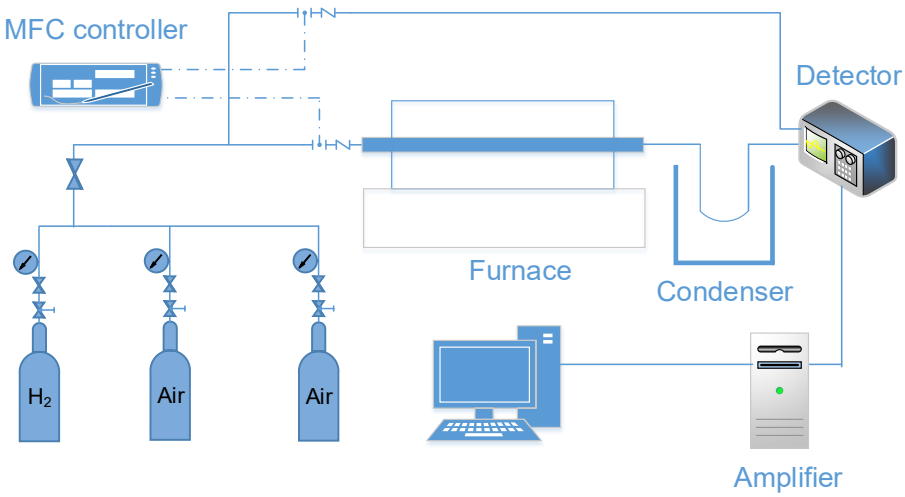

Figure 3.19 Schematic of temperature programmed reduction

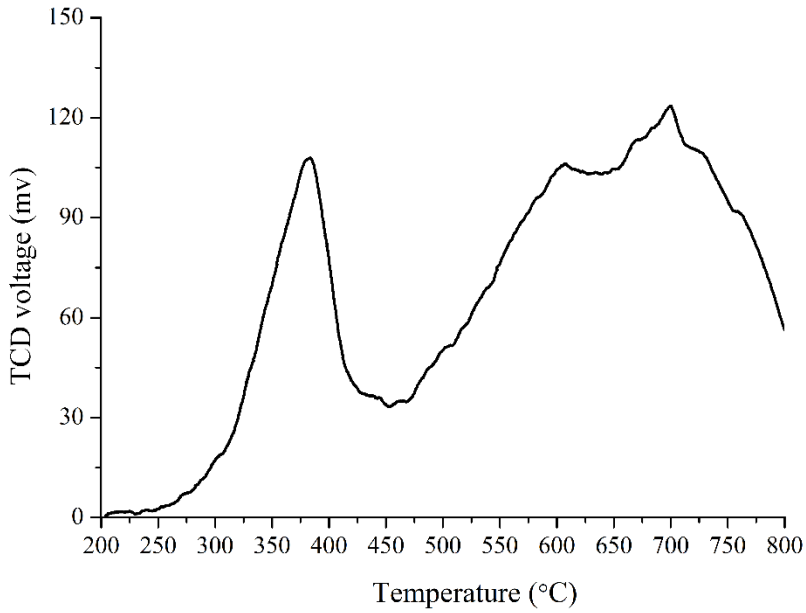

Figure 3.20 H_2-TPR profile of Fe-ZSM-5 (2.0 wt%)

When the H_2-TPR experiments were conducted, 300 mg catalyst was loaded in the quartz micro-reactor located in a furnace, quartz wool plugs were placed on both sides of the catalyst. The sample was first activated by purging in a stream of air or helium (30 ml/min) at 450 °C for 1 h, with a heating rate of 10 °C/min. Followed by reduction of sample by hydrogen in a H_2/Ar stream (2.04 vol% of H_2), with a total flow rate of 50 ml/min and a linear heating rate of 10 °C /min in the temperature range of 20–800 °C. N_2O or air pre-treatment,

if employed, was performed at required temperatures on the activated zeolites with a N_2O or air flow rate of 30 ml/min for 30 min or 1 h, and then cooled to room temperature, prior to reduction by the H_2/Ar stream.

3.4.7 *In situ* Fourier Transform Spectroscopy (*in situ* FTIR)

FTIR is a form of vibrational spectroscopy that is one of the most popular methods to characterize solid catalysts by providing the vibration information which are unique to each compound with different bonds [19]. The progress in FTIR spectrometer has remarkably promote the application. The advent of *in situ* FTIR enable one to acquire real-time information of interaction between adsorbed reactants and catalyst and hence lead to the deeper understanding of catalyst structure and catalytic reaction [20].

The method requires the utilization of mathematical process of Fourier transform to convert the raw data into a spectrum, where the intensity can be expressed as the percentage of either absorbance or transmittance at each wavenumber, and the two modes are interchangeable by using eq. 3. 13:

$$Absorbance = -log\frac{\%Transmittance}{100} \quad (13)$$

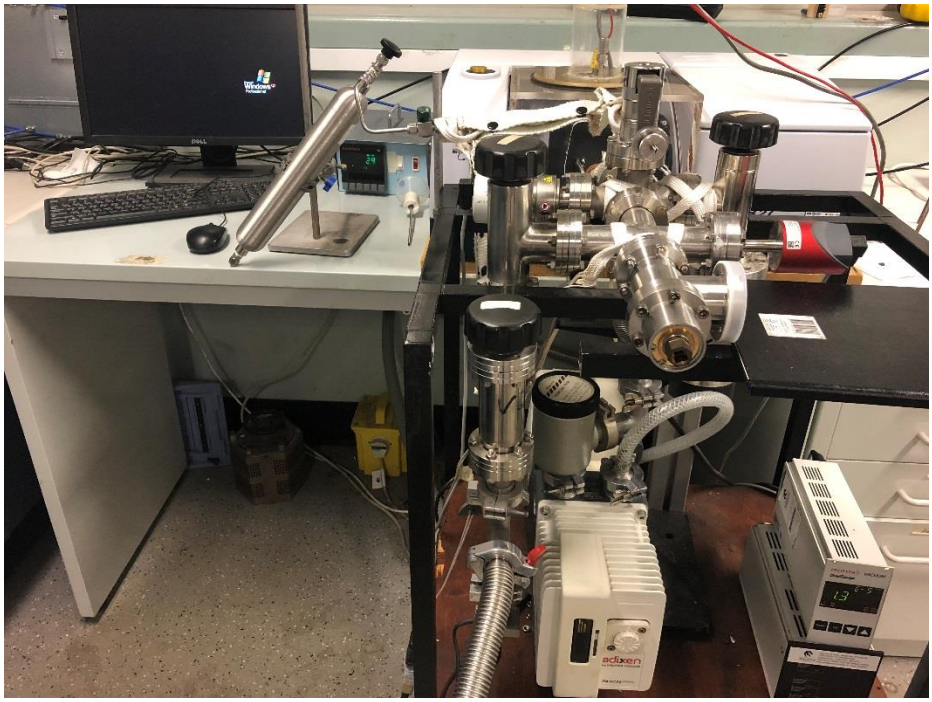

Figure 3.21 Custom-built in situ FTIR apparatus

The *in situ* FTIR spectrometer is shown in Fig. 3.21, and a schematic of the set-up is shown in Fig. 3.22. The apparatus consists a temperature controller to control the temperature to a required level, a dosing valve to control the flow rate of adsorbate, a sample chamber for loading the sample, a rotary pump and a turbo pump to evacuate the sample chamber, and a computer with OPUS collection data software and GRAMS data processing for data acquisition and processing.

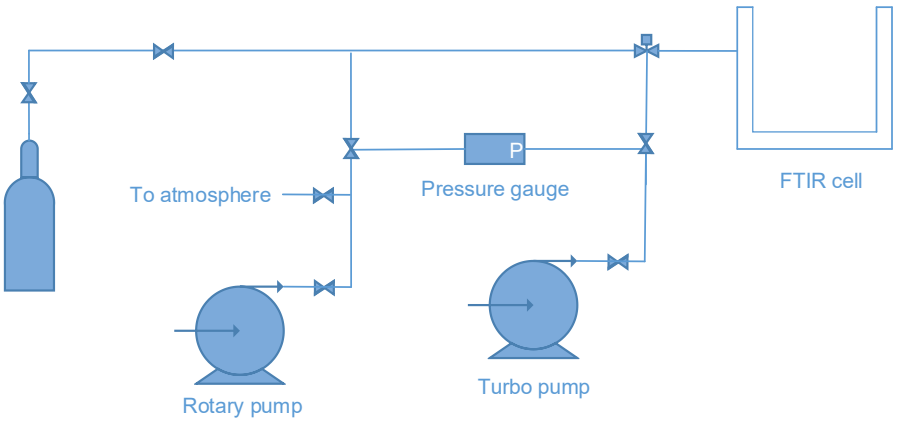

Figure 3.22 Schematic of in situ FTIR apparatus

In the project, infrared spectra were recorded using a Bruker Tensor 27 FTIR equipped with a liquid nitrogen-cooled mercury cadmium telluride detector. Measurements were conducted at a resolution of 4 cm^{-1} with a total of 3 scans per spectrum. Sample (30 mg) was ground into fine powder and was pressed into a self-supporting wafer at pressures of 3.76 t/cm^2, and subsequently placed into the sample cell equipped with CaF_2 IR windows. Prior to each experiment, the sample was evacuated (10^{-7} mbar) at 500 ℃ for 0.5 h. For NH_3 adsorption experiments, the FTIR spectra were monitored at 150 ℃ after adsorption of NH_3 (10 mbar). For NO adsorption experiments, the FTIR spectra were monitored at 150 ℃ after adsorption of NO ($5e^{-2}$ mbar), while for CH_4/N_2O adsorption experiments, the sample was exposed to CH_4 (5 mbar) first and then was exposed to N_2O (from 2 mbar to 15 mbar), or in a opposite order, and the FTIR spectra were monitored at various desired temperatures. For interaction of methanol with catalysts experiments, methanol was placed in a glass container which was connected with the IR cell via valves, and then was introduced into the cell in a pressure range from 5 mbar to 15 mbar. The overtones of zeolites lattice (1500-2000 cm^{-1}) were used to normalize the spectral intensity of the catalysts. An IR spectrum of H-ZSM-5 in the region of OH stretching vibrations is shown in Fig. 3.23.

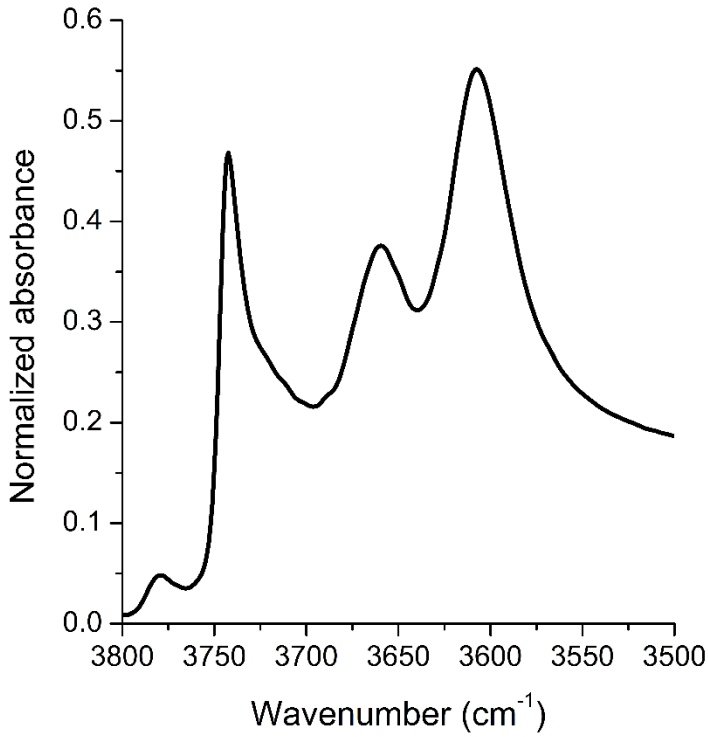

Figure 3.23 IR spectrum of H-ZSM-5 in the region of OH stretching vibrations

3.4.8 Ammonia temperature-programmed desorption (NH_3-TPD)

NH_3-TPD is another popular characterization techniques which allows the measurement of the amount and strength of acid sites in a material by determining the adsorption and desorption of ammonia on the sample [21]. The method is important and wildly used as acid sites are associated directly or indirectly with numerous catalytic reactions. Other adsorbate can be employed as well depending on experimental designs. In this project, N_2O decomposition over Fe-based catalysts in a batch mode reaction was analysed, by applying N_2O as the adsorbate which was adsorbed to the sample at various temperatures.

In this project, a built TPD apparatus equipped with a Pfeiffer Prisma quadrupole mass spectrometer as shown in Fig. 3.24 was used for

determination of desorption of adsorbates. The set-up consists of a quartz/stainless steel sample chamber, a furnace and temperature controller to elevate and control the temperature in the sample chamber, a rotary pump and a turbo pump to evacuate the sample chamber to a certain vacuum level, another turbo pump to maintain the chamber pressure in the desired range of operation, two pressure gauges, a dosing valve, a mass spectrometer, and a computer for processing the data. A schematic of the apparatus to exhibit the arrangement of TPD apparatus is shown in Fig. 3.25.

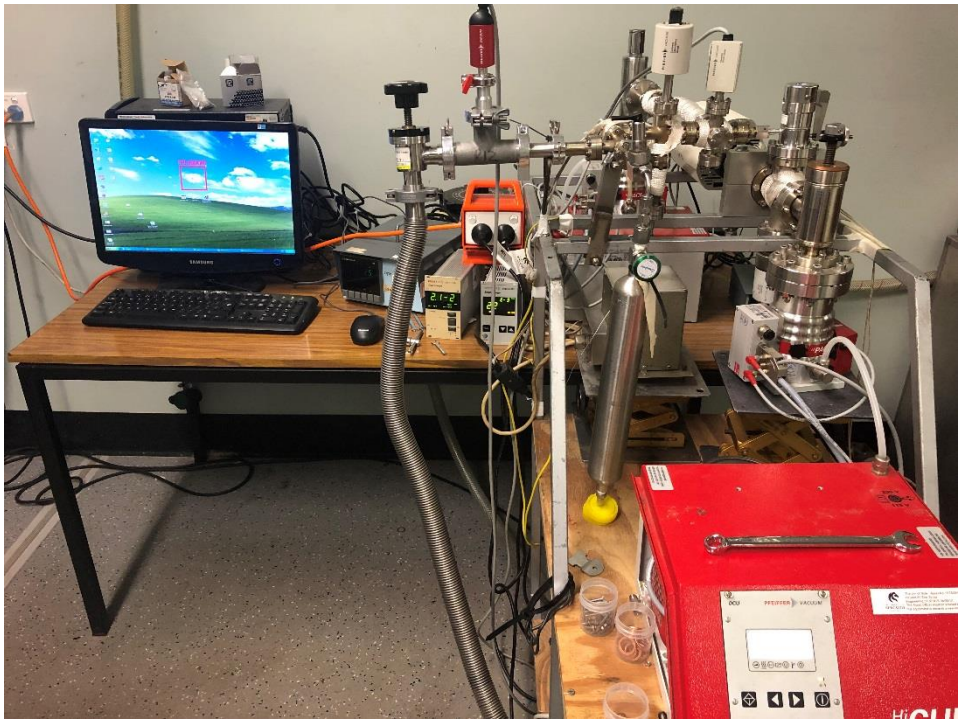

Figure 3.24 Custom-built TPD apparatus

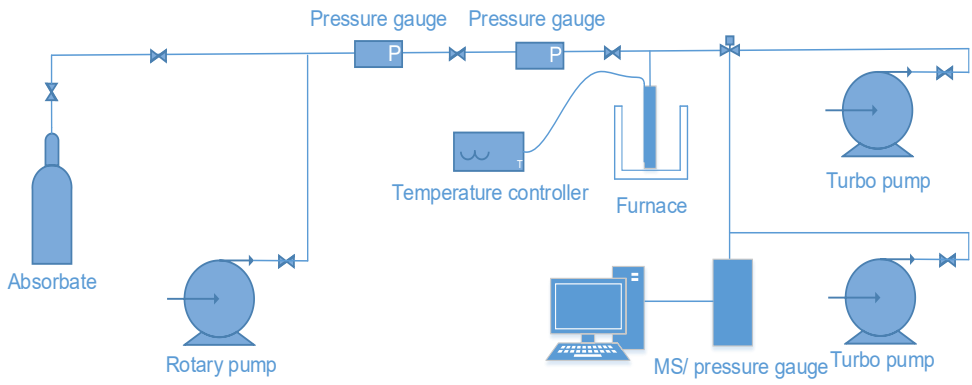

Figure 3.25 Schematic of TPD apparatus

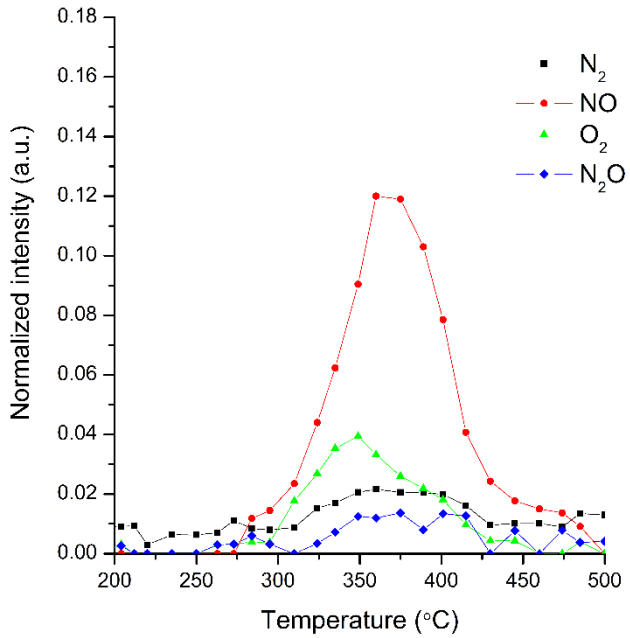

Figure 3.26 N_2O adsorption over Fe-FER (0.5 wt%) at 300 °C

The catalyst sample (100 mg) was loaded into the quartz tube which was evacuated in vacuum, followed by an activation at 550 °C for 1 h with a heating rate of 10 °C/min and was cooled to desired adsorption temperatures. For N_2O adsorption, N_2O was fed with a pressure of around 8 mbar at an adsorption temperature range of 250 °C to 350 °C. Subsequently, another evacuation was conducted to remove the additional adsorbate from the sample, and the adsorbed gases were desorbed by heating up the sample with a heating rate of 10 °C/min to 650 °C. The amount of desorbed gas was measured using the mass spectrometer and recorded for analysis. The

desorption of N_2O decomposition products over Fe-FER at 300 °C is shown in Fig. 3.26.

3.4.9 Thermal gravimetric analyses (TGA)

TGA is a thermoanalytical technique to study the weight loss of materials as a function of temperature in an oxidative, reactive or inert atmosphere, and hence the thermal stability or the composition of the sample can be estimated [22]. The mass loss can be attributed to multiple reasons, such as evaporation, decomposition and oxidation. The cause of mass loss can be distinguished by determining the emitting gas qualitatively and quantitatively during the temperature program using a Mass spectroscopy. Therefore, measurement of coke deposition in spent catalysts, where carbon formed due to the catalytic reactions, can be conducted by determining CO_2 emissions from the samples. In this study, analyses were performed in a Mettler Toledo TGA-DSC 1 STAR^e coupled with a ThermoStar Pfeiffer mass spectrometer. The spent catalyst was ground to fine powder, and around 10 mg sample was loaded in cylindrical alumina crucible with a height of 5 mm and an internal diameter of 4 mm. TGA analyses were performed in an air flow rate of 20 ml/min, with a heating rate of 5 °C/min from room temperature to 1000 °C. A TGA profile of spent Fe-ZSM-5 catalyst is shown in Fig. 3.27.

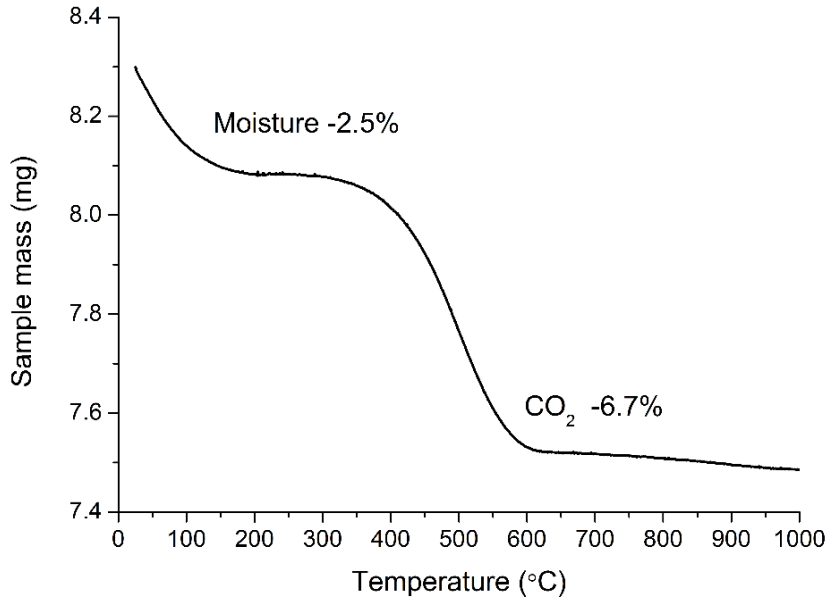

Figure 3.27 TGA profile of spent Fe-ZSM-5 catalyst (iron loading amount: 0.5 wt%, reaction temperature: 400°C)

3.4.10 Ultraviolet and visible spectroscopy (UV-vis spectroscopy)

UV-vis spectroscopy, which has been extensively used in identification of chemical substances, is a technique based on the measurement of absorption of incident light in a broad wavenumber range from UV (200 nm to 400 nm) to visible (400 nm to 800 nm) light by the sample. In the UV-vis spectra, the emerging bands and shoulders at given wavenumbers correspond to vibrational transitions which reflect the adsorption of energy from UV or visible light with different wavenumbers by the material [23]. The specific vibrations shown in the UV-vis spectra then can be used to analyze the compositional or structural features of the sample.

In this study, UV-Vis diffuse reflectance spectra were collected at ambient temperature on a Cary 5000 spectrophotometer equipped with a Praying Mantis attachment. $BaSO_4$ was used as a baseline and all samples were

ground into $BaSO_4$ prior to being analysed. Data was collected between 12500 cm^{-1} and 50000 cm^{-1} at a scan rate of 6000 cm^{-1}/min. The absorbance intensity was expressed using the Schuster-Kubelka-Munk function (1-R2)/(2R). A UV spectrum of Fe-FER catalyst is shown in Fig. 3.28.

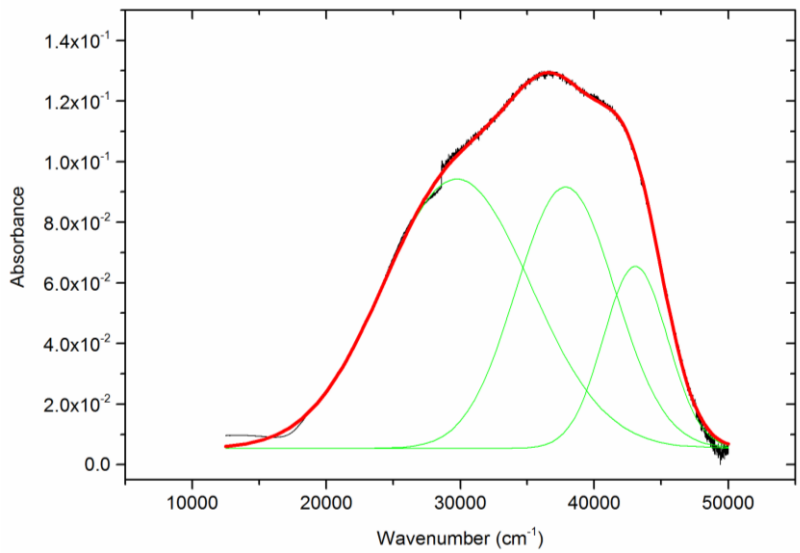

Figure 3.28 UV-vis spectrum of Fe-FER catalyst (0.5 wt%)

3.5 Reference

1. Delmon, B.; Jacobs, J.A.; Jacobs, P.A.; Poncelet, G. Preparation of Catalysts I: Scientific Bases for the Preparation of Heterogeneous Catalysts: Proceedings of the First International Symposium Held at the Solvay Research Centre, Brussels, Elsevier, **1975**.
2. Cabiac, A.; Delahay, G.; Durand, R.; Trens, P.; Coq, B.; Plée, D. Preparation of Pd/AC Catalyst by Ion Exchange, *Chem. Sustainable Dev.* **2006**, *14*, 553-558.
3. Abu-Zied, B.M.; Schwieger, W.; Unger, A. (2008). Nitrous oxide decomposition over transition metal exchanged ZSM-5 zeolites prepared by

the solid-state ion-exchange method. *Appl. Cata. B: Environ.* **2008**, *84*, 277-288.

4. Li, Y.; Armor, J.N. Ammoxidation of ethane: V. Solid-state ion exchange to prepare cobalt zeolite catalysts. *Applied Catalysis A: General*, **1999**, *188*, 211-217.
5. Karge, H.G. Solid-State Ion Exchange in Zeolites, Handbook of Heterogeneous Catalysis, Wiley-VCH Verlag GmbH & Co. KGaA. **2008**.
6. Dietz, W.A. Response factors for gas chromatographic analyses. *J. Chromatogr. Sci.* **1967**, *5*, 68-71.
7. Rabolt, J.F.; Burns, F.C.; Schlotter, N.E.; Swalen, J.D. Anisotropic orientation in molecular monolayers by infrared spectroscopy. *J. Chem. Phys.* **1983**, *78*, 946-952.
8. Harren, F.J.; Mandon, J.; Cristescu, S.M. Photoacoustic spectroscopy in trace gas monitoring. *Encyclopedia of Analytical Chemistry: Applications, Theory and Instrumentation*. **2006**.
9. Uvarov, V.L.A.D.I.M.I.R.; Popov, I. Metrological characterization of X-ray diffraction methods for determination of crystallite size in nano-scale materials. *Mater. Charact.* **2007***, 58*, 883-891.
10. Baskaran, S. *Structure and regulation of yeast glycogen synthase* (Doctoral dissertation). **2010**.
11. Goldstein, J. ed. Practical scanning electron microscopy: electron and ion microprobe analysis. Springer Science & Business Media. **2012**.
12. Williams, D.B.; Carter, C.B. The transmission electron microscope. In Transmission electron microscopy. Springer, Boston, MA. **1996**, 3-17.

13. Seaton, N.A.; Walton, J.P.R.B. A new analysis method for the determination of the pore size distribution of porous carbons from nitrogen adsorption measurements. *Carbon*, **1989**, *27*, 853-861.
14. Sing, K.S.W. Reporting physisorption data for gas/solid systems with special reference to the determination of surface area and porosity (Provisional). *Pure Appl. Chem.* 1982, *54*, 2201-2218.
15. Lohitharn, N.; Goodwin J.J.G. Impact of Cr, Mn and Zr addition on Fe Fischer–Tropsch synthesis catalysis: Investigation at the active site level using SSITKA. *J. Catal.* **2008**, *257*, 142-151.
16. Olesik, J.W. (1991). Elemental analysis using ICP-OES and ICP/MS. *Anal. Chem.* **1991**, *63*, 12-21.
17. Ghosh, S.; Prasanna, V.L.; Sowjanya, B.; Srivani, P.; Alagaraja, M.; Banji, D. Inductively coupled plasma–optical emission spectroscopy: a review. *Asian J. Pharm. Ana*. **2013**, *3*, 24-33.
18. Brito, J.L.; Laine, J.O.R.G.E. Reducibility of Ni-Mo/Al_2O_3 catalysts: a TPR study. *J. Catal.* **1993**, *139*, 540-550.
19. Baudot, C.; Tan, C.M.; Kong, J.C. FTIR spectroscopy as a tool for nano-material characterization. *Infrared Phys. Technol.* **2010**, *53*, 434-438.
20. Hunger, M.; Weitkamp, J. In situ IR, NMR, EPR, and UV/Vis spectroscopy: Tools for new insight into the mechanisms of heterogeneous catalysis. *Angew. Chem. Int. Ed.* **2001**, *40*, 2954-2971.
21. Lónyi, F.; Valyon, J. On the interpretation of the NH_3-TPD patterns of H-ZSM-5 and H-mordenite. *Micropor. Mesopor. Mat.* **2001**, *47*, 293-301.
22. Bottom, R. Thermogravimetric analysis principles and applications of thermal analysis, Blackwell Publishing Ltd, **2008**, 87-118.

23. Perkampus H.H. UV-VIS Spectroscopy and its Applications. Springer Science & Business Media. **2013**.

CHAPTER 4

4 DIRECT METHANE CONVERSION TO VALUE ADDED PRODUCTS BY N_2O OVER FE-ZSM-5 CATALYSTS

4.1 Introduction

The direct, catalytic partial oxidation of methane to value added products such as methanol, formaldehyde and DME have been paid extensive attention for many decades, and yet suffer from low selectivity and high cost due to severe reaction and process conditions [1-4]. Progress in research related to the use of methane monooxygenase (MMO) enzymes has inspired researches who are exploring biomimetic techniques for converting methane to desired products under mild conditions [5-7]. Among those activities, studies on catalytic partial oxidation of methane to value-added products by N_2O over Fe-ZSM-5 catalyst at low temperatures provides a promising approach [8, 9]. The generation of and subsequent reaction of so-called α-oxygen, readily developed at 200-250 °C in this process, can be used to convert methane to methanol at high selectivity and at low temperatures (normally less than 200 ℃) [10, 11]. However, at low temperature, methanol molecules generated tend to bind on the catalysts, and hence an extraction procedure is required to obtain the valuable product(s). As reported in previous studies, the rate of desorption of methanol molecules or methoxy groups is rate limited in the process and the regeneration of active sites on the catalysts is engendered by the migration of methanol molecules or methoxy groups to other surface site, which makes the reaction of methane conversion to methanol a quasicatalytic mode of reaction [7, 12, 13]. In addition, the additional extraction makes this process more complicated and challenging to apply in a commercial sense.

On the other hand, catalytic partial oxidation of methane conducted at elevated temperatures, which facilitates the desorption of methanol into gas phase, acts as a continuous mode reaction, but higher temperature (higher

than 400 ℃) tend to result in the deep oxidation of methanol to CO and CO_2 and decomposition of active oxygen species should be avoided in order to achieve reasonable methanol selectivities [14]. Therefore, study on catalytic partial oxidation of methane to value-added products at moderate temperatures to produce desired products continuously in gas phase is of fundamental and applied interest.

There are a relatively limited number of studies of the catalytic partial oxidation of methane by N_2O over Fe-ZSM-5 catalyst at temperature above 300 °C and the results obtained are somewhat controversial. The complete oxidation of methane at temperature above 250℃ was reported and low selectivities to methanol (less than 2.0%) was obtained [15]. Conversely, Panov and his co-workers showed the selectivity to methanol from catalytic partial oxidation of methane over Fe-ZSM-5 catalyst was ca. 25% ~30 % at 300°C with methane conversion at ca. 0.8% [13]. Further effort is necessary to examine the activity performance of direct methane conversion by N_2O over solid catalysts at moderate temperature.

Studies on the partial oxidation of methane over Fe-ZSM-5 catalysts at low temperatures are typically conducted at a fixed temperature. In this project, investigation of effect of temperature on the catalytic reaction was undertaken over the temperature range of 250 ℃ to 400 ℃ . Additionally, the effect of iron loading on the catalysts, feed gas composition and GHSV on methane conversion, N_2O decomposition and products selectivity was investigated, as the factors are necessary for the examination of feasibility of methane partial oxidation at moderate temperature, and are critical to obtain a better

understanding of the reaction mechanisms involved, and potentially beneficial to determine the appropriate reaction conditions for the process.

4.2 Experimental

4.2.1 Catalyst preparation

ZSM-5 (Si/Al=15) was purchased from Zeolyst and Fe $(NO_3)_3 \cdot 9H_2O$ (98%) was purchased from Sigma Aldrich. 0.1 wt%, 0.5 wt%, 1.0 wt% and 2.0 wt% of iron were incorporated with the ZSM-5 zeolite by incipient wetness method, and the pastes were dried at 110 °C overnight, followed by calcination at 550 °C for 5 hours at a heating rate of 3 °C/min. The powders were then pressed and sieved, and the particles with a diameter 250 μm to 425 μm were used as the catalysts for experiments.

4.2.2 Catalyst Characterization

Catalysts were characterized using various techniques. The surface area and pore volume and size of Fe-ZSM-5 catalysts with different iron loading amounts were measured by nitrogen adsorption. X-ray diffraction (XRD) measurements were conducted on Fe-ZSM-5 catalysts by a Phillips X'pert Pro diffractometer with Cu Kα incident radiation. A purpose built Temperature-programmed reduction (TPR) apparatus with a thermal conductivity detector was used for detection the reducibility of catalysts with various iron loading amounts. Mettler Toledo TGA-DSC 1 STAR^e coupled with a ThermoStar PFEIFFER mass spectrometer was employed for thermogravimetric analyses of spend Fe-ZSM-5 catalyst.

4.2.3 Catalytic activity test

Direct catalytic partial oxidation of methane by N_2O over a series of Fe-ZSM-5 catalysts was performed in a single-pass stainless steel tubular reactor in atmospheric pressure at a temperature range from 250 °C to 400 °C. In the feed gas, the ratio of He: CH_4: N_2O was 65:28:7, with a total gas hourly space velocity (GHSV) of 11000 h^{-1} and a total flow rate of 70 cm^3/min in the experiments unless stated otherwise. Various CH_4/N_2O ratios were investigated with the GHSV and flow rate of methane maintained, by adjusting the flow rates of He and N_2O to reach the different ratios of CH_4/N_2O without changing the GHSV. The effect of GHSV on the catalytic performance was investigated as well by adjusting the GHSV from 5500 h^{-1} to 28000 h^{-1}, the flow rates of methane and N_2O were maintained at 20 ml/min and 5 ml/min, respectively. The conversion of methane and N_2O was calculated based on determination of concentrations of methane and N_2O by a Varian micro-GC which contains Molsieve 5A and PoraPLOT Q (PPQ) columns. In the gaseous products, methanol, formaldehyde and dimethyl eithers (DME) were measured by a Fourier transform infrared spectroscopy (FTIR), while ethylene, CO and CO_2 were determined using a mirco GC.

4.3 Results and discussion

4.3.1 Catalytic partial oxidation of methane over Fe-ZSM-5 catalysts with various metal loading amounts

Fe-ZSM-5 catalysts with iron loading amounts of 0.1 wt%, 0.5 wt%, 1.0 wt% and 2.0 wt% were studied. As shown in Fig. 4.1, the XRD patterns of Fe-ZSM-5 catalysts with different iron loading showed that there was no apparent

change in crystal morphology observed, indicating that the zeolite crystal structure of all catalysts remained intact following iron loading and calcination. In addition, there were no extraneous reflections appearing in the XRD patterns of iron loaded zeolites, which is consistent with a good iron dispersion in the ZSM-5 zeolite [16, 17].

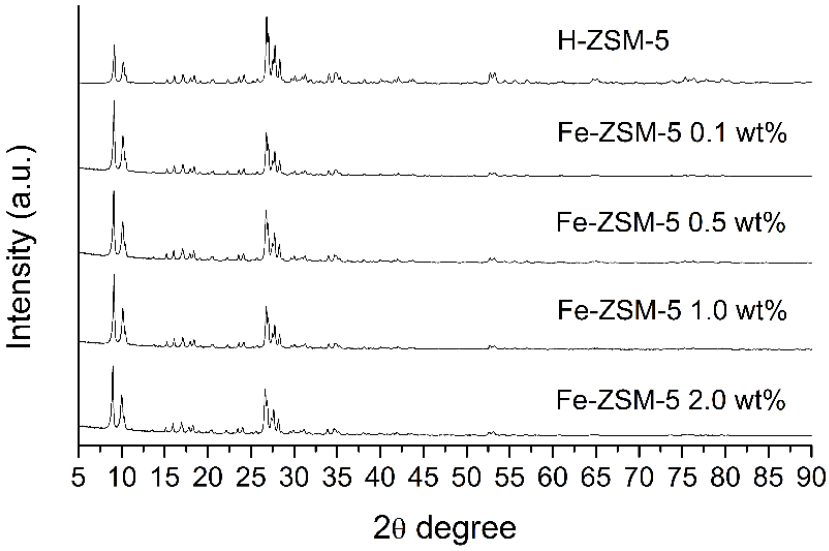

Figure 4.1 XRD patterns of H-ZSM-5 and Fe-ZSM-5 catalysts with iron loading amount of 0.1 wt%, 0.5 wt%, 1.0 wt% and 2.0 wt%

Table 4.1 Textual properties of H-ZSM-5 and Fe-ZSM-5 catalysts with different iron loading

	0 wt%	0.1 wt%	0.5 wt%	1.0 wt%	2.0 wt%
t-Plot micropore Area (m^2/g)	481.7	480.2	479.5	475.9	476.4
t-Plot micropore volume (cm^3/g)	0.11	0.11	0.11	0.11	0.11
Pore size (nm)	4.6	4.5	4.4	4.4	4.4

It is known that with increasing iron loading enhances the formation of iron oxides clusters and bulk particles, which block micropores in the zeolites [18, 19]. However, in this study the N_2 adsorption results as shown in Table 4.1 suggested that the loading of iron only led to a slight change in the textual properties of ZSM-5 zeolite, which may be due to the relatively low level of iron loading. The formed iron species over the Fe-ZSM-5 catalysts with various iron loading amounts were further investigated by H_2-TPR as shown in Fig. 4.2.

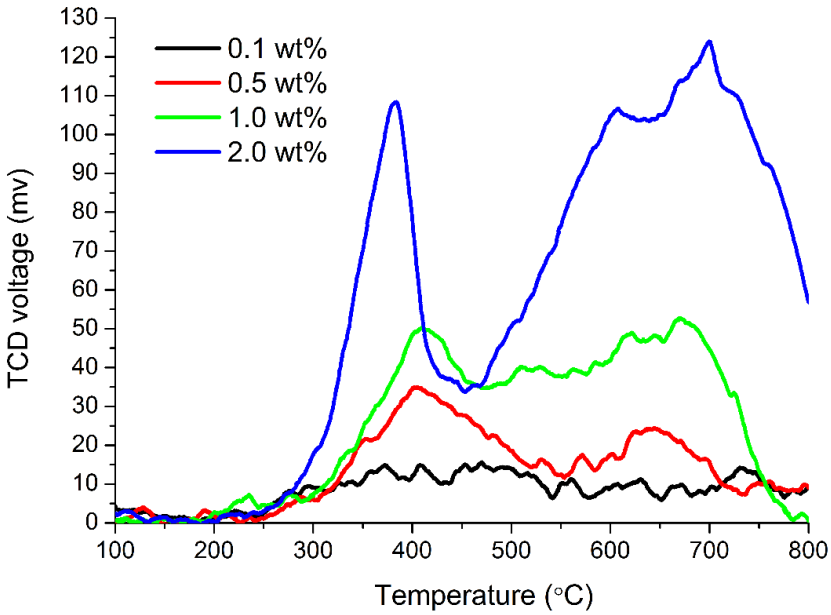

Figure 4.2 TPR profiles of Fe-ZSM-5 catalysts with iron loading amount of 0.1 wt%, 0.5 wt%, 1.0 wt% and 2.0 wt%

All the profiles showed nonspecific hydrogen consumption from 100 °C to 800 °C, indicating that various Fe species comprised in these catalysts. Two main hydrogen consumption peaks centred at around 400 °C and 650 °C were observed in all the profiles except in Fe-ZSM-5 catalyst with iron loading amount of 0.1 wt% due to the low amount of iron loading. The hydrogen

consumption peak at 400 °C is attributed to reduction of Fe_2O_3 to FeO or Fe_3O_4 [20], while the peak at higher temperatures is due to reduction of Fe^{2+} to Fe^0 [21]. The area of the hydrogen consumption peaks increased as the iron loading amount increasing from 0.1 wt% to 2.0 wt%, suggesting that higher iron loadings lead to the formation of Fe^{3+} species at elevated concentrations. In addition, and in comparison to Fe-ZSM-5 catalysts with iron loading amount of 0.5 wt%, the hydrogen reduction peak of Fe^{3+} to Fe^{2+} was observed at lower temperatures for Fe-ZSM-5 catalyst with iron loading amount of 2.0 wt%, which is in consistent with a previous report which indicated that more reducible Fe species were formed over Fe-ZSM-5 catalysts with higher iron loadings [22].

Catalytic partial oxidation of methane by N_2O over Fe-ZSM-5 catalysts with various Fe loading amounts was investigated at 400 °C, and the catalytic study results are shown in Fig. 4.3. H-ZSM-5 zeolite decompose N_2O and completely oxidize methane at 400 °C, which may be due to the presence of iron impurities on the zeolite. The addition of small amount of iron (0.1 wt%) on H-ZSM-5 zeolite enhances the level of methane conversion and N_2O decomposition remarkably. Methane conversion increased from 2.1% to 10.1% at a reaction time of 5 min after 0.1 wt% of iron was loaded on H-ZSM-5, and N_2O decomposition increased from 10.3% to 65.2%. Further increase of the iron loading amount to 2.0 wt% would increase methane conversion and N_2O decomposition gently as shown in Fig. 4.3.

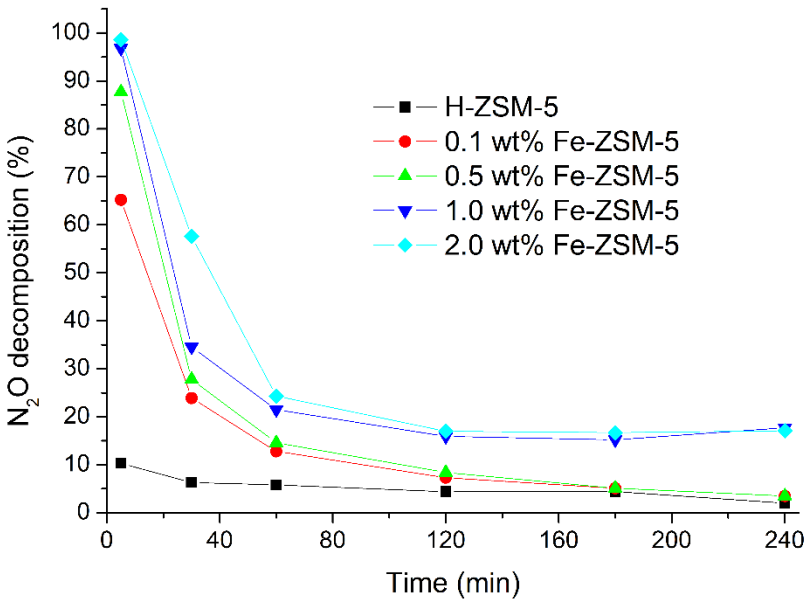

(a)

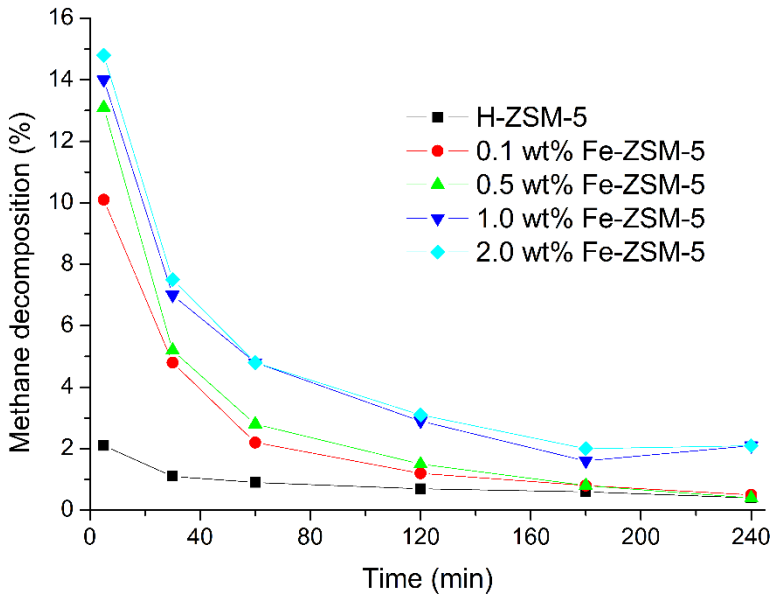

(b)

Figure 4.3 N_2O decomposition (a) and methane conversion (b) over catalysts with different Fe loading amounts at 400 °C

These results are in accordance with the observations published by other researchers, who reported that the active sites contained a small number of Fe atoms [23]. It has been suggested that the addition of a small amount of iron

on H-ZSM-5 zeolite results in the formation of iron species stabilized in the micropore of the zeolite, which were the unique active sites for N_2O decomposition [24]. N_2O decomposition on these iron species lead to the generation of active oxygen species, which subsequently react with methane. In addition, it was reported that extra-framework Fe species in the catalysts could be present as different forms, such as mono-, binuclear or oligonuclear cationic species, neutral iron oxide species with a varying degree of agglomeration and mixed oxide phases combining Fe and Al, and also bulk iron oxides on the external surface of ZSM-5 [25], but only mono-nuclear and binuclear iron species were proposed to be responsible for N_2O decomposition [10, 25, 26]. Higher Fe contents might lead to the formation of oligomeric clusters and particles of iron oxides because of lack of Al to anchor the Fe atoms [18, 19], and these iron species were not active for N_2O decomposition [25]. Therefore, it is conjectured that the increase of iron loading amount from 0.5 wt% to 2 wt% mainly leads to the formation of non-active sites and hence did noes improve the catalytic performance significantly.

In addition, it should be noted that upon all of the catalysts, both methane conversion and N_2O decomposition decreased over reaction time. It was reported that the deactivation of catalysts occurred because of coke formation on the catalysts surface [27]. The carbon balance within these experiments was estimated and the results are shown in Fig. 4.4. The poor carbon balance in the initial stage suggested that coke was formed when methane and N_2O were exposure to the zeolites.

Coke formation over Fe-ZSM-5 catalyst was further analysed by TGA-MS measurement of spent Fe-ZSM-5 catalyst. As shown in Fig. 4.5, the weight

loss in the temperature range of 25–200 ℃ and 250–600 ℃ which respectively represents mass loss due to the release of water and CO_2, were observed over Fe-ZSM-5 catalyst. The results confirmed the formation of coke on the catalyst, which may form via the transformation of methoxy groups or methanol over Fe-ZSM-5 catalysts to DME, ethylene, and aromatics which finally lead to carbon deposition [28, 29].

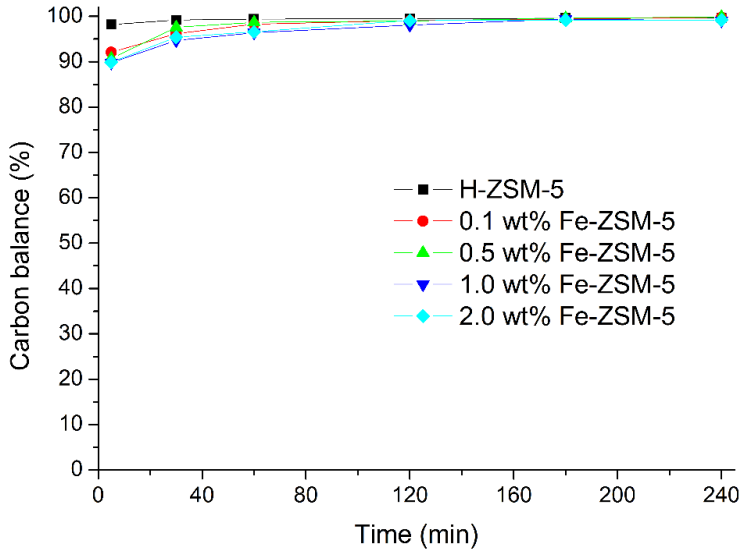

Figure 4.4 Carbon balance within Fe-ZSM-5 catalysts with various iron loading amounts over reaction time (reaction temperature: 400°C)

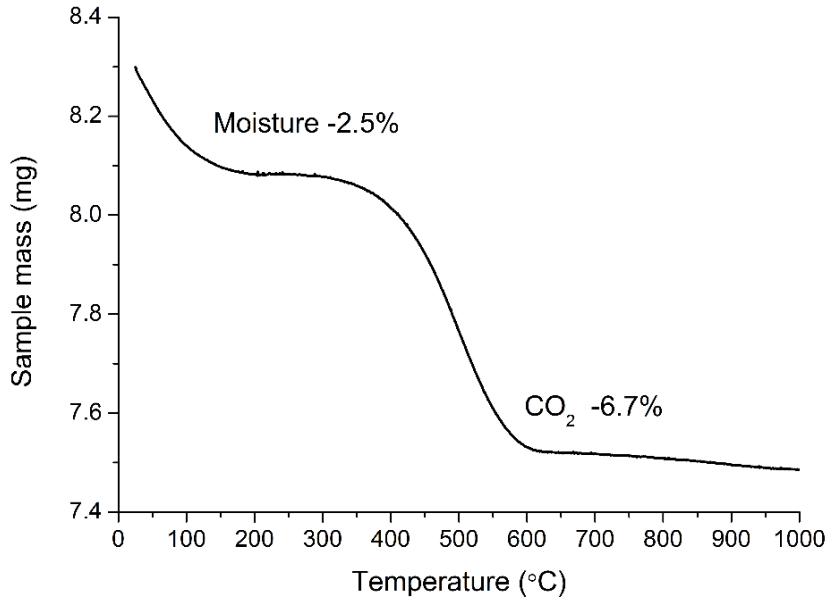

Figure 4.5 TGA profile of spent Fe-ZSM-5 catalyst (iron loading amount: 0.5 wt%, reaction temperature: 400°C)

The generation of reaction products was analysed and the results are shown in Fig. 4.6. All the data obtained following an average of 4 h reaction (from 60 min to 240 min). The result highlight that ethylene was the primary product which comprised 69.7% of all products over the H-ZSM-5 zeolite. Selectivity to C_1-oxygenates and carbon oxides was 1.5% and 28.7%, respectively. Addition of 0.1 wt% iron to the H-ZSM-5 zeolite enhanced the C_1-oxygenates selectivity to 4.2%, while the selectivity to carbon oxides increased to 54.3%, and the selectivity to ethylene dropped to 41.6%. The results show that methanol and formaldehyde were produced from reaction between methane and N_2O over Fe-ZSM-5 and H-ZSM-5 zeolites at moderate temperatures. The fact that addition of small amount of iron increased selectivity to C_1-oxygenates indicated that iron is critical for forming the active sites to active methane and form methanol.

It should be noted that, in all the experiments, ethylene was a product, especially over catalysts with low iron contents. The generation of ethylene might be due to the MTO (methanol-to-olefin) reaction [27, 30]:

$$2CH_3OH \rightarrow CH_3OCH_3 + H_2O \quad (1)$$

$$CH_3OCH_3 \rightarrow CH_2CH_2 + H_2O \quad (2)$$

It is suggested that the atomic oxygen in α–oxygen converted methane to methanol, which was subsequently dehydrated to DME and ethylene. It was reported that protonic sites and crystallites of catalysts were the keys to the reaction [31, 32]. In addition, a further increase in iron loading results in higher selectivity of carbon oxides but lower selectivity of C_1-oxygenates and ethylene, as shown in Fig. 4.6. The results agree with others who also reported that high iron content on catalysts tend to form bulky clusters iron species, and these iron species contribute to complete oxidation of benzene and its product phenol [25]. It was demonstrated that different forms of iron were present on the zeolites and that an increase in the loading changed the composition of iron species, which were responsible for the formation of different reaction products [33]. In this study, it is concluded that an increase in iron loading led to generation of oligomeric Fe clusters and bulk iron oxides which were not active sites for α–oxygen formation but resulted in the further oxidation of valuable products to carbon oxides.

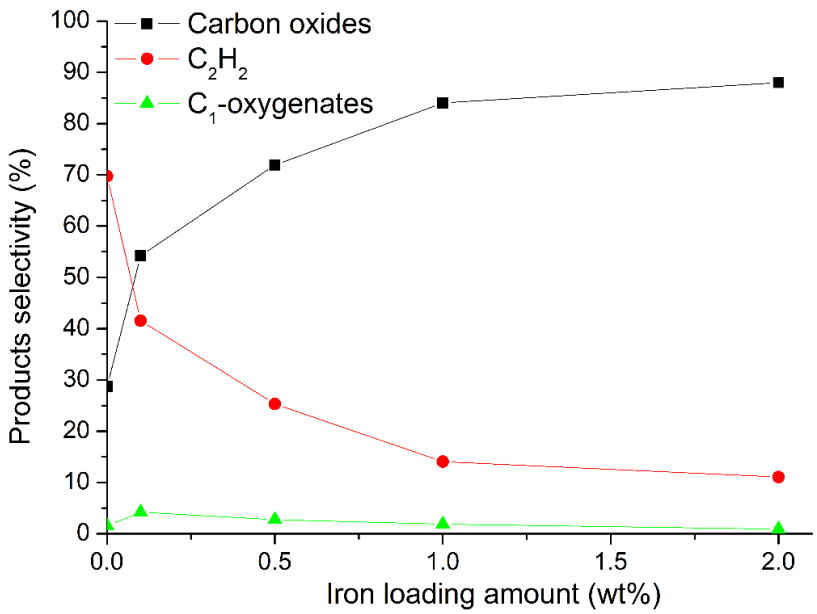

Figure 4.6 Products selectivity over Fe-ZSM-5 catalysts with various iron loading (reaction temperature: 400°C)

4.3.2 Effect of temperature on methane conversion and products generation

Methane conversion and N_2O decomposition over Fe-ZSM-5 catalyst with iron loading amount of 0.5 wt% were investigated at a temperatures range from 250°C to 400°C, and the results are shown in Fig. 4.7 and Fig. 4.8. As shown in Fig. 4.7, as temperature increased from 250°C to 400°C, the average methane conversion in a 4 h reaction (from 60 min to 240 min) increased from 0.3% to 1.4%, and the average N_2O decomposition increased from 2.8% to 7.7%. Product compositions under various temperatures were analysed as well and are shown in Fig. 4.8. At 250 ℃ , methanol and formaldehyde were not detected, presumably because methanol and formaldehyde bond strongly with Fe-ZSM-5 catalyst at this temperature, while carbon oxides and ethylene are released and detected as the primary products at 250 ℃ . At 300 ℃ ,

methanol and formaldehyde with selectivities of 5.7% and 1.9% were observed. The selectivity of ethylene and C_1-oxygenates decreased with the further increase of reaction temperature, while carbon oxides selectivity increased with temperature, and were the main products when the reaction temperature reached 400 °C. Under these conditions, over 70% of the products were carbon oxides. The results demonstrate that higher temperatures promote methane conversion by mean of complete oxidation over Fe-ZSM-5 catalysts. The effect of temperature on methoxy groups generation over Fe/Al-MFI was investigated using IR spectra, and it was found that the pair of bands assigned to methoxy groups decreased in intensity at higher temperature, and deep oxidation of surface methoxy groups was suggested to be the reason [19]. Therefore, relatively low temperature is suggested for obtaining high selectivity of methanol and formaldehyde.

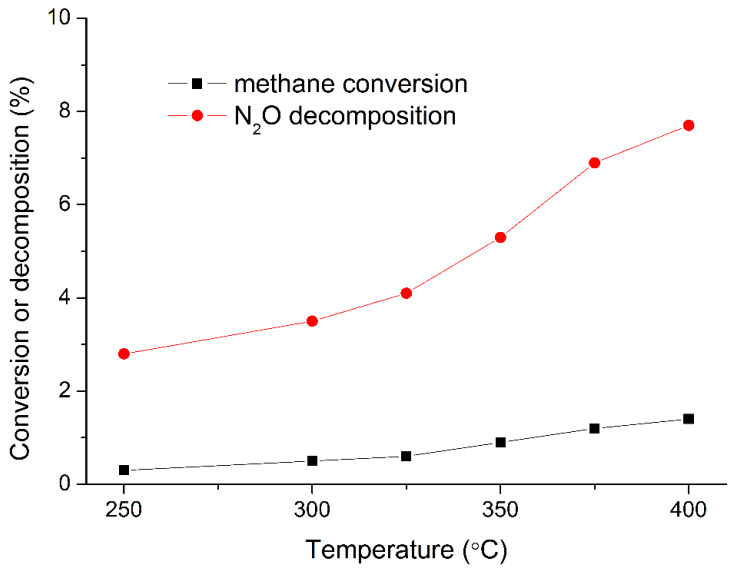

Figure 4.7 Catalytic partial oxidation of methane over Fe-ZSM-5 catalyst at various temperatures (iron loading amount: 0.5 wt%)

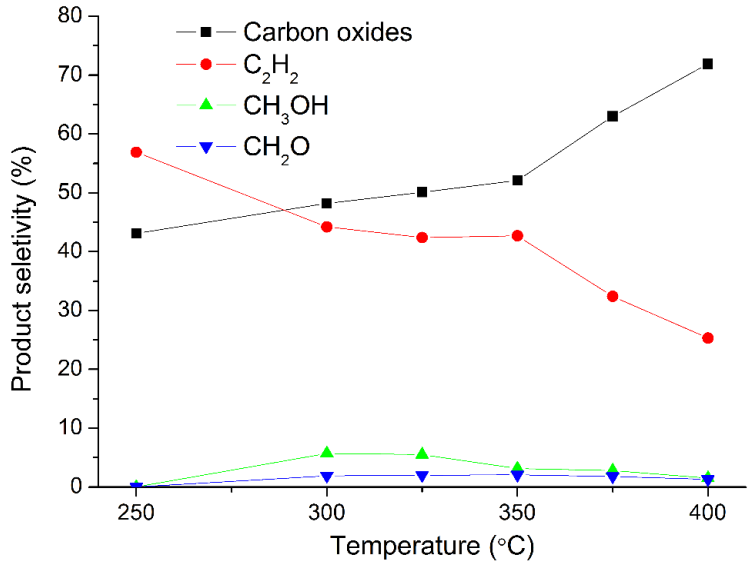

Figure 4.8 Products selectivity over Fe-ZSM-5 catalyst at various temperatures (iron loading amount: 0.5 wt%)

4.3.3 Effect of feed gas ratio on methane conversion and products generation

Methane conversion and N_2O decomposition and products selectivity over Fe-ZSM-5 catalyst with iron loading amount of 0.5 wt% at 400 °C were studied with different CH_4/N_2O ratios and the results are presented in Fig. 4.9 and Fig. 4.10. The flow rate of methane was maintained at 20 ml/min, the flow rate of N_2O was adjusted to reach desired CH_4/N_2O ratios, and the total flow rate was maintained at 70 ml/min by adjusting flow rate of helium. The conversion of N_2O and methane were determined and shown in Fig. 4.10. As the increase of CH_4/N_2O ratio from 4 to 12, average quantity of N_2O consumed decreased from 5390 ppm/min to 2570 ppm/min, while average amount of methane conversion showed a less remarkable decline from 3920 ppm/min to 2240 ppm/min. The resulted indicated that N_2O was the oxidant to generate active oxygen species for catalytic partial oxidation of methane, and hence methane

conversion decrease as lack of N_2O. In addition, the consumption of N_2O is elevated with respect to extent of methane conversion at all CH_4/N_2O ratios, indicating that self-decomposition of active oxygen species occurs, more dominantly at low CH_4/N_2O ratio as the more noticeable decrease in N_2O conversion amount in comparison to methane conversion amount was observed under these conditions as shown in Fig. 4.9.

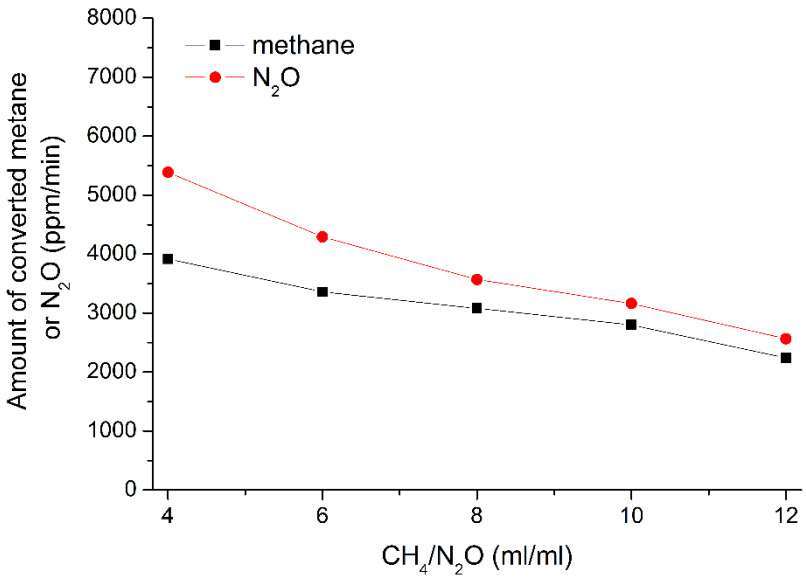

Figure 4.9 Amount of conversion of methane and N_2O over Fe-ZSM-5 catalyst with different CH_4/N_2O ratios (iron loading amount: 0.5 wt%, reaction temperature: 400°C)

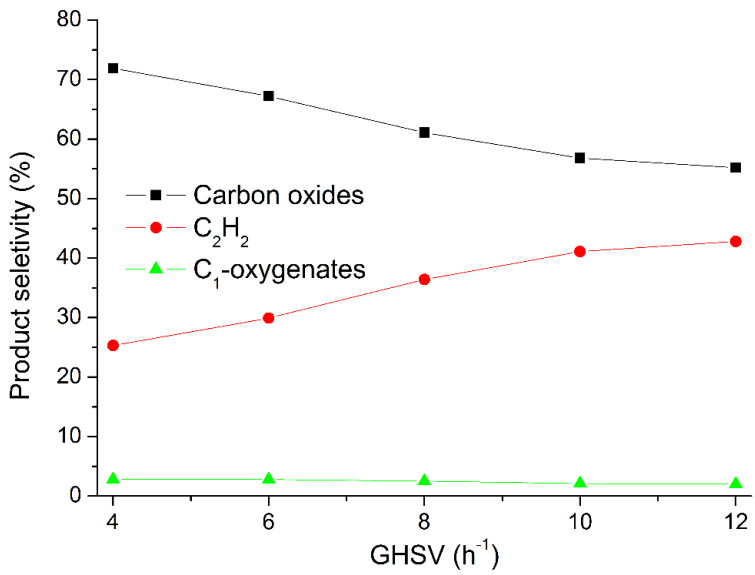

Figure 4.10 Products selectivity over Fe-ZSM-5 catalyst with different CH_4/N_2O ratios (iron loading amount: 0.5 wt%, reaction temperature: 400 °C)

As shown in Fig. 4.10, with an increase in the CH_4/N_2O ratio, selectivity of both carbon oxides and C_1-oxygenates decreased, which could be attributed to lack of oxidant since carbon oxides and C_1-oxygenates are products from catalytic partial oxidation of methane. Conversely, the selectivity of ethylene showed an opposite trend, which increased from 25.3% to 42.8% as the increase of CH_4/N_2O ratio from 4 to 12. The results indicated that ethylene was the product from dehydration of methanol, which was favorable when the concentration of oxidant was reduced.

4.3.4 Effect of feed gas GHSV on methane conversion and products generation.

The effect of GHSV on catalytic activity over Fe-ZSM-5 catalyst with iron loading amount of 0.5 wt% was investigated as shown in Fig. 4. 11.

With the increase of GHSV from 5500 h^{-1} to 28000 h^{-1}, the conversion of methane decreased from 2.0% to 0.9%, and decomposition of N_2O decreased from 12.0% to 5.7%. As shown in Fig. 4.12, an increase of GHSV impacted the selectivity of various products in different ways. The selectivity to carbon oxides decreased, while ethylene and C_1-oxygenates selectivity showed opposite trend with an increase of GHSV. The results are consistent with previous studies [34], which reported lower selectivity to methanol and higher selectivity to carbon dioxide when the contact time between Fe-ZSM-5 catalyst and mixture of methane and oxygen was extended.

It appears an increase in contact time, by using smaller GHSV, would be beneficial of oxidation of methane and intermediates, which resulted in higher methane conversion and carbon oxides selectivity. For obtaining elevated selectivity to desired products, a relatively larger GHSV is suggested but this requires increased amount of catalyst which in turn would lead to higher capital costs.

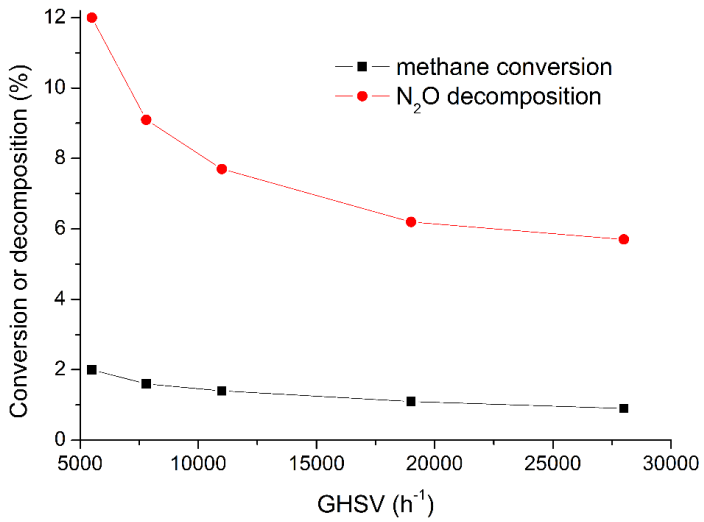

Figure 4.11 Methane conversion and N_2O decomposition over Fe-ZSM-5 catalyst with different GHSV (iron loading amount: 0.5 wt%, reaction temperature: 400 °C)

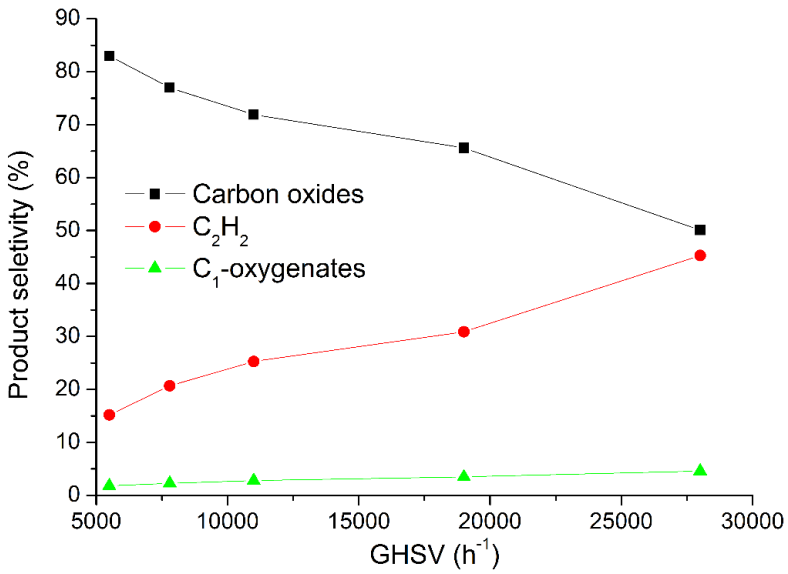

Figure 4.12 Products selectivity over Fe-ZSM-5 catalyst with different GHSV (iron loading amount: 0.5 wt%, reaction temperature: 400 °C)

4.4 Summary

Catalytic partial oxidation of methane by N_2O over Fe-ZSM-5 catalysts at moderate temperatures was investigated. Methanol and formaldehyde were

detected in the gas phase from catalytic partial oxidation of methane over H-ZSM-5 at 400 ℃ , and the loading of iron on ZSM-5 generates more active sites, which promote N_2O decomposition and methane conversion. A small amount of iron loading (0.1 wt%) was able to enhance the generation of C_1-oxygenates, while higher concentrations of iron on ZSM-5 would lead to complete oxidation of methane and enhance the generation of carbon oxides. Ethylene was shown to be one of the main products, especially when iron loading amount was low. The generation of ethylene appears to be result of methanol dehydration.

With an increase in reaction temperature, the extent of methane and N_2O reaction was enhanced, and carbon oxides selectivity increased while concomitantly, the selectivity to C_1-oxygenates and ethylene declined. An increase in the input CH_4/N_2O ratio increased the conversion of N_2O and subsequently leads to a decline in the selectivity to C_1-oxygenates and carbon oxides, but ethylene displayed an opposite trend, which indicates that the pathways of ethylene and carbon oxides generation from methanol are competing, with the generation of ethylene enhanced with a reduction in the feed concentration of N_2O. An increase in GHSV reduces the contact time of catalyst with gaseous reactants and reduces the rate of complete oxidation of intermediates, and hence is beneficial of methanol and formaldehyde generation.

4.5 Reference

1. Bendtsen, A.B.; Glarborg, P.; Dam-Johansen, K.I.M. Low temperature oxidation of methane: the influence of nitrogen oxides. *Combust. Sci.Technol.* **2000**, *151*, 31-71.

2. Arutyunov, V.S.; Strekova, L.N. The interplay of catalytic and gas-phase stages at oxidative conversion of methane: A review. *J. Mol. Catal. A: Chem.* **2017**, *426*, 326-342.

3. Holmen, A. Direct conversion of methane to fuels and chemicals. *Catal. Today* **2009**, *142*, 2-8.

4. da Silva, M. J. Synthesis of methanol from methane: Challenges and advances on the multi-step (syngas) and one-step routes (DMTM). *Fuel Process. Technol.* **2016**, *145*, 42-61.

5. Xu, J.; Zheng, A.; Wang, X.; Qi, G.; Su, J.; Du, J.; Gan, Z.; Wu, J.; Wang, W.; Deng, F. Room temperature activation of methane over Zn modified H-ZSM-5 zeolites: Insight from solid-state NMR and theoretical calculations. Chem. Sci. **2012**, *3*, 2932.

6. Wang, B.; Albarracín-Suazo, S.; Pagán-Torres, Y.; Nikolla, E., Advances in methane conversion processes. *Catal. Today* **2017**, *285*, 147-158.

7. Starokon, E. V.; Parfenov, M. V.; Arzumanov, S. S.; Pirutko, L. V.; Stepanov, A. G.; Panov, G. I., Oxidation of methane to methanol on the surface of FeZSM-5 zeolite. *J. Catal.* **2013**, *300*, 47-54.

8. Starokon, E.V.; Parfenov, M.V.; Pirutko, L.V.; Abornev, S.I.; Panov, G.I. Room-Temperature Oxidation of Methane by α-Oxygen and Extraction of Products from the FeZSM-5 Surface. *J. Phys. Chem. C* **2011**, *115*, 2155-2161.

9. Pirutko, L. V.; Chernyavsky, V. S.; Starokon, E. V.; Ivanov, A. A.; Kharitonov, A. S.; Panov, G. I., The role of α-sites in N_2O decomposition over FeZSM-5. Comparison with the oxidation of benzene to phenol. *Appl. Catal. B: Environ.* **2009**, *91*, 174-179.

10. Dubkov, K.A.; Ovanesyan, N.S.; Shteinman, A.A.; Starokon, E.V.; Panov, G.I. Evolution of Iron States and Formation of α-Sites upon Activation of Fe-ZSM-5 Zeolites. *J. Catal.* **2002**, *207*, 341-352.

11. Panov, G.; Dubkov, K.; Starokon, E., Active oxygen in selective oxidation catalysis. *Catal. Today* **2006**, *117*, 148-155.

12. Ravi, M.; Ranocchiari, M.; van Bokhoven, J. A., The Direct Catalytic Oxidation of Methane to Methanol-A Critical Assessment. *Angew. Chem. Int. Ed. Engl.* **2017**, *56*, 16464-16483.

13. Parfenov, M.V.; Starokon, E.V.; Pirutko, L.V.; Panov, G.I. Quasicatalytic and catalytic oxidation of methane to methanol by nitrous oxide over FeZSM-5 zeolite. *J. Catal.* **2014**, *318*, 14-21.

14. Nobukawa, T.; Sugawara, K.; Okumura, K.; Tomishige, K.; Kunimori, K. Role of active oxygen transients in selective catalytic reduction of N_2O with CH_4 over Fe-zeolite catalysts. *Appl. Catal. B: Environ.* **2007**, *70*, 342-352.

15. Wood, B.R.; Reimer, J.A.; Bell, A.T.; Janicke, M.T.; Ott, K.C. Methanol formation on Fe/Al-MFI via the oxidation of methane by nitrous oxide. *J. Catal.* **2004**, *225*, 300-306.

16. Pérez-Ramírez, J.; Groen, J.C.; Brückner, A.; Kumar, M.S.; Bentrup, U.; Debbagh, M.N.; Villaescusa, L.A. Evolution of isomorphously substituted iron zeolites during activation: comparison of Fe-beta and Fe-ZSM-5. . *J. Catal.* **2005**, *232*, 318-334.

17. Abdelsayed, V.; Shekhawat, D.; Smith, M.W. Effect of Fe and Zn promoters on Mo/HZSM-5 catalyst for methane dehydroaromatization. *Fuel* **2015**, *139*, 401-410.

18. Schwidder, M.; Kumar, M.; Klementiev, K.; Pohl, M.; Bruckner, A.; Grunert, W. Selective reduction of NO with Fe-ZSM-5 catalysts of low Fe contentI. Relations between active site structure and catalytic performance. *J. Catal.* **2005**, *231*, 314-330.

19. Wood, B.R.; Reimer, J.A.; Bell, A.T.; Janicke, M.T.; Ott, K.C. Methanol formation on Fe/Al-MFI via the oxidation of methane by nitrous oxide. *J. Catal.* **2004**, *225*, 300-306.

20. Qi, G.; Yang, R.T. Ultra-active Fe/ZSM-5 catalyst for selective catalytic reduction of nitric oxide with ammonia. *Appl. Catal. B: Environ.* **2005**, *60*, 13-22.

21. Guzmán-Vargas, A.; Delahay, G.; Coq, B. Catalytic decomposition of N_2O and catalytic reduction of N_2O and N_2O + NO by NH_3 in the presence of O_2 over Fe-zeolite. *Appl. Catal. B: Environ.* **2003**, *42*, 369–379.

22. Kameoka, S.; Nobukawa, T.; Tanaka, S.I.; Ito, S.I.; Tomishige, K.; Kunimori, K. Reaction between N_2O and CH_4 over Fe ion-exchanged BEA zeolite catalyst: A possible role of nascent oxygen transients from N_2O. *Phys. Chem. Chem. Phys.* **2003**, *5*, 3328-3333.

23. Zecchina, A.; Rivallan, M.; Berlier, G.; Lamberti, C.; Ricchiardi, G. Structure and nuclearity of active sites in Fe-zeolites: comparison with iron sites in enzymes and homogeneous catalysts. *Phys. Chem. Chem. Phys.* **2007**, *9*, 3483-99.

24. Parfenov, M.V.; Starokon, E.V.; Semikolenov, S.V.; Panov, G.I. O_2 isotopic exchange in the presence of O− anion radicals on the Fe-ZSM-5 surface. *J. Catal.* **2009**, *263*, 173-180.

25. Sun, K.; Xia, H.; Feng, Z.; van Santen, R.; Hensen, E.; Li, C. Active sites in Fe/ZSM-5 for nitrous oxide decomposition and benzene hydroxylation with nitrous oxide. *J. Catal.* **2008**, *254*, 383-396.

26. Yakovlev, A.L.; Zhidomirov, G.M.; van Santen, R.A. DFT Calculations on N_2O Decomposition by Binuclear Fe Complexes in Fe-ZSM-5. *J. Phys. Chem. B* **2001**, *105*, 12297-12302.

27. Khadzhiev, S.N.; Kolesnichenko, N.V.; Ezhova, N.N. Manufacturing of lower olefins from natural gas through methanol and its derivatives (review). *Petrol. Chem.* **2008**, *48*, 325-334.

28. Chen, D.; Moljord, K.; Holmen, A. A methanol to olefins review: Diffusion, coke formation and deactivation on SAPO type catalysts. *Micropor. Mesopor. Mat.* **2012**, *164*, 239-250.

29. Spencer, N. D. Partial oxidation of methane to formaldehyde by means of molecular oxygen. *J. Catal.* **1988**, *109*, 187-197.

30. Khadzhiev, S.N.; Magomedova, M.V.; Peresypkina, E.G. Mechanism of olefin synthesis from methanol and dimethyl ether over zeolite catalysts: A review. *Petrol. Chem.* **2014**, *54*, 245-269.

31. Sazama, P.; Sathu, N.K.; Tabor, E.; Wichterlová, B. Sklenák, Š.; Sobalík, Z. Structure and critical function of Fe and acid sites in Fe-ZSM-5 in propane oxidative dehydrogenation with N_2O and N_2O decomposition. *J. Catal.* **2013**, *299*, 188–203.

32. Chow, Y.K.; Dummer, N.F.; Carter, J.H.; Meyer, R.J.; Armstrong, R.D.; Williams, C.; Shaw, G.; Yacob, S.; Bhasin, M.M.; Willock, D.J.; Taylor, S.H.A. Kinetic Study of Methane Partial Oxidation over Fe-ZSM-5 Using N_2O as an Oxidant. *Chem. Phys. Chem.* **2018**, *19*, 402-411.

33. Ates, A.; Hardacre, C.; Goguet, A., Oxidative dehydrogenation of propane with N_2O over Fe-ZSM-5 and Fe–SiO_2: Influence of the iron species and acid sites. *Appl. Catal. A: Gen.* **2012**, *441-442*, 30-41.

34. Michalkiewicz, B. Kinetics of partial methane oxidation process over the Fe-ZSM-5 catalysts. *Chem. Pap.* **2005**, *59*, 403-408.

CHAPTER 5

5 COMPARISON OF DIRECT, SELECTIVE OXIDATION OF METHANE BY N_2O OVER FE-ZSM-5, FE-BETA AND FE-FER CATALYSTS

Introduction

Improvement of methane conversion and desired products selectivity has been the most critical target of study on direct methane conversion [1-5]. Among those factors that affect the catalytic performance of catalysts, zeolite structure plays an important role in the formation of Fe species, which in turn governs the methane conversion and products generation [6-8].

In addition to the extensive studies on hydrocarbons conversion by N_2O at low temperature have been performed over the MFI zeolite, researchers have explored the catalytic performance of other zeolites. Fe incorporated on TS-1 was reported to present contain active sites which decompose N_2O and convert benzene to phenol [9]. Fe-Al_2O_3 was proved to be able to remove N_2O and convert methane simultaneously [10, 11]. In addition, Beta zeolite is recognised as an attractive host for incorporating iron as previous works suggested that Fe-Beta presented higher activity with respect to Fe-ZSM-5 for N_2O decomposition, because two Fe(II) cations were successfully accommodated in two adjacent six-membered rings in the eight-membered ring channel (β sites) of Beta zeolite [12], while the geometrical arrangement of the cationic positions in Fe-ZSM-5 was reported to be quite different and less suitable for N_2O decomposition [6, 12, 13]. Ferrierite (FER) zeolite is suggested as another alternative of ZSM-5, since the N_2O decomposition over Fe-FER was reported to be times higher than that over Fe-ZSM-5. It was asserted that there was local structure with two β adjacent sites in the eight-member ring within FER zeolite, where the anchored Fe-Fe distance was calculated to be comparable to the length of N_2O molecular [7], the unique arrangement of the two Fe ions is favorable for N_2O splitting [12, 14, 15].

Even though the evidence proving better catalytic performance of Fe-Beta and Fe-FER zeolites on N_2O decomposition in comparison to Fe-ZSM-5 [6, 14], the application of iron incorporated Beta and FER zeolites for catalytic partial oxidation of methane by N_2O is rarely conducted and will be evaluated in this study.

Furthermore, the structure properties of zeolites are correlated to the active sites, which attract much attention and have been extensively studied. There are various characterization techniques aiming to analyse the nature of iron species over catalysts including XRD, EXAFS, XANES, Mossbauer spectroscopy, *in situ* FTIR, H_2-TPR, UV-vis spectroscopy, NH_3-TPD, etc. [7, 16-20]. However, the detailed structure of iron active sites is still controversial. Basing on the significant studies, researchers tend to agree that the active sites in iron-base catalysts for N_2O decomposition are binuclear or paired arranged mononuclear iron species locating at extra-framework, which are similar to the active sites of soluble methane mono-oxygenates [21-23]. Additional to the study aiming for clarifying nature of active sites, quantitative comparison of active sites formed in different circumstances is another attractive research area, which can be conducted by using a variety of characterization techniques with employment of probes. For example, NO adsorption on the active sites leads to the appearance of a band at 1874 cm^{-1} with a shoulder at 1892 cm^{-1} in FTIR spectra, which is a convenient approach to estimate the amount of active sites [18, 24]. N_2O can be used to pre-treat the catalysts to form α-oxygen species, which are reduced by H_2 in a H_2-TPR and hence a hydrogen consumption peak would be observed

and the peak area was reported to be correlated to the amount of active sites [6, 25].

In this study, catalytic partial oxidation of methane by N_2O over Fe-based catalysts were conducted in a continuous mode of operation at moderate temperatures (350 °C). Fe was incorporated into ZSM-5, Beta and FER frameworks, respectively, in order to obtain different Fe species. Effort was then made to correlate the nature of the Fe species within different catalysts with the catalytic activity in terms of methane and N_2O conversion and product selectivity. *In situ* FTIR, H_2-TPR, nitrogen adsorption, CO chemisorption and TGA-MS were employed to determine the nature and distribution of Fe in the catalysts, in an effort to explain the differing catalytic performance of catalysts.

5.2 Experimental

5.2.1 Catalysts preparation

The Fe-ZSM-5, Fe-Beta, and Fe-FER catalysts used in this study were prepared by incipient wetness impregnation technique. The parent NH_4-ZSM-5, NH_4-Beta, NH_4-FER with Si/Al ratios of 15, 12.5 and 10 were purchased from Zeolyst. $Fe(NO_3)_3 \cdot 9H_2O$ supplied by Sigma-Aldrich was weighed firstly according to the desired concentration of iron (2.0 wt%), and was dissolved in distilled water. The iron salt solution was then impregnated onto zeolites under ambient conditions. The well-mixed paste then was transferred to a crucible and dried for 2 hours and then calcined at 550 °C for 5 hours at a heating rate of 3 °C/min. The catalyst was then pressed and sieved, and the particles

within the size range of 250 μm to 425 μm were chosen to be used in the reaction.

5.2.2 Catalysts testing

Catalyst testing was performed in a fix-bed stainless steel tube reactor. 200 mg (unless stated elsewhere) catalyst was held in place by two quartz wool plugs and was activated in a flow of helium at a heating rate of 3 °C/min to 550 °C and was held at 550 °C for 3 h. The reaction was conducted at 350 °C with helium, methane and nitrous oxide being fed at a ratio of 65:28:7. The products were analysed using an online gas chromatography (Varian 490-GC) and a FTIR (Shimadzu IRPrestige21). The GC was equipped with a Molsieve column to detect CH_4 and CO, and a PoraPLOT Q (PPQ) column to detect N_2O, CO_2 and C_2H_4, while the FTIR was used to measure methanol, formaldehyde and dimethyl either (DME).

5.2.3 Catalysts characterization

Surface area and micropore analysis was performed at 77 K using a Micromeritics TriStar unit. The micropore volumes and micropore areas were measured using *t*-plot and Barrett-Joyner-Halenda (BJH) models. The Fe dispersion of the Fe-ZSM-5, Fe-Beta and Fe-FER catalysts was measured by volumetric chemisorption and the total amount of CO adsorbed on the catalysts were calculated applying the ideal gas law. In order to determine the Fe concentration of catalysts, analyses using an Inductively Coupled Plasma Atomic Emission Spectroscopy (ICP-AES) (Varian 715-ES) were performed. The temperature-programmed-reduction (TPR) experiments were carried out using a custom-built instrument equipped with a thermal conductivity detector

for hydrogen measurement to investigate the reducibility of catalyst. Prior to the H_2-TPR analysis, 300 mg of catalyst was placed in a quartz micro-reactor located in a furnace, and purged in a stream of air or helium (30 ml/min) at 450 °C for 1 h. Reduction by hydrogen was carried out in a H_2/Ar stream (2.04 vol% of H_2), with a total flow rate of 50 ml/min and a linear heating rate of 10 °C /min in the temperature range of 20–800 °C. N_2O pre-treatment, if employed, was performed at 250 °C on the dehydrated zeolites with a N_2O flow rate of 30 ml/min for 30 min, and then cooled to room temperature, prior to reduction by the H_2/Ar stream. Infrared spectra were recorded using a Bruker Tensor 27 FTIR equipped with an MCT detector. For NH_3 adsorption experiments, the FTIR spectra were monitored 150 ℃ after adsorption of NH_3 (10 mbar). For NO adsorption experiments, the FTIR spectra were monitored at 150 ℃ after adsorption of NO ($5e^{-2}$ mbar), while for CH_4/N_2O adsorption experiments, the sample was exposed to CH_4 (5 mbar) first and then was exposed to N_2O (from 2 mbar to 15 mbar), FTIR spectra were monitored at 350 ℃ . For interaction of methanol with catalysts experiments, methanol was placed in a glass container which was connected with the IR cell via valves, and then was introduced into the cell in a pressure range from 5 mbar to 15 mbar. The overtones of zeolites lattice (1500-2000 cm^{-1}) were used to normalize the spectral intensity of the catalysts. TGA analyses were performed in a Mettler Toledo TGA-DSC 1 STAR^e - coupled with a ThermoStar Pfeiffer mass spectrometer.

The carbon balance of the experiment was calculated by the following equation:

$$B=\left(\frac{\sum n_i+n_{p,CH_4}}{n_{f,CH_4}}+\frac{n_{coke}}{n_{f,CH_4}\times F\times T}\right)\times 100 \quad (1)$$

Where B is the total carbon balance, $\sum n_i$ is the sum of average concentration of the carbon in the product steam during the reaction (mole of carbon·L^{-1}), $n_{f, CH4}$ and $n_{p, CH4}$ is the average concentration of methane in the feed and outlet during the reaction (mole of carbon·L^{-1}), respectively. F is the flow rate of feed gas (L·min^{-1}), T is the reaction duration (min). n_{coke} represents the amount of coke formed during the reaction (mole of carbon), which can be calculated by:

$$n_{coke} = \frac{m_{CO2} \times m_c}{m_0 \times 13} \quad (2)$$

Where m_0 represents weight of sample for TGA analysis, m_{CO2} represents the weight loss due to oxidation of coke during TGA analysis (mg), m_c is the weight of catalyst for activity experiments (mg), we assumed C:H=1 and thus 13 is the molar mass of coke per carbon (g·mole of $carbon^{-1}$).

5.3 Results and discussion

5.3.1 Acidity study of H-form and Fe-modified zeolites

IR spectra of H-form zeolites in the region of OH stretching vibrations are shown in Fig. 5.1. Four bands were observed in the spectra of the three zeolites between 3500 cm^{-1} to 3800 cm^{-1}, the band at 3610 cm^{-1} is assigned to Si-OH-Al groups, which are associated with Brønsted-acid sites. The band at 3740 cm^{-1} is assigned to terminal Si-OH groups, and the band at 3780 cm^{-1} is due to hydroxyl groups on extra-framework Al oxide. The band at 3660 cm^{-1} is often attributed to OH groups associated with extra-framework or perturbed framework Al species [26], [27-30]. Among the different types of OH groups, the Si-OH-Al groups are crucial for N_2O conversion because they are the sites of the clustered Fe species, responsible for the selective oxidation [6, 31-34], and the concentration of framework Al species in the zeolites was

normally considered as equivalent to the concentration of Brønsted-acid sites [35-38], which can be determined quantitatively using IR spectra of ammonia adsorption on zeolites [26].

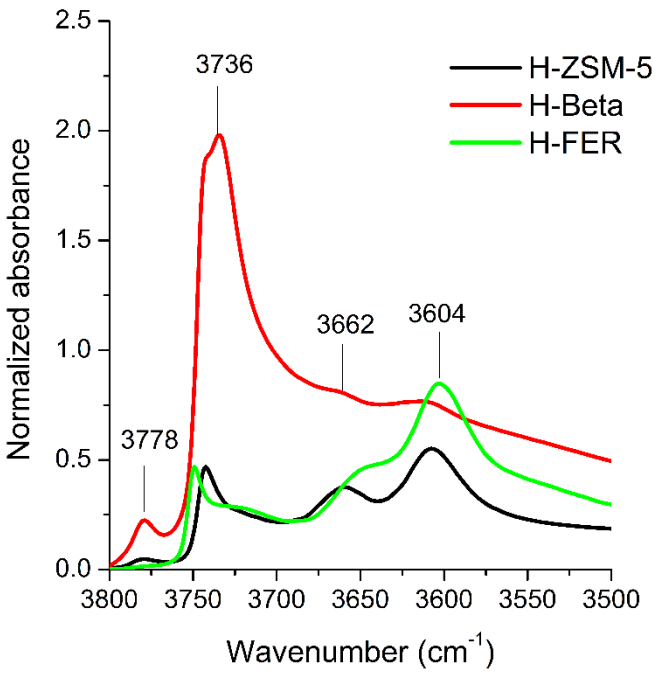

Figure 5.1 Normalized IR spectra of H-form zeolites in the region of OH stretching vibrations.

The normalized IR spectra of NH_3 adsorption over H-form and Fe-incorporated zeolites are shown in Fig. 5.2.

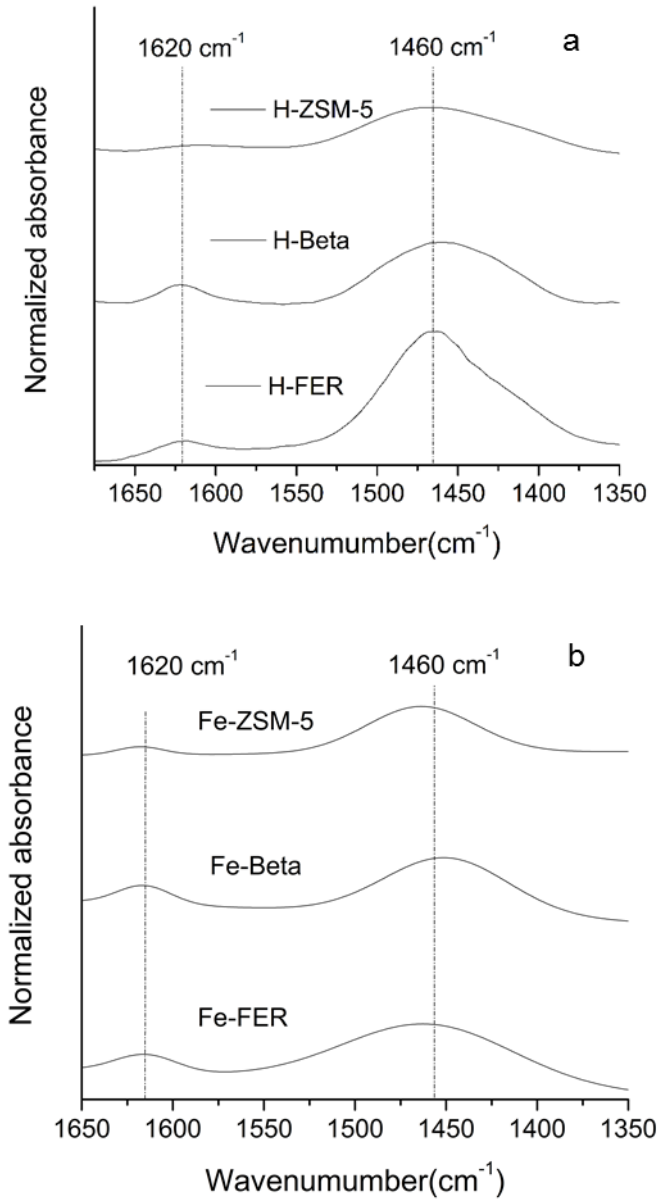

Figure 5.2 Normalized IR spectra of NH3 adsorbed (10 mbar) on H-form zeolites (a) and Fe-incorporated zeolites (b) at 150°C

As shown in Fig. 5.2, two bands related to ammonia adsorption on acid sites were observed in all the spectra at 1460 cm^{-1} and 1620 cm^{-1}, which were assigned to ammonia adsorbed on Brønsted-acid sites and Lewis-acid sites, respectively [39, 40]. The concentrations of Lewis-acid sites and Brønsted-acid sites over the H-form zeolites and Fe-modified catalysts are shown in Table. 5.1.

Table 5.1 Concentration of acid sites of H-form and Fe-modified zeolites (mmol/g)

	Brønsted-acid sites	Lewis-acid sites
H-ZSM-5	0.94	0.09
Fe-ZSM-5	0.86	0.12
H-Beta	1.09	0.34
Fe-Beta	0.97	0.38
H-FER	1.46	0.25
Fe-FER	1.26	0.30

As shown in Table. 5.1, among the three studied catalysts, H-FER exhibited the largest concentration of Brønsted-acid sites, which may result in more cationic sites and in turn Fe sites that are responsible for N_2O decomposition. In addition, the Fe-modified zeolites showed reduced amount of Brønsted-acid sites and enhanced amount of Lewis acid sites, suggesting that iron cations (replacing proton counter cations) exhibit Lewis acid properties acting as electron pair acceptor [26].

5.3.2 Textual properties, iron concentrations and dispersions over the catalysts.

t-plot micropore areas and volumes of the catalysts studied are listed in Table. 5.2. The textual properties indicated that Fe-Beta had the highest t-plot micropore area and volume among the three catalysts, while Fe-ZSM-5 presented higher t-plot micropore area than Fe-FER, but has the smallest t-plot micropore volume. ICP results showed that the zeolites with an iron concentration of 2.2wt%~2.3wt% were obtained. Chemisorption data showed that these catalysts had similar iron dispersion ranging from 12.1%~14.6%.

Table 5.2 Textual properties, iron concentrations and dispersions over the catalysts

	Fe-ZSM-5	Fe-Beta	Fe-FER
t-Plot micropore Area (m^2/g)	476	929	438
t-Plot micropore volume (cm^3/g)	0.11	0.17	0.13
Iron (wt%)	2.3	2.3	2.2
Iron dispersion (%)	12.1	12.8	14.6

5.3.3 H_2-TPR profile of catalysts

Fig. 5.3 compares the H_2-TPR profiles of Fe-ZSM-5, Fe-Beta and Fe-FER catalysts activated in a stream of air (at 450 °C) or He with extra N_2O pre-treatment (at 250 °C). All catalysts activated in air at 450 °C exhibited nonspecific hydrogen consumption from 200 to 800 °C, indicative of the presence of a broad range of Fe species formed in these zeolites. Different peak temperatures and net hydrogen consumption shown in Fig. 5.3 demonstrate that different Fe species are present within the three catalysts. For Fe-ZSM-5 and Fe-FER, two main hydrogen consumption peaks were detected at ca. 330~350 °C, and above 500 °C. The first hydrogen consumption peak is due to reduction of Fe^{3+} to Fe^{2+}, and the peak at high temperature can be attributed to reduction of Fe^{2+} to Fe^0. For Fe-Beta, only one broad hydrogen consumption peak with a maximum at around 400 °C was observed, which is consistent with previous reports[41]. This peak was reported to be responsible for the reduction of Fe^{3+} to Fe^{2+}, while the absence of a peak for reduction of Fe^{2+} to Fe^0 indicated that oxo-cations were the main component of reducible Fe species in the Fe-Beta catalyst [41].

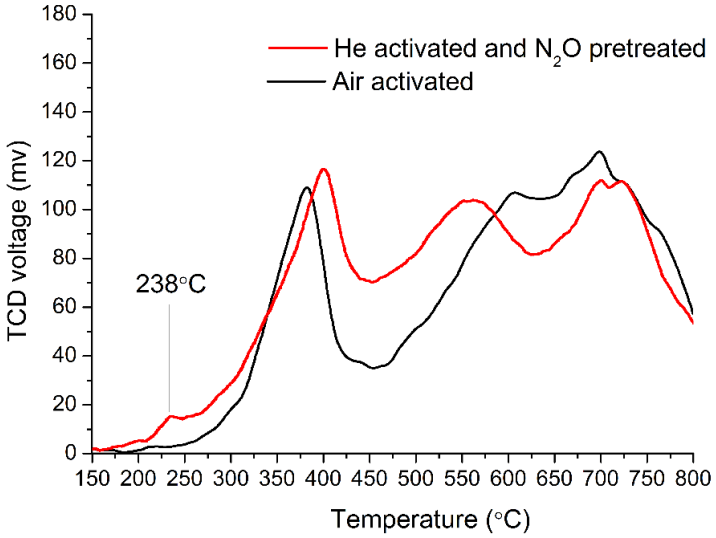

a. Fe-ZSM-5

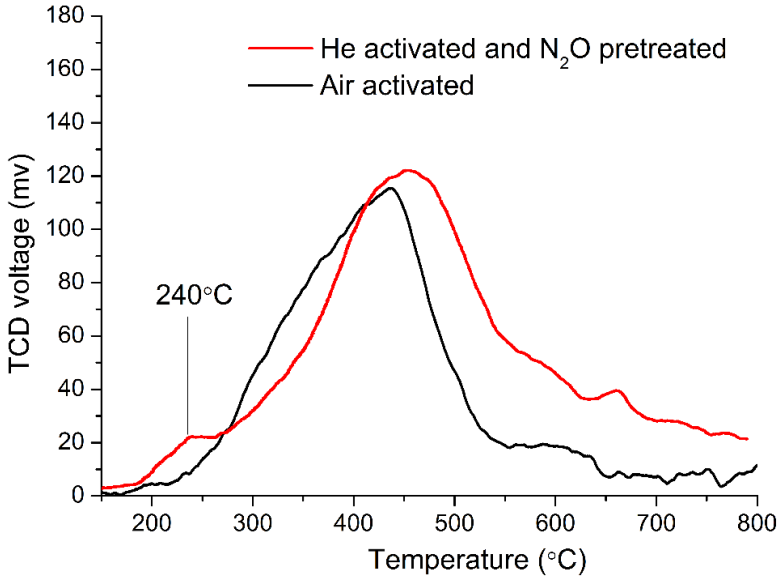

b. Fe-Beta

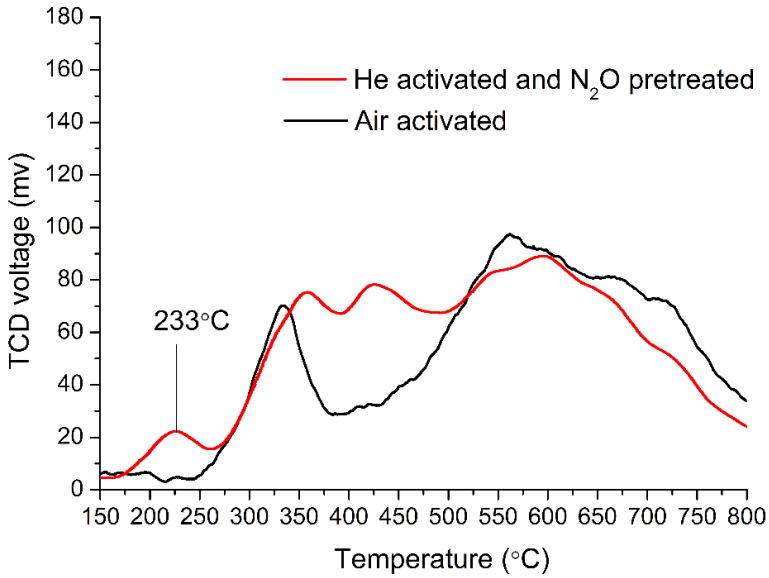

c. Fe-FER

Figure 5.3 Dependency of H_2-TPR profiles of catalysts on pre-treatment conditions (N_2O pre-treatment temperature: 250 °C)

In the three catalysts, the pre-treatment of the catalyst with N_2O resulted in to a new hydrogen reduction peak at 235 °C as shown in Fig. 5.3. It has been reported that N_2O pre-treatment of Fe-FER at 200 °C results in a TPR peak between 200 and 300 °C, which has been associated with a reduction in oxygen adsorbed on Fe cations during the N_2O pre-treatment, and the area of the low-temperature TPR peak observed was found to correlate with the number of active sites for the N_2O conversion [6]. In comparison to the hydrogen consumption peak at 235 °C present in Fe-ZSM-5 and Fe-Beta catalysts, the peak with a much higher area observed in Fe-FER indicated that Fe-FER contained more active sites for N_2O conversion, which is related to the higher concentration of framework Al atoms in the H-FER zeolites.

In addition, it should be noted that a new hydrogen consumption peak from 360 °C to 460 °C emerged in the TPR profile of N_2O pre-treatment Fe-FER

sample, indicating the generation of new form of Fe^{3+} species from oxidation of Fe^{2+} species by N_2O.

5.3.4 FTIR-NO adsorption.

To investigate the nature of specific iron species on the catalysts, an IR study of NO adsorption was undertaken and a comparison of the spectra of the catalysts following NO adsorption is presented in Fig. 5.4. Each of the spectra were deconvoluted to four components with a good fit. As shown in Fig. 5.4, bands at 1873 cm^{-1}, 1894 cm^{-1}, 1850 cm^{-1} and 1825 cm^{-1} were observed in the spectra of all three catalysts. The strong band at 1872 cm^{-1} has been attributed to high-spin Fe^{2+}-NO complex on small Fe clusters [42]. The band at 1892 cm^{-1} is assigned to NO adsorption on iron species that can transform from Fe^{3+} to Fe^{2+} [43], and it was reported that the calculated vibrational frequency of NO adsorption on a binuclear iron-oxo site matched well with the experimental value at 1892 cm^{-1} [44]. A similar band at 1874 cm^{-1} with a shoulder at 1892 cm^{-1} was assigned to NO adsorbed on extra-framework clustered Fe-O-Al species [45]. The band at 1850 cm^{-1} was extensively observed as well and was assigned to NO adsorption on oligonuclear Fe species [45, 46]. For the band at 1825 cm^{-1}, numerous studies have assigned bands between 1815 cm^{-1} to 1830 cm^{-1} to di-nitrosyls or poly-nitrosyls on (FeO_x) clusters [44-46].

The observation of the band at 1894 cm^{-1} over the three catalysts demonstrated the presence of extra-framework Fe clusters acting as counter ions for the negative framework Al atoms [43, 44], which are believed to be active sites for N_2O decomposition [6, 31, 32]. Additionally, it should be noted that, in comparison to the overall area of Fe species related bands, the much smaller

area of band at 1894 cm^{-1} indicated that only a small fraction of Fe cations is associated with the active sites, which has been suggested in previous publications [43, 45].

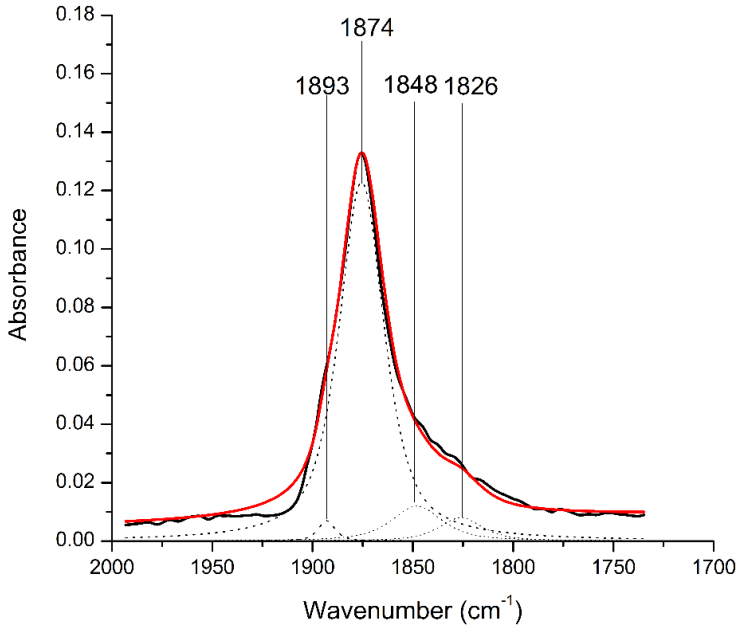

a. Fe-ZSM-5

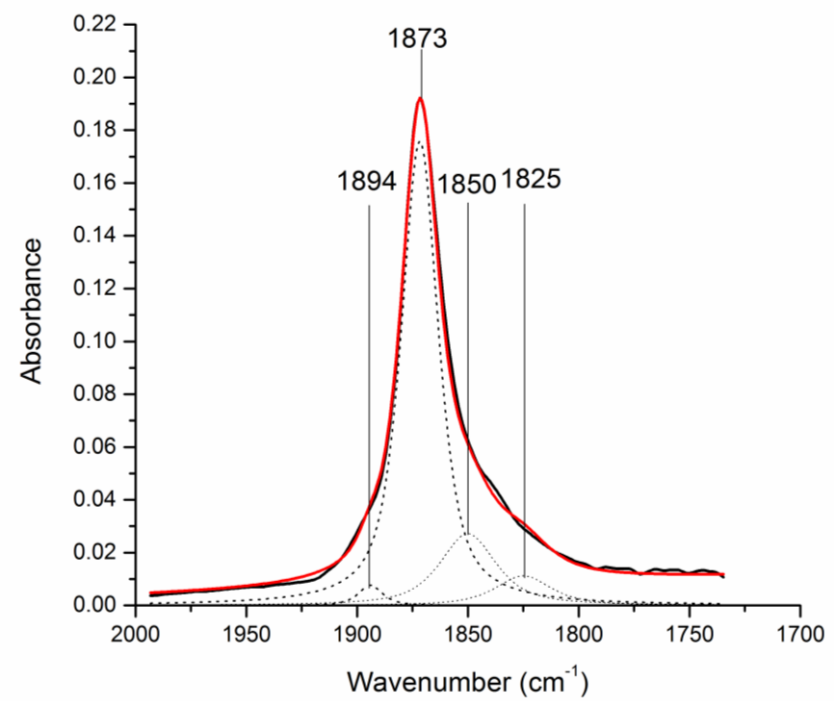

b. Fe-Beta

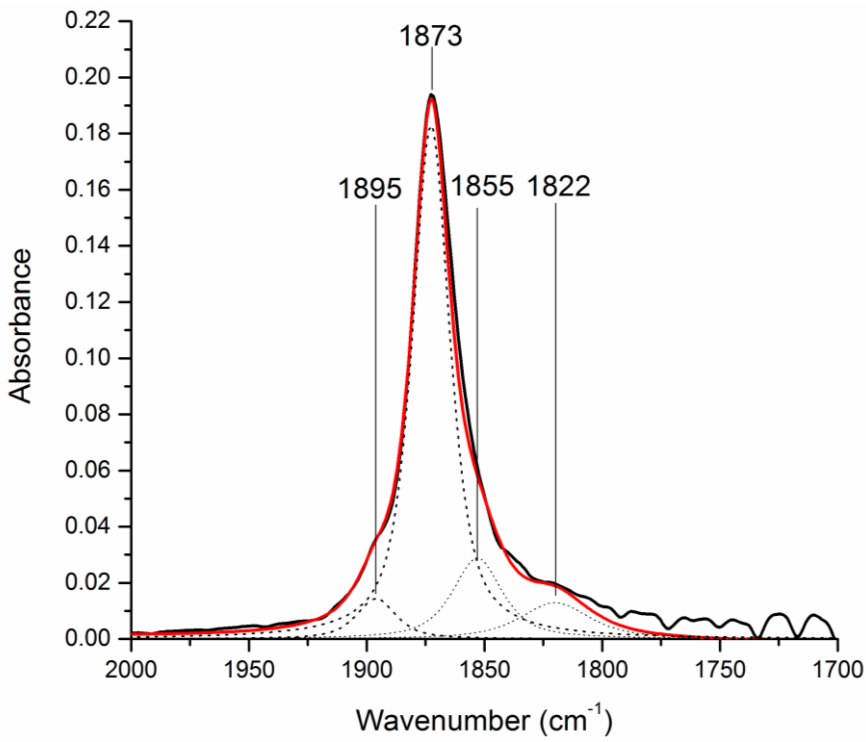

c. Fe-FER

Figure 5.4 Normalized spectra of NO adsorbed (NO pressure: 5e-2 mbar) on catalysts at 150 °C (black solid line: original trace, red solid line: fitted trace, dashed line: fitted peak)

5.3.5 FTIR profiles of catalysts with adsorption of methane and N_2O.

To investigate the reaction of CH_4 and N_2O over catalysts, CH_4 (5 mbar) was fed into the cell followed by the introduction of N_2O from 2 mbar to 15 mbar, and the FTIR spectra were monitored at 350 °C. Fig. 5.5 shows the IR spectra collected during the reaction between methane and N_2O over each of the three catalysts. Bands at 2973 cm^{-1}, 2920 cm^{-1}, 2861 cm^{-1} and 2822 cm^{-1} were observed over the three catalysts at all N_2O pressures applied. According to previous studies, these adsorption bands are caused by methoxy groups –OCH_3, where the bands at 2973 cm^{-1} and 2861 cm^{-1} were assigned to silanol-bound methoxy groups, while the bands at 2920 cm^{-1} and 2822 cm^{-1} were

attribute to Fe-bound methoxy groups [47, 48]. The appearance of methoxy groups demonstrated that methanol generated and bonded on Fe and Si species by the following reactions[49]:

$$CH_3OH+Z[Fe(OH)_2]\rightarrow H_2O+Z[Fe(OCH_3)(OH)] \quad (3)$$

$$CH_3OH+\equiv Si\text{-}OH\rightarrow H_2O+\equiv Si\text{-}OCH_3 \quad (4)$$

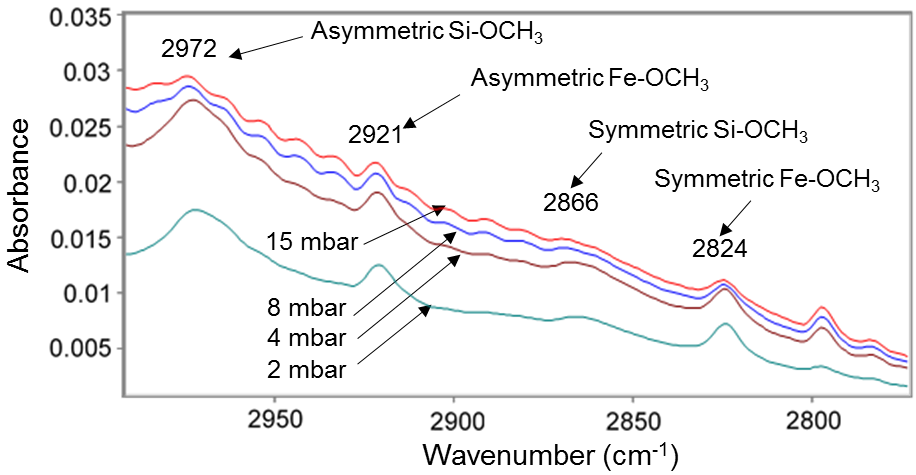

a. Fe-ZSM-5

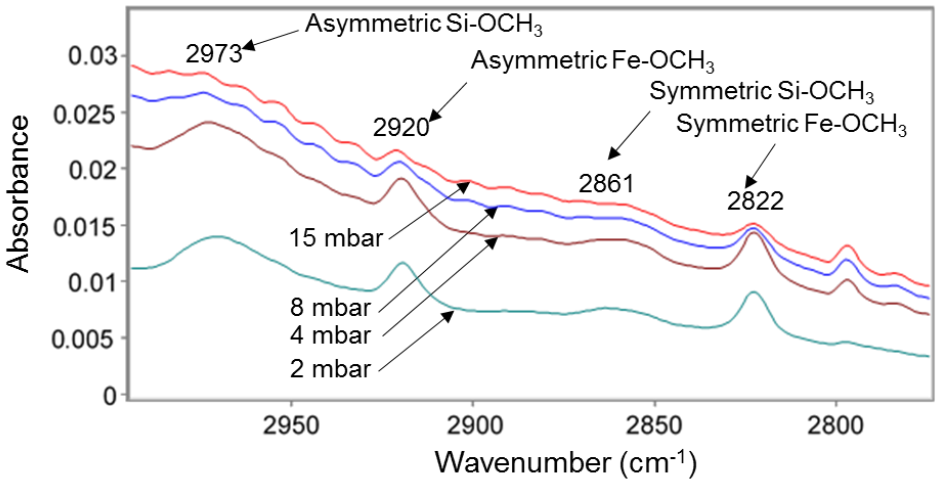

b. Fe-Beta

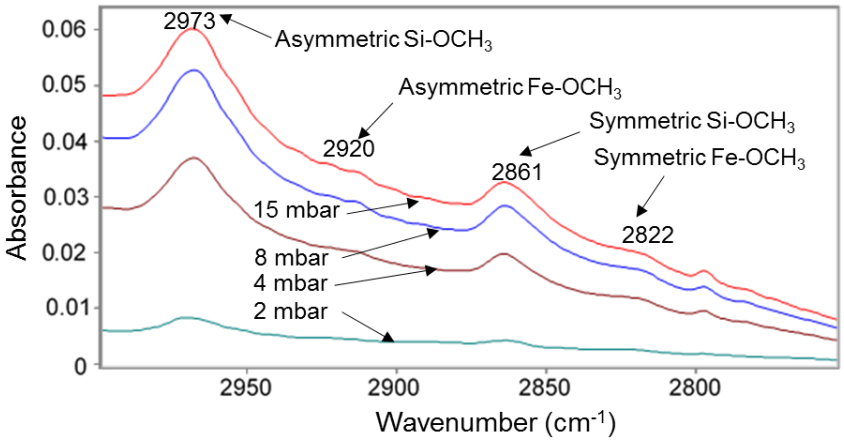

c. Fe-FER

Figure 5.5 CH stretching vibration region of catalysts during reaction of methane (5 mbar) with N_2O (from 2 mbar to 15 mbar) at 350 °C

Mechanistically, it is possible that methanol was initially generated on specific Fe species. The methanol species can either migrate to silicon groups and bond to them, (which would explain why silanol-bound methoxy groups were observed), or it can desorb into the gas phase, or transform into products such as DME, formaldehyde or ethylene. The IR spectra show that the distributions of Fe-bound and silanol-bound methoxy groups over the three catalysts are quite different. In contrast to Fe-ZSM-5 and Fe-Beta catalysts, the bands at 2920 cm^{-1} and 2822 cm^{-1} observed over Fe-FER were of much lower intensity than the bands at 2973 cm^{-1} and 2861 cm^{-1}.

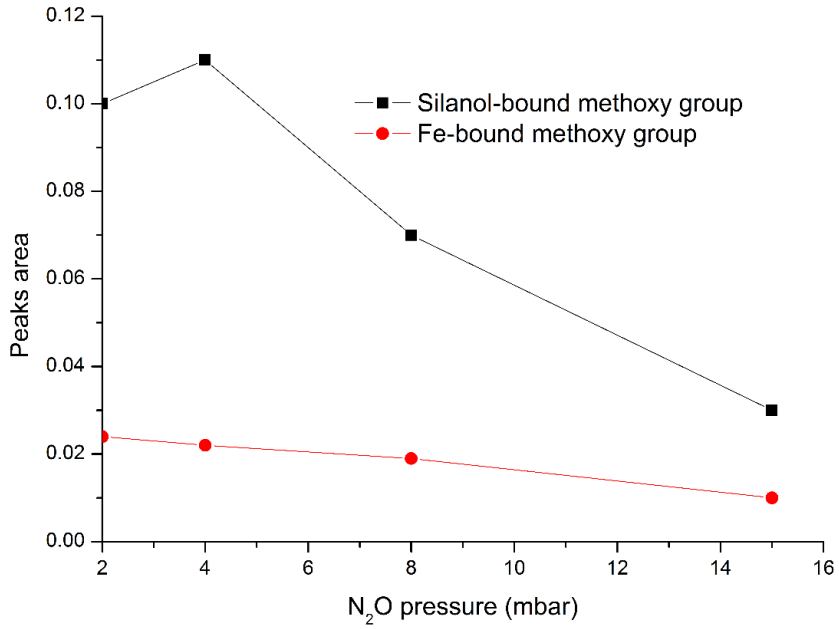

a. Fe-ZSM-5

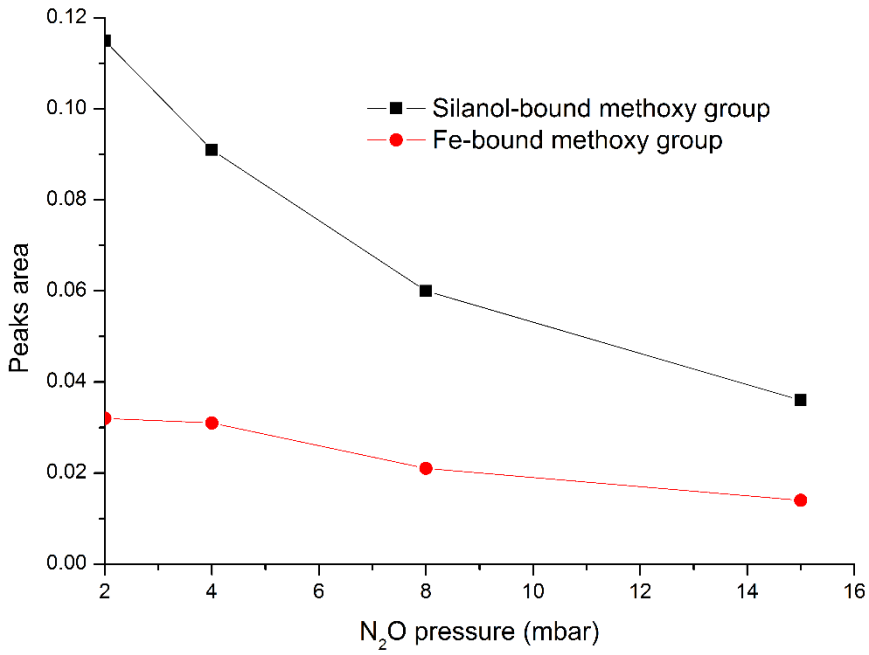

b. Fe-Beta

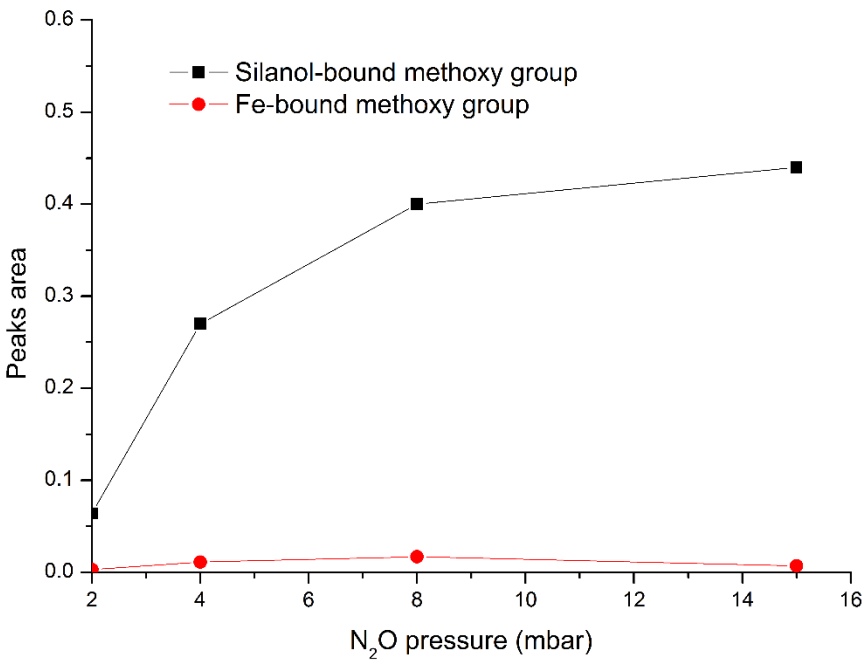

c. Fe-FER

Figure 5.6 Normalised peak areas of silanol and Fe-bound methoxy groups as a function of N_2O pressure

The areas of the asymmetric peaks assigned to Fe-bound and silanol-bound methoxy groups versus N_2O pressure are shown in Fig. 5.6. Over Fe-FER, the peak area of silanol-bound methoxy groups grew significantly as N_2O pressure increased from 2 to 8 mbar, and then increased at a much more moderate rate from 8 mbar to 15 mbar. Over the entire N_2O pressure range investigated, the peak areas of silanol-bound methoxy groups accounted for more than 95% of the total peak areas of all methoxy groups observed in Fe-FER. While the peak area of the Fe-bound methoxy groups initially increased with N_2O pressure it then decreased slightly when the N_2O pressure exceeded 8 mbar. It is asserted that as N_2O is exposed to the catalyst, an active oxygen species is generated which leads to the conversion of methane molecules to

methoxy groups, which subsequently and rapidly migrate and adsorb on silanol groups. However, as the N_2O pressure increases, a portion of the methanol is oxidized by the excess N_2O, resulting in a slight reduction in the concentration of methoxy groups.

For Fe-ZSM-5, silanol-bound methoxy groups accounted for 75%~80% of the total peak area of the methoxy groups, and a continual decrease in the peak area of Fe-bound methoxy groups was observed over Fe-ZSM-5 as the N_2O pressure increased from 2 to 15 mbar. The peak area of silanol-bound methoxy groups increased initially, but then decreased with the addition of N_2O. The peak area of silanol methoxy groups continually decreased over Fe-Beta, where silanol-bound methoxy groups accounted for 72%~78% of the total methoxy group peak areas. Therefore, it can be concluded that, compared to Fe-FER, the methoxy groups over Fe-ZSM-5 and Fe-Beta catalysts tend to accumulate on Fe sites rather than migrating to silicon species. It is believed that the accumulation of methoxy groups on Fe species hinders reaction between N_2O molecules and the Fe active sites, since these active sites are occupied by methoxy groups. Furthermore, the increased time of methoxy groups adsorbed on Fe species increases likelihood of transformation of methoxy groups to other products.

It should be noted that while no precise extinction coefficients for the methoxy groups are known, the peak areas shown in Fig. 5.6 suggest that the quantity of methoxy groups generated over Fe-FER was significantly higher than that of the methoxy groups generated over Fe-Beta and Fe-ZSM-5 catalysts (under the assumption of the same extinction coefficients). As a result, that

Fe-FER exhibits a higher propensity for methanol generation compared to the other catalysts studied.

In addition, the band at 3610 cm^{-1} remained relatively stable but a negative peak at 3740 cm^{-1} which is assigned to Si-OH groups [28, 50], appeared in all the catalysts studied as shown in Fig. 5.7, and the areas of the peak at 3740 cm^{-1}, as shown in Fig. 5.8, decreased in intensity with an increase of N_2O pressure over Fe-ZSM-5, Fe-Beta and Fe-FER catalysts.

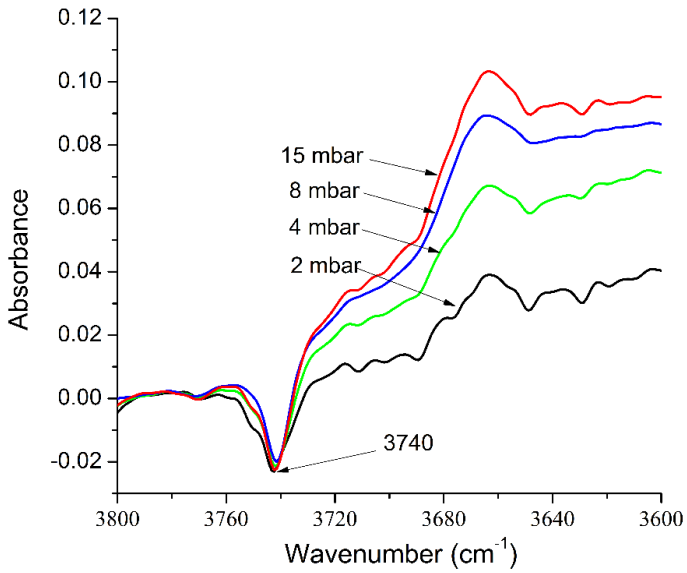

a. Fe-ZSM-5

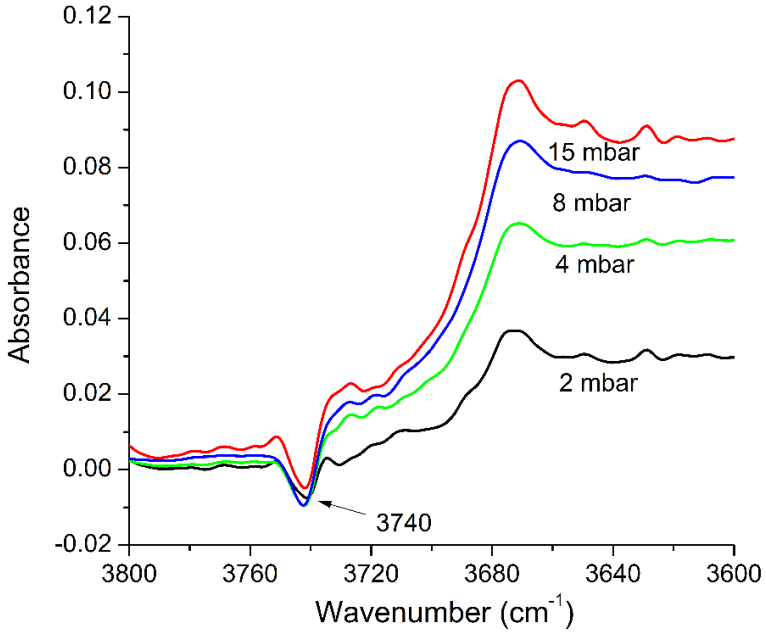

b. Fe-Beta

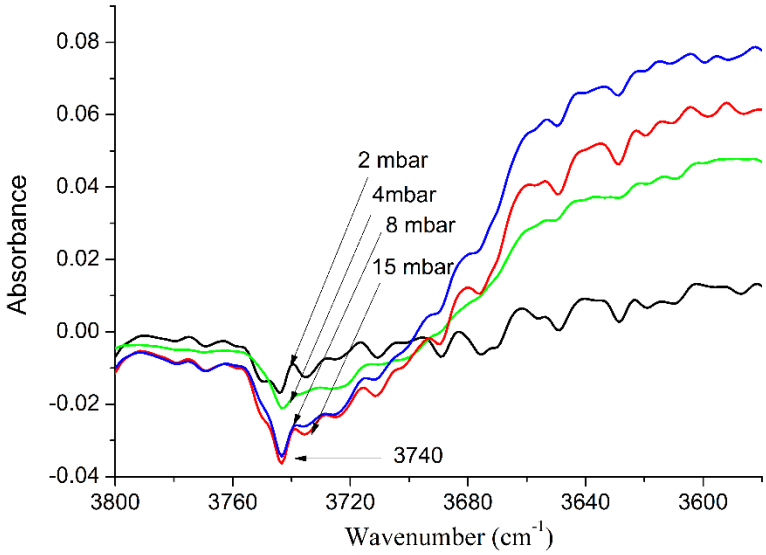

c. Fe-FER

Figure 5.7 Difference FTIR spectra of the Si-OH and Si-OH-Al region of catalysts when methane (5 mbar) and N_2O (from 2 mbar to 15 mbar) were reacted at 350 °C

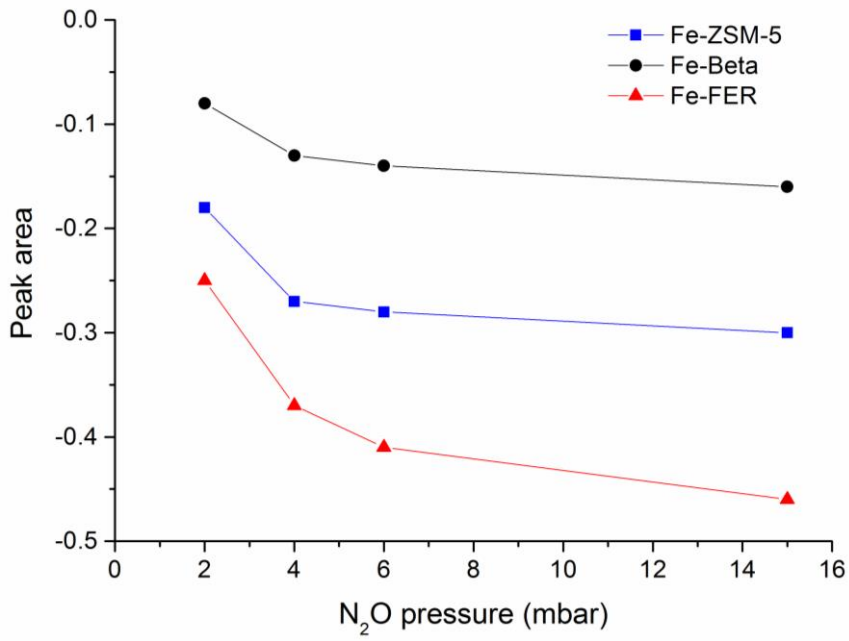

Figure 5.8 Si-OH peak (band at 3740 cm^{-1}) areas in catalysts during reaction of methane (5 mbar) withN_2O (from 2 mbar to 15 mbar) at 350 °C

However, the trends of peak area of Si-OH groups were not consistent with that of silanol-bound methoxy groups as shown in Fig. 5.6. Therefore, there should be other causes in addition to the reaction between methoxy groups with Si-OH groups that can affect the amount of Si-OH groups in the catalysts, and adsorption and desorption of methanol over Fe-FER were hence conducted as shown in Fig. 5.9 and Fig. 5.10.

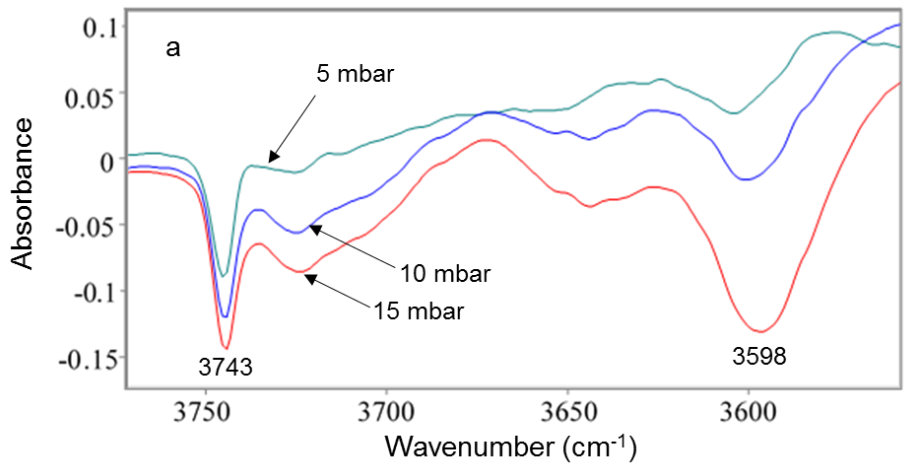

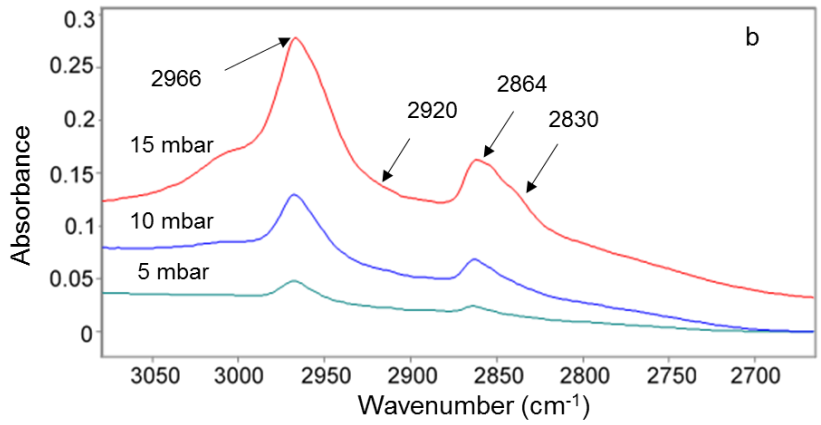

Figure 5.9 FTIR spectra (a: OH stretching vibration region b: CH stretching vibration region) of methanol adsorption over Fe-FER at 250 °C

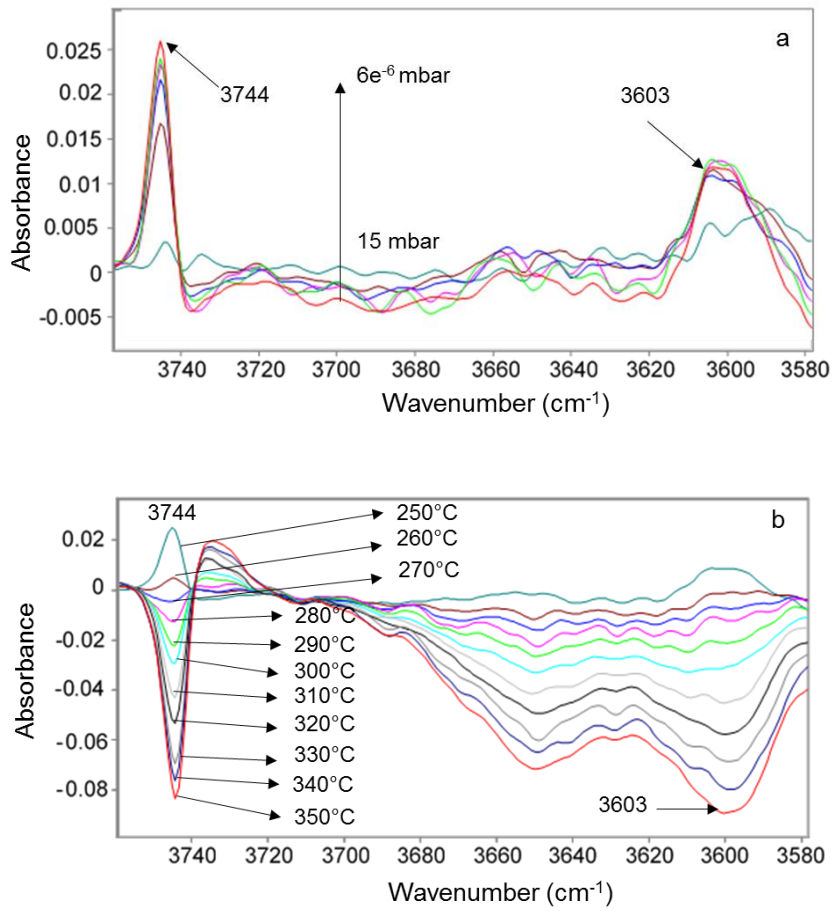

Figure 5.10 FTIR spectra of methanol desorption over Fe-FER (a: with decreased cell pressure from 15 mbar to 6e-6 mbar at 250 °C, b: with increased temperature from 250 to 350 °C)

Methanol adsorption IR spectra were shown in Fig. 5.9, the area of methoxy groups increased as the increase of methanol pressure from 5 mbar to 15 mbar. In addition to the negative peak at 3740 cm^{-1} observed in Fig. 5.7, another negative peaks at 3598 cm^{-1} which assigned to Brønsted acid sites was observed. As shown in Fig. 5.10, this negative peak became positive when methanol was desorbed at 250 °C indicating the regeneration of Si-OH groups and Brønsted acid sites. However, as the desorption temperature increased from 250 to 350 °C, the peak at 3740 cm^{-1} and 3603 cm^{-1} presented as negative again. It is believed that the Brønsted acid sites are able to convert methanol to alkanes and aromatics as well as coke, so the acid sites presenting as peak at 3603 cm^{-1} were interacting with carbonaceous species and thus a reduction in the OH stretching vibrations was observed [51]. These coke species were reported to grow out to the external surface of zeolites and hence lead to decrease of area of peak at 3740 cm^{-1} [52].

In addition, the areas of the band of Si-OH groups at 3740 cm^{-1} in the IR spectra of H-form zeolites shown in Fig. 5.1, Fig. 5.7 and Fig. 5.9 were integrated. The decrease of the peak area due to reaction of methoxy groups (which were formed due to reaction of 5 mbar methane with 2 ~ 15 mbar of N_2O) with Si-OH groups was calculated to be less than 3% in Fig. 5.7, while the adsorption of methanol with high pressure (5 mbar ~ 15 mbar) in Fig. 5.9 resulted in an area decrease of 10% ~ 25%. Therefore, the absence of negative peak at 3603 cm^{-1} in Fig. 5.7 (under reaction conditions) and the presence of the peak in Fig. 5.9 indicated that while methoxy groups formed on both silanol and bridging OH groups with methanol they are not observed under reaction conditions with N_2O and methane. It is suggested on Brønsted

acid sites other products formed from the methoxy groups in consecutive reactions.

5.3.6 Comparison of methane and N_2O conversion and products selectivity over catalysts.

Methane and N_2O conversion over Fe-ZSM-5, Fe-Beta and Fe-FER were compared at 350 °C, and the results is shown in Fig. 5.11. When 200 mg Fe-FER was used in the reaction (denoted as Fe-FER^a), methane conversion decreased from 2.8% to 2.0% over the four hours duration of the reaction, and N_2O conversion decreased from 22% to 19%. Lower methane (2%–0.8%) and N_2O (16.1%–9.5%) conversion was obtained when 100 mg Fe-FER was used in the reaction (denoted as Fe-FER^b). The average methane and N_2O conversion obtained by Fe-FER^a in the 4 hours reaction were 2.4% and 20%, which were 1.7 and 2.8 times of that over Fe-ZSM-5, and 1.8 and 2.2 times of that over Fe-Beta. The TOF of methane and N_2O conversion of Fe-ZSM-5, Fe-Beta and Fe-FER are shown in Table. 5.3. The TOF of N_2O over Fe-FER^a was 2.3 and 2.0 times of that over Fe-ZSM-5 and Fe-Beta, which is consistent with the areas of hydrogen consumption peak at around 235 °C, and the areas of band at 1894 cm^{-1} in the NO adsorption IR spectra as shown in Fig. 5.12. This confirmed that the hydrogen consumption correlates with the amount of active sites for N_2O conversion, and demonstrated the presence of extra-framework Fe clusters acting as the active sites for N_2O decomposition. This relationship suggests Fe clusters exhibiting an NO adsorption of 1894 cm^{-1} which can be reduced at 235 ℃ are most likely the main sites for N_2O activation under reaction conditions. These sites are suggested to be cationic

iron cluster sites. Carbon balance of the experiments is shown in Table. 5.3 as well, carbon balance in all of the experiments was above 99%.

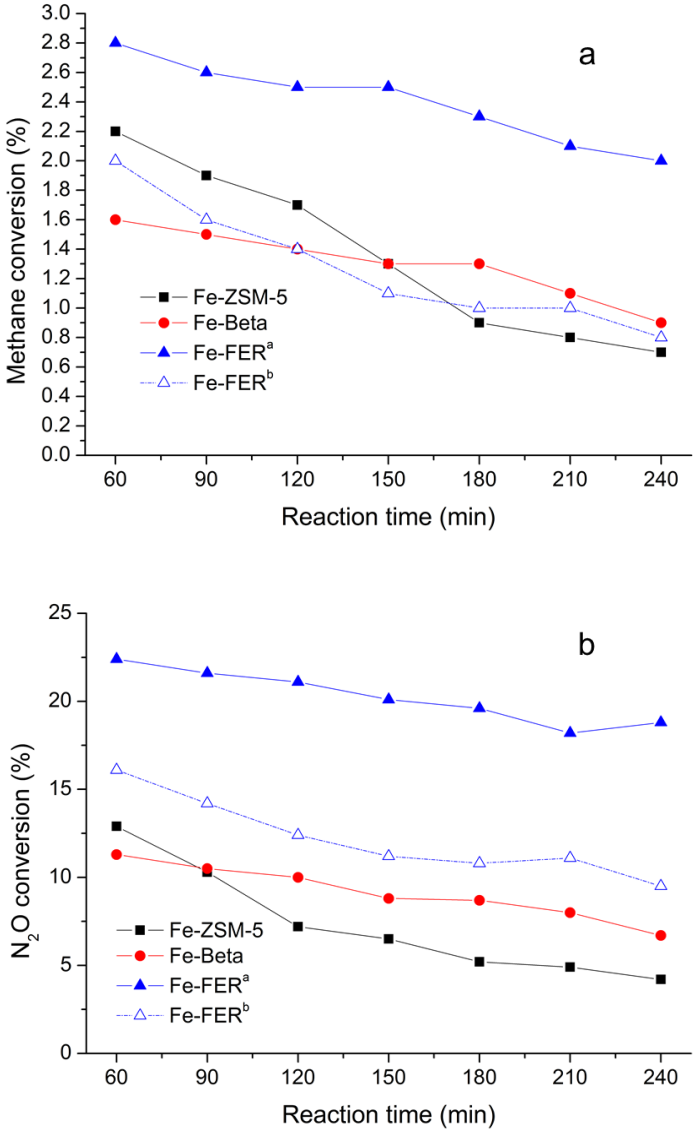

Figure 5.11 Methane conversion (a) and N_2O conversion (b) over catalysts at 350 °C (Fe-FER[a]–200 mg of catalyst, Fe-FER[b]–100 mg catalyst)

Table 5.3 TOF of CH_4 and N_2O and carbon balance over catalysts

Catalyst	TOF of CH_4 (h^{-1})	TOF of N_2O (h^{-1})	Carbon balance
Fe-ZSM-5	88.1	110.9	99.5%
Fe-Beta	77.3	130.7	99.3%
Fe-FER[a]	125.2	255.5	99.1%

Fe-FER[b]	140.3	307.1	99.1%

a–200 mg of catalyst, and the carbon balance was calculated with coke taken into account.

b–100 mg of catalyst.

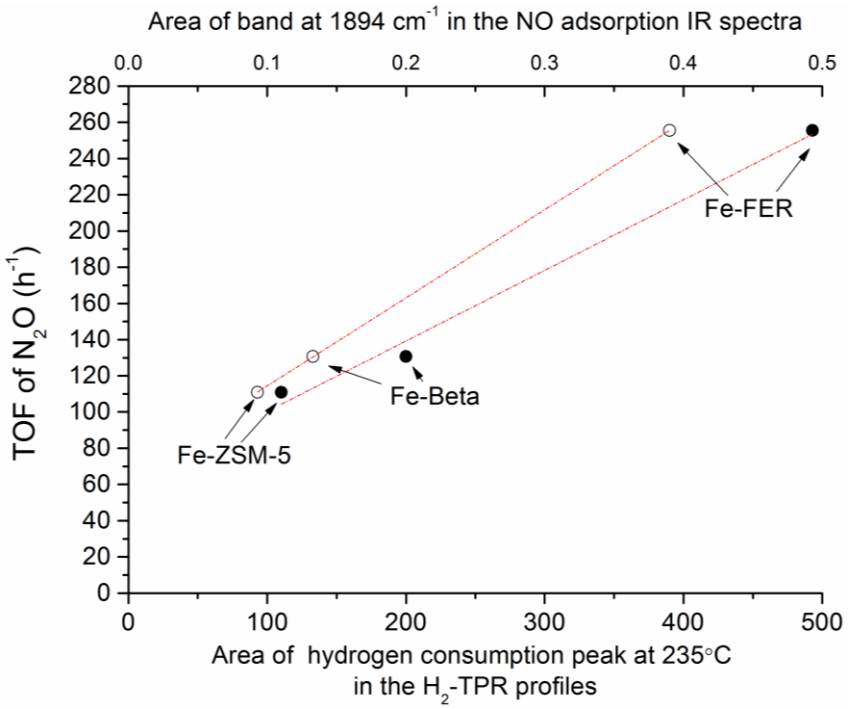

Figure 5.12 The integrated area of hydrogen consumption peak centred at 235 °C in the H_2-TPR profiles (solid circle) and peak area of band at 1894 cm^{-1} in the NO adsorption IR spectra (hollow circle) versus the TOF of N_2O conversion over catalysts

Product selectivity over the catalysts is presented in Fig. 5.13. Methanol and formaldehyde were produced under these experimental conditions over all catalysts. The average selectivity to methanol and formaldehyde over Fe-FER[a] were 21% and 4.8% at 350 °C, a slightly higher selectivity to desired products was obtained over the Fe-FER[b] as shown in Fig. 5.13. For Fe-ZSM-5, the average selectivity to methanol and formaldehyde were 3.1% and 4.7%, and that of Fe-Beta were 4.7% and 6.5%.

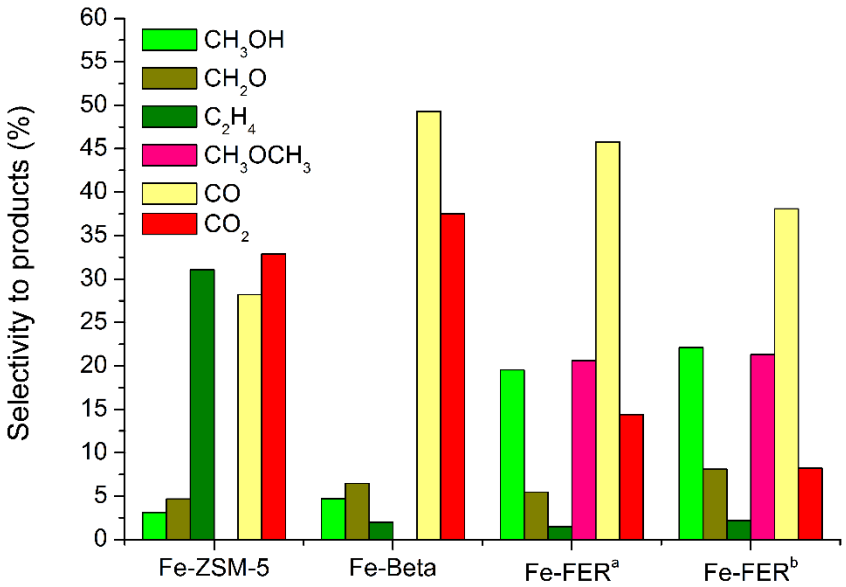

a. Comparison of average selectivity to products over catalysts

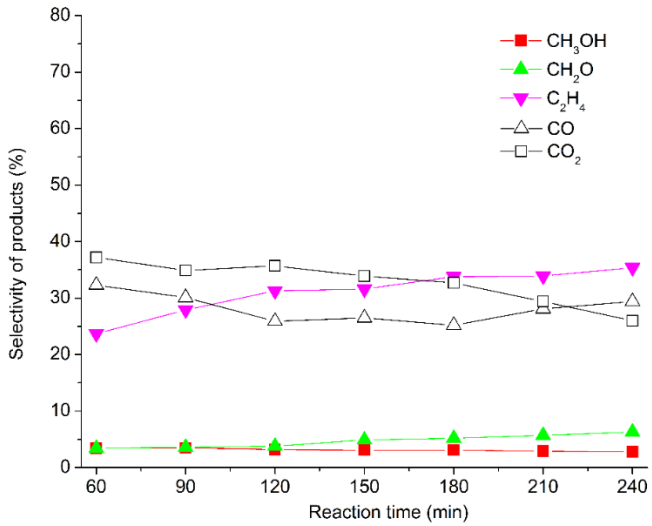

b. Product selectivity over Fe-ZSM-5 as a function of time on stream

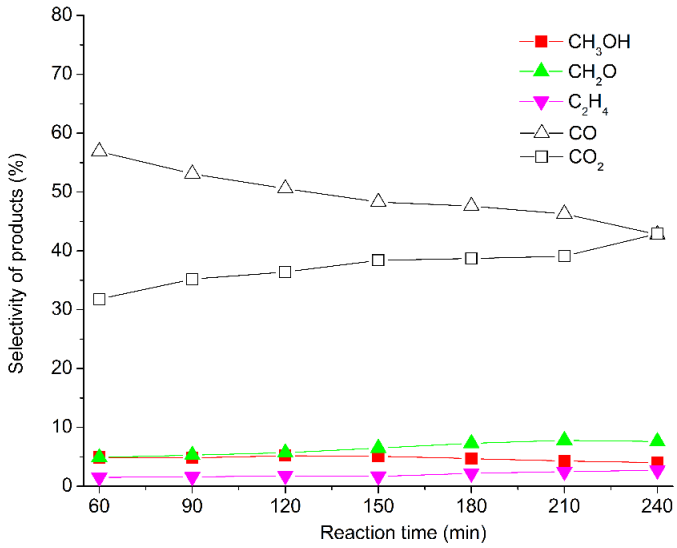

c. Product selectivity over Fe-Beta as a function of time on stream

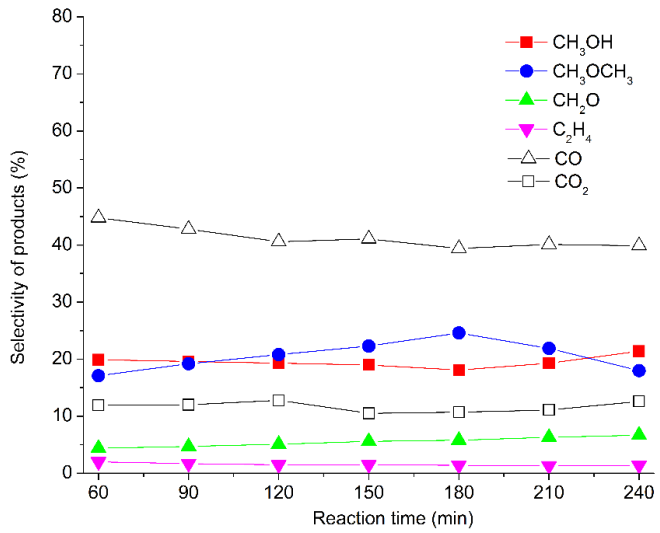

d. Product selectivity over Fe-FER[a] as a function of time on stream

Figure 5.13 Selectivity to products over catalysts at 350 °C (Fe-FER[a]–200 mg of catalyst, Fe-FER[b]–100 mg catalyst)

The results are consistent with the conclusions drawn from H_2-TPR profiles and IR spectral analysis where it is suggested that Fe-FER contains additional active sites for N_2O conversion than Fe-ZSM-5 and Fe-Beta catalysts. The active sites then resulted in more specific oxygen which is responsible for the

formation of C_1-oxygenates and DME, since the amounts of C_1-oxygenates and DME were negligible when O_2 was used as the oxidant (results not shown here). In addition, methanol intermediate species migrate more efficiently vacating active sites which are then available for reaction over Fe-FER, as demonstrated in Fig. 5.6 and Fig. 5.7.

Additionally, DME was detected over the three catalysts, but could only be quantified in samples from Fe-FER[a] and Fe-FER[b], where the selectivity to DME was 20.6% and 21.3%, respectively, as shown in Fig. 5.13. It is believed that methanol was firstly formed from methane partial oxidation, and then DME is generated from methanol dehydration. For Fe-ZSM-5 and Fe-Beta catalysts, a smaller fraction of formed methoxy groups desorbed from the catalysts to form methanol because of the lower migration efficiency of methoxy groups in comparison to Fe-FER as suggested in Fig. 5.5 and Fig. 5.6. The remained methoxy groups iron sites within Fe-ZSM-5 and Fe-Beta catalysts underwent further oxidation to CO and CO_2, while the desorbed methanol resulted in the formation of DME, which subsequently converted to light olefins, and as a consequence, the DME over Fe-ZSM-5 and Fe-Beta were unquantifiable. On the contrary, the efficient migration of methoxy groups to silicon species over Fe-FER is beneficial for achieving a much higher methanol selectivity, even though the dehydration of methanol to DME on Brønsted sites occurred.

It should be noted that a decrease in catalyst activity with time was observed in all the experiments in this study. As shown in Fig. 5.12, at 60 min, methane and N_2O conversion over Fe-ZSM-5 were 2.2% and 13%, 2.8% and 22% over Fe-FER[a], while at 240 min, the conversion of methane and N_2O over Fe-ZSM-

5 was 0.7% and 4.2%, compared to 2.0% and 19% over Fe-FER[a]. In comparison to the obvious decline of conversion of methane and N_2O, the product selectivities were relatively stable as shown in Fig. 5.11 and Fig. 5.13. It is suggested that coke was formed during the reaction, which led to the reduction of methane and N_2O conversion, and simultaneously mitigated deep oxidation of C_1-oxygenates and DME over Fe species.

Furthermore, the selectivity to ethylene over Fe-ZSM-5 at 350 ℃ was 31%, which was much higher compared to Fe-FER and Fe-Beta. It is conjectured that ethylene was generated via the methanol to olefins (MTO) reaction [53, 54].

$$2CH_3OH \leftrightarrow CH_3OCH_3 + H_2O \quad (5)$$

$$CH_3OCH_3 \leftrightarrow C_2H_4 + H_2O \quad (6)$$

An appropriate pore size and a low concentration of Lewis sites in the catalysts are suggested to be the two key factors for the MTO reaction [53]. In comparison with other catalysts, Fe-ZSM-5 has smaller pore volume as shown in Table. 5.2, and lower Lewis sites concentration as shown in Table. 5.1, which might be two of the reasons that resulted in higher ethylene selectivity over Fe-ZSM-5. In addition, carbon deposition was reported to enhance the generation of ethylene [55]. In order to investigate the coke formation over the catalysts, TGA-MS analyses were conducted.

5.3.7 TGA-MS analyses of used catalysts.

Coke formation over various catalysts was further analysed by TGA-MS measurement of the spent catalysts. As shown in Fig. 5.14, Fig. 5.15 and Table. 5.4, the weight loss in the temperature ranges of 25–200 °C and 250–

600 °C which respectively represents mass loss due to the release of water and CO_2, was observed over Fe-Beta and Fe-FER catalysts. For Fe-ZSM-5, in addition to the weight loss in the temperature ranges of 25–200 °C and 250–600 °C, a second CO_2 loss is present at higher temperatures (range of 750–900 °C). The total mass loss of CO_2 over the used Fe-ZSM-5, Fe-Beta and Fe-FER were 9.5%, 2.7% and 5.1%, respectively. The results are compatible with the results of FTIR spectra; the methanol formed over Fe-ZSM-5 is adsorbed on Fe species rather than migrating to silanol groups. As a consequence, the methoxy groups formed on Fe species underwent further reaction to carbon deposition. In addition, the more severe coke formation over Fe-ZSM-5 might enhance the generation of ethylene.

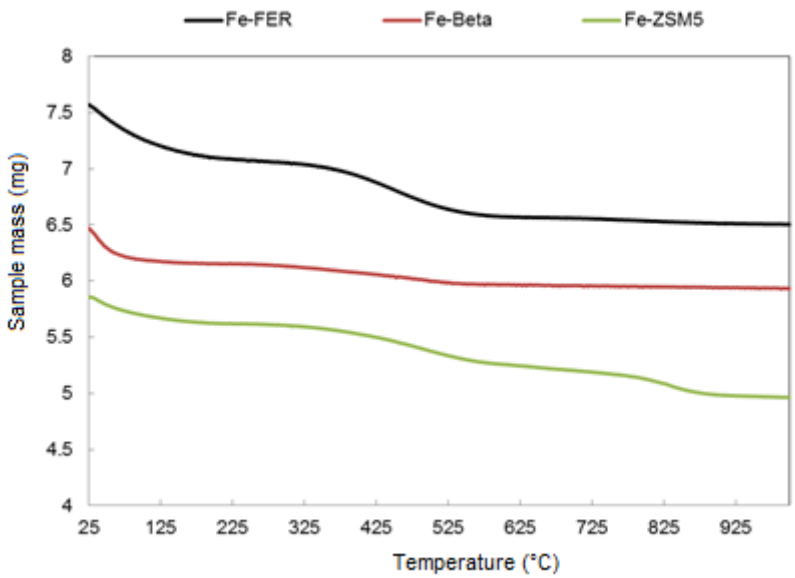

Figure 5.14 TGA profiles of the spent catalysts

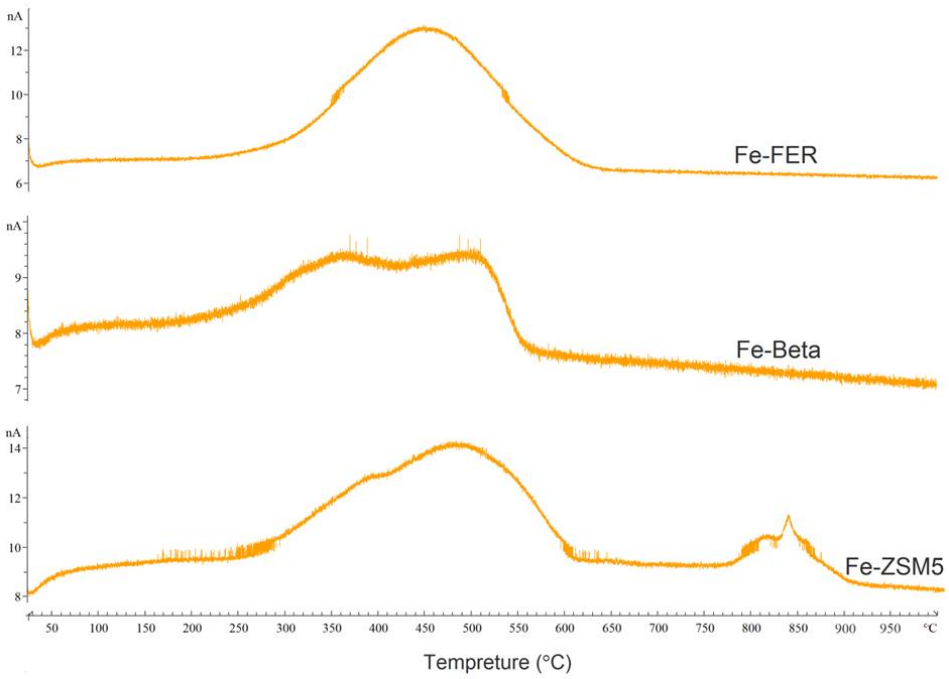

Figure 5.15 m/z=44 mass spectroscopy profiles of released CO_2 from spent catalysts

Table 5.4 Mass loss of used catalysts in different temperature ranges

Temperature range (°C)	25-200	250-600	750-900
Fe-FER	4.71%	5.06%	0.00%
Fe-Beta	4.58%	2.69%	0.00%
Fe-ZSM5	3.77%	5.92%	3.54%

5.4 Conclusion

Methane selective oxidation with N_2O over Fe-ZSM-5, Fe-Beta and Fe-FER catalysts was compared and characterization of catalysts was conducted. Among the three catalysts, H-FER contained the highest amount of framework Al atoms, which are essential for stabilizing Fe species to form the active sites for N_2O conversion. Based on the evidence provided by N_2O pre-treated H_2-TPR profiles, Fe-FER is suggested to contain more active Fe species

responsible for N_2O conversion, in comparison to Fe-ZSM-5 and Fe-Beta catalysts. The observation of a band at 1874 cm^{-1} with a shoulder at 1894 cm^{-1} when NO was adsorbed on the Fe containing zeolites suggested that they are due to extra-framework Fe clusters acting as counter ions of the negatively charged Al in the framework. Silanol-bound and Fe-bound methoxy groups were observed but displayed a different distribution of sites over the three catalysts, based on methane and N_2O adsorption FTIR studies. In contrast to Fe-ZSM-5 and Fe-Beta, the methanol generated on Fe species present in Fe-FER migrates to silanol groups more effectively.

The higher concentration of active sites and propensity for methoxy groups migration from Fe sites to silicon species over Fe-FER rendered the catalyst exhibiting the highest methane and N_2O conversion, and desired products selectivity among the three catalysts. During the reaction, the catalytic activity for methane and N_2O conversion of all the catalysts declined over time, due to carbon deposition. The most rapid decrease was observed over Fe-ZSM-5, and the TGA results demonstrated that the highest coke amount were obtained within Fe-ZSM-5. It is believed that the smaller pore size and lower Lewis acidity in Fe-ZSM-5 accelerated the MTO process, therefore, the resident methoxy groups on Fe species undergo coupling to aromatics and eventually to coke.

5.5 Reference

1. Abdelsayed, V.; Shekhawat, D.; Smith, M.W. Effect of Fe and Zn promoters on Mo/HZSM-5 catalyst for methane dehydroaromatization. *Fuel* **2015**, *139*, 401-410.

2. Bozbag, S.E.; Alayon, E.M.C.; Pecháček, J.; Nachtegaal, M.; Ranocchiari, M.; van Bokhoven, J.A. Methane to methanol over copper mordenite: yield improvement through multiple cycles and different synthesis techniques. *Catal. Sci. Technol.* **2016**, *6*, 5011-5022.

3. Periana, R. A.; Taube, D. J.; Gamble, S.; Taube, H.; Satoh, T.; Fujii, H.; Platinum catalysts for the high-yield oxidation of methane to a methanol derivative. *Sci.* **1998**, *280*, 560-564.

4. Takemoto, T.; He, D.; Teng, Y.; Tabata, K.; Suzuki, E. The optimization of methanol yield in direct selective oxidation of methane with O_2 and NO in the presence of Cu-ZnO/Al_2O_3. J. *Mol. Catal. A: Chem.* **2002**, *179*, 279-286.

5. Kondratenko, E.V.; Peppel, T.; Seeburg, D.; Kondratenko, V.A.; Kalevaru, N.; Martin, A.; Wohlrab, S. Methane conversion into different hydrocarbons or oxygenates: current status and future perspectives in catalyst development and reactor operation. *Catal. Sci. Technol.* **2017**, *7*, 366-381.

6. Jíša, K.; Nováková, J.; Schwarze, M.; Vondrová, A.; Sklenák, S.; Sobalik, Z. Role of the Fe-zeolite Structure and Iron State in the N_2O Decomposition: Comparison of Fe-FER, Fe-BEA, and Fe-MFI Catalysts. *J. Catal.* **2009**, *262*, 27-34.

7. Tabor, E.; Závěta, K.; Sathu, N.K.; Vondrova, A.; Sazama, P.; Sobalik, Z. N_2O decomposition over Fe-FER: A Mössbauer study of the active sites. *Catal. Today* **2011**, *175*, 238-244.

8. Ravi, M.; Ranocchiari, M.; van Bokhoven, J. A., The Direct Catalytic Oxidation of Methane to Methanol-A Critical Assessment. *Angew. Chem. Int. Ed. Engl.* **2017**, *56*, 16464-16483.

9. Pirutko, L.V.; Uriarte, A.K.; Chernyavsky, V.S.; Kharitonov, A.; Panov, G.I. Preparation and catalytic study of metal modified TS-1 in the oxidation of benzene to phenol by N_2O. *Micropor. Mesopor.Mat.* **2001**, *48*, 345-353.

10. Haneda, M.; Shinriki, M.; Nagao, Y.; Kintaichi, Y.; Hamada, H. N_2O removal by catalytic decomposition and reduction with CH_4 over Fe/Al_2O_3. *Bull. Chem. Soc. Jpn.* **2003**, *76*, 2329-2333.

11. Wang, Z. C.; Dietl. N.; Kretschmer, R.; Ma, J. B.; Weiske, T.; Schlangen, M.; Schwarz, H. Direct Conversion of Methane into Formaldehyde Mediated by $[Al_2O_3]^+$ at Room Temperature. *Angew. Chem., Int. Ed.* **2012**, *51*, 3703-3707.

12. Sklenak, S.; Andrikopoulos, P.C.; Boekfa, B.; Jansang, B.; Nováková, J.; Benco, L.; Bucko, T.; Hafner, J.; Dědeček, J.; Sobalík, Z. N_2O decomposition over Fe-zeolites: Structure of the active sites and the origin of the distinct reactivity of Fe-ferrierite, Fe-ZSM-5, and Fe-beta. A combined periodic DFT and multispectral study. *J. Catal.* **2010**, *272*, 262-274.

13. Sobolev, V.I.; Koltunov, K.Y. Location, stability, and reactivity of oxygen species generated by N_2O decomposition over Fe-ZSM-5 and Fe-Beta zeolites. *J. Mol. Catal. A: Chem.* **2011**, *347*, 22-27.

14. Čejka, J.; Centi, G.; Perez-Pariente, J.; Roth, W.J. Zeolite-based materials for novel catalytic applications: Opportunities, perspectives and open problems. *Catal. Today* **2012**, *179*, 2-15.

15. Sobalik, Z.; Novakova, J.; Dedecek, J.; Sathu, N. K.; Tabor, E.; Sazama, P.; Wichterlova, B. Tailoring of Fe-ferrierite for N_2O decomposition: On the decisive role of framework Al distribution for catalytic activity of Fe species in Fe-ferrierite. *Micropor. Mesopor. Mat.* **2011**, *146*, 172-183.

16. Zecchina, A.; Rivallan, M.; Berlier, G.; Lamberti, C.; Ricchiardi, G, Structure and nuclearity of active sites in Fe-zeolites: comparison with iron sites in enzymes and homogeneous catalysts. *Phys. Chem. Chem. Phys.* **2007**, *9*, 3483-99.

17. Sun, K.; Xia, H.; Feng, Z.; van Santen, R.; Hensen, E.; Li, C. Active Sites in Fe/ZSM-5 for Nitrous Oxide Decomposition and Benzene Hydroxylation with Nitrous Oxide. *J. Catal.* **2008**, *254*, 383-396.

18. Wood, B. R.; Reimer, J. A.; Bell, A. T.; Janicke, M. T.; Ott, K. C. Methanol Formation on Fe/Al-MFI via the Oxidation of Methane by Nitrous Oxide. *J. Cata.* **2004**, *225*, 300-306.

19. Grundner, S.; Markovits, M.A.; Li, G.; Tromp, M.; Pidko, E.A.; Hensen, E.J.; Jentys, A.; Sanchez-Sanchez, M.; Lercher, J.A. Single-site trinuclear

copper oxygen clusters in mordenite for selective conversion of methane to methanol. *Nat. Commun.* **2015**, *6*, 7546.

20. Tshabalala, T.E.; Coville, N.J.; Scurrell, M.S. Dehydroaromatization of methane over doped Pt/Mo/H-ZSM-5 zeolite catalysts: The promotional effect of tin. *Appl. Catal. A: Gen.* **2014**, *485*, 238-244.

21. Parfenov, M. V.; Starokon, E. V.; Pirutko, L. V.; Panov, G. I. Quasicatalytic and Catalytic Oxidation of Methane to Methanol by Nitrous Oxide over FeZSM-5 Zeolite. *J. Catal.* **2014**, *318*, 14-21.

22. Dubkov, K. A.; Ovanesyan, N. S.; Shteinman, A. A.; Starokon, E. V.; Panov, G. I. Evolution of Iron States and Formation of α-Sites upon Activation of FeZSM-5 Zeolites. *J. Catal.* **2002**, *207,* 341-352.

23. Park, J.H.; Choung, J.H.; Nam, I.S.; Ham, S.W. N_2O decomposition over wet-and solid-exchanged Fe-ZSM-5 catalysts. *Appl. Catal. B: Environ.* **2008**, *78*, 342-354.

24. Sun, K.; Xia, H.; Hensen, E.; van Santen, R.; Li, C. Chemistry of N_2O Decomposition on Active Sites with Different Nature: Effect of High-Temperature Treatment of Fe/ZSM-5. *J. Catal.* **2006**, *238*, 186-195.

25. Sazama, P.; Sathu, N.K.; Tabor, E.; Wichterlová, B.; Sklenák, Š.; Sobalík, Z. Structure and Critical Function of Fe and Acid Sites in Fe-ZSM-5 in Propane Oxidative Dehydrogenation with N_2O and N_2O Decomposition. *J. Catal.* **2013**, *299,* 188–203.

26. Góra-Marek, K.; Brylewska, K.; Tarach, K. A.; Rutkowska, M.; Jabłońska, M.; Choi, M.; Chmielarz, L. IR Studies of Fe Modified ZSM-5

Zeolites of Diverse Mesopore Topologies in the Terms of Their Catalytic Performance in NH_3-SCR and NH_3-SCO processes. *Appl. Catal. B* **2015**, *179*, 589-598.

27. Kiricsi, I.; Flego, C.; Pazzuconi, G.; Parker, W. J.; Millini, R.; Perego, C.; Bellussi, G. Progress Toward Understanding Zeolite. Beta. Acidity: an IR and ^{27}Al NMR Spectroscopic Study. *J. Phys. Chem.* **1994**, *98,* 4627-4634.

28. Bortnovsky, O.; Sobalík, Z.; Wichterlová, B.; Bastl, Z.; Structure of Al–Lewis Site in Beta Zeolite Active in the Meerwein–Ponndorf–Verley Reduction of Ketone to Alcohol. *J. Catal.* **2002**, *210*, 171-182.

29. Sazama, P.; Tabor, E.; Klein, P.; Wichterlova, B.; Sklenak, S.; Mokrzycki, L.; Pashkkova, V.; Ogura, M.; Dedecek, J. Al-Rich Beta Zeolites. Distribution of Al Atoms in the Framework and Related Protonic and Metal-Ion Species. *J. Catal.* **2016**, *333*, 102-114.

30. Guisnet, M.; Ayrault, P.; Coutanceau, C.; Alvarez, M. F.; Datka, J. Acid Properties of Dealuminated Beta Zeolites Studied by IR Spectroscopy. J. *Chem. Soc. Faraday Trans.* **1997**, *93*, 1661-1665.

31. Moretti, G.; Fierro, G.; Ferraris, G.; Andreozzi, G. B.; Naticchioni, V. N_2O Decomposition over [Fe]-MFI Catalysts: Influence of the Fe_xO_y Nuclearity and the Presence of Framework Aluminum on the Catalytic Activity. *J. Catal.* **2014**, *318*, 1-13.

32. Li, G.; Pidko, E. A.; Filot, I. A.; van Santen, R. A.; Li, C.; Hensen, E. J. Catalytic Properties of Extraframework Iron-Containing Species in ZSM-5 for N_2O Decomposition. *J. Catal.* **2013**, *308*, 386-397.

33. Melián-Cabrera, I.; van Eck, E. R.; Espinosa, S.; Siles-Quesada, S.; Falco, L.; Kentgens, A. P.; Kapteijn, F.; Moulijn, J. A.; Tail Gas Catalyzed N_2O Decomposition over Fe-Beta Zeolite. On The Promoting Role of Framework Connected AlO_6 Sites in the Vicinity of Fe by Controlled Dealumination During Exchange. *Appl. Catal. B* **2017**, *203*, 218-226.

34. Hansen, N.; Heyden, A.; Bell, A. T.; Keil, F. J. Microkinetic Modeling of Nitrous Oxide Decomposition on Dinuclear Oxygen Bridged Iron Sites in Fe-ZSM-5. *J. Catal.* **2007**, *248,* 213-225.

35. Brus, J.; Kobera, L.; Schoefberger, W.; Urbanová, M.; Klein, P.; Sazama, P.; Tabor, E.; Sklenak, S.; Fishchuk, A. V.; Dědeček, J. Structure of Framework Aluminum Lewis Sites and Perturbed Aluminum Atoms in Zeolites as Determined by ^{27}Al {^{1}H} REDOR (^{3}Q) MAS NMR Spectroscopy and DFT/Molecular Mechanics. *Angew. Chem., Int. Ed.* **2015**, *54,* 541-545.

36. Lónyi, F.; Valyon, J. On the Interpretation of the NH_3-TPD Patterns of H-ZSM-5 and H-Mordenite. *Micropor. Mesopor.Mat.* **2001**, *47*, 293-301.

37. Kresnawahjuesa, O.; Gorte, R. J.; De Oliveira, D.; Lau, L. Y. A simple, Inexpensive, and Reliable Method for Measuring Brønsted-Acid Site Densities in Solid Acids. *Catal. Lett.* **2002**, *82*, 155-160.

38. Gao, Y.; Zheng, B.; Wu, G.; Ma, F.; Liu, C. Effect of the Si/Al Ratio on the Performance of Hierarchical ZSM-5 Zeolites for Methanol Aromatization. *RSC Adv.* **2016**, *6*, 83581-83588.

39. Bonelli, B.; Cozzolino, M.; Tesser, R.; Di Serio, M.; Piumetti, M.; Garrone, E.; Santacesaria, E. Study of the Surface Acidity of TiO_2/SiO_2

Catalysts by Means of FTIR Measurements of CO and NH_3 Adsorption. *J. Catal.* **2007**, *246*, 293-300.

40. Bortnovsky, O.; Melichar, Z.; Sobalık, Z.; Wichterlová, B. Quantitative Analysis of Aluminium and Iron in the Framework of Zeolites. *Micropor. Mesopor. Mat.* **2001**, *42*, 97-102.

41. Guzmán-Vargas, A.; Delahay, G.; Coq, B. Catalytic Decomposition of N_2O and Catalytic Reduction of N_2O and N_2O+ NO by NH_3 in the Presence of O_2 over Fe-Zeolite. *Appl. Catal. B* **2003**, *42*, 369-379.

42. Joyner, R.; Stockenhuber, M.; Preparation, Characterization, and Performance of Fe-ZSM-5 Catalysts. *J. Phys. Chem. B* **1999**, *103*, 5963-5976.

43. Blasin-Aubé, V.; Marie, O.; Saussey, J.; Plesniar, A.; Daturi, M.; Nguyen, N.; Hamon, C.; Mihaylov, M.; Ivanova, E.; Hadjiivanov, K. Iron Nitrosyl Species in Fe-FER: a Complementary Mossbauer and FTIR Spectroscopy Study. *J. Phys. Chem. C* **2009**, 113, 8387-8393.

44. Fellah, M. F. CO and NO Adsorptions on Different Iron Sites of Fe-ZSM-5 Clusters: a Density Functional Theory Study. *J. Phys. Chem. C* **2010**, *115*, 1940-1951.

45. Sun, K.; Xia, H.; Hensen, E.; van Santen, R.; Li, C. Chemistry of N_2O Decomposition on Active Sites with Different Nature: Effect of High-Temperature Treatment of Fe/ZSM-5. *J. Catal.* **2006**, *238*, 186-195.

46. Mul, G.; Perez-Ramirez, J.; Kapteijn, F.; Moulijn, J. A. NO Adsorption on Ex-Framework [Fe, X] MFI Catalysts: Novel IR Bands and Evaluation of Assignments. *Catal. Lett.* **2002**, *80*, 129-138.

47. Kameoka, S.; Nobukawa, T.; Tanaka, S. I.; Ito, S. I.; Tomishige, K.; Kunimori, K. Reaction Between N_2O and CH_4 over Fe Ion-Exchanged BEA Zeolite Catalyst: A Possible Role of Nascent Oxygen Transients from N_2O. *Phys. Chem. Chem. Phys.* **2003**, *5,* 3328-3333.

48. Stockenhuber, M.; Hudson, M.J.; Joyner, R.W. Preparation, Characterization, and Unusual Reactivity of Fe-MCM-41. *J. Phys. Chem.* B **2000**, *104*, 3370-3374.

49. Wood, B. R.; Reimer, J. A.; Bell, A. T.; Janicke, M. T.; Ott, K. C. Methanol Formation on Fe/Al-MFI via the Oxidation of Methane by Nitrous Oxide. *J. Catal.* **2004**, *225*, 300-306.

50. Campbell, S.M.; Jiang, X. Z.; Howe, R. F. Methanol to Hydrocarbons: Spectroscopic Studies and the Significance of Extra-Framework Aluminium. *Micropor. Mesopor. Mat.* **1999**, *29,* 91-108.

51. Pinard, L.; Tayeb, K. B.; Hamieh, S.; Vezin, H.; Canaff, C.; Maury, S.; Delpoux, O.; Pouilloux, Y. On the Involvement of Radical “Coke” in Ethanol Conversion to Hydrocarbons over HZSM-5 Zeolite. *Catal. Today* **2013**, *218*, 57-64.

52. Caeiro, G.; Lopes, J. M.; Magnoux, P.; Ayrault, P.; Ribeiro, F. R. A FT-IR Study of Deactivation Phenomena during Methylcyclohexane Transformation on H-USY Zeolites: Nitrogen Poisoning, Coke Formation, and Acidity–Activity Correlations. *J. Catal.* **2007**, *249*, 234-243.

53. Khadzhiev, S. N.; Magomedova, M. V.; Peresypkina, E. G. Mechanism of Olefin Synthesis from Methanol and Dimethyl Ether over Zeolite Catalysts: A Review. *Petrol. Chem.* **2014**, *54*, 245-269.

54. Chow, Y. K.; Dummer, N. F.; Carter, J. H.; Meyer, R. J.; Armstrong, R. D.; Williams, C.; Shaw, G.; Yacob, S.; Bhasin, M. M.; Willock, D. J. *et al.* A Kinetic Study of Methane Partial Oxidation over Fe-ZSM-5 Using N_2O as an Oxidant. *ChemPhysChem* **2018**, *19*, 402-411.

55. Aihua, X.; Li, W.; Yulin, S. Evolution of Coke Deposit and its Effect on Product Selectivity for Methanol-to-Olefin Reaction in Fluidized Bed. *Energ. Fuel.* **2014**, *28*, 3339-3344.

CHAPTER 6

6 DIRECT METHANE CONVERSION TO VALUE ADDED PRODUCTS BY N_2O OVER FE-FER CATALYSTS PREPARED BY DIFFERENT METHODS

6.1 Introduction

Iron incorporated FER zeolites exhibited improved catalytic performance in terms of N_2O and methane conversion, and higher selectivity to desired products, i.e. methanol, formaldehyde and DME in comparison to Fe-ZSM-5 and Fe-Beta catalysts. This is attributed to the higher concentration of active sites that are responsible for N_2O conversion, and the greater efficiency of migration of formed methoxy groups from iron sites to silicon species, as demonstrated in the previous chapter. The active sites were proposed to be extra-framework Fe clusters acting as counter ions of the negatively charged Al in the framework.

As reported in previous publications, the state of iron species incorporated in zeolites strongly depends on preparation method [1-4]. Further enhancement of selectivity to valuable products can be achieved by preparing catalysts by applying the aqueous ion exchange method, which leads to higher dispersion and greater level of protons exchange in zeolites by iron ions in comparison to impregnation method [4]. Solid state ion exchange is another attractive preparation method which mixes precursor and zeolite mechanically without involvement of water [3, 5-7], and hence forms distinctive difference metal sites in comparison to aqueous ion exchange method [5, 7-9]. Comparison of activity of Fe-based catalysts prepared by aqueous ion exchange and solid state ion exchange for N_2O decomposition has been extensively studied, however presented contradictory results [3, 6, 10-12].

To investigate the effect of preparation method on catalytic performance of catalysts, in the present chapter, incipient wetness impregnation (IMP),

aqueous ion exchange (IE) and solid state ion exchange (SSIE) methods were used to load 0.5wt% iron on FER zeolite to make Fe-FER catalysts. This research will contribute to determining the number and the nature of the active sites for N_2O conversion and methanol formation, as the various preparation methods lead to formation of different Fe species on the zeolites [5, 13]. Catalytic partial oxidation of methane by N_2O in a continuous mode at moderate temperature (350 ℃) was to investigate the catalytic performance of Fe-FER catalysts synthesised by different preparation methods. Characterisation techniques including H_2-TPR, *in situ* FTIR, UV-vis spectroscopy, XRD and SEM were employed to reveal the relation between catalytic activity and nature of the Fe species over Fe-FER catalysts.

6.2 Experimental

6.2.1 Catalyst preparation

The Fe-FER (0.5 wt%) catalysts used in this study were prepared by incipient wetness impregnation, aqueous ion exchange and solid state ion exchange method. The parent NH_4-FER with Si/Al ratios of 10 was purchased from Zeolyst. $FeCl_3 \cdot 6H_2O$ supplied by Sigma-Aldrich was weighed firstly according to the desired concentration of iron (0.5 wt%). For incipient wetness impregnation method, the $FeCl_3 \cdot 6H_2O$ was dissolved in distilled water to make iron salt solution, which then was then impregnated onto NH_4-FER under ambient conditions. The well-mixed paste then was transferred to a crucible and dried for 2 hours and then calcined at 550 °C for 5 hours at a heating rate of 3 °C/min. The powder was then pressed and sieved, and the particles within the size range of 250 μm to 425 μm were chosen to be used in the reaction.

When the aqueous ion exchange method was performed, calcined FER zeolite was added into $FeCl_3$ solution, and the mixture was then heated to 80°C and stirred for 24 h in a fume cupboard. The solution was washed extensively and centrifuged 5 times, and the remaining paste was dried over night at 80°C. The powder thus obtained was then pressed and sieved. When the solid state ion exchange method was employed, the iron salt was weighed and then was mechanically mixed with the appropriate amount of zeolite for the desired Fe-exchange level. The mixture was then placed in a crucible and rapidly heated to 500 °C in half hour and maintained at 500 °C for 3 h, and then cooled to room temperature, followed by calcination at 550 °C for 5 hours at a heating rate of 3 °C/min, following which the powder was then pressed and sieved.

6.2.2 Catalyst performance studies

Catalyst studies were performed in a fix-bed stainless steel tube reactor. 200 mg (unless stated elsewhere) catalyst was held in place by two quartz wool plugs and was activated in a flow of helium at a heating rate of 3 °C/min to 550 °C and was held at 550 °C for 3 h. The reaction was conducted at a temperature range from 250 ℃ to 350 °C with helium, methane and nitrous oxide being fed at a ratio of 65:28:7 and a total flow rate of 70 $ml \cdot min^{-1}$. The products were analysed using an online gas chromatography (Varian 490-GC) and a FTIR (Shimadzu IRPrestige21). The GC was equipped with a Molsieve column to detect CH_4 and CO, and a PoraPLOT Q (PPQ) column to detect N_2O, CO_2 and C_2H_4, while the FTIR was used to detect methanol, formaldehyde and DME.

6.2.3 Characterization

XRD was performed on a Phillips X'pert Pro diffractometer utilizing Cu Ka radiation. SEM images were provided by a Zeiss Sigma VP Field Emission SEM. UV-Vis diffuse reflectance spectra were collected at ambient temperature on a Cary 5000 spectrophotometer equipped with a Praying Mantis attachment. IR spectra were recorded using a Bruker Tensor 27 FT-IR equipped with an MCT detector. Samples (30 mg) were pressed into self-supporting wafer and subsequently placed into an IR cell equipped with CaF_2 IR windows. For NO adsorption experiments, the FTIR spectra were monitored at 150 ℃ after adsorption of NO (5 x 10^{-2} mbar). The H_2-TPR experiments were carried out using a custom-built instrument equipped with a thermal conductivity detector for hydrogen measurement to investigate the reducibility of catalyst. Prior to the H_2-TPR analysis, 300 mg of catalyst was placed in a quartz micro-reactor located in a furnace, and purged in a stream of air or helium (30 ml/min) at 450 °C for 1 h. Reduction by hydrogen was carried out in a H_2/Ar stream (2.04 vol% of H_2), with a total flow rate of 50 ml/min and a linear heating rate of 10 °C /min in the temperature range of 20–800 °C. N_2O pre-treatment, if employed, was performed at 250 °C or 350 °C on the dehydrated zeolites with a N_2O flow rate of 30 ml/min for 1 hour, and then cooled to room temperature, prior to reduction by the H_2/Ar stream.

6.3 Results and discussions

6.3.1 XRD pattern

The X-ray diffraction pattern of parent zeolites and catalysts are shown in Fig. 6.1. All the Fe loaded catalysts exhibited the typical diffraction pattern of

parent zeolite, indicating that the zeolite crystal structures of all catalysts remained intact following iron loading and calcination. In addition, there were no extraneous reflections appearing in the XRD patterns of iron-loaded zeolites, consistent with the small amount of iron loading and a relatively high level of iron dispersion in the zeolite [14].

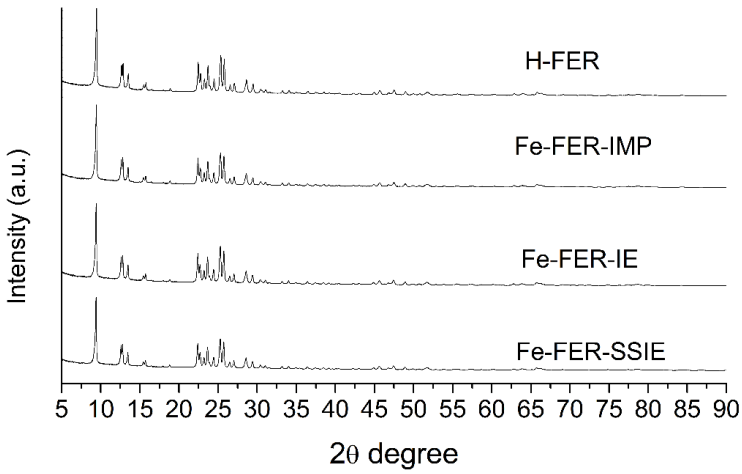

Figure 6.1XRD pattern of Fe-FER catalysts prepared by different methods

6.3.2 SEM images

The SEM images of Fe-FER catalysts as shown in Fig. 6.2 demonstrated that there were iron oxides aggregation formed over Fe-FER prepared by IMP. SSIE obtained better dispersion, but the big iron particles were still observable. Fe-FER-IE exhibited the best dispersion among the three samples as shown in Fig. 6.2.

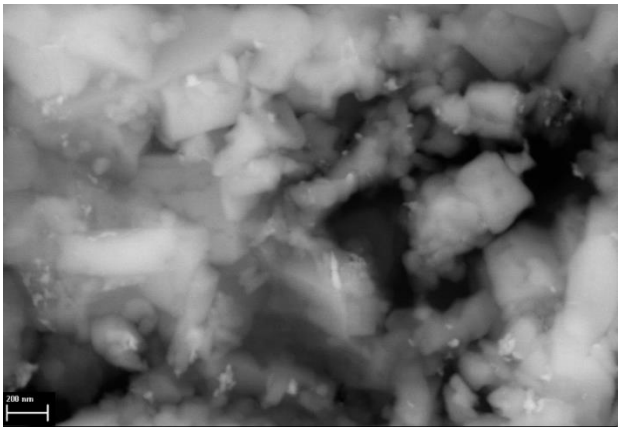

a. Fe-FER-IMP

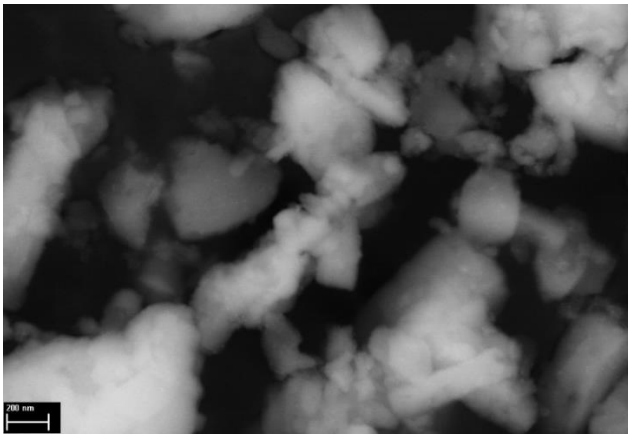

b. Fe-FER-IE

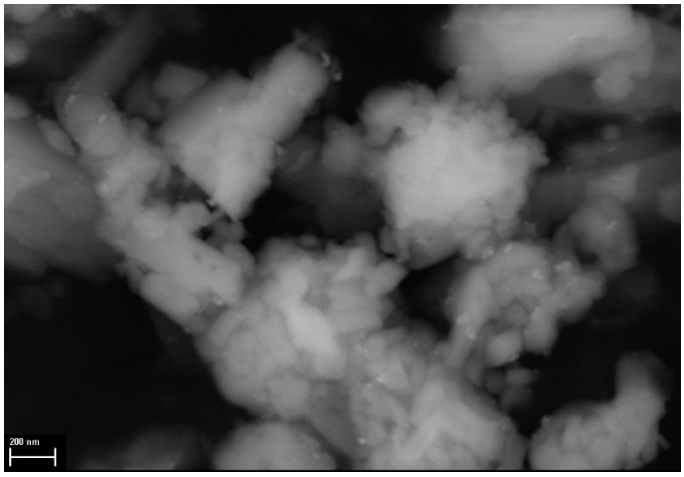

c. Fe-FER-SSIE

Figure 6.2 SEM images of Fe-FER catalysts prepared by different methods

6.3.3 UV-vis spectra

UV-vis spectra of Fe-FER catalysts prepared by IMP, IE and SSIE are decomposed and displayed in Fig. 6.3. The spectra of Fe-FER catalysts presents intense bands at below 30000 cm^{-1}, between 35000 cm^{-1} and 38000, and above 40000 cm^{-1}, respectively. There have been extensive studies regarding assignment of the bands, and it is generally accepted that the wavelength between 15000 cm^{-1} and 50000 cm^{-1} can be divided into three zones in which the bands are assigned to mononuclear, oligomeric and aggregated iron species, respectively [15]. Normally the bands at high wavelength (above 33000 cm^{-1}) are assigned to ligand to metal charge transform (LMCT) transitions of isolated Fe^{3+} species in tetrahedral or octahedral coordination, the bands at between 30000 cm^{-1} and 25000 cm^{-1} are typically attributed to oligomeric Fe_xO_y clusters, and bands below 25000 cm^{-1} are assigned to large Fe_2O_3 particles [16, 17]. The assignment of band at round 28200 cm^{-1} to dinuclear Fe^{3+} complexes was suggested [18], which however was rejected by subsequent studies. It was proposed that the bands above 40000 cm^{-1} are assigned to isolated Fe^{3+} species in framework sites, the bands between 40000 cm^{-1} and 28500 cm^{-1} are assigned to isolated or oligomeric extra-framework Fe species in zeolites channels, bands between 28500 cm^{-1} and 22000 cm^{-1} are assigned to iron oxide clusters, and bands below 22000 cm^{-1} are assigned to large surface oxide species [19, 20]. The assignment of bands above 33000 cm^{-1} have been deeply studied based on the assistance from EXAFS and Mossbauer results, and the physical origin of red-shift of the LMCT bands of oxygen bridged iron dimers relative to

isolated iron ions were observed and explained [21], therefore the bands above 33000 cm^{-1} could be due to isolated and dimeric ion species [22].

Table 6.1 Distribution of Fe species shown in UV-vis spectra

	Area percentage of various bands (%)			
	Ca. 21000	ca. 29000	ca. 37000	ca. 42000
IMP	-	51.4	33.5	15.1
IE	-	2.9	38.3	58.9
SSIE	9.3	31	47.7	11.9

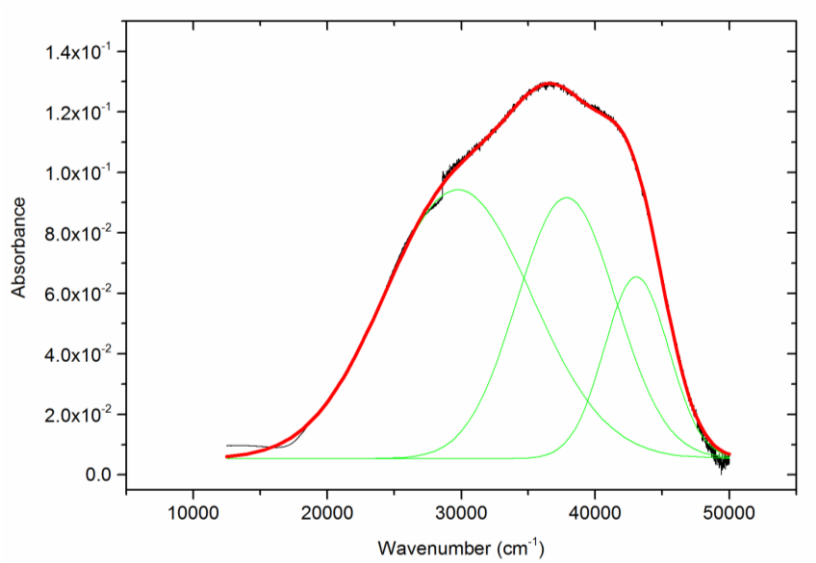

a. Fe-FER-IMP

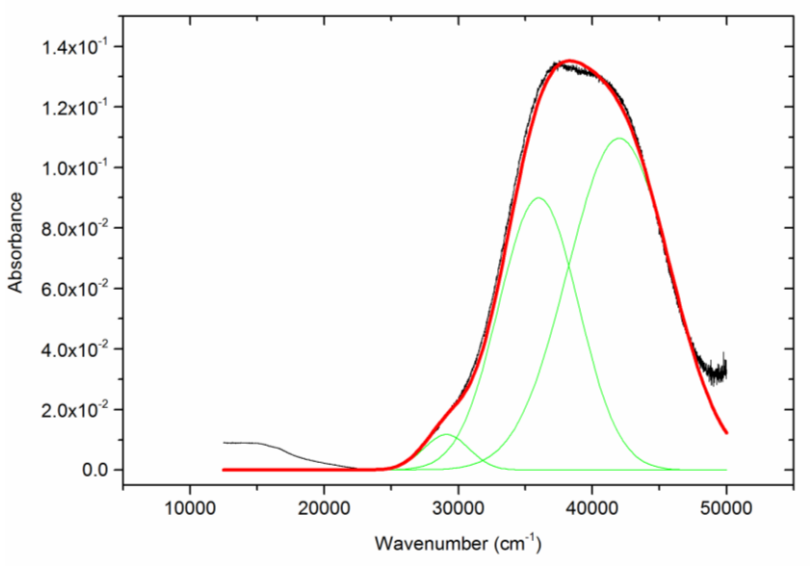

b. Fe-FER-IE

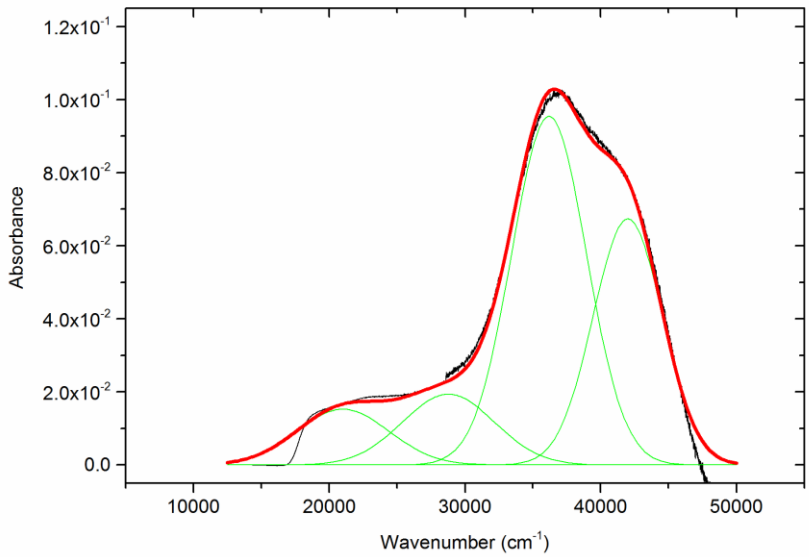

c. Fe-FER-SSIE

Figure 6.3 UV-vis spectra of Fe-FER catalysts prepared by different methods

In this study, the band at a wavelength centred around 42000 cm^{-1} is assigned to isolated Fe^{3+} species at framework sites, while the band at around 37000 cm^{-1} are ascribed to dimeric extra-framework Fe^{3+} species, and the band at

around 29000 cm^{-1} is attribute to oligomeric Fe_xO_y clusters. In addition, in the spectra of Fe-FER-IMP and Fe-FER-SSIE, broad signals at around 21000 cm^{-1} were observed and the signals are assigned to the bulk Fe iron oxide. The relative percentage of deconvoluted band area is estimated and shown in Table. 6.1. It is shown that the Fe species with dominate percentage in the three Fe-FER catalysts are isolated extra-framework Fe species for Fe-FER-IE, and dimeric extra-framework Fe species for Fe-FER-SSIE, and oligomeric oxide clusters for Fe-FER-IMP, respectively. Even though the UV-vis spectroscopy is more of a qualitative characterization technique, and the wavelength dependence of the absorption coefficient is unknown, the relative percentage of the components still presents crucial information related to the composition of iron species in the Fe-FER catalysts. The large portion of isolated Fe^{3+} species within Fe-FER-IE indicates the ion exchange of Fe ions into the zeolite and enhanced iron dispersion than Fe-FER-SSIE and Fe-FER-IMP. Conversely, the main Fe species within Fe-FER-IMP were oligonuclear clusters and big iron oxide particles, suggesting a reduced level of dispersion within Fe-FER-IMP. For Fe-FER-SSIE, a major peak assigned to dimeric extra-framework Fe species were observed.

6.3.4 IR spectra of NO adsorption

IR study of NO adsorption is known as an effective technique to investigate the nature of specific iron species on the catalysts, as NO molecules adsorb on various Fe sites and exhibit distinguishable vibration bands. NO adsorption in the *in situ* FTIR was undertaken for the three catalysts and a comparison of the spectra of the catalysts following NO adsorption is presented in Fig. 6.4 and Fig. 6.5. As shown in Fig. 6.4, between 1840 cm^{-1} to 1940 cm^{-1}, each of

the spectra were deconvoluted to two peaks at 1870 cm^{-1} and 1892 cm^{-1}. The strong band centred at 1870 cm^{-1} has been extensively observed and is generally assigned to a mononitrosyl species on the Fe^{2+} species [18, 23-25]. The band at 1892 cm^{-1} was proposed to assign to NO adsorption on Fe sites which can be easily oxidized to Fe^{3+} species, and these sites were suggested to be the α-sites [25]. A similar band at 1892 cm^{-1} was observed and assigned to binuclear iron-oxo sites, and the reported experimental value of vibrational frequency matched with calculated value of vibrational frequency of band at 1897 cm^{-1} in followed study [26, 27].

Comparison of the band centred at 1892 cm^{-1} is shown in Fig. 6.5. The intensity order of the band shown in the three catalysts is: Fe-FER-SSIE > Fe-FER-IE > Fe-FER-IMP, indicating that Fe-FER-SSIE contained the largest amount of dimeric Fe species, which is consistent with the results from the UV-vis spectra as shown in Fig. 6.3.

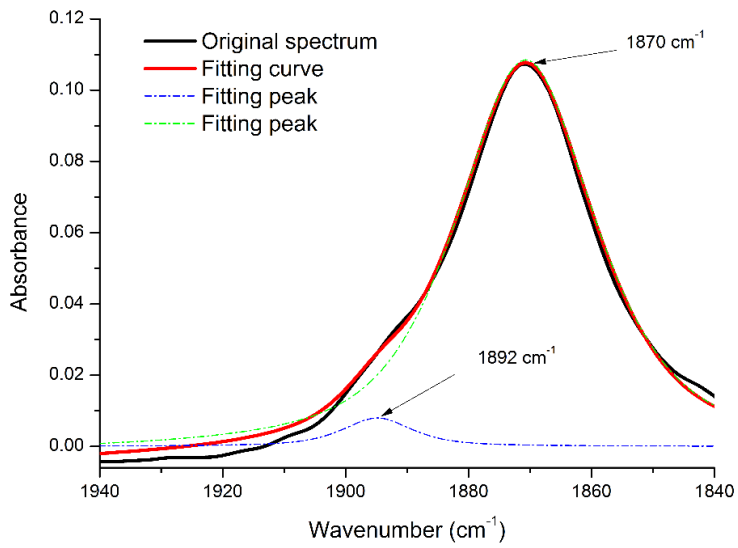

a. Fe-FER-IMP

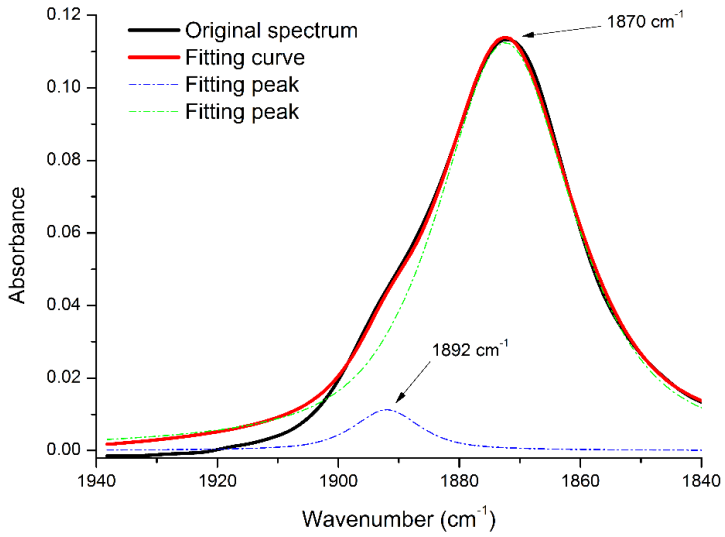

b. Fe-FER-IE

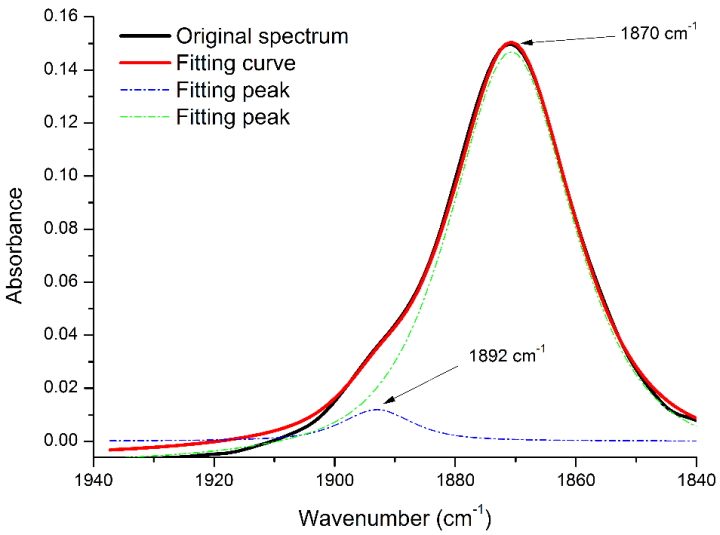

c. Fe-FER-SSIE

Figure 6.4 IR spectra of NO adsorption on Fe-FER catalysts prepared by different methods at 150 °C

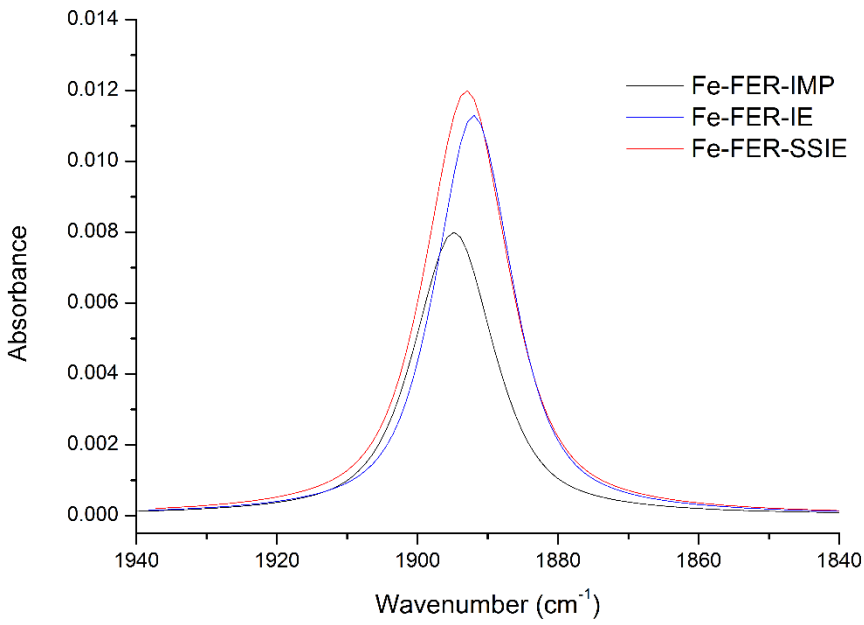

Figure 6.5 Comparison of the band at 1892 cm^{-1} in IR of NO adsorption over Fe-FER catalysts prepared by different methods

6.3.5 H_2-TPR profiles

In the H_2-TPR profiles of catalysts, hydrogen consumption peaks at different temperatures were observed as shown in Fig. 6.6. Hydrogen consumption observed in a broad temperature range indicated that there were a variety of Fe species associated with zeolite framework. The reduction of Fe-FER-IMP led to two main peaks, a sharp peak at ca. 330 °C due to the reduction of the Fe^{3+} to Fe^{2+} species, followed by a broad peak from 380 °C to 650 °C, which corresponded to reduction of FeO to Fe^{0} species, and indicated the presence of small Fe_2O_3 aggregates [4, 6, 28]. For Fe-FER-IE, a broad peak of reduction at ca. 390 °C with a shoulder at ca. 380 °C was observed, and the intensity of band ranged from 380 °C to 650 ℃ was much lower than that observed in Fe-FER-IMP. Therefore, the shoulder at ca. 380 °C and the peak centred at 393 °C are believed to be attributed to the reduction of Fe^{3+} to Fe^{2+} species and

Fe^{2+} to Fe^{0} species. The results are in accordance with that from previous studies, indicating that, compared to the Fe species in Fe-FER-IMP catalysts, the main Fe species in Fe-FER-IE are well-dispersed ion exchanged Fe^{3+} species which are readily reduced [4]. While in Fe-FER-SSIE, two stronger hydrogen consumption peaks were observed to centre at 480 °C and 590 °C, which reflected the reduction of Fe^{2+} to Fe^{0} species and the presence of iron oxides particles. Two shoulders at ca. 330 °C and ca. 390 °C are suggested an association with the reduction of Fe^{3+} to Fe^{2+} species.

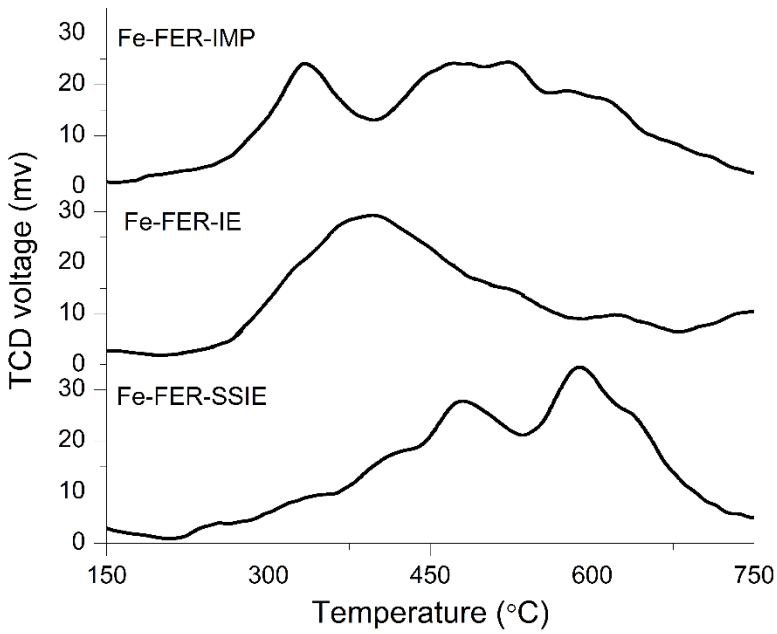

Figure 6.6 H_2-TPR profiles of Fe-FER catalysts

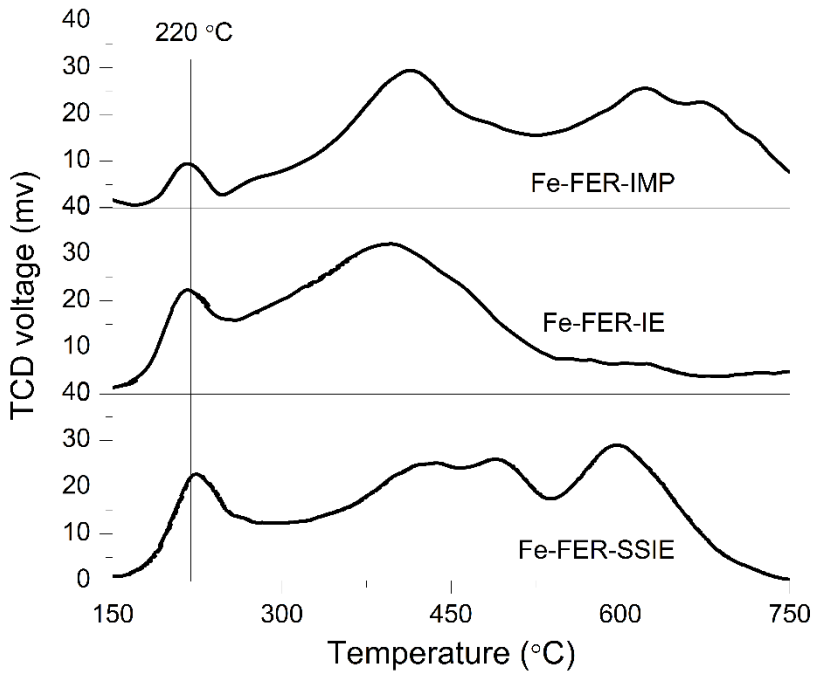

Figure 6.7 H_2-TPR profiles of Fe-FER catalysts pre-treated by N_2O at 250 °C

To investigate the concentration of active sites for N_2O decomposition over the catalysts, H_2-TPR was undertaken for samples pre-treated with N_2O at 250 ℃ . As shown in Fig. 6.7, the pre-treatment of N_2O results in shift in the reduction peaks, indicating that new Fe species were formed during the oxidation of original Fe species by N_2O. Particularly, a new hydrogen consumption peak at 220 °C was observed over all samples. The results are in good agreement with previous publications that reported that N_2O pre-treatment at 200 °C would lead to a hydrogen consumption peak at lower temperature in H_2-TPR profiles, and the peak reflects the reduction of monoatomic oxygen stabilized on originally Fe^{2+} species [29]. In addition, the area of the peak was reported to correlate with the amount of active sites for N_2O decomposition [30]. As shown in Fig. 6.7, Fe-FER-SSIE displayed the hydrogen consumption peak with the highest area among the three catalysts, and the area of the peak at 220 °C is in accordance with the area of band at

1892 cm^{-1} in the IR spectra as shown in Fig. 6.8. This suggests that the number of active oxygen species correlates with the amount of binuclear extra-framework Fe species, which could subsequently undergo a reversible redox transition between $Fe^{2+} \leftrightarrow Fe^{3+}$ and are thus the active sites for N_2O decomposition. Fe-FER-SSIE contained the greatest number of active sites for N_2O decomposition, while the mononuclear Fe species and big particles of iron oxides observed in Fe-FER-IE and Fe-FER-IMP catalysts are less active.

In addition, it should be noted that the intensity of band at 1892 cm^{-1} in the IR spectra of NO adsorption was much lower than that of the overall Fe species, suggested that only a small fraction of Fe cations are associate with active sites for N_2O decomposition [25, 31].

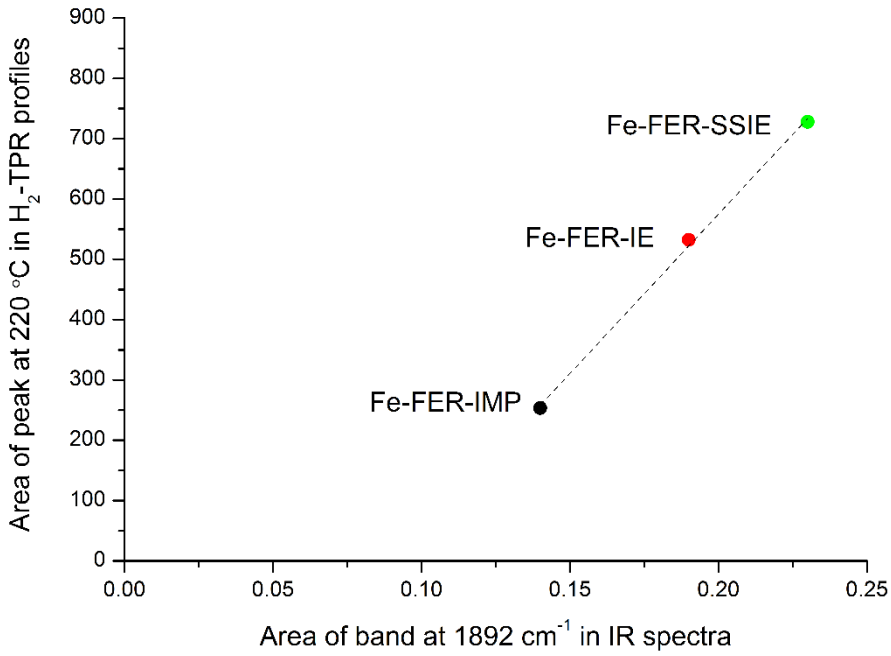

Figure 6.8 The integrated area of hydrogen consumption peak centred at 220 °C in the H_2-TPR profiles versus the peak area of band at 1892 cm^{-1} in the NO adsorption IR over catalysts

It should be noted that, at temperatures above 250 °C, the active oxygen species are unstable and may transform to oxygen molecules which are not able to activate methane [32, 33]. Therefore, H_2-TPR of samples that pre-treated by N_2O at 350 °C was undertaken to investigate the stability of active oxygen species formed over the catalysts.

As shown in Fig. 6.9, pre-treatment of catalysts by N_2O at 350 °C also led to the formation of hydrogen reduction peaks at 220 °C over the catalysts studied, but displayed a significant decrease in area in comparison to the area of the peak when the samples were pre-treated with N_2O at 250 °C as shown in Fig. 6.7. The results demonstrate that the active oxygen species are readily transformed at elevated temperature. As shown in Fig. 6.10, the decrease in area of the peak over the three catalysts was calculated, and the most notable reduction (90.4%) of the area was observed over Fe-FER-IE, followed by Fe-FER-IMP and Fe-FER-SSIE. It was reported that the solid state ion exchange method allows metal atom to migrate into the ion-exchangeable positions of lower accessibility [13], and hence may form the active oxygen species that require higher temperatures to decompose. In addition, the formation of oxygen molecules are initiated with the recombination of two surface oxygen atoms, which is the rate-limiting step for decomposition of the active oxygen species [34], and the relatively low concentration of active sites over Fe-FER-IMP may contribute to enhanced stability of active oxygen species than Fe-FER-IE.

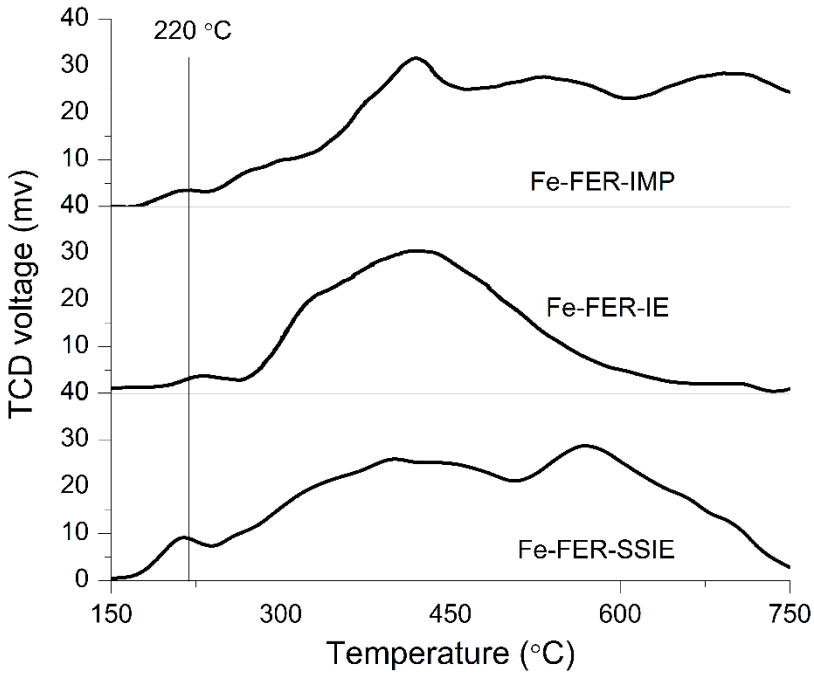

Figure 6.9 H_2-TPR profiles of Fe-FER catalysts pre-treated by N_2O at 350 °C

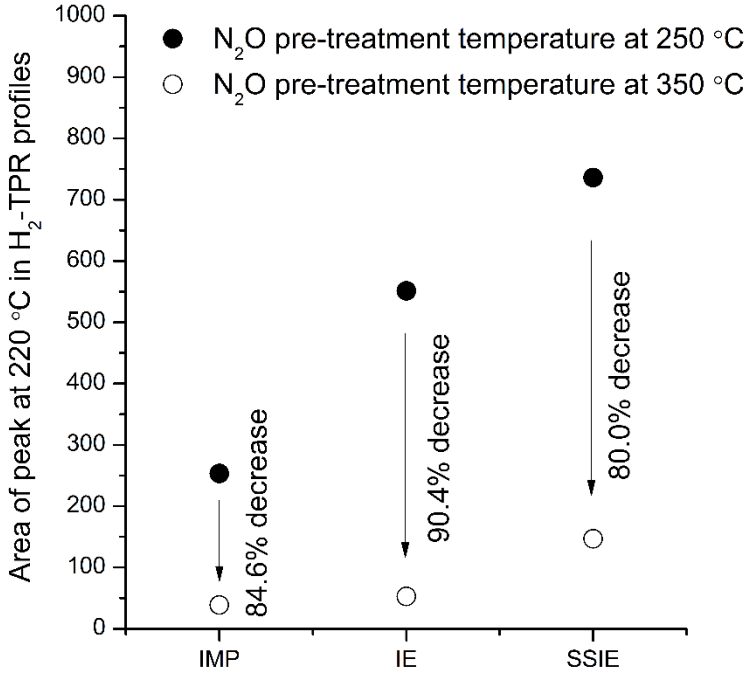

Figure 6.10 Decrease on area of peak at 220 °C in the H_2-TPR profiles

6.3.6 Catalytic activity test

N_2O decomposition at a temperature range of 250 °C to 350 °C over Fe-FER-IMP, Fe-FER-IE and Fe-FER-SSIE catalysts was compared as shown in Fig. 6.11.

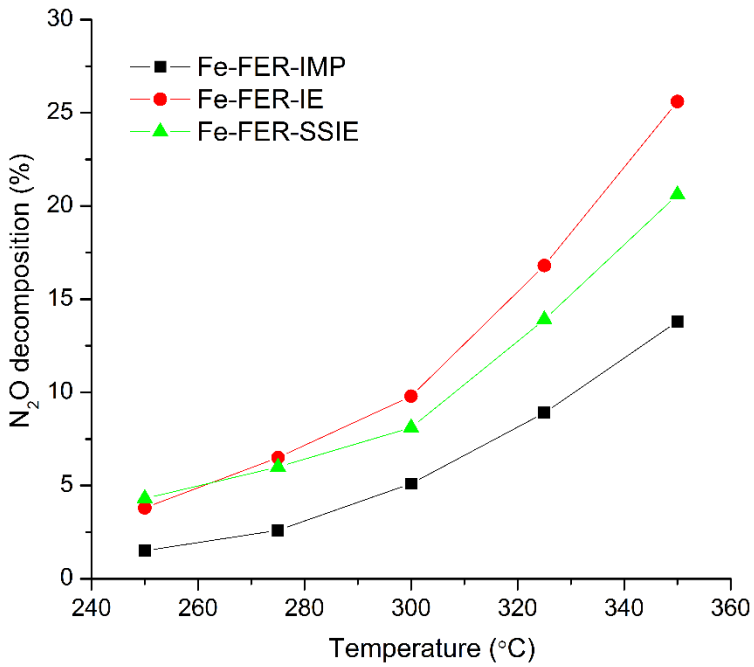

Figure 6.11 N_2O decomposition over Fe-FER catalysts prepared by different methods at different temperatures

N_2O decomposition increased with temperature over three catalysts, and Fe-FER-IMP obtained the lowest N_2O decomposition at all the reaction temperatures. Fe-FER-SSIE showed slightly higher activity for N_2O decomposition than Fe-FER-IE at 250 °C, however a lower N_2O decomposition than Fe-FER-IE was observed at elevated temperatures. As shown in Fig. 6.10, the active oxygen species formed over Fe-FER-IE are less stable and more readily decompose to form oxygen molecules. As a consequence, at elevated temperatures, large portion of formed Fe^{3+}-O

species from N_2O decomposition over Fe-FER-IE catalyst were subsequently transformed to O_2 with a higher efficiency than Fe-FER-SSIE, Fe-FER-IE hence exhibited better performance on N_2O decomposition even though contained a lower concentration of active sites in comparison to Fe-FER-SSIE.

N_2O decomposition and methane conversion as a function of time on stream over the Fe-FER catalysts prepared by different methods at 350 ℃ was compared as shown in Fig. 6.12. To obtain methane conversion with a similar level over the three catalysts, 200 mg of Fe-FER SSIE and IE, and 200 mg and 280 mg of Fe-FER IMP were used for the activity test. The application of larger amount Fe-FER-IMP catalyst obtained higher N_2O decomposition but still less than 17.5% due to lack of active sites. Fe-FER-IE catalyst achieved the highest N_2O conversion, however, Fe-FER-SSIE obtained an average methane conversion of 2.8%, which is slightly higher than that over Fe-FER-IE and Fe-FER-IMP (280 mg).

The relationship between N_2O decomposition and methane conversion reflects a fact that the utilization efficiencies of active oxygen species for methane conversion over Fe-FER-IE and Fe-FER-SSIE were different in the continuous mode reaction. As shown in Fig. 6.10, a more significant decrease in the area of the H_2 peak at 220 °C over Fe-FER-IE in comparison to Fe-FER-SSIE suggested a higher likelihood of self-decomposition of the active oxygen species to oxygen molecules, and the O_2 failed to activate methane and hence led to lower methane conversion. For Fe-FER-SSIE, the active oxygen species are more stable and tend to maintain in the micropores and react with methane instead.

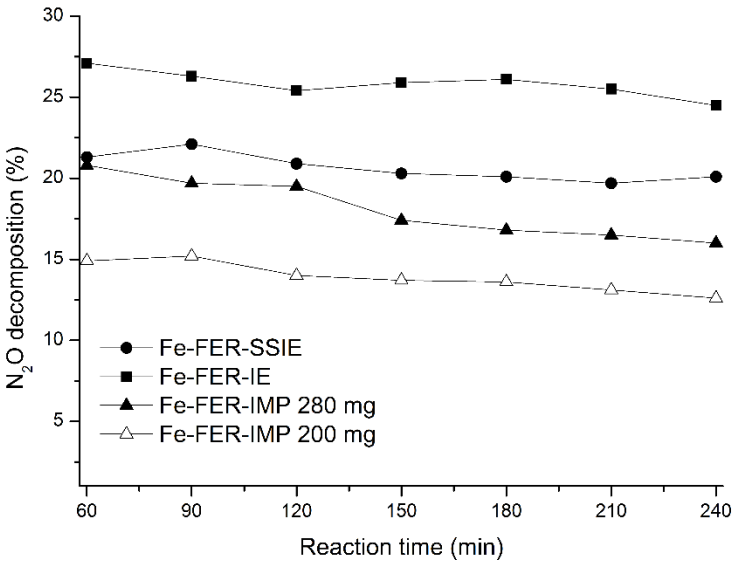

a. N_2O decomposition

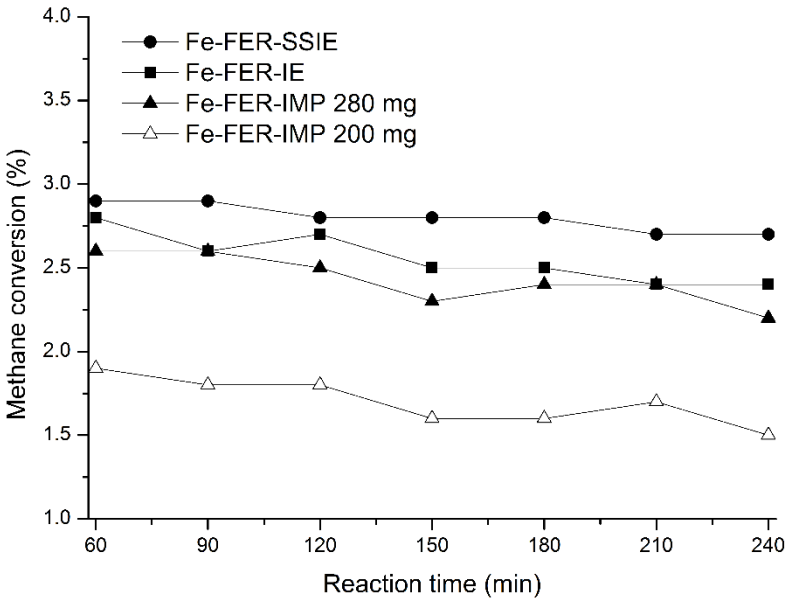

b. Methane Conversion

Figure 6.12 N_2O decomposition (a) and methane conversion (b) over Fe-FER catalysts prepared by different methods

In addition, a slight decrease in methane conversion and N_2O decomposition was observed in the 4 h reaction over the studied catalysts, which might be due to the formation of coke during the reaction between methane and N_2O.

In this study, the unknown carbon was assumed to be carbon deposition in the catalysts, and the products selectivity (coke took into account) was accordingly estimated over the studied catalysts is shown in Fig. 6.13. Over the three catalysts, coke was remarkably formed with a selectivity above 50%. Fe-FER-IE contained the lowest selectivity to coke but highest selectivity to carbon oxides. It is known that the generated methanol either undergo further oxidation to form formaldehyde, CO and CO_2, or dehydrate to DME, ethylene, aromatics and finally forms coke [35, 36]. The higher selectivity to CO and CO_2 observed over Fe-FER-IE suggests an elevated rate of complete oxidation of intermediates (methanol, DME, formaldehyde and ethylene), which is due to the larger concentration of oxygen molecules released from decomposition of active oxygen species (from N_2O). Fe-FER-IMP obtained the lowest methane conversion, N_2O decomposition but highest coke, due to lower concentration of active sites. Fe-FER SSIE obtained the highest selectivity to desired products, i.e. methane, formaldehyde, DME and ethylene, which accounted for 22%, the selectivity to desired products over Fe-FER IE and IMP was 16.5% and 12.5%, respectively. In addition, Fe-FER-SSIE was less selective to methanol formation compared to Fe-FER-IE, but the selectivity to DME over Fe-FER-SSIE was 1.6 times of that over Fe-FER-IE, which may relate to the longer pathway of methanol desorption from the lower accessible Fe sites enhanced the chance of DME formation from methanol dehydration.

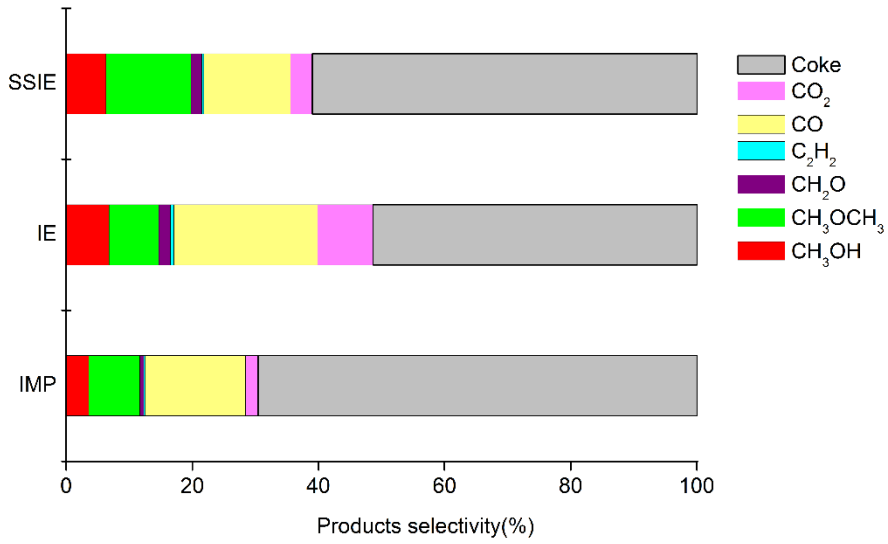

Figure 6.13 Product selectivity over Fe-FER catalysts prepared by different methods (Fe-FER-IMP: 280 mg, Fe-FER-IE: 200 mg. Fe-FER-SSIE: 200 mg).

6.4 Conclusion

Catalytic partial oxidation of methane with N_2O at moderate temperature over Fe-FER catalysts prepared by different methods was compared and characterization of catalysts was undertaken. UV-vis spectra suggested that iron species were well-dispersed in the ferrierite zeolite over Fe-FER-IE, primarily leading to the formation of isolated Fe sites; while dimeric Fe species and oligomeric Fe_xO_y clusters exhibited as the main component over Fe-FER-SSIE and Fe-FER-IMP catalysts, respectively. Comparison of area of the IR band at 1892 cm^{-1} in IR spectra of NO adsorption on the studied catalysts demonstrated that Fe-FER-SSIE contained the highest concentration of binuclear extra-framework Fe species, which was in agreement with the observation that the most prominent hydrogen consumption peak at 220 ℃ in H_2-TPR profiles of Fe-FER-SSIE pre-treated with N_2O at 250 °C. Based on

the evidence from UV-vis spectra, IR spectra of NO adsorption and H_2-TPR profiles, the active sites for N_2O decomposition over Fe-FER are suggested to be binuclear extra-framework Fe species, and Fe-FER-SSIE contained the greatest amount of active Fe species.

In contrast, catalyst activity studies showed that Fe-FER-IE displayed the highest rate of N_2O decomposition at temperatures above 250 ℃ among the three catalysts, due to the instability of active oxygen species formed from N_2O decomposition, according to H_2-TPR profiles of samples pre-treated with N_2O at 350 ℃ . However, the oxygen molecule released from these sites does not appear to active methane but leads to the complete oxidation of intermediates to CO and CO_2. The active oxygen species formed over Fe-FER-SSIE exhibited the highest stability, which might be related to the active sites located at less accessible positions. Among the studied catalysts, Fe-FER-SSIE achieved the greatest methane conversion (2.8%) and selectivity to desired products (22%).

6.5 Reference

1. Capdeillayre, C.; Mehsein, K.; Petitto, C.; Delahay, G. Fe-ZSM-5 Catalyst Prepared by Ion Exchange from Fe $(acac)_3$: Application into NH_3-SCR of NO. *Top. Catal.* **2016**, *59*, 901-906.

2. Delahay, G.; Bichon, P.; Capdeillayre, C.; Petitto, C. Past and recent approaches of preparing Fe-ZSM-5. **2007**.

3. Pérez-Ramırez, J.; Kapteijn, F.; Mul, G.; Moulijn, J. Highly active SO_2-resistant ex-framework FeMFI catalysts for direct N_2O decomposition. *Appl. Catal. B: Environ.* **2002**, *35*, 227-234.

4. Romero-Sáez, M.; Divakar, D.; Aranzabal, A.; González-Velasco, J.; González-Marcos, J. Catalytic oxidation of trichloroethylene over Fe-ZSM-5: Influence of the preparation method on the iron species and the catalytic behavior. *Appl. Catal. B: Environ.* **2016**, *180*, 210-218.

5. Abu-Zied, B.M.; Schwieger, W.; Unger, A. Nitrous oxide decomposition over transition metal exchanged ZSM-5 zeolites prepared by the solid-state ion-exchange method. *Appl. Catal. B: Environ.* **2008**, *84*, 277-288.

6. Guzmán-Vargas, A.; Delahay, G.; Coq, B. Catalytic decomposition of N2O and catalytic reduction of N_2O and N_2O+ NO by NH_3 in the presence of O_2 over Fe-zeolite. *Appl. Catal. B: Environ.* **2003**, *42*, 369-379.

7. Sainz-Vidal, A.; Balmaseda, J.; Lartundo-Rojas, L.; Reguera, E. Preparation of Cu–mordenite by ionic exchange reaction under milling: A favorable route to form the mono-(μ-oxo) dicopper active species. *Micropor. Mesopor. Mat.* **2014**, *185*, 113-120.

8. Li, Y.; Armor, J. Ammoxidation of ethane: V. Solid-state ion exchange to prepare cobalt zeolite catalysts. *Appl. Catal. A: Gen.* **1999**, *188*, 211-217.

9. Rauscher, M.; Kesore, K.; Mönnig, R.; Schwieger, W.; Tissler, A.; Turek, T. Preparation of a highly active Fe-ZSM-5 catalyst through solid-state ion exchange for the catalytic decomposition of N_2O. *Appl. Catal. A: Gen.* **1999**, *184*, 249-256.

10. Park, J.-H.; Choung, J.H.; Nam, I.S.; Ham, S.W. N_2O decomposition over wet-and solid-exchanged Fe-ZSM-5 catalysts. *Appl. Catal. B: Environ.* **2008**, *78*, 342-354.

11. Heyden, A.; Hansen, N.; Bell, A.T.; Keil, F.J. Nitrous oxide decomposition over Fe-ZSM-5 in the presence of nitric oxide: a comprehensive DFT study. *J. Phys. Chem. B* **2006**, *110*, 17096-17114.

12. Hall, W. K.; Feng, X.; Dumesic, J.; Watwe, R. Problems in preparation of FeZSM-5 catalysts. *Catal. Lett.* **1998**, *52*, 13-19.

13. Le, H.V.; Parishan, S.; Sagaltchik, A.; bel, C.; Schlesiger, C.; Malzer, W.; Trunschke, A.; Schom cker, R.; Thomas, A. Solid-state ion-exchanged Cu/mordenite catalysts for the direct conversion of methane to methanol. *ACS Catal.* **2017**, *7*, 1403-1412.

14. Abdelsayed, V.;Shekhawat, D.; Smith, M.W. Effect of Fe and Zn promoters on Mo/HZSM-5 catalyst for methane dehydroaromatization. *Fuel*, **2015**, *139*, 401-410.

15. Schwidder, M.; Kumar, M.S.; Klementiev, K.; Pohl, M.M.; Brückner, A.; Grünert, W. Selective reduction of NO with Fe-ZSM-5 catalysts of low Fe content: I. Relations between active site structure and catalytic performance. *J. Catal.* **2005**. *231*, 314-330.

16. Pérez-Ramírez, J.; Groen, J.C.; Brückner, A.; Kumar, M.S.; Bentrup, U.; Debbagh, M.N.; Villaescusa, L.A. Evolution of isomorphously substituted iron zeolites during activation: comparison of Fe-beta and Fe-ZSM-5. *J. Catal.* **2005**. *232*. 318-334.

17. Kumar, M.S.; Schwidder, M.; Grünert, W.; Brückner, A. On the nature of different iron sites and their catalytic role in Fe-ZSM-5 $DeNO_x$ catalysts: new insights by a combined EPR and UV/VIS spectroscopic approach. *J. Catal.* **2004**. *227*, 384-397.

18. Čapek, L.; Kreibich, V.; Dědeček, J.; Grygar, T.; Wichterlova, B.; Sobalik, Z.; Martens, J.A.; Brosius, R.; Tokarova, V. Analysis of Fe species in zeolites by UV–VIS–NIR, IR spectra and voltammetry. Effect of preparation, Fe loading and zeolite type. *Micropor. Mesopor. Mat.* **2005**. *80,* 279-289.

19. Xu, J.; Armstrong, R.D.; Shaw, G.; Dummer, N.F.; Freakley, S.J.; Taylor, S.H.; Hutchings, G.J. Continuous selective oxidation of methane to methanol over Cu-and Fe-modified ZSM-5 catalysts in a flow reactor. *Catal. Today*, **2016**. *270*, 93-100.

20. Pérez-Ramírez, J.; Groen, J.C.; Brückner, A.; Kumar, M.S.; Bentrup, U.; Debbagh, M.N.; Villaescusa, L.A. Evolution of isomorphously substituted iron zeolites during activation: comparison of Fe-beta and Fe-ZSM-5. *J. Catal.* **2005**. *232*, 318-334.

21. Brown, C.A.; Remar, G.J.; Musselman, R.L.; Solomon, E.I. Spectroscopic and electronic structure studies of met-hemerythrin model complexes: A description of the ferric-oxo dimer bond. *Inorg. Chem.* **1995**. *34*, 688-717.

22. Pirngruber, G.D.; Roy, P.K.; Prins, R. On determining the nuclearity of iron sites in Fe-ZSM-5—a critical evaluation. *Phys. Chem. Chem. Phys.* **2006**, *8*, 3939-3950.

23. Joyner, R.; Stockenhuber, M., Preparation, characterization, and performance of Fe− ZSM-5 catalysts. *J. Phys. Chem. B* **1999**, *103*, 5963-5976.

24. Ates, A.; Hardacre, C.; Goguet, A., Oxidative dehydrogenation of propane with N_2O over Fe-ZSM-5 and Fe–SiO_2: Influence of the iron species and acid sites. *Appl. Catal. A: Gen.* **2012**, *441-442*, 30-41.

25. Blasin-Aubé, V.; Marie, O.; Saussey, J.; Plesniar, A.; Daturi, M.; Nguyen, N.; Hamon, C.; Mihaylov, M.; Ivanova, E.; Hadjiivanov, K. Iron Nitrosyl Species in Fe-FER: a Complementary Mossbauer and FTIR Spectroscopy Study. *J. Phys. Chem. C* **2009**, 113, 8387-8393.

26. Fellah, M. F. CO and NO Adsorptions on Different Iron Sites of Fe-ZSM-5 Clusters: a Density Functional Theory Study. *J. Phys. Chem. C* **2010**, *115*,1940-1951.

27. Sun, K.; Xia, H.; Feng, Z.; van Santen, R.; Hensen, E.; Li, C. Active Sites in Fe/ZSM-5 for Nitrous Oxide Decomposition and Benzene Hydroxylation with Nitrous Oxide. *J. Catal.* **2008**, *254*, 383-396.

28. Guzmán-Vargas, A.; Delahay, G.; Coq, B. Catalytic Decomposition of N_2O and Catalytic Reduction of N_2O and N_2O+ NO by NH_3 in the Presence of O_2 over Fe-Zeolite. *Appl. Catal. B* **2003**, *42*, 369-379.

29. Sazama, P.; Sathu, N.K.; Tabor, E.; Wichterlová, B.; Sklenák, Š.; Sobalík, Z. Structure and Critical Function of Fe and Acid Sites in Fe-ZSM-5 in Propane Oxidative Dehydrogenation with N_2O and N_2O Decomposition. *J. Catal.* **2013**, *299,* 188–203.

30. Jíša, K.; Nováková, J.; Schwarze, M.; Vondrová, A.; Sklenák, S.; Sobalik, Z. Role of the Fe-zeolite Structure and Iron State in the N_2O Decomposition: Comparison of Fe-FER, Fe-BEA, and Fe-MFI Catalysts. *J. Catal.* **2009**, *262*, 27-34.

31. Sun, K.; Xia, H.; Hensen, E.; van Santen, R.; Li, C. Chemistry of N_2O Decomposition on Active Sites with Different Nature: Effect of High-Temperature Treatment of Fe/ZSM-5. *J. Catal.* **2006**, *238*, 186-195.

32. Fellah, M.F.; Onal, I. Direct methane oxidation to methanol by N_2O on Fe-and Co-ZSM-5 clusters with and without water: A density functional theory study. *J. Phys. Chem. C* **2010**, *114*, 3042-3051.

33. Starokon, E.V.; Parfenov, M.V.; Arzumanov, S.S.; Pirutko, L.V.; Stepanov, A.G.; Panov, G. I. Oxidation of methane to methanol on the surface of FeZSM-5 zeolite. *J. Catal.* **2013**, *300*, 47-54.

34. Pirngruber, G.D.; Roy, P.K.; Prins, R. The role of autoreduction and of oxygen mobility in N_2O decomposition over Fe-ZSM-5. *J. Catal.* **2007**, *246*, 147-157.

35. Chen, D.; Moljord, K.; Holmen, A. A methanol to olefins review: Diffusion, coke formation and deactivation on SAPO type catalysts. *Micropor. Mesopor. Mat.* **2012**, *164*, 239-250.

36. Spencer, N. D. Partial oxidation of methane to formaldehyde by means of molecular oxygen. *J. Catal.* **1988**, *109*, 187-197.

CHAPTER 7

7 FORMATION OF SURFACE OXYGEN SPECIES AND THE CONVERSION OF METHANE TO VALUE ADDED PRODUCTS WITH N_2O AS OXIDANT OVER FE-FER CATALYST

7.1 Introduction

Direct methane conversion by N_2O over Fe-based catalysts at low temperature has been extensively studied as a pathway to produce value-added products including methanol, formaldehyde and dimethyl ether (DME) [1-3], since N_2O was found to form active oxygen species, so called α-oxygen, over Fe-ZSM-5, and these unique surface oxygen species are able to activate methane which is subsequently converted to methanol and formaldehyde at low temperatures, even at room temperature [4, 5].

It was reported that α-oxygen is stable at temperatures up to 250 ℃ , above which it transforms into molecular oxygen which is non-selective for methane conversion [6-8]. However, catalytic trials demonstrate that methane can be transformed to methanol over Fe-based catalysts using N_2O at temperatures above 300 °C [7, 9-11]. The selectivity to methanol over Fe/Al-MFI reported to be less than 2% at temperatures above 250°C, which was attributed to the high rate of the complete oxidation of methane [9]. Panov and co-workers established that the inclusion of water vapour in the feed could enhance the selectivity to methanol over Fe-ZSM-5 by ca. 25%~30 % at 300°C where methane conversion of ca. 0.8%, and DME was not detected [10]. A similar observation was noted elsewhere, and carbon balance data showed that over 60% of methane was converted to coke [7]. Zeolite Beta is another zeolite which has been investigated for the conversion of CH_4 and N_2O, and it was observed that during the reaction of CH_4 and N_2O over Fe ion exchanged Beta zeolite in the temperature range of 200 ℃ to 400 ℃ , the reactivity of the surface

oxygen species with CH_4 was very low at 350 °C and no product selectivity information was provided in the manuscript [11]. In an effort to explain this apparent contradiction, it has been suggested that methane might be oxidized by as yet uncharacterised short-lived oxygen species which are formed *in operando* during N_2O dissociation [12].

In the present study, the formation and decomposition of active oxygen species over Fe-ferrierite (Fe-FER) catalyst prepared by solid state ion exchange method over the temperature range of 250 ℃ to 350 ℃ was studied using H_2-TPR and N_2O-TPD, and catalyst activity trials were conducted in batch mode using an *in situ* FTIR and continuous mode in a fix-bed stainless steel tube reactor. Optimization aimed at maximising products yield was undertaken by controlling the ratio of CH_4/N_2O in the feed gas.

7.2 Experimental

7.2.1 Catalysts preparation

The Fe-FER catalyst used in this study was prepared by solid state ion exchange method. The parent NH_4-FER, with a Si/Al ratio of 10, was purchased from Zeolyst. $FeCl_3 \cdot 6H_2O$ supplied by Sigma-Aldrich, and was weighed according to the desired concentration of iron (0.5 wt%). The powder was mechanically mixed with the appropriate amount of FER zeolites. Then the mixture was placed into a crucible and heated up quickly to 500 °C in half an hour and kept at 500 °C for 3 h, and then was cooled to room temperature, followed by calcination at 550 °C for 5 hours at a heating rate of 3 °C/min. The catalyst was then pressed and sieved, and the particles within the size range of 250 μm to 425 μm were chosen to be used in the reaction.

7.2.2 Catalysts characterization

H_2-TPR experiments were conducted in a custom-built instrument. Prior to the H_2-TPR analysis, 300 mg of catalyst was placed in a quartz micro-reactor located in a furnace, and purged in a stream of He or air (30 ml/min) at 450 °C for 1 h. Reduction of catalyst by hydrogen was carried out in a H_2/Ar stream (2.04 vol% of H_2), with a total flow rate of 50 ml/min and a linear heating rate of 10 °C /min in the temperature range of 20–800 °C. N_2O or air pre-treatment, if employed, was performed at various temperatures on the dehydrated zeolites with a N_2O or air flow rate of 30 ml/min for 1 h, and then the sample was cooled to room temperature in Ar, prior to reduction by the H_2/Ar stream. The FTIR spectra were monitored at 150 ℃ during adsorption of NO (from $8e^{-4}$ to $5e^{-2}$ mbar). N_2O temperature-programmed desorption (N_2O-TPD) was carried out to investigate the decomposition of N_2O on the catalyst. The catalyst sample (100 mg) was introduced into the desorption cell, followed by activation at 550 °C for 1 h with a heating rate of 10 °C/min and was cooled to various temperatures for adsorption of N_2O on sample. Subsequently, N_2O and the products were desorbed using a heating rate of 10 °C/min from 100 °C to 650 °C, and the desorbed gases were analyzed using the mass spectrometer.

7.2.3 Catalysts activity examination

Catalyst studies were performed either in a batch mode using an *in situ* FTIR or in a fix-bed stainless steel tube reactor. For the batch mode reaction, 30 mg of the sample was pressed into self-supporting wafer and activated in vacuum at 500 ℃ for 1 h, followed by cooling to reaction temperatures. The activated sample was exposed to CH_4 (10 mbar) first and then was exposed

to N_2O (from 1 mbar to 5 mbar), or in an opposite order with N_2O pressure of 5 mbar and CH_4 pressure of 10 mbar.

For studies involving the continuous reaction of N_2O, 200 mg catalyst was held in place by two quartz wool plugs and was activated in a flow of helium at a heating rate of 3 °C/min to 550 °C and was held at 550 °C for 3h. The reaction was conducted over the temperature range of 250 °C to 350 °C, with helium and nitrous oxide being fed at a ratio of 93:7, or helium, methane and N_2O fed at a ratio of 65:28:7. The investigation of effect of CH_4/N_2O ratio on catalytic activity was conducted with CH_4/N_2O ratio from 0.5 to 6 at 350 °C. The flow rate of methane was maintained and N_2O flow rate was tuned to reach desired ratios, and the GHSV was kept constant by adjusting the helium flow rate. The concentration of feeding gases and gaseous products were analysed using an online gas chromatography (Varian 490-GC) and a FTIR (Shimadzu IRPrestige21).

7.3 Results and discussion

7.3.1 Formation and stability of active oxygen species during the reaction between catalyst and N_2O as a function of temperature

To monitor the presence of active oxygen species, H_2-TPR, N_2O-TPD and NO adsorption on catalyst surface by FTIR were used. Fig. 7.1 compares the H_2-TPR profiles of catalysts that were activated in helium or air followed by the pre-treatment by N_2O or air at a variety of temperatures. Multiple hydrogen consumption peaks at different temperatures were observed in the H_2-TPR profiles, presumably related to various Fe species on the catalyst. In particular, a hydrogen consumption peak centred at 220 °C was observed

over samples that were activated in helium and pre-treated by N_2O at temperatures of 350 °C, 300 °C and 250 °C as shown in Fig. 7.1 a, b and c.

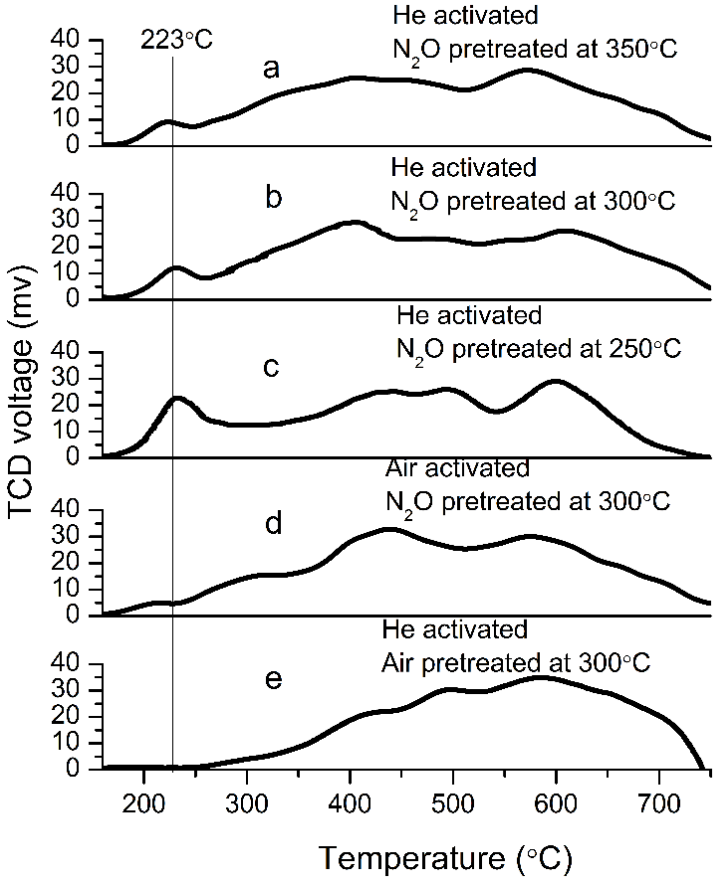

Figure 7.1 H_2-TPR profiles of samples

In contrast, this peak is absent when the catalyst was activated in air followed by pre-treatment in N_2O or activated in helium, as shown in Fig. 7.1 (d and e). This suggests that the hydrogen consumption peak at 220 °C was not caused by reduction of adsorbed N_2O or O_2 over catalysts, but instead reduction of species which were generated from the reaction of N_2O with catalysts activated in helium. The results are consistent with previous findings suggesting the hydrogen consumption peak is a result of the reduction of Fe(III)—O^- to Fe(II) species, where Fe(III)—O^- species are formed by oxidation of Fe in cationic positions [13].

In addition, the disappearance of the hydrogen consumption peak over the catalyst that was activated in air as shown in Fig. 7.1d indicates that activation of Fe-FER catalyst in helium is beneficial for the formation of active species. To investigate the effect of activation methods on catalytic activity of catalyst, IR spectra with NO adsorption over samples activated in inert and air atmosphere were compared.

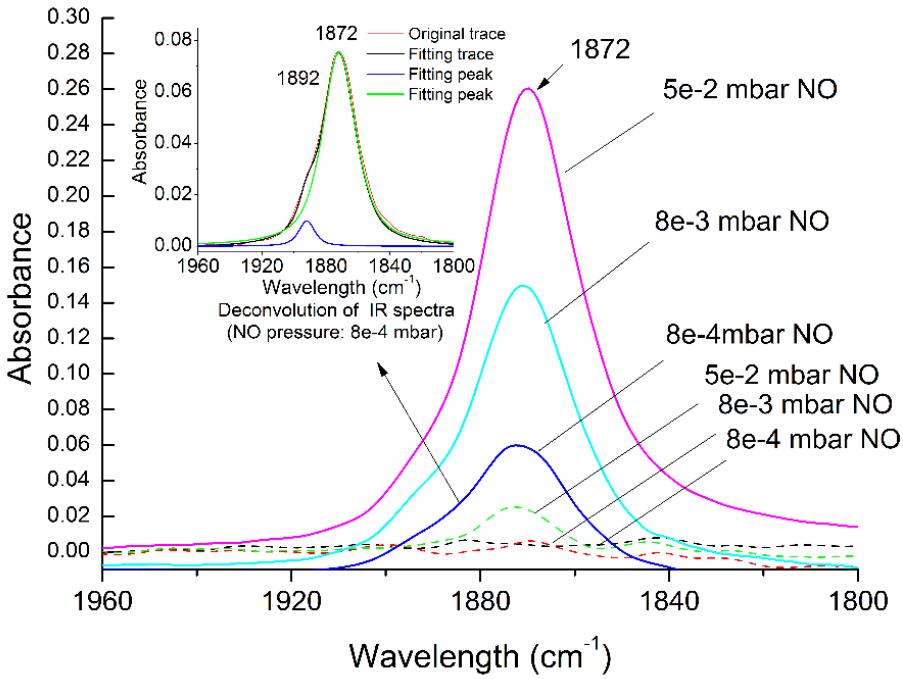

Figure 7.2 NO adsorption IR spectra of Fe-FER catalysts activated in inert and air atmosphere (dash line: activated in air atmosphere, solid line: activated in inert atmosphere)

As shown in Fig. 7.2, an NO adsorption band at 1872 cm^{-1} with a shoulder at 1892 cm^{-1} was observed in the spectra of sample that was activated under vacuum. The band centred at 1872 cm^{-1} has been observed in the spectra of NO adsorption on Fe-based catalysts, and it has been assigned to mononitrosyl species on the Fe^{2+} sites [14-19]. This band, with a shoulder at 1892

cm^{-1}, has also been attributed to NO adsorbed on extra-framework Fe-O-Al species, which are the active sites for N_2O decomposition [20]. It should be noted that the band at 1872 cm^{-1} was significantly attenuated in the spectra of air activated samples, compared to samples activated under an inert atmosphere.

In addition, the area of hydrogen consumption peak at 220 °C decreased with increasing pre-treatment temperature, as shown in Fig. 7.1 (a to e), which is consistent with the inference that the decomposition of the oxygen species to molecular oxygen is accelerated as temperature increases [21].

To investigate the decomposition of N_2O over Fe-FER catalyst, N_2O-TPD was performed with N_2O adsorption taking place at 250 °C, 300 °C and 350 °C, and the desorption species were monitored using a mass spectrometer. As shown in Fig. 7.3, a mixture of N_2, NO and O_2 were observed as the products of N_2O decomposition over Fe-FER catalyst. The N_2O-TPD was performed in previous studies at 280 and 320 °C [22, 23], and it is asserted that N_2O decomposed over Fe-based catalysts to form N_2 and active oxygen species. The active oxygen species was subsequently released as O_2 (at temperature higher than 250 °C) or reacted with N_2O to form Fe(III)—NO_x, which decomposed to NO and O_2 at temperature higher than 300 °C. During the decomposition of N_2O, N_2 was formed and released from the catalyst, while O_2, NO and NO_2 remained captured in the zeolites and hence lead to desorption peaks [22].

O_2 and NO were observed as the main decomposition species as shown in Fig. 7.3 and the peak area of products decreased sharply with increase of

adsorption temperature, indicating a reduced concentration of active oxygen species remain after N_2O adsorption at elevated temperatures. In addition, with the increase in N_2O adsorption temperature, the O_2 desorption peak shifted towards higher temperatures and coincided with NO desorption temperature when N_2O was adsorbed at 350 °C. The phenomenon was observed previously; the increasing N_2O adsorption temperature enhanced the interaction of N_2O with Fe(III)—O^- to form non-active Fe(III)—NO_x, which subsequently decomposed to NO, NO_2 and O_2 and desorbed at nearly the same temperatures [24]. Therefore, it is suggested that the O_2 desorption peak is attributed to decomposition of Fe(III)—O^- at lower temperature and Fe(III)—NO_x at higher temperature. Upon N_2O adsorption temperature, the transformation from Fe(III)—O^- to Fe(III)—NO_x was favoured, and resulted in the shift of O_2 desorption peak towards higher temperature.

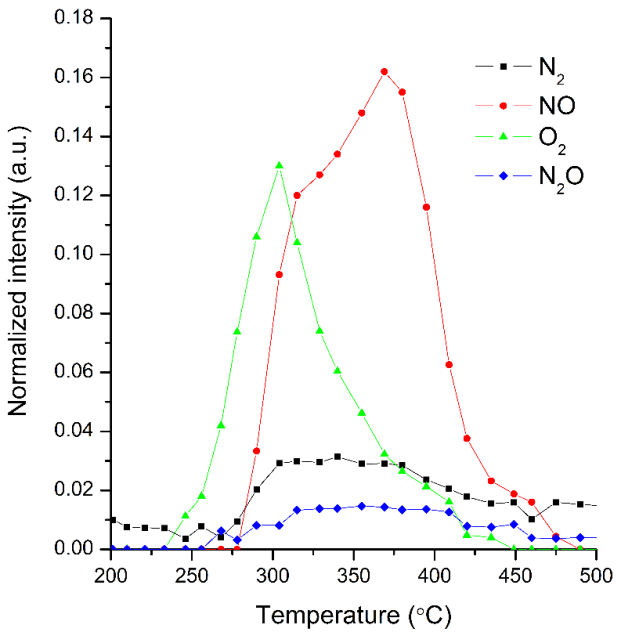

a. N_2O adsorption at 250 °C

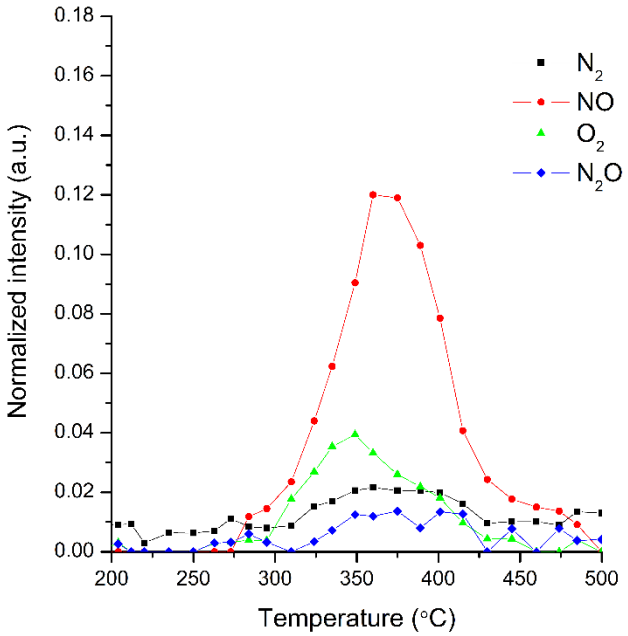

b. N_2O adsorption at 300 °C

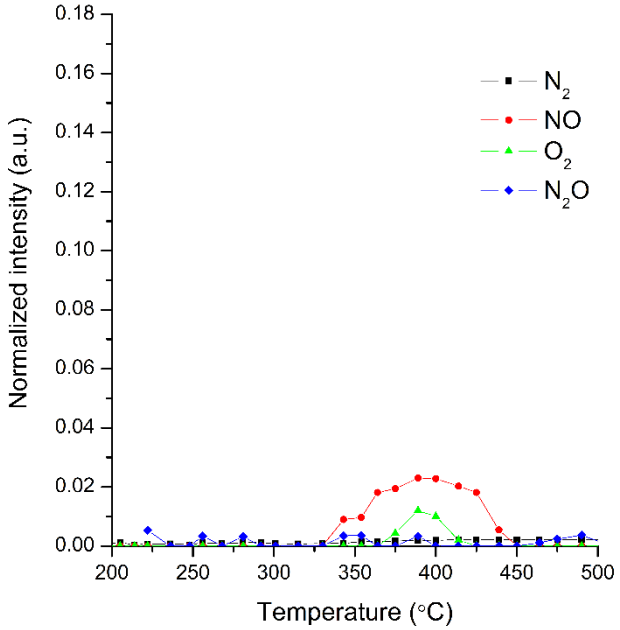

c. N_2O adsorption at 350 °C

Figure 7.3 N_2O-TPD with N_2O adsorption at various temperatures

The formation of NO from N_2O decomposition was further investigated by IR spectroscopy [25], and the results are shown in Fig. 7.4. As the pressure of N_2O

increased from 0.5 mbar to 5 mbar, four main Bands at 2235 cm^{-1}, 1945 cm^{-1}, 1843 cm^{-1} and 1605 cm^{-1} were observed. The band at 2235 cm^{-1} is attributed to adsorbed N_2O on the catalyst [25], and the band at 1945 cm^{-1} was assigned to stretching vibrations of symmetric NO in $Fe(NO)_3^+$ complexes [26]. For bands at 1843 cm^{-1} and 1605 cm^{-1}, similar bands were observed and assigned to $FeAlO_x$-NO and $FeAlO_x$-NO_2 [27]. The observation of NO associated bands confirmed the production of NO from N_2O decomposition, and the generation of NO_2 was attributed to the reaction of NO with active oxygen species [24].

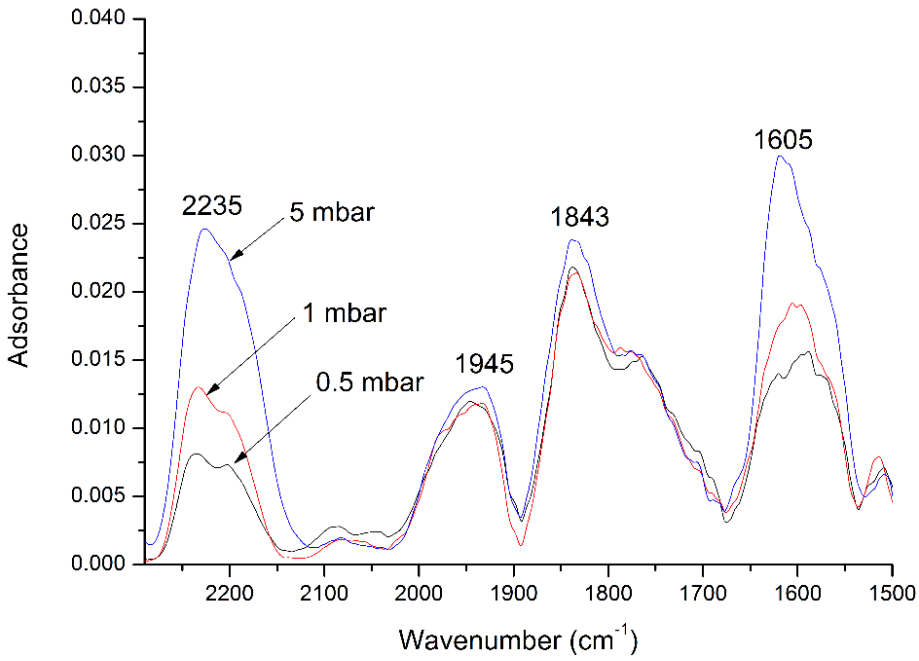

Figure 7.4 N_2O adsorption IR spectrum of Fe-FER catalysts (N_2O pressure: 0.5 ~ 5 mbar)

According to the results from N_2O-TPD and H_2-TPR profiles, active oxygen species tend to decompose to O_2 at high temperature, and hence the concentration of residual active oxygen species decreased with increasing reaction temperature. However it should be noted that the peak of hydrogen consumption at 220 °C was observable in the H_2-TPR profiles of the samples

that were pre-treated by N_2O at 300 °C and 350 °C, indicating that there are Fe(III)—O^- species remaining and reactive at moderate temperatures. Therefore, methane can be oxidised by the active oxygen species to methanol and other valuable products at temperatures above 250 °C.

7.3.2 Batch mode reactions of methane and N_2O

To investigate the reaction of methane and N_2O at moderate temperatures, batch mode reactions were conducted using an *in situ* FTIR by sequentially feeding and exposing methane and then N_2O to the catalyst and the resulting spectra were monitored at 250 °C, 300 °C and 350 °C, respectively.

As shown in Fig. 7.5, the bands at 2969 cm^{-1}, 2914 cm^{-1}, 2864 cm^{-1} and 2816 cm^{-1} were observed in all spectra obtained at different N_2O pressures and temperatures studied. The bands at 2969 cm^{-1} and 2860 cm^{-1} are assigned to asymmetric and symmetric Si-bound methoxy groups, and the bands at 2914 cm^{-1} and 2816 cm^{-1} are assigned to asymmetric and symmetric Fe-bound methoxy groups, respectively [9, 28]. The spectra confirm that methane can be activated by N_2O to form methoxy groups at moderate temperatures.

The peak area of asymmetric methoxy groups was integrated and the results are shown in Fig. 7.6. Apparently, the area of the CH stretching vibrations of the methoxy group increased with an increase in reaction temperature when N_2O with pressure of 1 mbar and 2 mbar was used. Upon further increase of N_2O pressure to 5 mbar, the area of the methoxy group peak kept increasing to 0.3 and 0.8 for reactions at a temperature of 250 °C and 300 °C, but at a reaction temperature of 350 °C, the methoxy group peak area decreased sharply to 0.6, which is less than that of reaction at 300 °C. It is suggested

that methoxy groups are generated from reaction between methane and active oxygen species, and undergo further oxidation to CO and CO_2. In the spectra monitored at 350 °C, the band at 2350 cm^{-1} was observed as shown in Fig. 7.7, which is the IR feature of adsorbed CO_2 [29]. The significant increase of the CO_2 peak area as the pressure of N_2O increased from 2 mbar to 5 mbar (as shown in Fig. 7.7) coincided with a decline in the methoxy group concentration appears to be related to the higher level of combustion occurring when 5 mbar N_2O was applied at 350 °C. However, the areas of the CO_2 peak were much lower in the reactions conducted at 250 °C and 300 °C (results not shown). It is suggested, based on the data presented in Fig. 7.3 that the Fe(III)—O^- species generated from N_2O decomposition another Fe(III)—O^- species form O_2 on neighbouring sites and NO on isolated Fe sites. Molecular oxygen then results in combustion of methoxy groups to CO_2.

Therefore, methane appears to be converted to methoxy groups at moderate temperatures, and non-selective oxidation can be inhibited by feeding a stoichiometric quantity of N_2O at 350 °C, to lead to the generation of more methoxy groups in comparison to the concentration of methoxy groups at 300 °C and 250 °C.

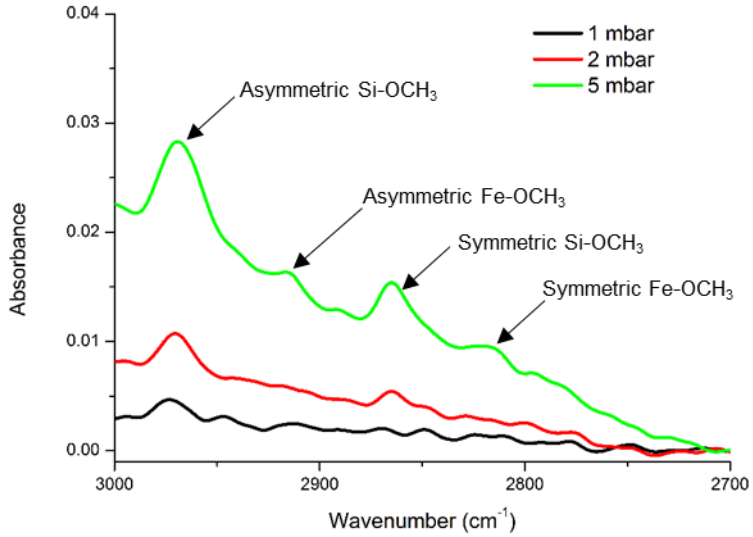

(a) 250 °C

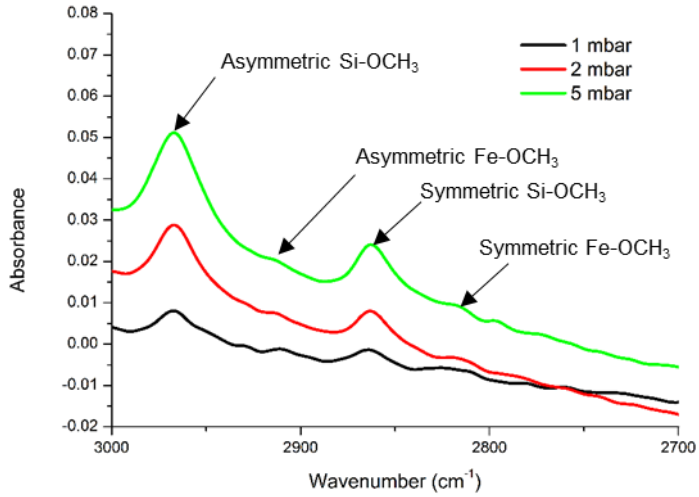

(b) 300 °C

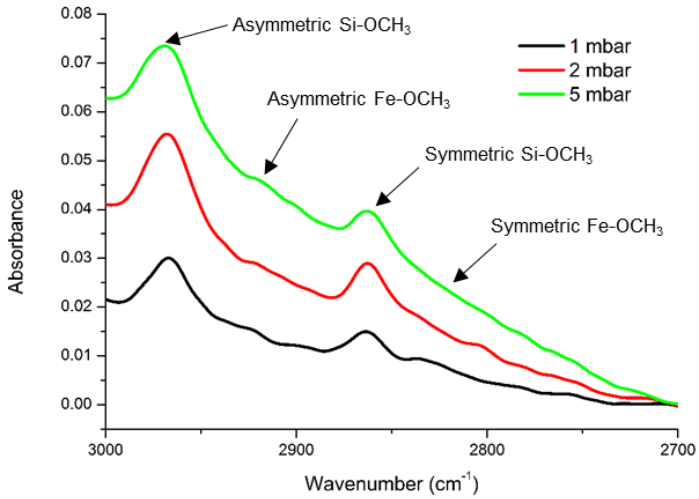

(c) 350 °C

Figure 7.5 IR spectra of sequential methane (10 mbar) and N_2O adsorption (1 mbar, 2 mbar and 5 mbar) at different temperatures

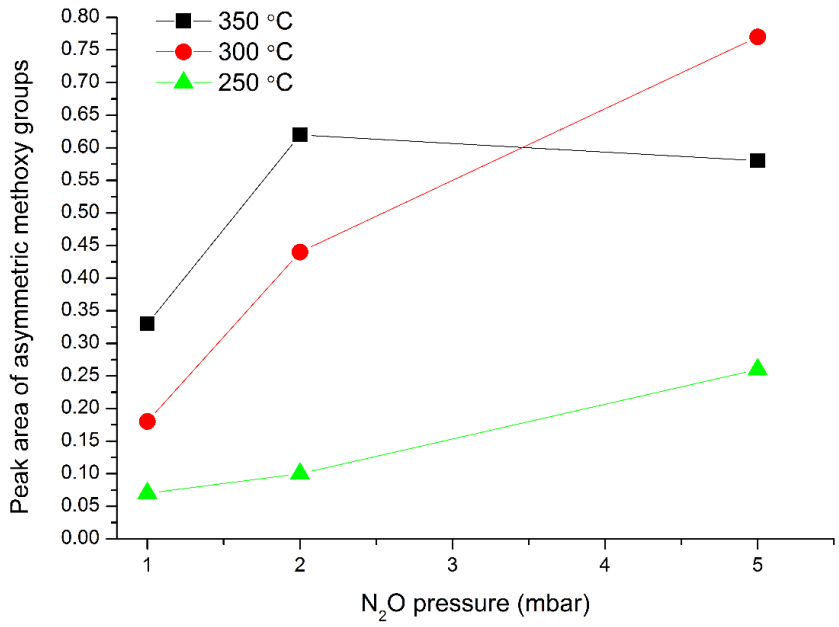

Figure 7.6 Comparison of methoxy group band intensity at different adsorption temperatures (methane pressure: 10 mbar)

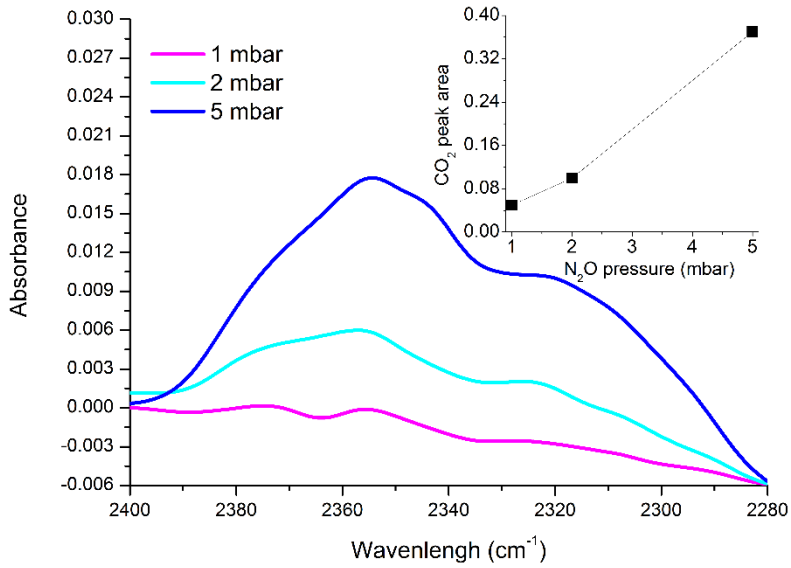

Figure 7.7 Adsorbed CO_2 band intensity at 350 °C (methane pressure: 10 mbar, N_2O pressure: 1 mbar to 5 mbar)

To explore the nature of the reaction between methane and Fe(III)—O^- species further, methane and N_2O were exposed to the catalysts in the opposite order described previously.

When N_2O was fed in the cell with a pressure of 5 mbar, followed by the introduction of methane with a pressure of 1 mbar, 5 mbar and 10 mbar at 300 °C, methoxy group were detected, but with a significantly reduced peak areas, as shown in Fig. 7.8, in comparison to feeding methane first followed by N_2O as shown in Fig. 7.6. These results suggest that in the absence of methane, active oxygen species were formed upon N_2O adsorption and were subsequently transformed to NO and O_2. As a consequence the concentration of residual active oxygen species was reduced. In the presence of methane, the simultaneous consumption of Fe(III)—O^- species and formation of methoxy groups is observed. In addition the reaction between methane and active oxygen species should be favourable compared to the pathway in which active oxygen species react with N_2O to form Fe-NO_x, and hence would in turn result in a higher level of N_2O conversion.

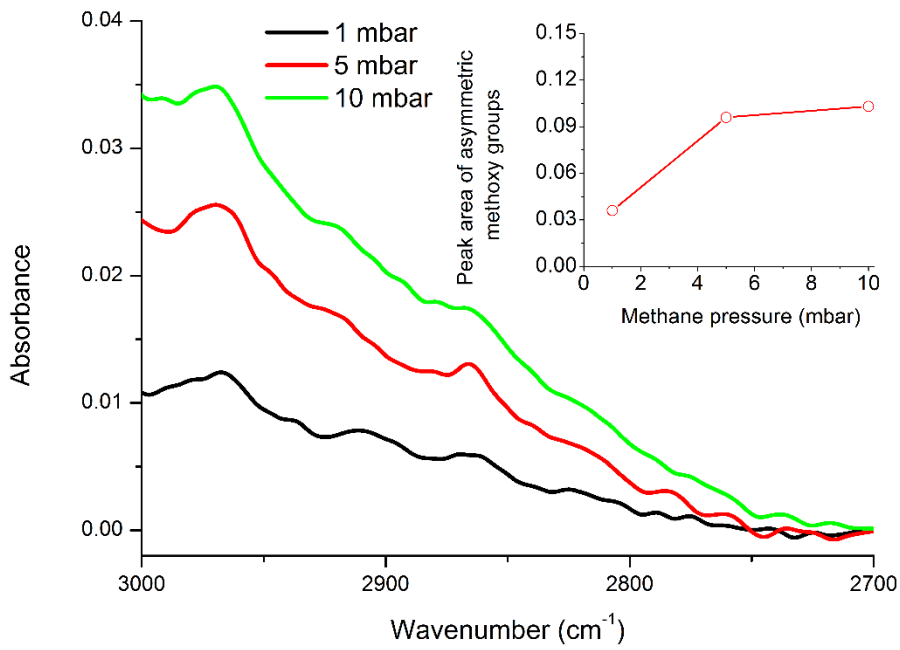

Figure 7.8 Methoxy groups bands formed upon sequential adsorption of N_2O (5 mbar) and CH_4 (1 mbar, 5 mbar and 10 mbar) over Fe-FER at 300 °C

7.3.3 N_2O decomposition with or without methane addition in a continuous reaction over Fe-FER

N_2O decomposition over Fe-FER catalysts over the temperature range from 250 °C to 350 °C was investigated and the results are shown in Figure 9. N_2O decomposition increased from 1.3% to 3.9 % as the temperature increased from 250 °C to 350 °C when N_2O alone reacted with Fe-FER. Co-feeding of methane with N_2O led to a notably higher level of N_2O decomposition as shown in Fig. 7.9. 4.3%, 8.1% and 20.6% of N_2O was converted at 250 °C, 300 °C and 350 °C, which is 3.3, 4.3 and 4.8 times of that obtained without co-existence of methane, respectively. These results are consistent with previous conclusion that the catalytic activity of a combination of methane and N_2O showed significantly higher N_2O conversion at 350 °C, in comparison to the activity of N_2O decomposition at 400 °C [6]. It is suggested that methane

reduces the concentration of active oxygen species on the surface of the catalyst.

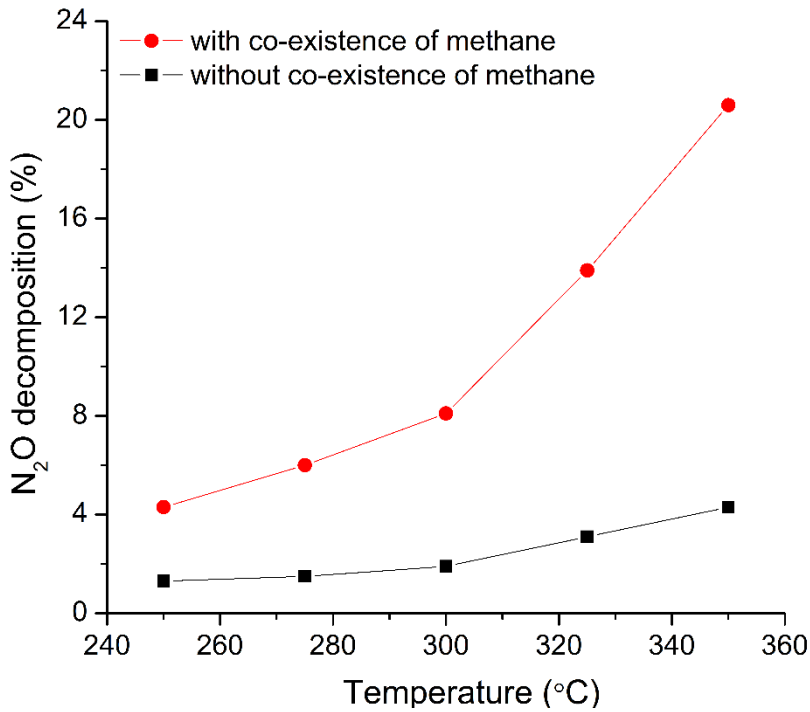

Figure 7.9 N_2O decomposition with or without co-existed methane over Fe-FER catalysts at various temperatures

7.3.4 Activity examination with a variety of CH_4/N_2O ratios

As indicated by the batch mode reactions results shown in Fig. 7.5, Fig. 7.6 and Fig. 7.7, additional N_2O in the feed promotes complete oxidation of methane and a reduction in the formation of methoxy groups. In order to obtain desired products at the highest yield, the catalytic activity of Fe-FER catalysts with different CH_4/N_2O ratios was investigated. The conversion of methane, decomposition of N_2O and generation of products over Fe-FER catalysts are shown in Fig. 7.10 and Fig. 7.11. As the increase of ratio of CH_4/N_2O from 0.5 to 2, methane conversion and N_2O decreased sharply from 57% to around 2.0%, and from 95% to around 20%, respectively. The

conversion of methane and N_2O decreased slightly upon further increase of CH_4/N_2O.

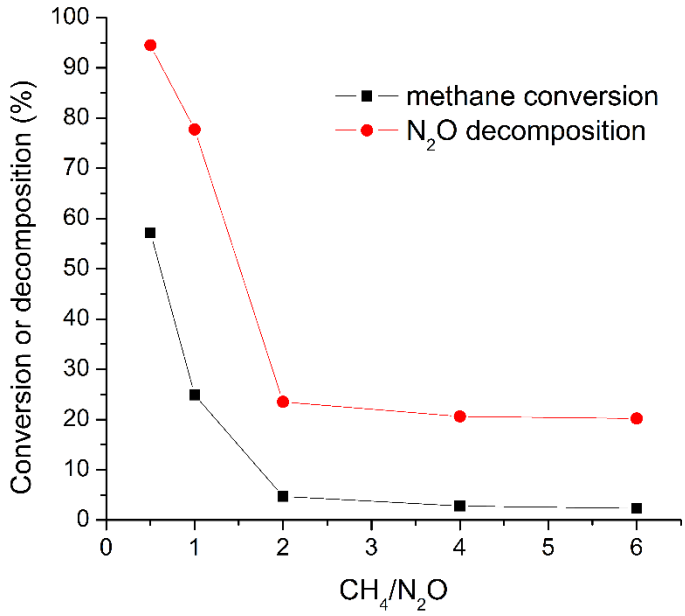

Figure 7.10 Methane conversion and N_2O decomposition over Fe-FER with different CH_4/N_2O ratios at 350 °C

With respect to product selectivity, with an increase in the ratio of CH_4/N_2O from 0.5 to 6, the yield of methanol, formaldehyde and DME initially increased and then decreased, while the concentration of CO, CO_2 and ethylene decreased as shown in Fig. 7.11. The total concentration of value-added products i.e. methanol, formaldehyde and DME is shown in Fig. 7.12, and the total yield increased to a maximum at a CH_4/N_2O of 4, and decreased as the increase of the ratio to 6. The results are consistent with the results from the IR studies shown in Fig. 7.6, indicating the excess addition of N_2O will reduce the amount of generated valuable products, and lead to the generation of CO and CO_2 as the main products.

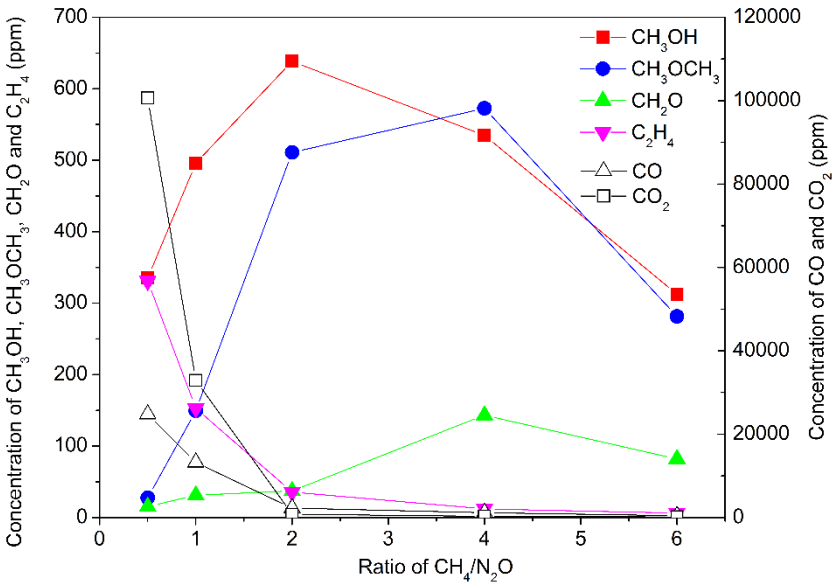

Figure 7.11 Products generation from methane conversion by N_2O over Fe-FER with different CH_4/N_2O ratios at 350 °C

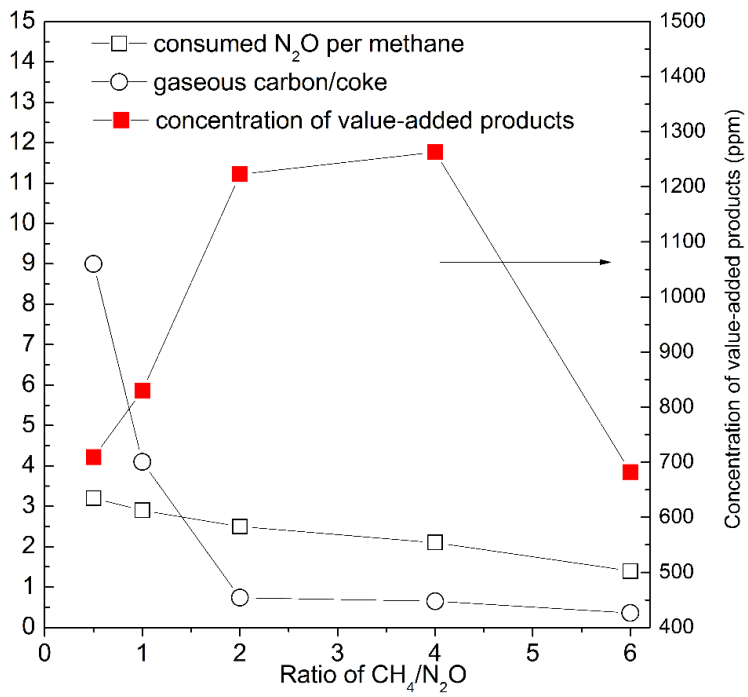

Figure 7.12 The ratio of converted CH_4/ N_2O, gaseous carbon/coke, and the total concentration of value-added products

To explain the activity test results, the carbon balance of each reaction was estimated in an effort the study the effect of the ratio of carbon in gaseous products to undetected products which are categorised as coke. These results are shown in Table. 7.1 and Fig. 7.12. This ratio decreased from 9 to 0.36 as the increase of CH_4/N_2O from 0.5 to 6, indicating the extent of carbon deposition increased with a reduction on the feed concentration of N_2O. In addition, the fractional conversion of N_2O per CH_4 molecule decreased with increasing CH_4/N_2O as shown in Fig. 7.12, suggesting reducing the feed concentration of N_2O reduces the consumption of N_2O on a per CH_4 molecule basis which appears to reduce the extent of methanol, formaldehyde and DME decomposition, which would otherwise be oxidized to CO and CO_2. When the ratio of CH_4/N_2O is low, N_2O was consumed and methane was oxidised to CO and CO_2. As the increase of the ratio of CH_4/N_2O, the combustion of desired products was mitigated, however the level of carbon deposition was enhanced, which resulted in loss of catalysts activity. Therefore, the generation of desired products can be optimized by controlling the CH_4/N_2O ratio to balance deep oxidation and coke formation. In this study, the optimum catalytic performance was obtained when the ratio of CH_4/N_2O was 4, and concentrations of methanol, formaldehyde and DME were 534 ppm, 143 ppm and 573 ppm, respectively, and the selectivity of desired products was 55%.

Table 7.1 Methane conversion, carbon balance and products distribution with different CH_4/N_2O ratios at 350 °C

CH_4/N_2O ratio	Methane conversion (%)	Carbon balance (%)	Gaseous products (%)	Undetected products (%)

0.5	57.2	94.3	51.5	5.7
1	24.9	95.1	20.0	4.9
2	4.7	97.3	2.0	2.7
4	2.8	98.3	1.1	1.7
6	2.3	98.3	0.6	1.7

7.4 Conclusion

Formation of active oxygen species from N_2O decomposition over Fe-FER catalysts was studied at moderate temperatures, and the generation of methoxy groups and valuable products from the reaction between N_2O and methane was investigated. A low temperature reduction peak which is attributed to reduction of active oxygen species was observed in the H_2-TPR profiles of samples activated in helium and pre-treated by N_2O. This feature decreased in area with an increase in catalyst pre-treatment temperature, indicating the active oxygen species are decomposed at higher temperatures. The N_2O-TPD results disclose that N_2O decomposes to N_2, O_2 and NO at moderate temperatures. Activation of Fe-FER catalyst in helium promotes the formation of Fe^{2+} species in comparison to activation in air, according to the NO adsorption IR spectra. N_2O and Fe^{2+} species were shown to be essential for the formation of active oxygen species active in selective oxidation of methane.

Introduction of methane to the Fe-FER sample pre-treated by N_2O at moderate temperature led to the emergence of methoxy groups bands in the FTIR spectrum, which are the active surface species resulting in the formation of selective products. The direct catalytic partial oxidation of methane by N_2O

over Fe-FER catalysts at moderate temperatures proceeds via the formation of active oxygen species from N_2O, and the generation of oxygenates was promoted by optimization of the ratio of CH_4/N_2O to balance the level of methane combustion and coke formation.

7.5 Reference

1. Hammond, C.; Forde, M.M.; Ab Rahim, M.H.; Thetford, A.; He, Q.; Jenkins, R.L.; Dimitratos, N.; Lopez-Sanchez, J.A.; Dummer, N.F.; Murphy, D.M. et al. Direct catalytic conversion of methane to methanol in an aqueous medium by using copper-promoted Fe-ZSM-5. *Angew. Chem., Int. Ed.* **2012**, *51*, 5129–5133.
2. Mahyuddin, M.H.; Staykov, A.; Shiota, Y.; Yoshizawa, K. Direct conversion of methane to methanol by metal-exchanged ZSM-5 zeolite (Metal= Fe, Co, Ni, Cu). *ACS Catal.* **2016**, *6*, 8321-8331.
3. Li, G.; Vassilev, P.; Sanchez-Sanchez, M.; Lercher, J.A.; Hensen, E.J.; Pidko, E.A. Stability and reactivity of copper oxo-clusters in ZSM-5 zeolite for selective methane oxidation to methanol. *J. Catal.* **2016**, *338*, 305-312.
4. Panov, G.I.; Uriarte, A.K.; Rodkin, M.A.; Sobolev, V.I. Generation of active oxygen species on solid surfaces. Opportunity for novel oxidation technologies over zeolites. *Catal. Today* **1998**, *41*, 365-385.
5. Starokon, E.V.; Parfenov, M. V.; Pirutko, L. V.; Abornev, S. I.; Panov, G. I. Room-Temperature Oxidation of Methane by α-Oxygen and Extraction of Products from the FeZSM-5 Surface. *J. Phys. Chem. C* **2011**, *115,* 2155-2161.
6. Kameoka, S.; Nobukawa, T.; Tanaka, S. I.; Ito, S. I.; Tomishige, K.; Kunimori, K. Reaction Between N_2O and CH_4 over Fe Ion-Exchanged BEA

Zeolite Catalyst: A Possible Role of Nascent Oxygen Transients from N_2O. *Phys. Chem. Chem. Phys.* **2003**, *5,* 3328-3333.

7. Starokon, E. V.; Parfenov, M. V.; Arzumanov, S. S.; Pirutko, L. V.; Stepanov, A. G.; Panov, G. I. Oxidation of Methane to Methanol on the Surface of FeZSM-5 Zeolite. *J. Catal.* **2013**, *300*, 47-54.
8. Sun, K.; Xia, H.; Feng, Z.; van Santen, R.; Hensen, E.; Li, C. Active Sites in Fe/ZSM-5 for Nitrous Oxide Decomposition and Benzene Hydroxylation with Nitrous Oxide. *J. Catal.* **2008**, *254*, 383-396.
9. Wood, B. R.; Reimer, J. A.; Bell, A. T.; Janicke, M. T.; Ott, K. C. Methanol Formation on Fe/Al-MFI via the Oxidation of Methane by Nitrous Oxide. *J. Catal.* **2004**, *225*, 300-306.
10. Parfenov, M. V.; Starokon, E. V.; Pirutko, L. V.; Panov, G. I. Quasicatalytic and Catalytic Oxidation of Methane to Methanol by Nitrous Oxide over FeZSM-5 Zeolite. *J. Catal.* **2014**, *318*, 14-21.
11. Chow, Y. K.; Dummer, N. F.; Carter, J. H.; Meyer, R. J.; Armstrong, R. D.; Williams, C.; Shaw, G.; Yacob, S.; Bhasin, M. M.; Willock, D. J. *et al.* A Kinetic Study of Methane Partial Oxidation over Fe-ZSM-5 Using N_2O as an Oxidant. *ChemPhysChem* **2018**, *19*, 402-411.
12. Kondratenko, E.V.; Pérez-Ramírez, J. Importance of the lifetime of oxygen species generated by N_2O decomposition for hydrocarbon activation over Fe-silicalite. *Appl. Catal. B* **2006**, *64*, 35-41.
13. Sazama, P.; Sathu, N.K.; Tabor, E.; Wichterlová, B.; Sklenák, Š.; Sobalík, Z. Structure and critical function of Fe and acid sites in Fe-ZSM-5 in propane oxidative dehydrogenation with N_2O and N_2O decomposition. *J. Catal.* **2013**, *299,* 188-203.

14. Berlier, G.; Zecchina, A.; Spoto, G.; Ricchiardi, G.; Bordiga, S.; Lamberti, C. The role of Al in the structure and reactivity of iron centers in Fe-ZSM-5-based catalysts: a statistically based infrared study.*J. Catal.* **2003**, *215*, 264-270.

15. Berlier, G.; Spoto, G.; Fisicaro, P.; Bordiga, S.; Zecchina, A.; Giamello, E.; Lamberti, C. Coordination and oxidation changes undergone by iron species in Fe-MCM-22 upon template removal, activation and red–ox treatments: an in situ IR, EXAFS and XANES study. *J. Catal.* **2005**, *229*, 45-54.

16. Rivallan, M.; Berlier, G.; Ricchiardi, G.; Zecchina, A.; Nechita, M.T.; Olsbye, U. Characterisation and catalytic activity in de-NO_x reactions of Fe-ZSM-5 zeolites prepared via ferric oxalate precursor.*Appl. Catal. B* **2008**, *84*, 204-213.

17. Benco, L.; Bucko, T.; Grybos, R.; Hafner, J.; Sobalik, Z.; Dedecek, J.; Hrusak, J. Adsorption of NO in Fe^{2+}-exchanged ferrierite. A density functional theory study. *J. Phys. Chem. C* **2007**, *111*, 586-595.

18. Benco, L.; Bucko, T.; Grybos, R.; Hafner, J.; Sobalik, Z.; Dedecek, J.; Sklenak, S.; Hrusak, J. Multiple Adsorption of NO on Fe^{2+} Cations in the α-and β-Positions of Ferrierite: An Experimental and Density Functional Study. *J. Phys. Chem. C* **2007**, *111*, 9393-9402.

19. Blasin-Aubé, V.; Marie, O.; Saussey, J.; Plesniar, A.; Daturi, M.; Nguyen, N.; Hamon, C.; Mihaylov, M.; Ivanova, E.; Hadjiivanov, K. Iron Nitrosyl Species in Fe-FER: a Complementary Mossbauer and FTIR Spectroscopy Study. *J. Phys. Chem.* C **2009**, 113, 8387-8393.

20. Li, G.; Pidko, E.A.; van Santen, R.A.; Li, C.; Hensen, E.J. Stability of extraframework iron-containing complexes in ZSM-5 zeolite, *J. Phys. Chem.* C **2012**, 117, 413-426.

21. Wood, B.R.; Reimer, J.A.; Bell, A.T.; Janicke, M.T.; Ott, K.C. Nitrous oxide decomposition and surface oxygen formation on Fe-ZSM-5. *J. Catal.* **2004**, *224*, 148-155.

22. Nováková, J.; Sobalík, Z. N_2O decomposition and formation of NO_x species on Fe–ferrierite. Effect of NO and CO addition on the decomposition and the role of surface species. *Catal. Lett.* **2005**, *105*, 169-177.

23. El-Malki, E.M.; Van Santen, R.A.; Sachtler, W.M.H. Active sites in Fe/MFI catalysts for NO_x reduction and oscillating N_2O decomposition.*J. Catal.* **2000**, *196*, 212-223.

24. Sobalík, Z.; Tabor, E.; Nováková, J.; Sathu, N.K.; Závěta, K. Role of active oxygen and NO_x species in N_2O decomposition over Fe-ferrierite. *J. Catal.* **2012**, *289*, 164-170.

25. Grubert, G.; Hudson, M.J.; Joyner, R.W.; Stockenhuber, M. The Room Temperature, Stoichiometric Conversion of N_2O to Adsorbed NO by Fe-MCM-41 and Fe-ZSM-5. *J. Catal.* **2000**, *196*, 126-133.

26. Wang, L.; Wang, G.; Qu, H.; Wang, C.; Zhou, M. Infrared Photodissociation Spectroscopy of Iron Nitrosyl Cation Complexes: $Fe(NO)_n^+$ (n = 1−5), *J. Phys. Chem. A* **2014**, 118, 1841-1849.

27. Mul, G.; Perez-Ramirez, J.; Kapteijn, F.; Moulijn, J. A. NO Adsorption on Ex-Framework [Fe, X] MFI Catalysts: Novel IR Bands and Evaluation of Assignments. *Catal. Lett.* **2002**, *80*, 129-138.

28. Wang, X.; Shishkin, A.; Hemmingsson, F.; Skoglundh, M.; Martinez-Casado, F.J.; Bock, L.; Idström, A.; Nordstierna, L.; Härelind, H.; Carlsson, P.A. Methane adsorption and methanol desorption of copper modified boron silicate. *RSC Adv.* **2018**, *8*, 36369-36374.
29. Szanyi, J.; Gao, F.; Kwak, J.H.; Kollár, M.; Wang, Y.; Peden, C.H. Characterization of Fe^{2+} ions in Fe, H/SSZ-13 zeolites: FTIR spectroscopy of CO and NO probe molecules. *Phys. Chem. Chem. Phys.* **2016**, *18*, 10473-10485.

CHAPTER 8

8 CONCLUSIONS AND RECOMMENDATIONS

8.1 Conclusions

A laboratory scale process for catalytic partial methane oxidation to methanol and derivatives by N_2O over Fe-based catalysts in a continuous operation mode at moderate temperatures was developed to examine the catalytic activity and study the involved mechanisms. This work focused on optimizing catalytic performance and obtaining insights of the nature of active sites and formation of surface oxygen species. An important contribution of this work relates to the production of methanol and derivatives from catalytic partial methane oxidation at moderate temperatures by analysing the formation and disassociation of surface oxygen species, and the proposition of active iron sites to extra-framework binuclear Fe clusters in ion exchange positions.

The major finds in this work are described as follows:

- Demonstrated the successful, continuous production of methanol and formaldehyde from catalytic partial oxidation of methane by N_2O over Fe-ZSM-5 catalysts at moderate temperatures. The activity was further promoted by optimizing reaction conditions, employing superior zeolites and catalyst preparation methods. At 350 °C, Fe-FER (0.5 wt%) catalysts prepared by solid state ion exchange methods obtained methane conversion of 2.8% with desired products (methanol, formaldehyde and dimethyl ether) selectivity of 46%. A comparison of catalytic performance obtained from previous studies and this work is shown in Table 8.1. Fe-FER presented better performance comparing to most of the studies as shown in Table 8.1 except for one study which was conducted at 0.45 MPa. The results confirm the feasibility of

conducting catalytic partial oxidation of methane by N_2O over Fe-FER at moderate temperature.

Table 8.1 Comparison of methane conversion and desired products concentrations over different catalysts

Material	T (°C)	Converted CH_4 (μmol/min·g cat.)	HCHO concentration (μmol/ min·g cat.)	CH_3OH concentration (μmol/ min·g cat.)	DME concentration (μmol/ min·g cat.)	Ref.
MoO_3/SiO_2	500	9	6.6	1.2	-	1
V_2O_5/SiO_2	550	201	112.6	39.6	-	2
Fe-ZSM-5	160	4.2	-	2.1	0.3	3
Fe-ZSM-5	200	2.7	-	0.3	0.1	4
Fe-ZSM-5	300	5.6	-	2.4	-	4
Fe-FER	350	122.5	0.8	6.1	6.6	This work

- Zeolites structure showed critical effect on formation of active sites and methanol production. Among H-ZSM-5, H-Beta and H-FER zeolites, H-FER contained the highest amount of framework Al atoms, which are essential for stabilizing Fe species to form the active sites for N_2O conversion. In addition, the methoxy groups generated on Fe species present in Fe-FER migrated to silanol groups more effectively in comparison to Fe-ZSM-5 and Fe-Beta catalysts. The higher concentration of active sites and propensity for methoxy groups migration from Fe sites to silicon species over Fe-FER led to the best catalytic performance.
- The active sites over catalysts was proposed to be extra-framework binuclear Fe clusters in ion exchange positions, basing on the

correlation of results from UV-vis spectroscopy, H_2-TPR, *in situ* FTIR and activity test.

- Formation and disassociation of surface oxygen species were studied over Fe-FER catalysts at various temperatures. These species decomposed to oxygen molecules readily at elevated temperatures but were still available with a small amount at 350 °C. Various stabilities of surface oxygen species were observed over Fe-FER catalysts prepared by different techniques.
- Different from a batch mode reaction, the conducting of catalytic partial methane oxidation in a continuous mode fed methane and N_2O simultaneously, in this way the conversion of N_2O to active oxygen species and utilization of these short-live oxygen species were enhanced to produce more methanol.
- Coke formation is inevitable during the reaction, however catalytic performance can be optimized by adjusting the ratio of CH_4/N_2O to balance the coke formation and complete oxidation of methane.

8.2 Recommendations

The study on catalytic partial oxidation of methane to valuable products by N_2O over Fe-based catalysts at moderate temperatures are currently limited and further efforts are expected to be made to:

- Further characterise the nature of active sites. In this study, the active sites for N_2O decomposition and methanol formation were proposed to be extra-framework binuclear Fe clusters in ion exchange positions. However, this is a controversial issue over various zeolite structures,

and there have been types of iron sites (isolated, mononuclear, binuclear, oligonuclear iron species) suggested to be the active sites, basing on DFT calculation, XAFS spectroscopy, Mössbauer spectroscopy, IR spectroscopy, UV–vis spectroscopy, etc [5-10]. Further investigation is required for determination of nature of the active sites.

- Study the mobility of methoxy groups over zeolites. Fe-ZSM-5, Fe-Beta and Fe-FER exhibited different mobility of methoxy groups from iron sites to silicon sites, which played an important role on products selectivity. Further study on the mobility of methoxy groups over zeolites will contribute to enhancement of methanol selectivity.
- Expand the study to other zeolites. Current studies for this purpose mainly focuses on Fe-ZSM-5 [4, 11]. This study demonstrated the superior catalytic performance of Fe-FER over Fe-ZSM-5 in terms of methane conversion and desired products selectivity. There could be potential zeolites that are favorable for N_2O decomposition and value-added products generation.
- Explore strategies to obtain higher yield of desired products. It was reported that high-temperature pre-treatment of catalysts promoted formation of active sites [12], and co-feeding of vapor was beneficial for the formation of methanol by preventing coke formation [4]. These strategies can be applied to achieve better catalytic performance.

8.3 Reference

1. Sugino, T.; Kido, A.; Azuma, N.; Ueno, A.; Udagawa, Y. Partial Oxidation of Methane on Silica-Supported Silicomolybdic Acid

Catalysts in an Excess Amount of Water Vapor. *J. Catal.* **2000**, *190*, 118-127.

2. Wang, C. B.; Herman, R. G.; Shi, C.; Sun, Q.; Roberts, J. E. V_2O_5-SiO_2 xerogels for methane oxidation to oxygenates: preparation, characterization, and catalytic properties. *Appl. Catal. A: Gen.* **2003**, *247*, 321-333
3. Starokon, E. V.; Parfenov, M. V.; Arzumanov, S. S.; Pirutko, L. V.; Stepanov, A. G.; Panov, G. I. Oxidation of methane to methanol on the surface of FeZSM-5 zeolite. *J. Catal.* **2013**, *300*, 47-54.
4. Parfenov, M. V.; Starokon, E. V.; Pirutko, L. V.; Panov, G. I. Quasicatalytic and Catalytic Oxidation of Methane to Methanol by Nitrous Oxide over FeZSM-5 Zeolite. *J. Catal.* **2014**, *318*, 14-21.
5. Snyder, B. E.; Vanelderen, P.; Bols, M. L.; Hallaert, S. D.; Böttger, L. H.; Ungur, L.; Pierloot, K.; Schoonheydt, R. A.; Sels, B. F.; Solomon, E. I. The active site of low-temperature methane hydroxylation in iron-containing zeolites. *Nat.* **2016**, *536*, 317.
6. Dubkov, K. A.; Ovanesyan, N. S.; Shteinman, A. A.; Starokon, E. V.; Panov, G. I. Evolution of Iron States and Formation of α-Sites upon Activation of FeZSM-5 Zeolites. *J. Catal.* **2002**, *207*, 341-352.
7. Li, G.; Pidko, E. A.; Filot, I. A.; van Santen, R. A.; Li, C.; Hensen, E. J. Catalytic properties of extraframework iron-containing species in ZSM-5 for N_2O decomposition. *J. Catal.* **2013**, *308*, 386-397.
8. Yakovlev, A. L.; Zhidomirov, G. M.; van Santen, R. A. DFT Calculations on N_2O Decomposition by Binuclear Fe Complexes in Fe-ZSM-5. *J. Phys. Chem. B* **2001**, *105*, 12297-12302.

9. Park, J. H.; Choung, J. H.; Nam, I. S.; Ham, S. W. N_2O decomposition over wet-and solid-exchanged Fe-ZSM-5 catalysts. *Appl. Catal. B: Environ.* **2008**, *78*, 342-354.

10. Choi, S. H.; Wood, B. R.; Ryder, J. A.; Bell, A. T. X-ray Absorption Fine Structure Characterization of the Local Structure of Fe in Fe-ZSM-5. *J. Phys. Chem. B* **2003**, *107*, 11843-11851.

11. Chow, Y. K.; Dummer, N. F.; Carter, J. H.; Meyer, R. J.; Armstrong, R. D.; Williams, C.; Shaw, G.; Yacob, S.; Bhasin, M. M.; Willock, D. J. *et al.* A Kinetic study of methane partial oxidation over Fe-ZSM-5 using N_2O as an oxidant. *ChemPhysChem* **2018**, *19*, 402-411.

12. Sun, K.; Xia, H.; Feng, Z.; van Santen, R.; Hensen, E.; Li, C. Active sites in Fe/ZSM-5 for nitrous oxide decomposition and benzene hydroxylation with nitrous oxide. *J. Catal.* **2008**, *254*, 383-396.